LATERAL BUCKLING OF STEEL I-SECTION BRIDGE GIRDERS BRACED BY U-FRAMES

by

ROSE MUI YUEN
B.Eng

Submitted in accordance with the requirements for the degree of Doctor of Philosophy

(The Candidate confirms that the work submitted is her own and appropriate credit has been given where reference has been made to the works of others.)

The University of Leeds
Department of Civil Engineering
October 1992

ACKNOWLEDGEMENTS

I would like to express my sincere thanks to my supervisor, Mr. J.O. Surtees not only for his constant guidance and encouragement throughout the period of my study, but also for the inspiring discussions and candid criticism which proved invaluable.

My entry to postgraduate study would not have been possible without support from the Tetley and Lupton Scholarship Fund and Overseas Research Studentship Committee. Thanks are also due to the Department of Transport for their funding of part of this study and Travers Morgan Limited who, through Mr. E. Jeffers, provided essential ideas and background information.

Thanks also go to Dr. J. Schmidt of the University's Computing Services and to technical staff of the Department of Civil Engineering for their helpful assistance.

Special thanks are also due to my friends in Leeds for their moral support and, in particular, Dr. F.B. Mok who has been most helpful.

I am deeply indebted to my dear parents for their love, patience and support throughout my years of study in this country. Through the dedication of this work to them, I would like to express my heartfelt love and gratitude.

Last, but certainly not least, I wish to express my profound gratitude to Advin K.S.Teh who shared with me, willingly and patiently, the stressful as well as the joyful times of this period and whose relentless encouragement I could not have done without.

ABSTRACT

The study consists of an experimental and analytical investigation into the lateral buckling behaviour of steel I-section girders braced by continuous or discrete U-frames. Scaled down laboratory tests on twin I-section girders have been carried out under full instrumentation and are reported. Lateral deflection of the compression flanges and final buckling modes were recorded and the coupling effect of U-frame action is clearly demonstrated. The failure loads obtained were generally higher than the corresponding design values according to BS5400.

Using a large displacement elasto-plastic finite element package, ABAQUS, finite element idealisations of the tests were established and analysed. Good correlation between the experiments and the numerical analyses was reached. Validity of the ABAQUS package was confirmed and first order elements were sufficiently effective for the analysis.

This was followed by further investigation of a wider range of I-section girders using ABAQUS. The ultimate bending resistance of the girders obtained from finite element analysis was in general greater than the corresponding design values to BS5400, particularly so with girders of high slenderness. Thus, the present design method is considered to be unduly conservative.

The cause of this conservatism in BS5400 is discussed. The expression for the calculation of effective length of U-frame braced girders was found to be reasonable. Based on the results from ABAQUS and reviews of the limited research directly related to this study, two main parameters in the BS5400 expression for beam slenderness seem inappropriate for lateral buckling of an I-section girder under U-frame restraint. These are the radius of gyration of the whole girder section and the ratio of overall depth of a girder to mean flange thickness. Instead, radius of gyration of the compression flange together with a contribution from the adjoining web section was found to be more appropriate as also was the web slenderness. In addition, a modification is proposed to the present limiting stress curve for lateral buckling of bare steel I-section girders. Empirically derived factors have been introduced. The general procedures in the existing design method to BS5400 remain similar, however.

TABLE OF CONTENTS

CHAPTER 4 FINITE ELEMENT IDEALISATION OF EXPERIMENTAL TEST MODELS

CHAPTER 5 FINITE ELEMENT MODELLING OF BRIDGE GIRDERS

CHAPTER 6 FINITE ELEMENT IDEALISATION OF DISCRETE U-FRAMES

LIST OF TABLES

LIST OF FIGURES

CHAPTER 5

CHAPTER 7

NOTATION

A:	area of a cross-section
B:	distance between girders
D:	overall depth of a girder
d:	depth of web
d_1:	distance from centroid of a compression flange to the nearer face of the cross member of the U-frame
d_2:	distance from centroid of compression flange to the centroidal axis of cross member of the U-frame
E:	Young's modulus of elasticity
I_1:	second moment of area of an effective vertical element of the U-frame about its axis of bending
I_2:	second moment of area of the cross member of the U-frame about its axis of bending
I_c:	second moment of area of the compression flange about its centroidal axis parallel to the web of the beam
I_t:	second moment of area of the tension flange about its centroidal axis parallel to the web of the beam
i:	$\frac{I_c}{I_c+I_t}$
k:	elastic spring stiffness
k_3:	a coefficient for restraint against rotation at supports
k_4:	a coefficient for type of beam
L:	span length
l_e:	effective length
l_u:	distance between U-frames
M_b:	buckling moment capacity
M_{cr}:	elastic moment capacity
M_D:	ultimate bending resistance
M_p:	plastic moment capacity
m:	number of half-waves
P:	axial force
P_E:	Euler load
r_y:	radius of gyration of whole beam section about its weaker axis

S: shape factor, ($\frac{Z_{pe}}{Z_{pc}}$ for compact sections or $\frac{D}{2y_t}$ for non-compact sections)

t_f: mean thickness of the two flanges of an I-section girder

t_w: thickness of girder web

y_c: distance from the axis of zero stress to the extreme compression fibre of a girder section

y_t: distance from the axis of zero stress to the extreme tension fibre of a girder section

Z_{pe}: plastic modulus of a section

Z_{xc}: elastic modulus of a section with respect to the extreme compression fibre

Z_{xt}: elastic modulus of a section with respect to the extreme tension fibre

β: beam/girder slenderness function, defined as $\lambda_{LT}\sqrt{\frac{\sigma_{yc}}{355}}$

β: a non-dimensional quantity, defined as $(\frac{k}{EI_c})^{0.25}$

δ: lateral deflection which would occur in a U-frame at the level of the centroid of the compression flange when a unit force acts laterally on the U-frame at this point simultaneously with an equal and opposite force on the other compression flange associated with the U-frame

η: a coefficient for bending moment variation in the λ_{LT} expression or an imperfection constant in the Perry-Robertson formula

λ_{LT}: slenderness parameter

λ_F: $(\frac{le}{r_y})(\frac{t_f}{D})$

σ_{cr}: elastic critical stress

σ_{lc}: limiting compressive stress

σ_{li}: basic limiting stress

σ_{yc}: nominal yield stress of the compressive flange

υ: a factor for the shape of a cross-section, dependent on i and λ_F or Poisson's ratio.

ABBREVIATIONS

BS5400	British Standard BS5400: Part 3: 1982
CPU	Central Processing Unit
ECCS	European Convention for Constructional Steelwork 1976
F.E.	Finite Element
LH	Left Hand
LVDT	Linear Variable Differential Transformer
MCC	Manchester Computing Centre
MPC.	Multi-Point Constraint
RH	Right Hand
SHS	Square Hollow Section
TRRL	Transport and Road Research Laboratory
UDL	Uniformly Distributed Load
WI	Welding Institute

CHAPTER 1

INTRODUCTION

1.1 GENERAL

In choosing the structural arrangement for a steel girder bridge, various forms of bracing may be used. The primary function of bracing is to limit undesirable out-of-plane deformation. For medium span bridges, the half-through girder system, as illustrated in Figure 1.1 in which cross members (for example, deck slabs or cross-beams) are located at the lower flange level with no interconnection at the upper flange level, is in common use.

For a simply supported span, the compression flange of the girder is obviously unsupported in the transverse direction and its stability must, therefore, be provided by U-frame bracing action from the cross members and the web of the girder. Such a bracing device may be either discrete or continuous depending on the form of cross members. An inverted U-frame (as shown in Figure 1.2) is applicable if the positions of the compression and tension flanges are reversed. This condition occurs over internal supports in continuous spans, where stability of the unsupported lower flange depends on the restraining force from the cross members acting through the stiffened or unstiffened girder webs.

Because of the popularity of such bridge configurations, it is important to study the stability of girders braced by U-frames and to seek an effective and economical design method.

It is widely believed that design according to the current BS5400[1] can significantly underestimate the bending capacity of steel girders restrained by U-frames. This has led to excessive and unnecessary bracing of I-section girders and, therefore, to uneconomical bridge structures with perhaps added maintenance burdens and fatigue susceptibilities. A better appreciation of the way in which U-frame action actually functions and its qualification to ensure the stability of girders is clearly necessary.

In BS5400, instability of the compression flange of I-section girders braced by U-frames is treated as lateral torsional buckling of beams. No special adjustment is provided for the presence of lateral restraint to the tension flange, for example.

1.2 LATERAL BUCKLING

Buckling, is a form of unstable behaviour in which a sudden large increase in deformation in a plane normal to the applied force occurs after a small increase in the applied force. Beams which transfer load through bending are often regarded as uniaxially effective and major axis bending, therefore, becomes a principle design consideration. I-beams or girders are often selected on this basis and further possibility of lateral buckling or, as sometimes called, lateral torsional buckling, in which collapse is initiated as a result of lateral deflection and twisting of the cross-section, must be considered.

However, in the form of instability associated with I-section bridge girders braced by U-frames, buckling of the compression flange is accompanied by distortion of the cross-section[2], as illustrated in Figure 1.3. This is mainly because the tension flange is laterally and torsionally restrained so that twisting and lateral movement of the entire section (as in the case of lateral torsional buckling of I-sections mentioned above) are very much limited by the restraint from cross members.

Buckling behaviour of unrestrained beams[3,4] is well comprehended as a result of the vast amount of study and research carried out to date. The effect of lateral or torsional bracing on struts and I-section beams has also been examined to a limited extent [5,6]. However, rather less has been done in relation to girders subject to U-frame bracing. Even so, the characteristics of buckling under U-frame support have become clearer through studies conducted in the last decade. It is felt that the present design approach needs to be improved if economical design is to be achieved. It is the purpose of this research to study the instability of I-section girders under U-frame bracing action with a view to refining the present design procedures.

The behaviour of steel bridge girders may be examined through experimental tests. However, the cost would be high and the number of parameters studied would be limited. This can be overcome by analytical modelling, for instance by the finite element method, provided that the validity of the models is verified by experimental tests.

In the work presented here, experimental observations and numerical modelling have been applied to the study of lateral 'torsional' buckling of I-girders under U-frame bracing. An understanding of the failure mechanisms of such type of bridge structure has been sought. Geometrical and material non-linearity have been included. The appropriateness of the effective length concept used in the Code has been examined. The bending capacity of girders under continuous or discrete U-frame bracing has been

evaluated by finite element analysis and compared with values derived according to BS5400. Modification of present design to BS5400 is ultimately proposed.

1.3 ORGANISATION OF THE THESIS

A review of previous work on the lateral buckling of I-section girders under U-frame action is presented in Chapter 2.

In Chapter 3, a description of settings of laboratory tests on three U-frame bridge models is presented and the results are discussed in detail.

Main characteristics of the finite element package used in this project are outlined in Chapter 4. Idealisations of the three laboratory tests are given and finite element results are presented and compared with those from the tests.

Having confirmed the suitability of the package, idealisation of two practical deck forms which use continuous U-frame support is described in Chapter 5. In this case, the effect of uniform bending moment on a single span and varying moment due to UDL on two continuous spans is studied.

Chapter 6 presents a number of finite element analyses of girders braced by equally spaced cross-beams representing discrete U-frame action. The effect of the size and spacing of cross-beams on load capacity of the girders and buckling mode of the compression flange is addressed.

Based on the findings from numerical results, a proposed modification of the present Code is described and tested on girders of various geometries. The validity of the modification in predicting the load capacity of girders is discussed in relation to BS5400 in Chapter 7.

Chapter 8 summarises the work carried out and the conclusions drawn. Further studies are also suggested.

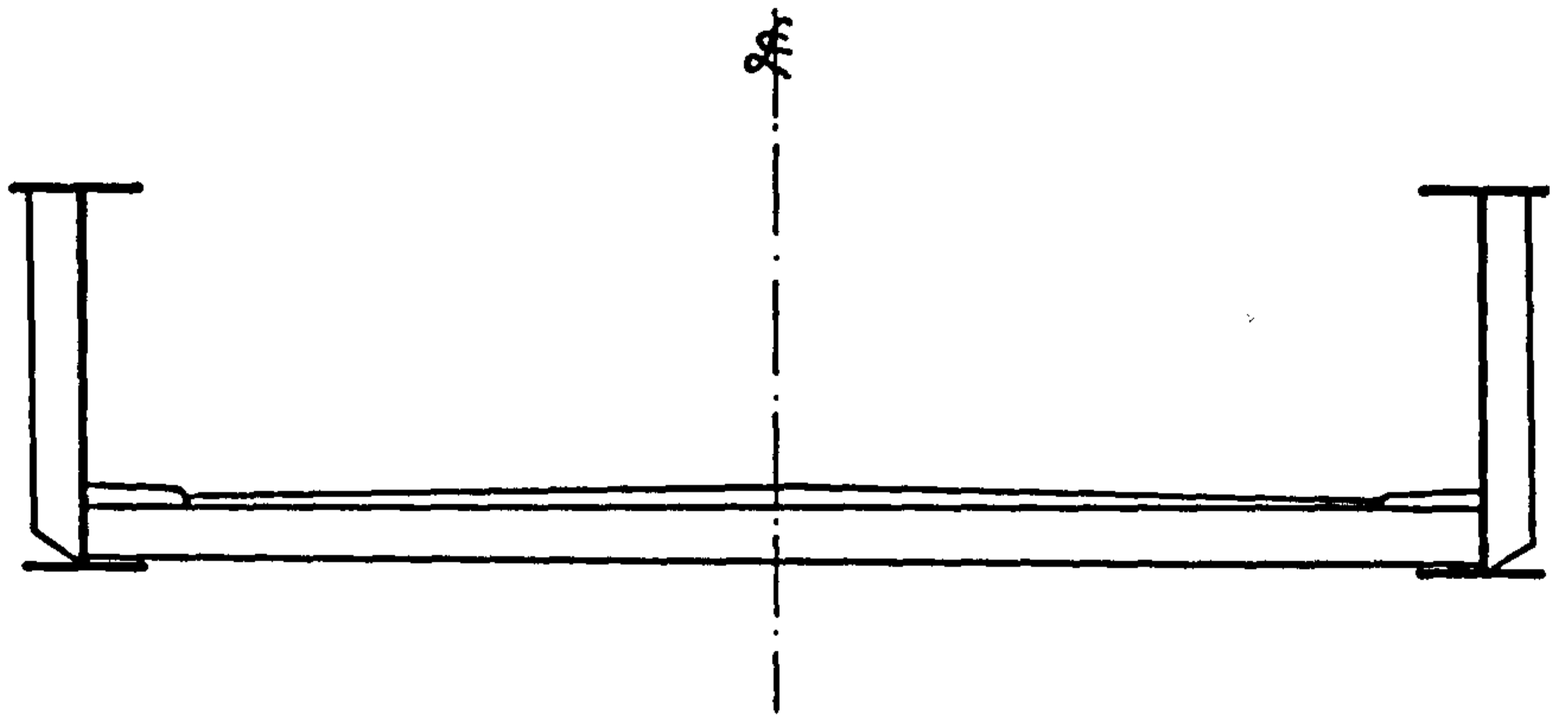

Figure 1.1 Typical half-through bridge section

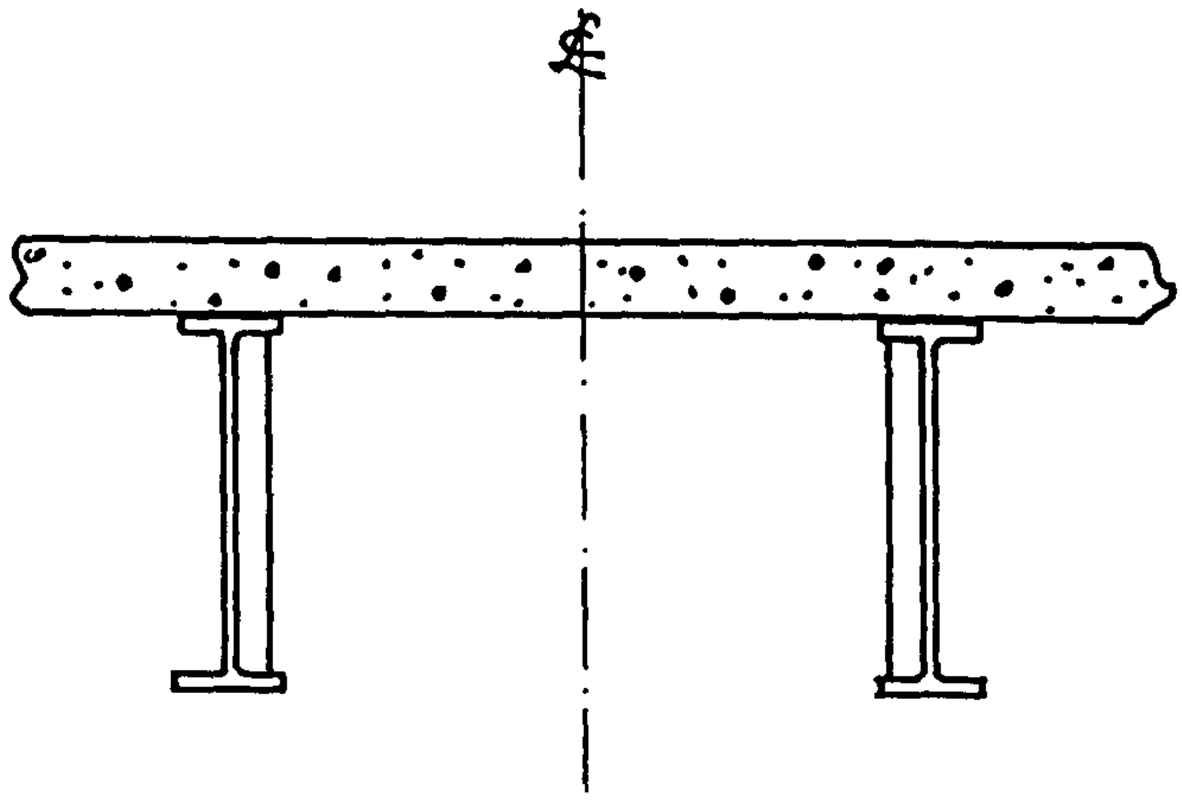

Figure 1.2 Inverted U-frame

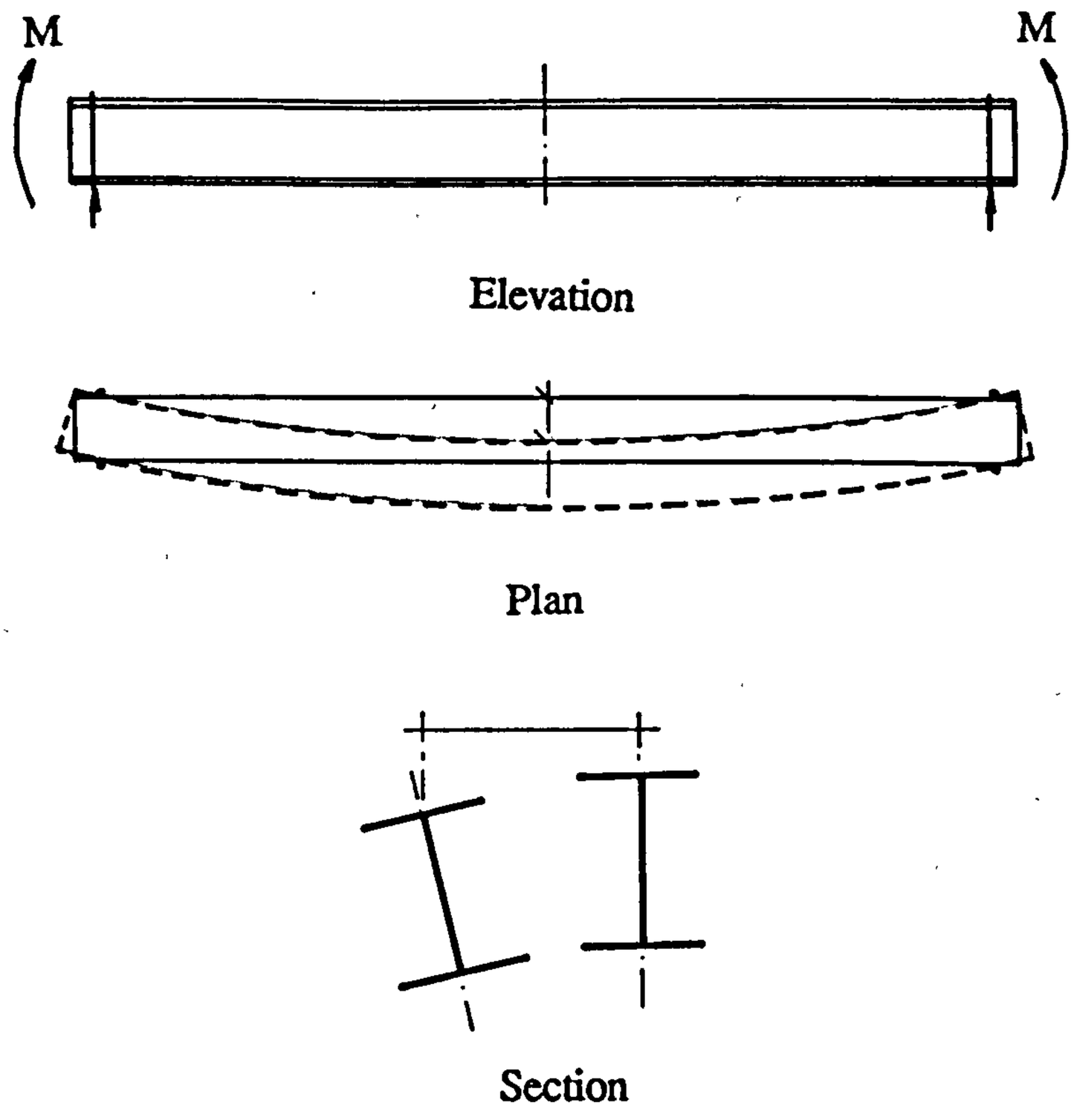

Figure 1.3 Lateral torsional buckling of beams

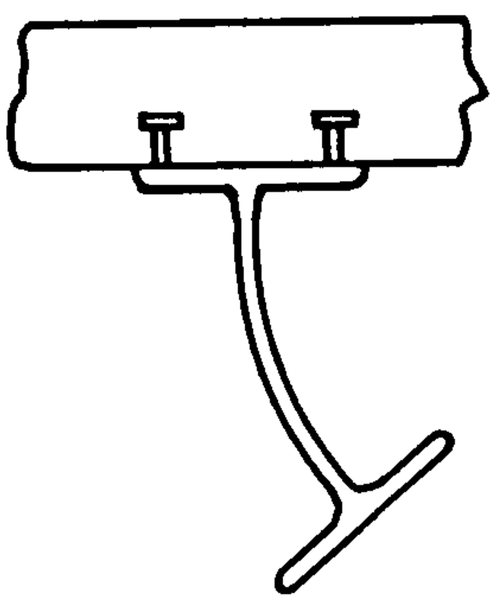

Figure 1.4 Distortion of a girder cross-section braced by concrete deck

CHAPTER 2

RECENT DEVELOPMENT IN U-FRAME STRUCTURES

2.1 INTRODUCTION

Owing to the complexity of the behaviour of a compression flange over an internal support, many problems associated with instability in this region are not resolved yet and still attract attention from research investigators and practising engineers[7].

To provide a better understanding of the behaviour and its relation to design, the basis of the BS5400 criteria are discussed and research directly related to this study is reviewed.

2.2 EXISTING BRITISH STANDARD

2.2.1 Effective Length

In current design to BS5400: Part 3, lateral buckling of compressive flanges of steel girders restrained by U-frames, continuous or discrete, is treated as a strut on an elastic foundation[8]. The strut represents the flange whereas the stiffness of the elastic foundation is an idealisation of the restraining action from the U-frames.

The strut is assumed to be simply supported at both ends with elastic spring supports along its length and subjected to an axial force P. At a certain loading stage, lateral buckling occurs with a buckling mode of m half sine waves and the relation between P and m can be written as :

$$P = \frac{\pi^2 EI}{L^2}\left(m^2 + \frac{\beta L^4}{m^2 \pi^4 EI} \right),$$

where β = rigidity of elastic medium;

L = length of the strut ; and

EI = bending rigidity.

When $m = 1$, $\beta = k$, $P = \frac{\pi^2 EI}{L^2}\left(1 + \frac{kL^4}{\pi^4 EI} \right)$

To obtain minimum buckling load, $\frac{dP}{dL} = 0$

$$L = \pi(EIk)^{0.25}$$

$P_{min} = 2(EIk)^{0.5} = \frac{\pi^2 EI}{l_e^2}$, which is the Euler load with effective length

$$l_e = \frac{\pi}{\sqrt{2}}\left(\frac{EI}{k}\right)^{0.25} \quad . \quad . \quad . \quad . \quad . \quad . \quad . \quad . \quad . \quad . \quad . \quad . \quad (2.1)$$

Based on the derivation of l_e in equation (2.1), the effective length is defined in BS5400: Part 3, Clause 9.6.5 for discrete U-frames as:

$$l_e = 2.5k_3(EI_c l_u \delta)^{0.25} \quad . \quad . \quad . \quad . \quad . \quad . \quad . \quad . \quad . \quad . \quad . \quad (2.2)$$

where EI_c is the bending stiffness of the compression flange about its weaker axis;

l_u is the distance between U-frames; and

δ represents the flexibility of U-frames as shown in Figure 2.1. It is defined in BS5400 as the lateral deflection which would occur in a U-frame at the level of the centroid of the flange being considered, when a unit force is applied at this point.

An increase of 12.5% in l_e (from equation (2.1) to (2.2)) is given as an allowance for rotation of the compression flange in plan at supports.

For continuous U-frames, l_u is taken as 1.0 and $l_e = 2.5k_3(EI_c\delta)^{0.25}$ as defined in Clause 9.6.6.

From both expressions of δ in continuous or discrete U-frame structures, it can be seen that the compressive flange is restrained by the web cantilevered in simple bending from the cross members. Therefore, distortion, of the web is not represented in the design Code. The shear connection between the top flange and the concrete slab is assumed to be rigid (whereas in practice, some degree of flexibility would be present).

2.2.2 Limiting Stress Curve and Slenderness Ratio

The limiting stress design curve in Figure 10 of BS5400: Part 3, with $\frac{\sigma_{li}}{\sigma_{yc}}$ plotted against slenderness function λ_{LT}, is deduced from the Perry-Robertson equation:

$$(M_p - M_b)(M_{cr} - M_b) = \eta M_b M_{cr} \quad . \quad . \quad . \quad . \quad . \quad . \quad . \quad . \quad . \quad . \quad (2.3)$$

on the analogy of buckling of a strut. The effects of initial geometrical imperfection, residual stress and material yielding with respect to lateral buckling of the compression

flange of a U-frame braced girder are assumed to be the same as in the overall buckling of a bare steel beam. The imperfection constant, η, is taken as 0.005 (β-45).

As $M_p = Z_{pe}\,\sigma_{yc}$, $M_{cr} = Z_{xc}\,\sigma_{cr}$ and $M_b = Z_{pe}\,\sigma_{li}$ (for compact section) equation (2.3) can then be expressed as:

$$\frac{\sigma_{li}}{\sigma_{yc}} = 0.5\left[1+(1+\eta)\frac{5700}{\beta^2} - \sqrt{\left\{1+(1+\eta)\frac{5700}{\beta^2}\right\}^2 - \frac{22800}{\beta^2}}\ \right]$$

assuming that: $\frac{\sigma_{cr}}{\sigma_{yc}} = \frac{5700}{\beta^2}$

where β, the slenderness parameter, can be expressed as: $\lambda_{LT}\left(\frac{\sigma_{yc}}{355}\right)^{0.5}$; and

$$\lambda_{LT} = \left(\frac{l_e}{r_y}\right)k_4\eta\upsilon,$$

where l_e is the effective length as defined in BS5400 for either continuous or discrete U-frame structures;

r_y is the radius of gyration of the whole beam section about its weak axis;

η is a coefficient for the effect of moment gradient;

k_4 is a factor for a type of girder section; and

υ[9] is approximated by $\frac{1}{\{1+0.05[(\frac{l_e}{r_y})(\frac{D}{t_f})]^2\}^{0.25}}$ for doubly symmetrical beams. When the flanges of I-section beams are of different sizes, then υ has to be represented as:

$$\upsilon = [(4i(1-i) + 0.05(\frac{l_e}{r_y})(\frac{D}{t_f})^2+\psi^2)^{0.5}+\psi]^{-0.5}$$

in which $i=\frac{I_c}{I_c+I_t}$

where I_c and I_t are the second moments of area of the compression and tension flange respectively about their minor axes and ψ is a mono-symmetry index.

The variation of υ related to flange sizes can be expressed graphically as shown in Figure 2.2.

Limiting compressive stress, σ_{lc}, for compact section will be taken as σ_{li} but in the case of non-compact sections, a correction factor $\frac{D}{2y_t}$ is introduced in BS5400 to modify σ_{li} to enable the calculation of limiting compressive stress using Z_{xc} rather than Z_{pe}.

The Perry-Robertson formula is used for lateral torsional buckling of the entire beam. The effect of distortion of the beam section is, however, not dealt with. Only

rotation of the beam section about its longitudinal axis is considered. Even so, it is employed in the design of girders braced by U-frames.

2.2.3 Comments on BS5400

It is therefore seen that an effective length and the limiting stress both obtained from buckling of a simple elastically supported strut, are assumed to be valid for the design of the bridge girders braced by concrete slabs or cross-beams in BS5400. As the main feature of girders braced by U-frames is excluded, the assessment of lateral buckling of compression flanges using BS5400 is likely to be very conservative and this conservatism is exacerbated because the girders also receive a significant amount of assistance from the remainder of the structure. A case study of an existing railway bridge in Australia[10] suggested that the elastic buckling load of the bridge was approximately 6.5 times the design value according to BS5400.

The inappropriateness of the design code was discussed in depth by Johnson and Buckby[2] and Nethercot[11]. Their observations may be summarised as:

(a) the effective length of a compression flange is based on a partially restrained strut with constant axial compression (and the buckling mode is presumed to be a single half-wave, ie, m = 1), thus the beneficial effect of moment gradient is neglected;

(b) the torsional and warping stiffnesses of the compression flange at supports are ignored; and

(c) the δ value in l_e expressions is not constant in the compression region as explained by Nethercot[11].

A review of past research work, numerical and experimental, confirmed that the design method in BS5400 for lateral buckling of flanges in compression under U-frame restraints is indeed questionable. It has been widely recognised that the so-called lateral buckling of a compression flange involves two main features:

(a) the tension flange is restrained laterally by a relatively stiff concrete slab and lateral movement is virtually impossible. Rotation of the tension flange about an axis perpendicular to the plane of the U-frame may also be negligible; and

(b) there is no rotation of the girder as a whole, as in the case of overall lateral buckling of a bare steel beam, to generate the lateral displacement of a compression flange. Therefore, section distortion, for example, distortion of the web (as shown in Figure 1.4), is definitely involved (especially in the absence of transverse web stiffeners) and hence, the assumptions made in BS5400 are not applicable.

2.3 DEVELOPMENT

2.3.1 General

The research literature on elastic or inelastic overall lateral torsional buckling of unbraced steel beams, based on rigid web theory[8], has been well documented[2,12,13]. However, web distortion was hardly considered although it could be a practical problem for the design of girders of slender or unstiffened webs. Distortion of web can apparently reduce the torsional rigidity of cross-sections of girders and their buckling resistance would then be lower than the calculated value using classical rigid web theory. Research in this field became active when Hancock[14,15] dealt with distortional lateral buckling (ie, lateral torsional buckling coupled with web distortion) in the elastic range and provided a better understanding about distortional behaviour of steel I-beams. Afterwards, Bradford[16,17] studied the effect of web distortion systematically and concluded that load capacity would not be significantly affected.

Investigations have been carried out on lateral buckling of I-beams braced by side rails, cladding or shear diaphragm[18,19]. However, the characteristics of this kind of bracing are hardly applicable to bridge U-frame situations. Studies on the effect of rigid bracing together with distortion of girder webs were comparatively few and it is clear that the behaviour is insufficiently understood.

2.3.2 Numerical and Theoretical Study

The limited research done in the field before the 1950's has been described by Bleich[12].

In preparing a revised version of BS153 (the former British Bridge Code), Kerensky et al[20,21] published a series of results from theoretical analysis and experimental tests related to the bending and buckling strength of bare steel girders. The influence of sectional distortion in slender and unstiffened webs had long been recognised at the time and the contribution of torsional rigidity to the stability of the girders was apparently reduced. Nevertheless, they argued that the reduction was only of slight importance in beams of conventional proportion and might also be insignificant for deep plate girders, even if unstiffened. In addition, they claimed that the application of simple column analogy to analyse U-frame structures was justified and the ultimate strength curve for any practical girders was in fact of the Perry-Robertson type. U-frame action had been implicitly discussed but no laboratory tests had been carried out. It has been, since then, customary to use the Perry-Robertson formula for girders braced by U-frames.

In the experimental study of lateral torsional buckling of bare steel beams, they found a family of curves based on $\frac{D}{t_f}$ ratio of beam/girder cross-sections, as shown in Figure 2.3, amongst which, the Perry-Robertson formula is a special case with torsional index value approaching to infinity (ie, T-beams).

Bradford and Johnson[22] emphasized that classical theory of elastic lateral torsional buckling was not applicable to buckling of compression flanges close to internal supports in U-frame structures because it assumed that the cross-section of the member rotates as a whole without distortion. They carried out a study of elastic distortional lateral buckling for this type of girder, using elastic finite element analysis. Beams or girders under consideration were partitioned into a number of longitudinal member elements, each of them consisting of a web panel having membrane, torsional and bending flexibilities and two flange sub-elements with membrane and torsional flexibility only. Thus, there was no allowance for distortion of flange members. Eigenvalue analyses were used to determine the critical loads. To simulate the continuity of the compression flange over an internal support in the case of multi-span bridges, fixed-end spans under UDL were examined.

Parametric studies with main variables including span to compression flange width ratio $\frac{L}{B}$ (from 48 to 90), compression flange width to thickness ratio $\frac{B}{t_f}$ (from 9.6 to 15), web depth to thickness ratio $\frac{d}{t_w}$, width of concrete slab and percentage of reinforcement were undertaken. It was observed that the critical compressive stresses were mainly influenced by web slenderness ratio and the influence of other variables was small. The critical buckling mode, which was defined as the lateral displacement of the compression flange, was always symmetrical about mid-span. A tentative design curve which related the ratio of σ_{li} (limiting design stress) to σ_{yc} (nominal yield stress) and the ratio of σ_{yc} to σ_{cr} (elastic critical stress) instead of beam slenderness by taking:

$$\beta = 3.4\,(\frac{d}{t_w})^{0.7} \text{ and } \frac{\sigma_{cr}}{\sigma_{yc}} = 600\,(\frac{d}{t_w})^{-1.4} \text{ and, therefore, } \frac{\sigma_{cr}}{\sigma_{yc}} = \frac{7000}{\beta 2} \text{ rather than}$$

$$\beta = \lambda_{LT}(\frac{\sigma_{yc}}{355})^{0.5} \text{ and } \frac{\sigma_{cr}}{\sigma_{yc}} = \frac{5700}{\beta 2}$$

was proposed, based on the Perry-Robertson formula used in BS5400.

The design moment obtained by this method suggested that values calculated according to BS5400 could be doubled. It implied that the beneficial effects of top flange restraint and variation of moment distribution outweigh the inclusion of cross-sectional distortion. These results could be slightly unconservative as the tension flange was

restrained against lateral displacement and twist whereas it could actually rotate in a real situation.

The scope of the work was limited to spans without any intermediate transverse web stiffeners. Due to the much higher proposed design stress, it is perhaps questionable whether the local (inelastic) buckling near an internal support is comparable with the form of lateral buckling assumed in the analysis. Interaction between these two modes of buckling could have an adverse effect, preventing the proposed stresses from being realised. It is understood from theoretical study and laboratory tests[23] that local buckling (over a much shorter yield length), is associated with lateral buckling in hogging moment region and always occurs before the lateral buckling in composite girders. Therefore, it is necessary to study the effect of local buckling on the lateral stability of compression flanges braced by U-frames.

Bradford and Johnson[24], in 1987, presented a series of inelastic analyses of composite U-frame bridges buckling near to internal supports. Together with the other theoretical and experimental evidence [23,25], they stated that inelastic local buckling will usually precede lateral distortional buckling in hogging regions of continuous composite beams with non-compact cross-sections. There was, however, an exceptional situation in the finite element analysis where the flange was just within the class of compact classification and yet local buckling occurred first. Bradford and Johnson extended the previously proposed design method to cover both lateral distortional and local buckling situations. Two slenderness parameters β_D and β_L representing the occurrence of lateral distortional buckling and local buckling, respectively, were defined as:

$$\beta_D = 3.1\left(\frac{S\sigma_{yc}}{355}\right)^{0.5}\left(\frac{d}{t_w}\right)^{0.7} \text{ and } \beta_L = 3.5(\beta_f\,\beta_w)^{0.5}$$

S is the shape factor, equal to $\frac{Z_{pc}}{Z_{xc}}$ for the steel compression flange in the hogging region;

β_f, is the flange slenderness, assumed as $\left(\frac{B}{t_f}\right)\left(\frac{\sigma_{yc}}{355}\right)^{0.5}$;

β_w, is the web slenderness and expressed as $\left(\frac{\alpha d}{t_w}\right)\left(\frac{\sigma_{yc}}{355}\right)^{0.5}$, where αd is the depth between the elastic neutral axis of the beam and the compressive edge of the web.

The higher of β_D and β_L, representing the more critical buckling condition was taken as β. β was used in place of $\lambda_{LT}\left(\frac{\sigma_{yc}}{355}\right)^{0.5}$ in the design curve (Figure 10 in BS5400: Part 3). The limiting compressive stress in the compression flange was then obtained. Lateral distortional buckling appears to be the critical mode of failure for compact sections.

The improved design method yielded moments of resistance which, once again, doubled, on average, those given by BS5400. However, the method was only applicable to U-frame braced girders without intermediate web stiffeners. Again, a fixed-end span under UDL was the only case considered. Yet, direct use of the design curve $\frac{\sigma_{li}}{\sigma_{yc}}$ versus λ_{LT}, which is based on a strut subjected to constant axial force, is doubtful.

A more detailed numerical investigation of the stability of the compressive flange in the support region of U-frame braced bridge girders was carried out by Weston et al[26,27,28]. A large deflection elasto-plastic finite element programme developed by Crisfield[29,30] was employed. As in the approach by Bradford and Johnson, only fixed-end spans under UDL with unstiffened webs were considered.

Girder webs were modelled as rectangular plate elements and flanges as beam elements. The concrete slab attached to girders forming the tension flange in the composite section was transformed to an equivalent steel section in the sagging and hogging moment regions. Cracking of the concrete slab and the resultant loss of girder stiffness in the hogging region was assumed to be uniform over the whole hogging region and was modelled as part of the top flange whereas the elastic neutral axis position for the model still coincided with that of uncracked girder. Ivanov's yield criterion[31] was used to simulate the spread of plasticity rather than the usual von Mises' yield criterion. A total of 19 girders were analysed and, depending on the different geometric properties, three types of failure were observed, namely:

(a) local web buckling, leading to significant lateral flange movement in the vicinity of the web only;

(b) lateral buckling of the compressive flange, extending over a substantial portion of the half spans; and

(c) combined buckling, involving large displacement in both web and flange.

Because of the simplified modelling of flanges with beam elements, local flange buckling was not detectable and, thus, was precluded from the analysis. In this work, it was noted that when the ratio of web depth to thickness $\frac{d}{t_w}$ exceeds about 60, failure is likely to be caused by lateral buckling of the compression flange near the internal supports. The compression flange slenderness $\frac{L}{r_y}$, in which L is the span and r_y is the lateral radius of gyration of the compression flange, proved to be as significant as the web slenderness $\frac{d}{t_w}$. From the numerical results, a newly defined slenderness parameter involving both $\frac{L}{r_y}$ and $\frac{d}{t_w}$ was proposed as:

$$\beta = 1.28\,[(\frac{L}{r_y})^{0.5}\,(\frac{d}{t_w})(\frac{1}{3})]\text{-}29,$$

Then, in conjunction with the basic limiting stress curve (ie, Figure 10 of BS5400: Part 3), the limiting compressive stress σ_{li}, was determined. β was also presented in chart form in the paper, from which it was possible to determine immediately whether or not a particular girder geometry was susceptible to lateral buckling.

The influence of the form and magnitude of initial imperfection on loaded behaviour was observed. It was seen that the load capacity of the girders was reduced by only 5% if the number of half-waves in the initial lateral imperfection in the compression flange was changed between one half-wave to six half-waves. The magnitude of the initial bows only affected the rate at which out-of-plane deformation developed but not the ultimate capacity of the girders. The effect of residual stress on the behaviour of the girder was similar to that of initial imperfection, while there was little change when torsional rigidity of the tension flange varied.

In common with other work (notably by Bradford & Johnson and Svensson[32]), the results suggested that BS5400 drastically underestimated the lateral buckling capacity of U-frame braced girders as the computed load capacities were four to five times greater than the design values obtained according to BS5400. The results also confirmed that local buckling would be a critical factor for non-compact girders.

On the other hand, in contrast with the findings of Bradford & Johnson, Weston[26] stated that the dominant mode of failure in compact or near-compact bridge girders is likely to be inelastic local buckling adjacent to an internal support and Bradford and Johnson's method may give an unsafe estimate of the ultimate bending moment of girders with slender flanges because $\frac{d}{t_w}$ ratio, only, had been considered. A detailed comparison of the work done by Bradford and Johnson[22,24] and Weston et al[26,27] was presented by Fan[33].

The drawback of references (22), (24) and (26), (27) is that the only boundary conditions and variation of moment distribution considered were those corresponding to a fixed-end span under UDL.

Local (web or flange) buckling seems to be invariably associated with the failure of U-frame braced girders with non-compact cross-sections. It was observed that severe local buckling occurred even when very stocky joints were used[23,34,35]. Hamada and Longworth[34] studied local flange buckling and lateral buckling in a negative moment region theoretically and experimentally. They found that the ultimate moment capacity of

a composite beam was affected by local flange buckling unless the compression flange was stiffened by a cover plate.

Several investigators[36,37,38,39,40] have attempted to obtain a general closed form of solution for elastic lateral buckling of continuously restrained beams and columns. Because of the general complexity of the problem, the influence of various factors (for example, web distortion and moment variation) were not covered. Also, application of the theoretical solutions to practical situations was not easy.

The problem of stability of compression flange in composite girders near to the support had been tackled by Svensson[32] using a different approach. The compression flange was modelled as a column subject to various axial P(x) force distributions (see Figure 2.4), whereas the web of the girder was idealised as a Winkler foundation elastically supporting the column. The modulus of the foundation was actually the flexural stiffness of the web of distorted profile per unit length and defined as:

$$k=\frac{Et_w^3}{4(1-\upsilon^2)h^3} \quad \ldots\ldots\ldots\ldots\ldots\ldots\ldots\ldots\ldots\ldots \quad (2.5)$$

where h is the distance between the centroids of compression and tension flanges.

The simplified problem could be represented mathematically by the differential equation:

$$EI(\frac{d^4w}{dx^4})+\frac{d}{dx}[P(x)(\frac{dw}{dx})]+kw=0 \quad \ldots\ldots\ldots\ldots\ldots\ldots\ldots\ldots\ldots\ldots \quad (2.6)$$

where w is the lateral displacement.

By introducing various non-dimensional quantities and using a Fourier expansion, he produced a series of equations using the Galerkin's method as:

$$\frac{d^4w}{d\xi^4}+\pi^4\lambda\{\frac{d}{d\xi}[p(\xi)(\frac{dw}{d\xi})]\}+(\beta L)^4w=0$$

where $\xi=\frac{x}{L}$, $\beta L=(\frac{k}{EI})^{0.25}L$ and $\lambda=\frac{P_o}{P_E}$

The series of equations constituted an eigenvalue problem. The smallest positive eigenvalue λ_e, for an infinitely long strut , was found as:

$$\lambda_e=\frac{2}{\pi^2}(\beta L)^2$$

for any particular spring stiffness k under different axial loading $p(\xi)$.

It is not difficult to see that $\lambda_e^{-0.5} = \frac{l_e}{L}$ where l_e is the effective buckling length and L the length of the column. The effective buckling length could be used to find σ_{el} which is the elastic buckling stress, given by $\sigma_{el} = \frac{\pi E}{(\frac{l_e}{r_y})^2}$ and then the dimensionless slenderness ratio given by $\lambda_r = \sqrt{\frac{\sigma_{yc}}{\sigma_{el}}}$.

The limiting compressive stress was then obtained from one of ECCS[41] strut design curves (plotted with $\frac{\sigma_{li}}{\sigma_{yc}}$ against λ_r ,which is similar to Figure 10 in BS5400). It is worth noting that Svensson did not propose relationship in terms of web or flange slenderness as Bradford and Johnson and Weston et al had done, but the idea of effective buckling length used in BS5400 was extended for different loading cases and end conditions.

Since the flexibility of the concrete slab was neglected, the spring modulus k would be slightly over-stiff and the ultimate capacity of the column would be exaggerated. However, the model was still considered conservative because the contribution to torsional stiffness of the compression flange was disregarded. Weston has shown that the error in this method was on the safe side.

To improve the accuracy of predicting the elastic critical stress, Svensson together with Goltermann[42] presented a refined method based on this elastically supported column analogy. According to Williams and Jemah[43], approximately 15% of the area of the web, should be integrated with the compression flange to constitute the column including the torsional restraints from concrete slab. Svensson and Goltermann replaced the previous spring stiffness k by k_{eq}, as suggested by Nakamur and Wakayabashi[44],

where $\frac{1}{k_{eq}} = \frac{1}{k_f} + \frac{1}{k_w}$ . . . . . (2.7)

$k_w = k = \frac{Et_w^3}{4(1-\upsilon^2)h^3}$ as before;

$k_f = \frac{2(EI)_c}{h^2 B}$, $(EI)_c$ being the flexure stiffness of a unit strip of the concrete slab in the transverse direction; and

B is the distance between two parallel beams.

A close examination of expression (2.7) reveals that it is in fact the same as the δ expression for U-frames defined in BS5400. k_w is the first term in δ whilst k_f is the second.

Equation (2.6) will be modified as:

$$\frac{d^4w}{dx^4}+\pi^4k_1\lambda\left(\frac{d}{dx}\left[n(x)-\frac{k_2}{k_1\lambda}\left(\frac{dw}{dx}\right)\right]\right)+(\beta L)^4w=0 \quad \ldots\ldots\ldots\ldots (2.8)$$

where k_1 and k_2 are in terms of k_w and k_f. Details of the derivation are given in the paper.

The smallest eigenvalue of λ, ie, λ_e, as defined before was sought and followed by seeking the value of σ_{el}.

A simply supported column subject to eight variations of axial force, as a simulation of the compression flange in girders under various moment distribution, was studied in detail and presented in tabular form. The critical stress σ_{cr} of the column could then be determined by:

$$\frac{\sigma_{cr}}{\sigma_{yc}}=\frac{1}{\sqrt{1+\lambda_r^4}}, \text{ where } \lambda_r=\sqrt{\frac{\sigma_{yc}}{\sigma_{el}}}.$$

It is unfortunate that the lateral movement of the column was not traced for various loading situations and hence no indication of the buckling mode or half-wave length at the buckling stage was expressed in this refined evaluation procedure. The occurrence of any local buckling (web or flange) or the interaction of local and lateral distortional buckling could not be detected in the analysis based on the spring supported column analogy. Therefore, for beams or girders susceptible to local buckling, the above analogy may not be applicable. In addition, the only boundary condition considered was for a simply supported situation which may not be practical when analysing real bridges.

2.3.3 Experimental Work

Little useful information has been produced from experimental work. The cost of test specimens and set up to model a U-frame structure accurately in a continuous girder situation can be quite high.

In 1986 Nakamura and Wakabayashi[45] tested a series of H-shaped steel girders, with and without concrete slab or purlins, under uniform bending moment and various other moment profiles. Load carrying capacity and deformability of the girders were recorded and analysed.

It was the first time that observations from experiments had shown that the lateral displacement and the twist of the tension flange, which was attached to a reinforced concrete slab, were very small even when the slab was relatively flexible. The effect of

the reinforced concrete slab on the lateral buckling strength of the girders was compared with previous work done by Wakabayashi[46], where secondary beams or purlins were large and the maximum load carrying capacity had increased significantly.

Under a triangular bending moment profile, the maximum load carrying capacity of the beams braced by the slab was higher than the plastic moment of resistance of the steel beam despite a high slenderness ratio about the weaker axis of 600. But when a uniform moment profile was applied, the maximum load capacity was less than the plastic moment of the steel section. Therefore, the benefit of a non-uniform bending profile was clearly demonstrated. The buckled shape of the compression flange was not described or evaluated in the study and no information was given on the final buckled shapes in the experiments.

Recently, a more elaborate experiment was published by Fan[33,47] from Warwick University. A series of tests on full scale isolated T-beams and inverted U-frames were carried out to investigate the distortional feature of lateral buckling of the compression flange in the negative moment region. Beams with near-compact section were used as they frequently occur in the practical bridges. Vertically unstiffened webs were used throughout the whole series of tests as it was assumed that the transverse flexibility of shear connectors was negligible and this assumption was only valid in the absence of vertical web stiffeners[2,27].

The tests were done in double cantilevered fashion to simulate the hogging moment region near an internal support in a continuous beam. The initial lateral imperfection was recorded and the buckled shapes at the final loading stage were observed in detail.

In two of the U-frame tests, the results showed that the ultimate strength of the beams forming the U-frames was largely dependent upon the interaction of local flange buckling and distortional lateral buckling of the compression flange, which in turn was strongly influenced by the initial lateral imperfection. However, in Weston's finite element analyses of the girders, he formed a quite different view as far as the effect of initial lateral imperfection was concerned.

The maximum experimental hogging moments exceeded the predictions according to BS5400 by 200%, and this seemed to confirm the previous conclusion that BS5400 is over conservative.

2.4 CONCLUSION

From previous numerical and experimental investigations into the stability of compression flanges of U-frame braced girders, the common finding shared by

researchers is that the BS5400 method of evaluation of the load capacity of this type of structure may be extremely conservative.

Local buckling of the compression flange or web near an internal support region seems always to be associated with lateral buckling in either compact or non-compact sections. Lateral buckling of the compression flange of a vertically unstiffened girder certainly involves distortion of the web. Thus, lateral distortional buckling is a more suitable description of instability in U-frame braced, unstiffened, composite beams. However, to what extent distortion affects the load capacity is not yet clear.

The effect of variation of moment distribution has not been studied intensively nor has the influence of the torsional rigidity of a beam cross-section.

Research work so far has dealt with composite beams which only form continuous U-frames. Little work has been carried out for discrete U-frames consisting of plate girders with vertical stiffened webs and evenly spaced cross-beams.

Therefore, instability of the compression flange still remains an active research area. It is the aim of this study to investigate buckling behaviour of U-frame braced girders with a view to refining the present design procedure.

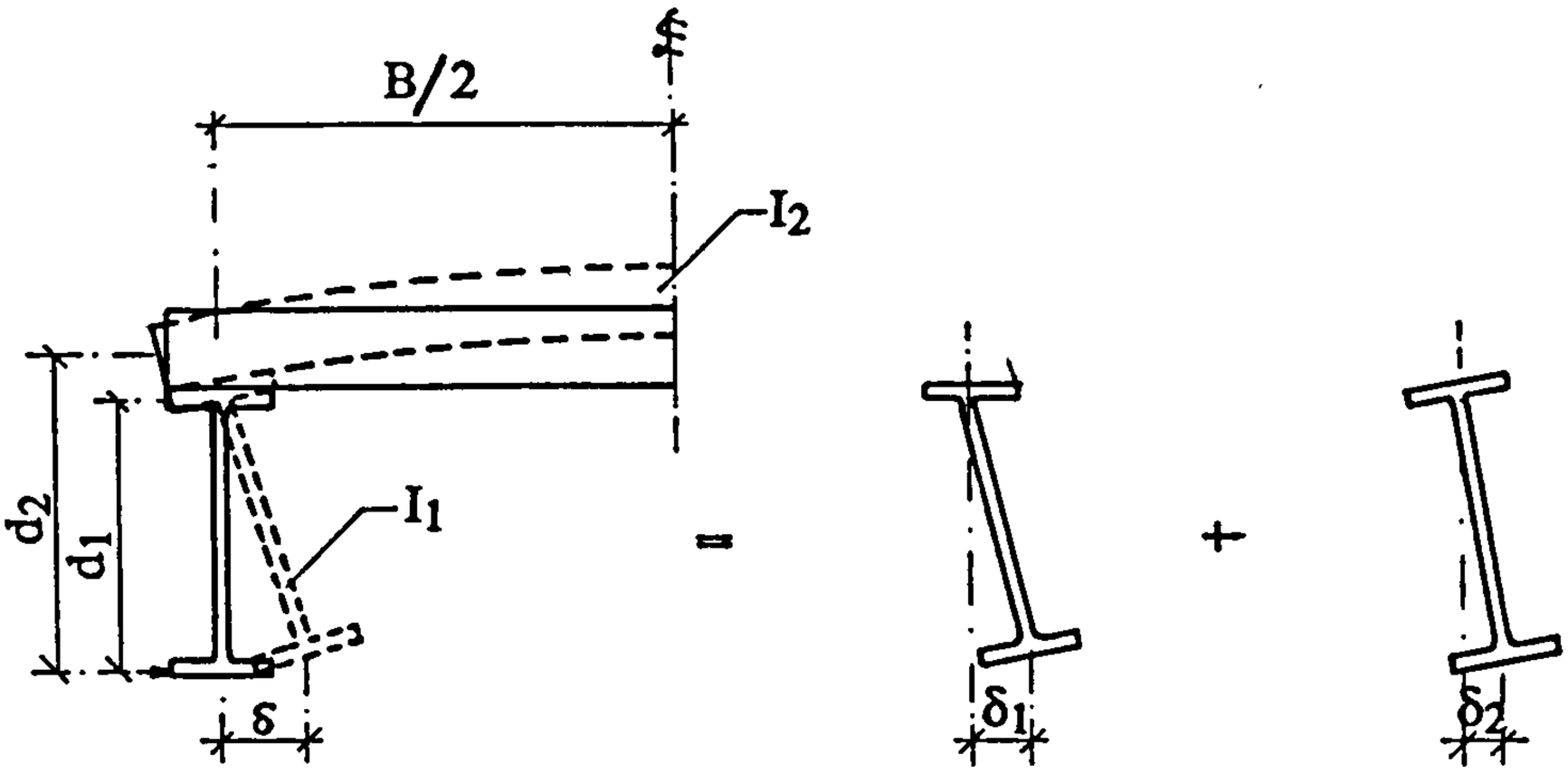

Deformation due to web bending $\delta_1 = \frac{d_1^3}{3EI_1}$

Deformation due to web bending $\delta_2 = \frac{Bd_2^2}{3EI_2}$

Figure 2.1 Flexibility of U-frame

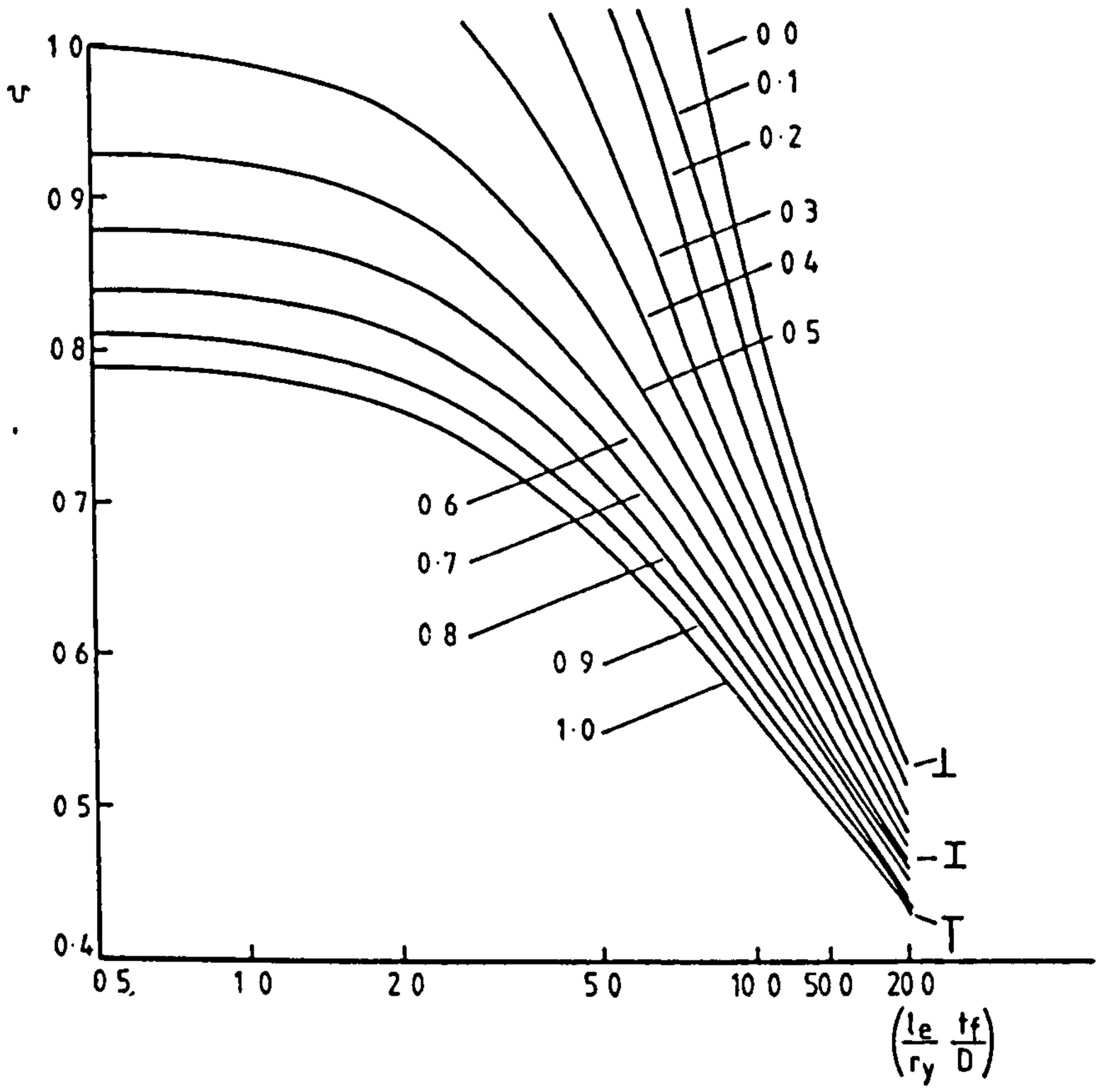

Figure 2.2 Variation of υ with $(\frac{l_e}{r_y})(\frac{t_f}{D})$

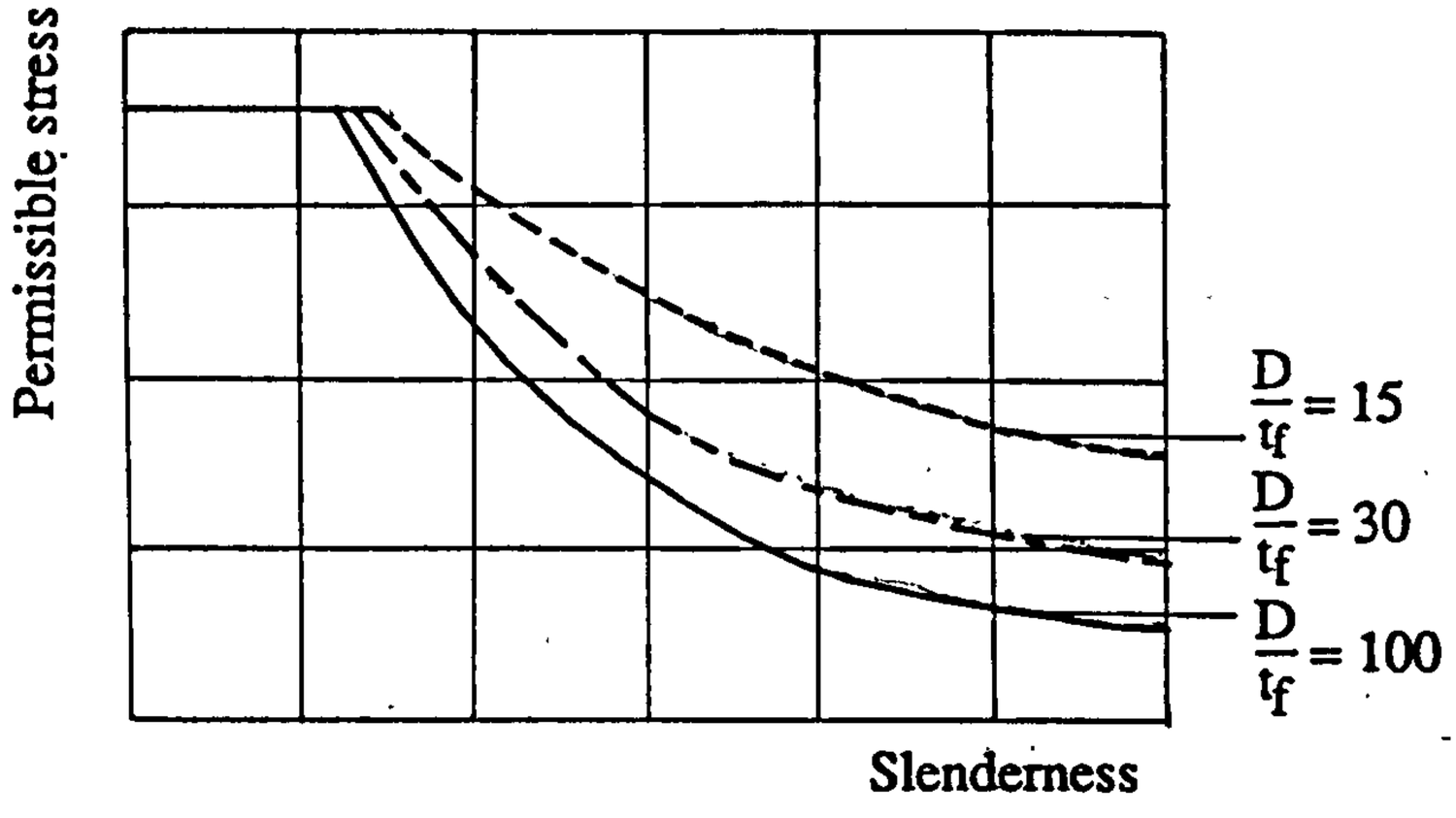

Figure 2.3 Effect of $\frac{D}{t_f}$ ratio on bending stress

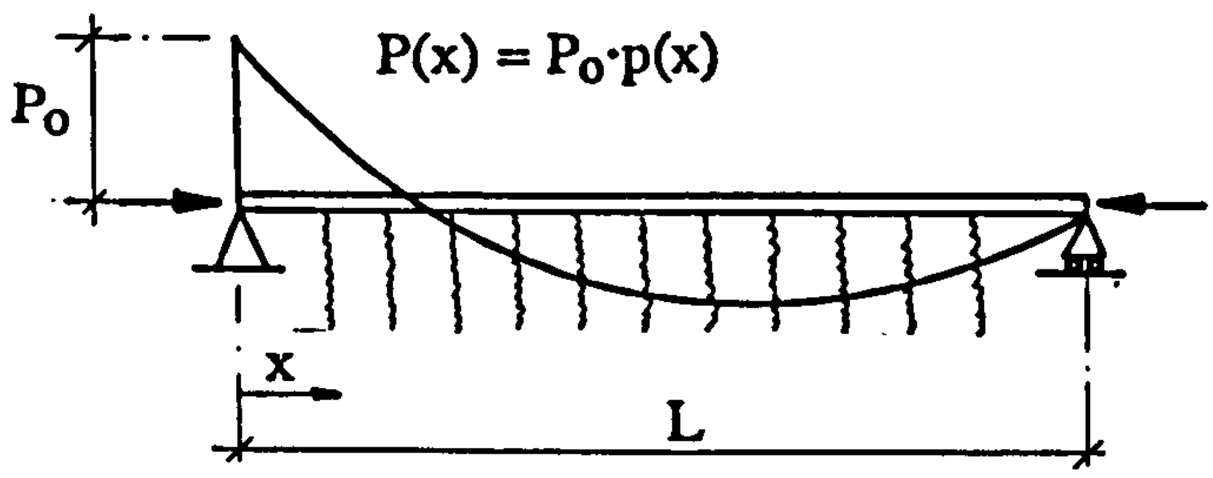

Figure 2.4 Strut on elastic foundation

CHAPTER 3

EXPERIMENTAL WORK AND RESULTS

3.1 INTRODUCTION

Three steel model U-frame bridges were loaded to collapse with a view to validating of the finite element results. The first of these was a one-tenth scale model, designed by Travers Morgan[48] and manufactured by the Welding Institute[49]. Discrete U-frame restraint was provided to the compression flange and uniform bending moment was applied by means of cantilever extensions to the model. This test will be referred as the WI test in the following sections.

To supplement the data from the WI test and to verify the effectiveness of finite element analysis in dealing with other forms of loading and support, two smaller models were subsequently tested at Leeds. The first of these consisted of composite U-frame deck and main girders under uniform bending moment, while the second was of discrete U-frame form and with triangular bending moment applied. The tests were designed and constructed at Leeds University and are named as Leeds Test 1 and Leeds Test 2 respectively. Because of the difficulty of constructing small scale composite concrete models, the latter test model employed an equivalent composite steel deck.

3.2 WELDING INSTITUTE TEST

3.2.1 Geometry and Material

The test piece was a one-tenth scale model of a 40m span steel plate girder bridge. The overall geometry, member sizes and loading arrangement of the model is shown in Figures 3.1 and 3.2.

Basically, it consisted of two parallel plate girders simply supported over a span of 3.96m with transverse web stiffeners on the inside faces at U-frame positions. Cross members connecting with the tension flanges, were positioned at each web stiffeners to form discrete U-frames. Twisting and lateral movements of the girders at the supports were limited by plate diaphragms directly over the latter.

Cantilevers of 0.8m were provided to generate a constant hogging bending moment over the span without affecting the large deflection of the flanges in compression. Cross-bracings were used to prevent any instability in the cantilever loading arms. Two very stiff steel box beams, together with two bearing stiffeners were welded to the ends of the both arms.

The dimensions of the components were chosen to ensure that local buckling was eliminated. Flanges, webs and stiffeners were made from two 4.0mm thick grade 50A steel sheets (to BS4360). Originally, the cross members were to be 30x15mm. However, for a clear manifestation of the final buckling mode, a more sensitive model, with a more flexible U-frame bracing, was adopted. The cross members were chosen to be 15x15mm. Typical details were shown in Figure 3.3.

3.2.2 Manufacture

Due to the lack of availability of long steel sheets for the 3.96m span, full penetration butt welds were used to join shorter strips in the webs and flanges, to make up the required length.

The flanges, web plates and web stiffeners of each girder were assembled and lightly tacked together using TIG weld. Then cross members, diaphragms and loading beams were placed in position and finally, the model was fully welded and loading arms cross-braced. Greater detail of the manufacture of the model is described in the WI test report[49].

Initial lateral imperfection was measured after installation in the test rig and just before loading and is shown in Figure 3.4. The flexibility of the U-frame was measured approximately as follows. A pair of equal but opposite forces was applied laterally to the compression flanges at mid-span by means of a spring balance, the resulting displacement was measured as 0.52mm under 27.0lb lateral force. Tensile tests[49] were carried out on each steel sheet and the results are shown in Figure 3.5.

3.2.3 Loading Arrangement

The structure was located on small bearing plates, which in turn rested on two steel rollers placed transversely. The flanges were, therefore, allowed to rotate in plan as well as in elevation. It is assumed that horizontal restraints on the model were negligible.

Loads were applied by two 100kN nominal capacity hydraulic jacks to steel balls at the centre of loading beams, to ensure that the distribution of load to the two girders was equal. The jacks were identical and were connected to a common hydraulic pressure line. The jacking forces applied were measured by a Novatech load cell instrumented

with digital read-out. Four dial gauges were used to measure the lateral and vertical displacements of both compression flanges at mid-span.

3.2.4 Test Sequence

The model was initially loaded to 35kN at each jack in 5kN increments and unloaded. This was done to relax the residual welding stresses and also to check the entire system. The model was then loaded in increments of 10kN up to 40kN followed by increments of 5kN to 65kN. Load increment was reduced to 2.5kN to the collapse load. This was followed by unloading to zero. Lateral and vertical deflections of the compression flange at mid-span were measured and recorded at each loading increment and the residual deformed shape after complete unloading was recorded as well.

During the second loading cycle, one of the dial gauges for measuring lateral movement of the compression flange was dislodged from the edge of the flange due to excessive vertical displacement of the latter. This occurred in spite of an articulated link between the dial gauge and flange tip.

3.2.5 Results

The structure was loaded as described until failure. The maximum load recorded at each end of the girders was 72.5kN, and therefore, its ultimate bending moment capacity was 29.0kNm.

The load-deflection curves are showed in Figure 3.6. The equivalent bending moment generated in the span was plotted against horizontal (lateral) and vertical displacements of the compression flange at mid-span.

In general, the vertical deflection of both girders was virtually identical until maximum load had almost been reached. However, the lateral deflection was somewhat different. The directions of the lateral displacements of the two girders were mutually opposite throughout the loading process; their magnitudes were only comparable at the initial loading stage.

Development of the three half-wave mode only became obvious after the maximum load had been reached and the load was starting to reduce. In this post-buckling stage, the half-wave adjacent to the LH support (at the position of the 14th U-frame in Figure 3.4) grew in amplitude and length whilst the other half-waves stabilised. This stage was characterised by steady creep. At no time was any sudden snap-through evident. After 30 seconds of continuously decreasing vertical displacement and increasing horizontal displacement, load fall-off was observed at around 55.0kN. The jacks were then gradually released.

There were no strain measurements in the WI test as the main aim of the experiment was to observe the deformation of the girders up to and beyond the instant of buckling. No signs of local buckling were observed in any of the members, nor was there any evidence of weld failure, in spite of high plastic deformation of the bottom flanges and cross members. The first sign of lateral instability of the compression flange (see Figure 3.7) was noticed at the position of the 11th U-frame, though this was not obvious until maximum load had been reached.

The final lateral buckling mode, comprising three unequal half-waves in the compression flanges, is shown after unloading in Figure 3.8. The buckled modes for the girders were mirror images of each other. As illustrated in Figure 3.9, the cross members hogged or sagged in unison with the inward or outward bow of the compression flanges. The permanent deformation of the U-frames was associated with plastic deformation of the compression flanges and the cross-beams whilst the web stiffeners and weld joints appeared to be unstrained.

3.2.6 Discussion

It is obvious that the final deformed shape of both compression flanges did not share any similarity with their initial lack of straightness, which consisted of single inward bowing. It seemed to be logical to assume that buckled shapes would follow the trend of their initial imperfection and half-waves would be formed with the middle one bowing inwardly.

This 'assumption' was obviously proved incorrect from the evidence obtained from the test. The phenomenon might be explained in terms of strain energy.

Other factors which might encourage the resultant deformed shape would be uneven seating at the supports and rigid bracing in the loading arms applying additional constraints to the compression flanges.

Girder A had a larger initial lack of straightness than Girder B, but the magnitudes of the final residual buckled shape were almost the same. This is due to the restraining action of the U-frames. Moreover, there was no dominant failure in one girder preceding the other, despite the difference in magnitude of the initial imperfections. Thus, it was illustrated that the influence of initial imperfections on the ultimate load capacity of girders braced by U-frames is insignificant.

3.3 LEEDS TEST 1

3.3.1 Geometry and Material

The test model was approximately one-third of the size of the WI test. The overall geometry and member details are shown in Figures 3.10 and 3.11.

Compared with the WI test, the essential difference was the deployment of continuous U-frame action from the composite deck. Web stiffeners were not used except at load and support points.

The test piece represented twin plate girders interconnected by a steel plate over a total span of 1.82m, the maximum length to fit in the INSTRON loading machine. However, two load points were arranged 0.25m from the supported ends of the model. This arrangement induced a uniform sagging bending moment over the inner 1.32m of the whole span. It was assumed that the distance between the load and support points was sufficiently long for the behaviour of the uniform bending moment region not to be influenced by conditions in the loading arms.

To simplify the manufacture of the test piece, separated steel tension flanges were omitted. A continuous steel plate 1.5mm thick provided U-frame restraint to the compression flanges and represented concrete deck. The compression flanges were, hence, unbraced along the section under uniform bending moment.

Two plate diaphragms were connected to the twin girders at the load points to prevent cross-sectional distortion. Additional partial restraint against rotation in plan of the compression flange at these points was imposed by the proximity of the end support cross-heads which were made of two stiff SHS cross-beams. Detailed dimensions of cross-sections and arrangement of load and support points are shown in Figure 3.12.

The initial lack of lateral straightness in one of the compression flanges was measured before the instalment in the test rig and is shown in Figure 3.19.

To determine the properties of the material employed, three simple tensile specimens were cut from the steel plates used and each specimen was machined to a nominal waisted width of 25mm. Two electrical strain gauges (in fact, a strain gauge rosette consisting of two strain gauges) perpendicular to each other were attached to mid-section of each specimen. These tests were carried out in a 200kN Denison test machine and strains induced were measured by Peekle strain indicator. The load-displacement curves are shown in Figure 3.13(a). Young's modulus was taken as the slope of initial linear segment of stress-strain curve. The measurements of

longitudinal and transverse strains were made to obtain Poisson's ratio of the material (see Figure 3.13(b)).

3.3.2 Manufacture

Components were tacked and clamped firmly to prevent distortion during a balanced welding process. Also, to minimize the effects of distortion from welding, only intermittent TIG welds were adopted throughout because of the thinness of the plates.

3.3.3 Loading arrangement

An INSTRON 8033 servo-hydraulic testing machine was employed. Upper stationary and lower moving horizontal steel beams fixed to the loading faces of the machine were used to support and load the model respectively, ie, the model was loaded upside down. As illustrated in Figure 3.12, two solid steel bars were placed in line with the plate diaphragms and support was provided to the centre of the bars through two ball bearings. Therefore, rotation of the compression flange was permitted in elevation and initial adjustment of bearing in the transverse direction was possible. The cross-beams at the ends of the model were loaded on knife-edge blocks to minimize the effect of rotational restraint on the model.

Few lateral movements between the knife-edge load points and the supports were assumed because the loading arms were considered as rigid in plan under the combined effect of diaphragm plate, deck and SHS cross-beam. Therefore, ball bearing supports and knife-edge blocks were assumed on the longitudinal centre line of the model. The load was, hence, assumed to be applied to the knife-edges and transferred to the two girders.

3.3.4 Instrumentation

A load cell measured the total load applied to the rig. Nine electrical resistance strain (ERS) gauges were placed on the outer faces of the webs and deck plate at a cross-section close to a quarter-span position to monitor the bending strain distribution. The gauge positions are defined in Figures 3.14 and 3.15. To detect the development of the buckled shape and to establish the buckling moment precisely, lateral displacements of both compression flanges were detected by six LVDT of 25mm travel gauges which were placed at one-quarter, centre and three-quarter span positions. The LVDT gauges were mounted to the lower loading beam and, therefore, the measured horizontal movements were relative to the outer knife-edge load points which had few movements relative to the supports as explained before. Two dial gauges attached to the upper and lower steel beam as shown in Figure 3.16 were used to measure average vertical displacement of the model at mid-span and RH load point respectively. One data logger with 100 channels

was used to scan and record all strain and LVDT measurements at each loading increment. Vertical movement of the loading beam was recorded and plotted automatically against loading by the INSTRON recording system.

3.3.5 Test Sequence

A loading rate of 1.333 kN/min. was used throughout the test. To dampen the effects of residual stress and ensure that the model rested on the supports properly, as well as to check the functioning of the instruments and the set up of the loading system, the model was initially loaded to 8kN and unloaded. A second load cycle was continued up to failure and then unloaded back to zero.

3.3.6 Results

Although an increase in the rate of change of lateral deflection of the compression flange, which signified the occurrence of buckling, was observed at a total applied load of approximately 9.5kN, the ultimate load capacity reached at the end of the test was 9.9kN, which indicated a uniform bending moment of 618.75Nm over the central span.

The actual vertical deflection at mid-span was measured as the relative movement of the girders (Girder A) to the stationary supporting beam above. As illustrated in Figure 3.16, the reading from a dial gauge at point B, which was the distance travelled by the lower loading platten (the upper platten was locked) and automatically recorded by the INSTRON machine, in fact represented the deflection of the RH loading point relative to the RH support. The load-deflection curves are plotted and compared with the estimated vertical deflections in Figure 3.17.

The lateral deflections of the compression flange at the six LVDT positions are illustrated in Figure 3.18. From each plot, it is clear that lateral displacements are not linearly related to loading during the first loading cycle. This is likely to have been caused by weld shrinkage stresses and uneven seating at bearings. The second loading run was accompanied by linear displacements up to the previous loading stage. Further loading gave significant increases in the rate of change of lateral displacements until failure. The direction of the displacements in the compression flanges were again, as in the WI test, mutually opposite.

The lateral deformation of the compression flanges followed by rapid development of the buckling mode was visualized. Because of this rapid development, there was no time to record the fast on-going buckling shape.

From the onset of buckling, lateral displacements of the flanges conformed to dual half-waves rather than their initial shape. The skew of the half-waves was reversed for

the two girders, ie, at a given cross-section, the two compression flanges moved either towards or away from each other as a result of the cross-coupling action of the U-frames. The lateral deflection at quarter-span positions are shown at various stages of loading in Figure 3.19 together with the initial lateral imperfection of Girder A.

The residual shapes of the unloaded girders are shown in Figures 3.20 and 3.21. At post-buckling stage, there was large deformation adjacent to mid-span and hence permanent yielding in the compression flanges. As a consequence of local weld failure, there was also major loss of bracing effect from the U-frames at this stage.

3.3.7 Discussion

The response of the test model was essentially linear up to about 60% of the failure load. Beyond this point, the bending stiffness of the model declined gradually until the sudden occurrence of buckling. The loss of stiffness was due to premature yielding as a consequence of residual stress introduced during fabrication of the specimen. This was borne out by the extended linear response during the second loading run.

The final buckling mode bore no relation to the initial unloaded shape of the compression flange.

3.4 LEEDS TEST 2

3.4.1 General

To explore the beneficial effect of moment gradient on the stability of a U-frame structure, I-section girders of identical dimensions to the Leeds Test 1 specimen, were tested under a triangular bending moment distribution.

The general arrangement and detailed design dimensions are shown in Figures 3.22 and 3.23. Instead of using a plate deck, discrete U-frames composed of 4.75x4.75mm cross members and 7x1mm inner vertical web stiffeners were placed at 187.5mm. To impose a triangular moment distribution, the LH point, in Figure 3.10, was moved to coincide with the LH support position. Thus the span between loading points became 1.5m, compared with 1.32m for Leeds Test 1. Plate diaphragms were provided to interconnect both girders and restrain twisting and lateral movement at the loading positions.

The material used was the same as in the previous test and a similar welding procedure was adopted during the manufacture of the model.

The initial lateral lack of straightness of both compression flanges was measured and is shown in Figure 3.19. The vertical convex curvature of the girders caused by weld shrinkage amounted to an initial bow of 14mm near mid-span.

3.4.2 Loading Arrangement

The loading rig for Leeds Test 1 was also used for this test. The upper and lower steel beams were used to support and load the model respectively. The applied load was transferred equally to the girders, as sketched in Figure 3.24, through two balls and seats at the LH load points and a knife-edge block at RH side.

The upper supporting platten resisted the load applied to the upper supporting beam (resting freely on two transverse steel bar placed on greased bearing pads centred on each girder) through a ball and seat at mid-point of another transverse bar. From Figure 3.25, it can be seen that applied load was not shared equally between the LH and RH supports.

3.4.3 Instrumentation

In order to detect lateral horizontal movement of the top (compression) flanges under the central moment gradient region, six LVDT gauges were also used at the positions shown in Figure 3.26, along the span between the diaphragms. One dial gauge was employed to monitor mean horizontal movement of the girder A at the RH load point and another two for the vertical displacements of both girders at the rightmost LVDT gauge position. Because of the movement of both the loading and supporting beams, as shown in Figure 3.25, the dial gauge reading is not the absolute value of vertical displacement at the gauge position.

Strain gauges were not used on the test model because of the symmetry of cross-section of both girders.

3.4.4 Test Sequence

A similar procedure to that for Test 1 was carried out except that the structure was loaded and unloaded twice before starting the final loading run. The first loading cycle started with an initial bedding down load of 2kN followed by increments of 1kN up to 5kN and then unloaded to 0.5kN. The second loading cycle was loaded straight up to 4kN and then, by increments of 1kN, up to 8kN. This cycle was completed with the unloading down to 0.5kN. In the final loading run, the model was loaded from 0.5kN to 2kN and then to 8kN by increments of 2kN. The increment rate was then reduced to 1kN and 0.5kN respectively in the next two loading stages and then to 0.1kN until failure at 10.1kN.

3.4.5 Results

An ultimate total load of 10.1kN was attained at the end of the final loading run and, thus, the ultimate bending moment capacity of the structure was 631.25Nm.

The vertical deflections of Girder A and B at the rightmost LVDT position in the final loading cycle are plotted in Figure 3.27 together with the theoretically estimated vertical displacement at that position, assuming equally shared load on load points. The horizontal dial gauge at the RH load points showed that there was little lateral movement of the girders at that position.

Variation of lateral displacement with load at the six LVDT gauge positions is presented in Figure 3.28 and the change of lateral deflection along the compression flange was shown in Figure 3.29. All the curves exhibit a distinct change of stiffness at a total applied load of 2kN. Above this threshold, there was a significant increase in the stiffness of the structure. Towards the end of the final loading cycle, an obvious increase in the lateral displacement (see Figure 3.28) indicated the commencement of buckling as depicted in Figure 3.30. Changes in directions of the displacement (see Figure 3.29), in both girders, took place at gauge position 1 in Figure 3.26, reversing the lateral deflection at that position and altering the developing buckling mode.

The convex load-displacement curves obtained in Test 1 for lateral deflection of the compression flange were not repeated in Test 2, neither was the opposing movement of the two compression flanges due to cross coupling of the U-frames. The direction of displacement of the compression flanges at all the gauge positions was consistently the same even after failure.

Instead of forming a characteristic buckling mode of a symmetrical buckled shape about the longitudinal central line of the model, the buckled modes in the compression flanges were almost identical from the onset of the buckling until failure as shown in Figures 3.29, 3.31 and 3.32. Consequently, the residual buckled mode was of two flanges deformed in the same direction as pictured in Figure 3.33.

3.4.6 Discussion

Vertical deflection of Girder A was always greater than that of Girder B, thus the applied load transferred to the two girders might not be the same. In retrospect, monitoring of strain in the girder flanges could have provided some confirmation on the load-sharing between the two girders.

Little change in the lateral gauge reading proved that the outer supports and load point remained virtually in a straight line, in plan, up to collapse. This was achieved by

locking the loading machine ball joint against rotation about an axis parallel to the longitudinal beam axis during the test. The intent was to force a purely vertical displacement on the ball bearing at the load point.

The sudden increase in the slope of the load-deflection curves in Figure 3.27 (in the second and final loading runs) could be explained in terms of a change in support conditions. A second possibility was that the upper supporting beam was restrained at the ball joint instead of resting freely on the bridge model at the two load points. If the ball joint had been mistakenly locked about the horizontal transverse axis as well as the longitudinal axis, a stiffening effect similar to that observed in the LVDT readings would have occurred. The loading beams would tend to remain parallel and a greater proportion of the load would pass through the stiffer LH load path. Eventually, the bending moment caused by the reaction from the load point would overcome the locking resistance of the ball joint and change the balance of force between the two load points. The machine operator is, however, firmly of the opinion that the ball joint was not locked against rotation about the transverse horizontal axis.

The above possibilities do not, in any case, explained the sudden change of buckling mode. Perhaps the only interpretation of the situation could be attributed to the exchange (releasing or restoring) of strain energy when the structure deformed. Besides, premature yielding as a result of residual welding stress in the compression flange would have a radical effect on the deformation of compression flange and, therefore, promote a change in the buckling mode.

The residual buckled shape shown in Figure 3.33, surprisingly, demonstrated a breakdown in the cross-coupling effect of the U-frames, even when the initial lateral deviation from straightness of the two compression flanges were symmetrically disposed.

3.5 CONCLUSION

Three laboratory tests of U-frame braced girders were described and their results are postulated in this chapter.

Much attention was paid to the behaviour of the girders, particularly, the compression flanges. In both the Welding Institute Test and Leeds Test 1, sudden occurrences of buckling were visualised together with the coupling effect of U-frames which were satisfactorily demonstrated. It was also found that initial lack of lateral straightness in compression flanges did not affect the final buckled mode and load capacity of the girders.

Unfortunately, Leeds Test 2 did not proceed well. This was possibly caused by the misuse of the locking system of the loading machine which induced different reactions at supports than originally expected, and hence, a different bending moment distribution over the main span. Moreover, the load-deflection curves consistently showed that there was an increase in the stiffness of the model at a total load of 2kN. The U-frame restraining effect on compression flange also failed. As a whole, results from these three tests will provide an essential data-base for the finite element modelling of these models and verify the suitability of ABAQUS finite element package in modelling of lateral buckling behaviour of U-frame braced I-section girders bridges.

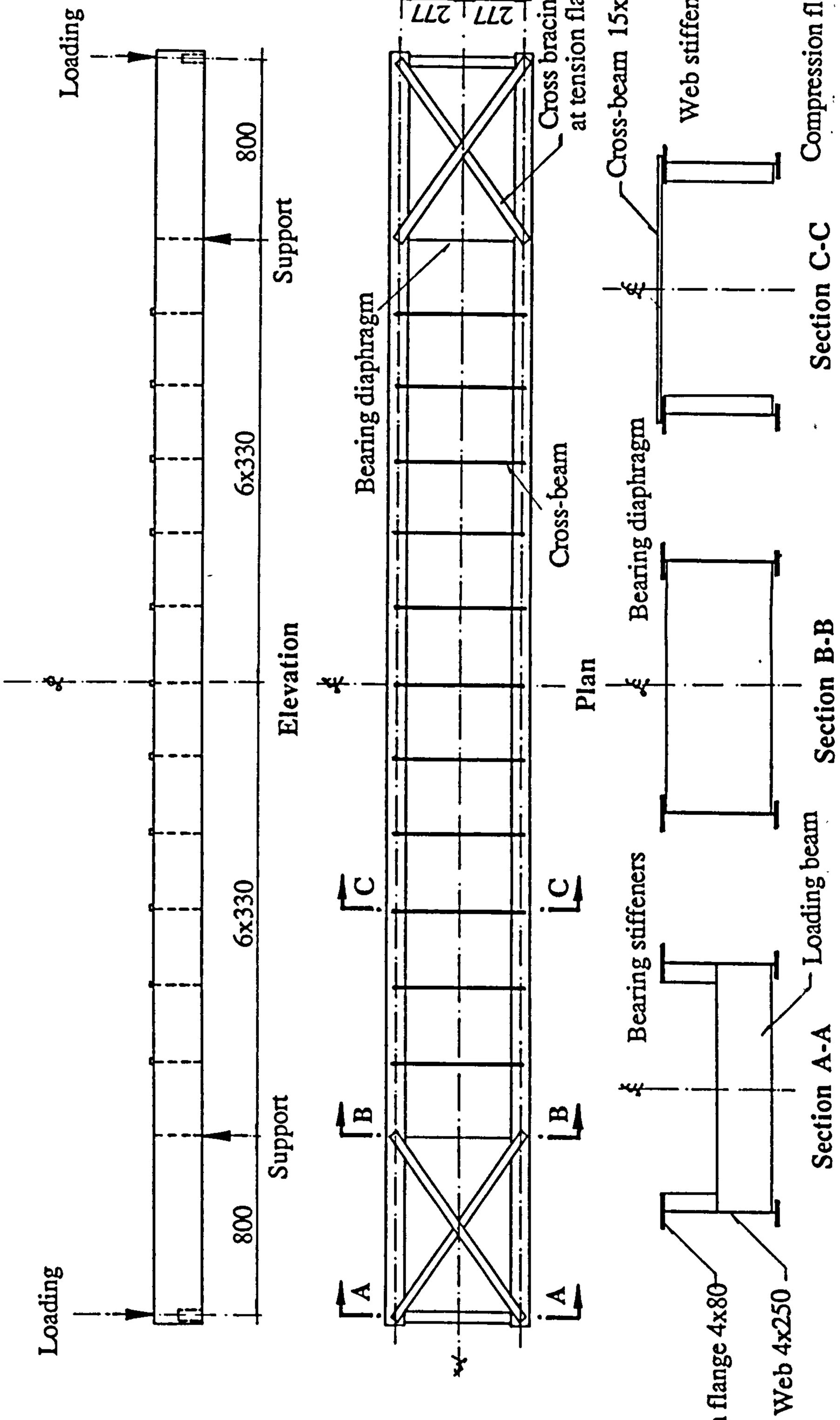

Figure 3.1 General arrangement of the Welding Institute test

Figure 3.2 Loading arrangement and instrumentation for the Welding Institute test

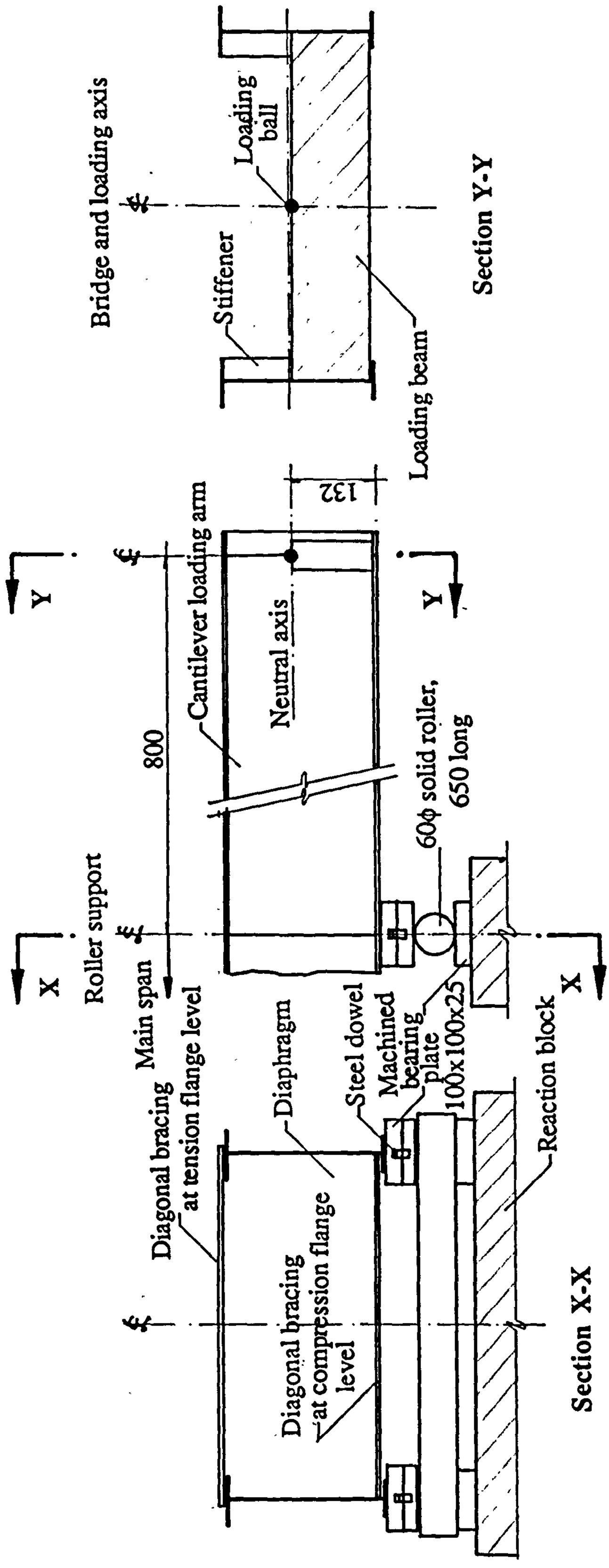

Figure 3.3 Detailof the Welding Institute test

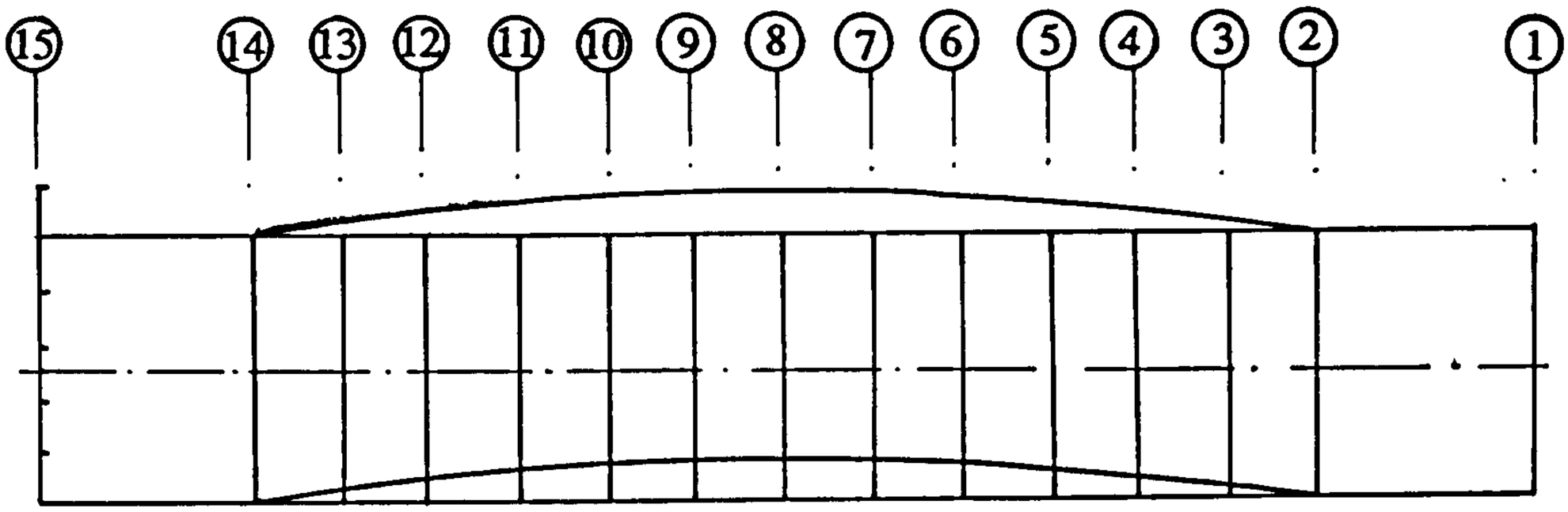

Figure 3.4 Initial lateral imperfection of flanges for the Welding Institute test

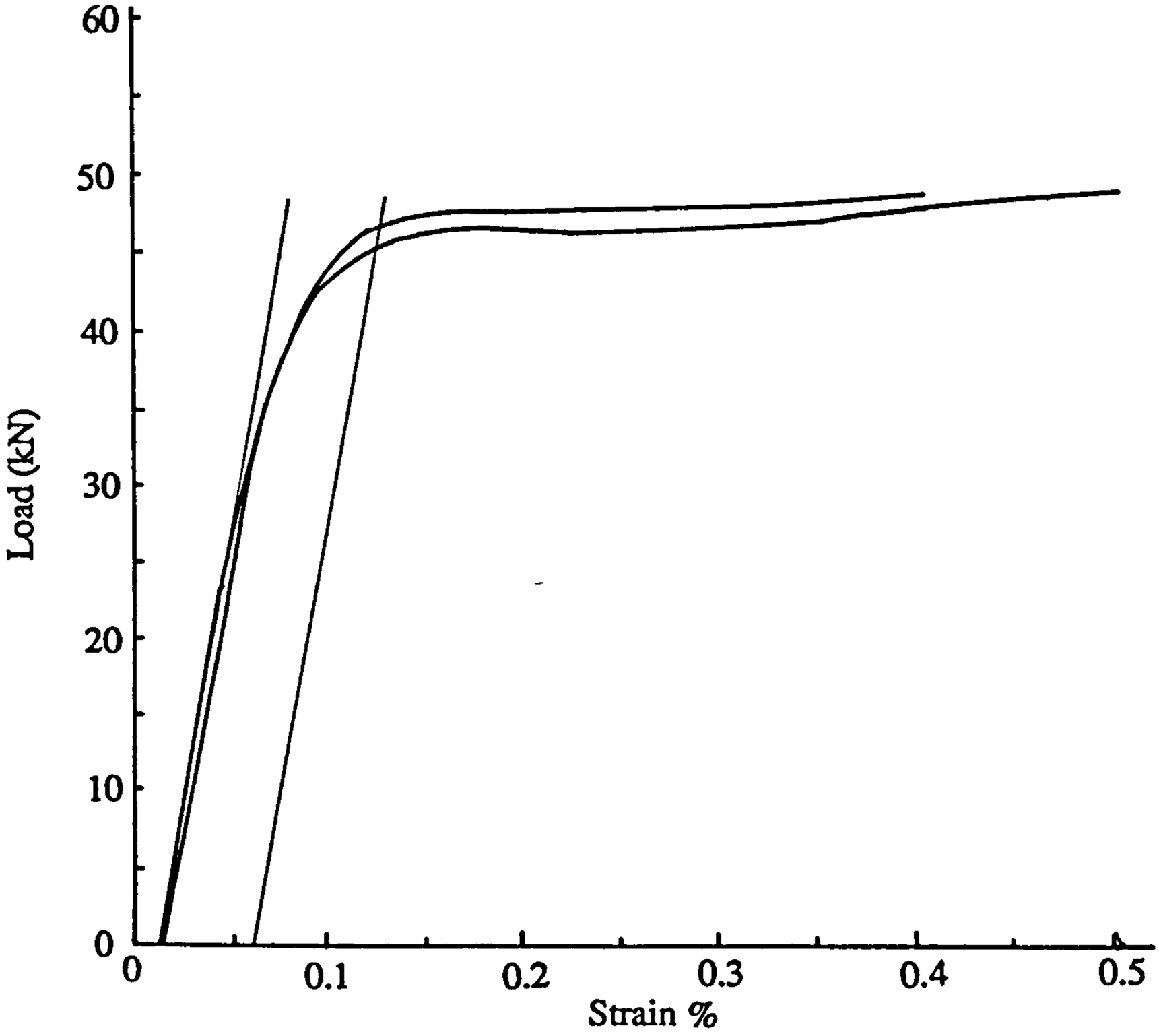

Figure 3.5 Tensile test results for material used in the Welding Institute test

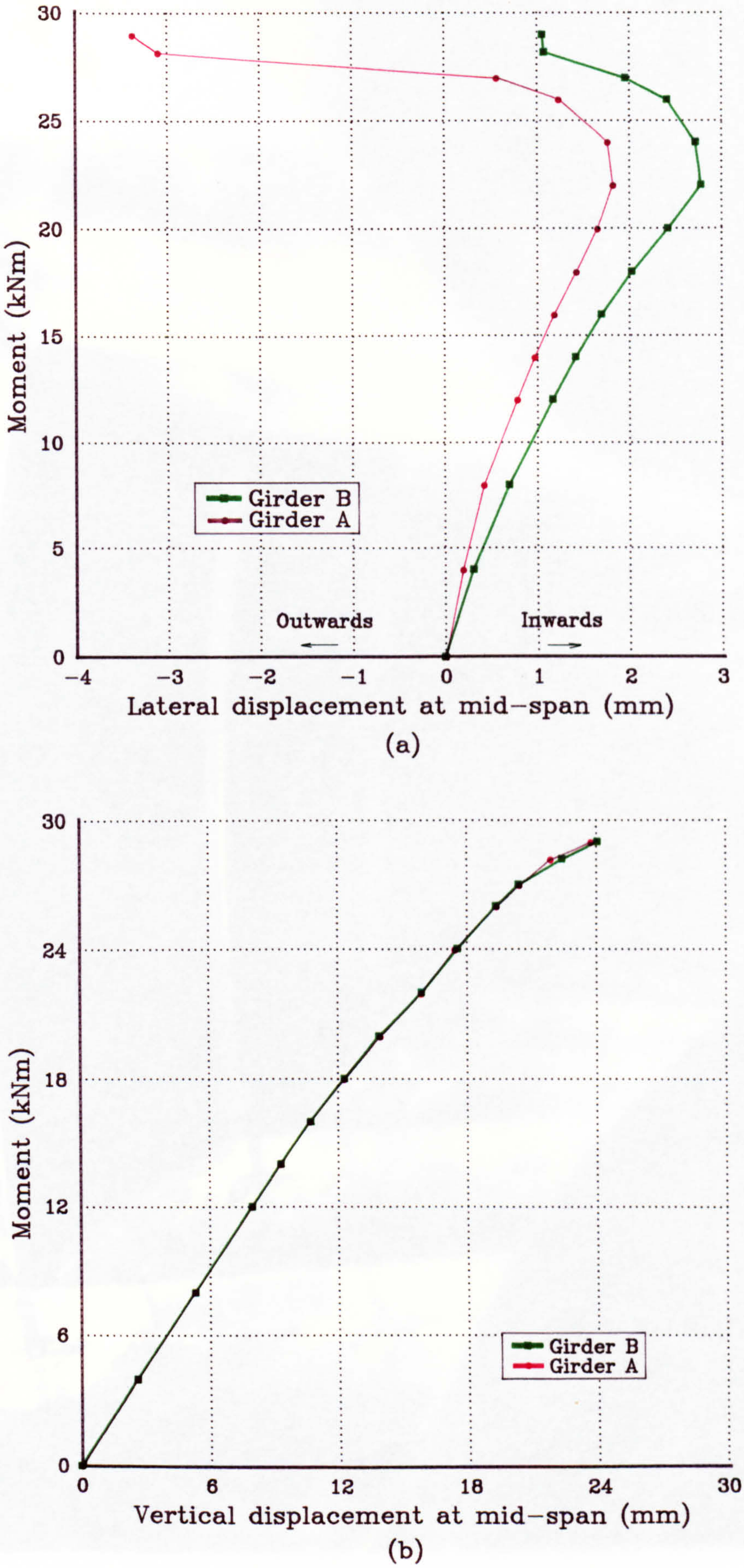

Figure 3.6 Load v. displacement relationship for the Welding Institute test

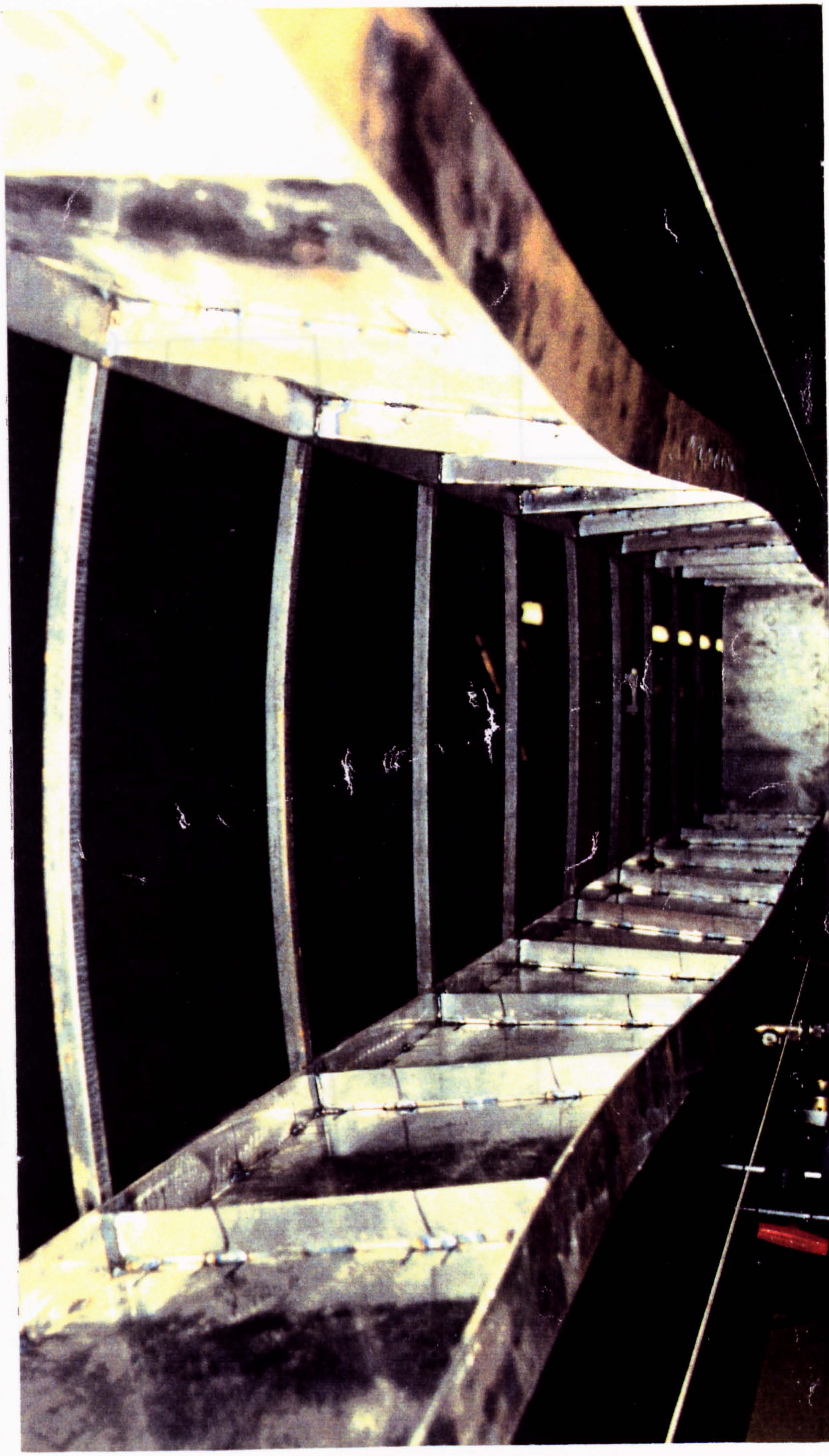

Figure 3.7 Onset of buckling for the Welding Institute test

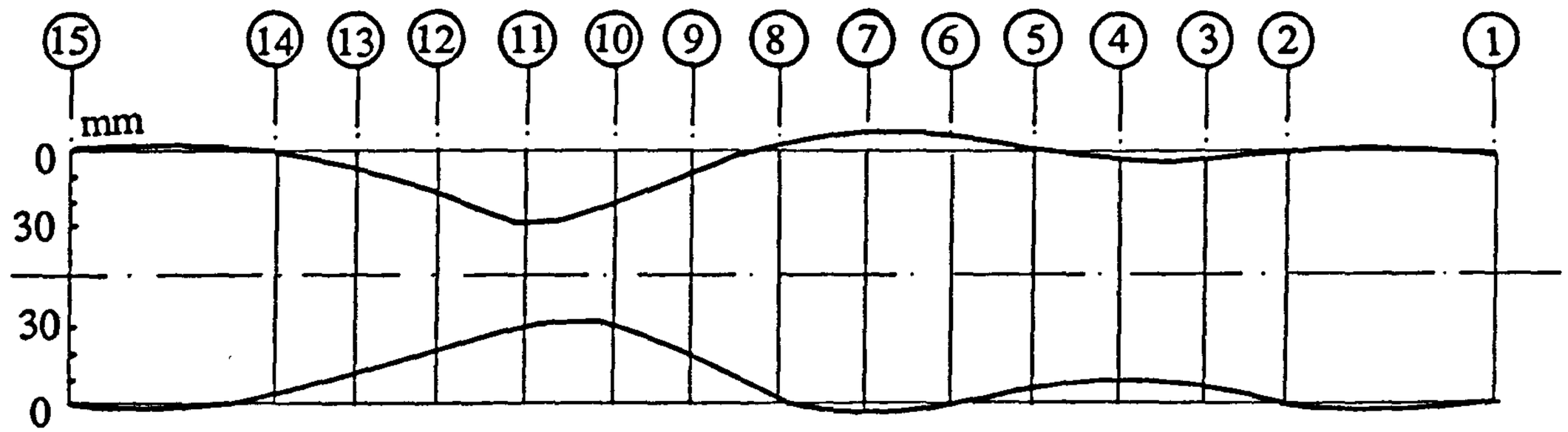

Figure 3.8 Residual buckled shape of the Welding Institute test

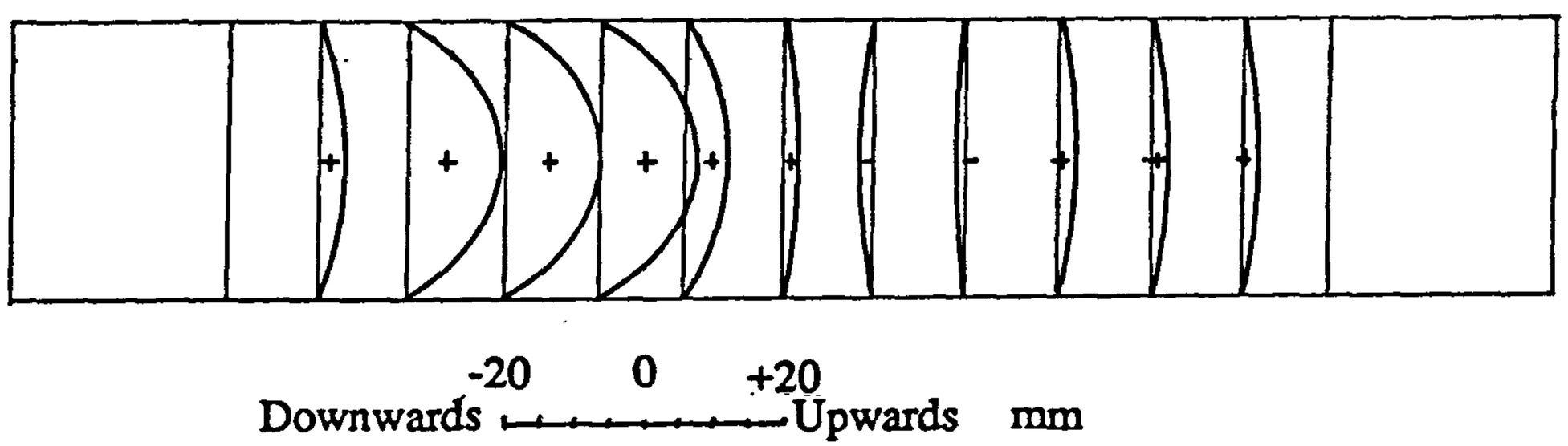

Figure 3.9 Deformation of cross-beams of the Welding Institute test

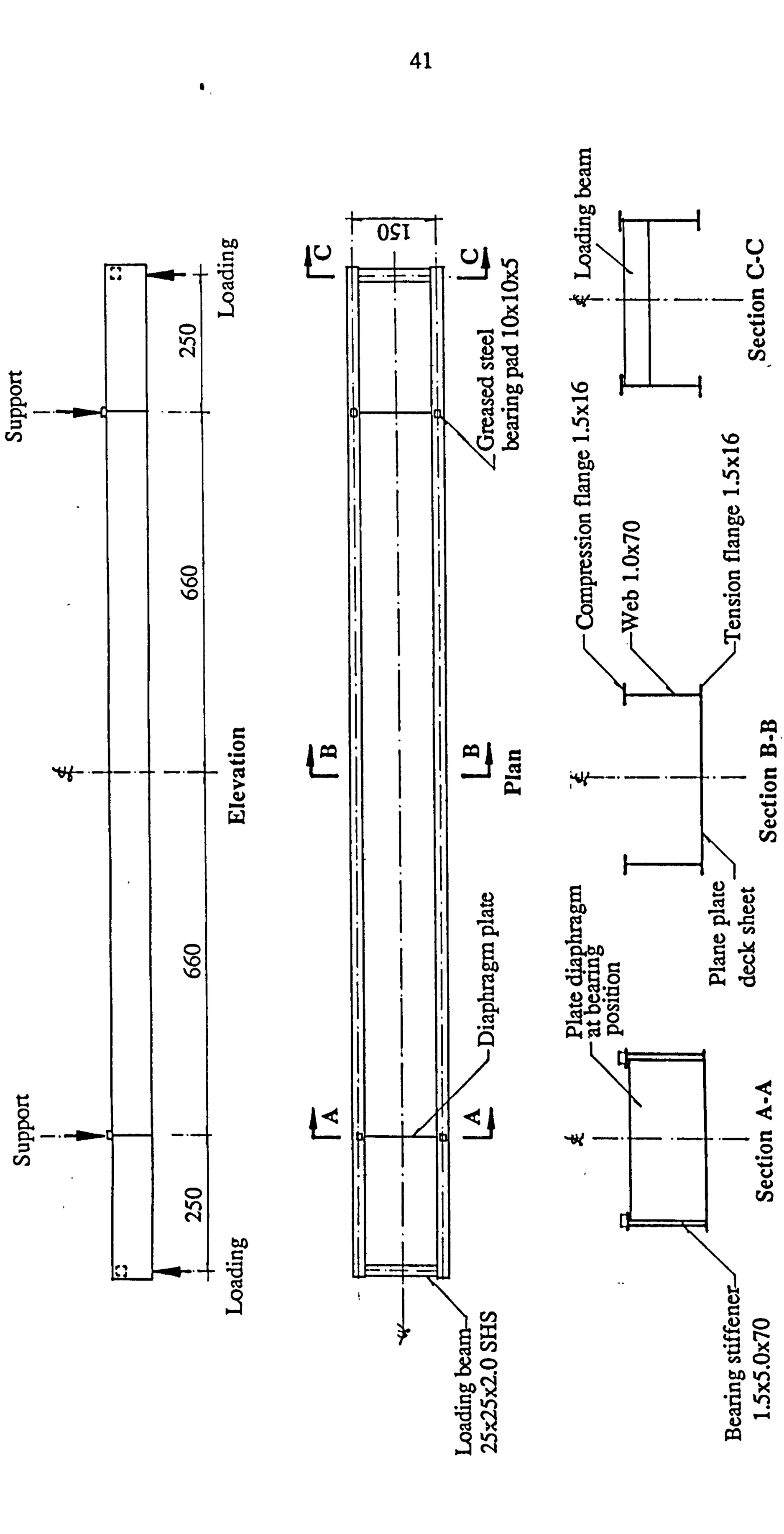

Figure 3.10 General arrangement of Leeds Test 1 Unit : mm

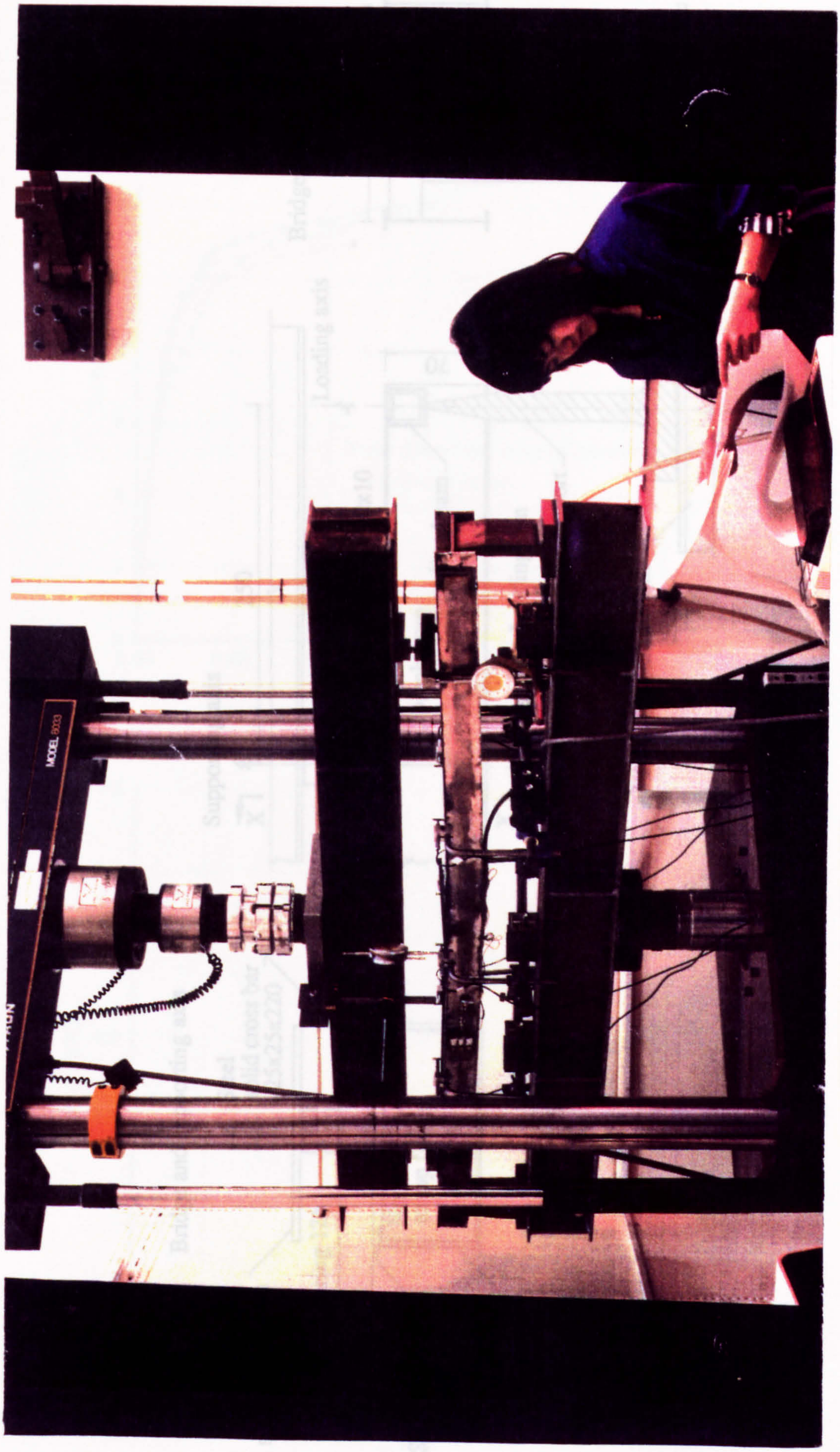

Figure 3.11 Loading arrangement and instrumentation for Leeds Test 1

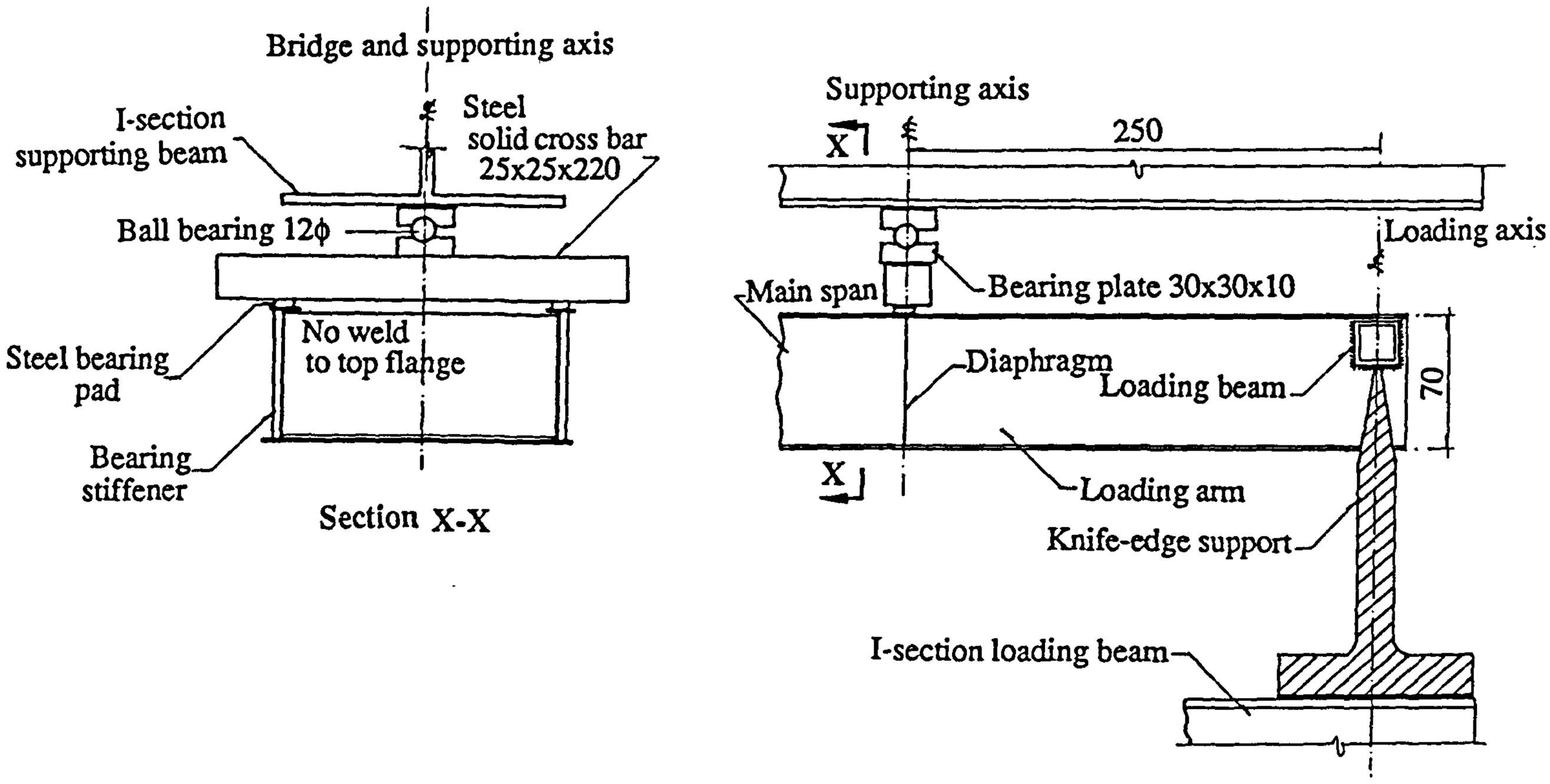

Figure 3.12 Details of Leeds Test 1

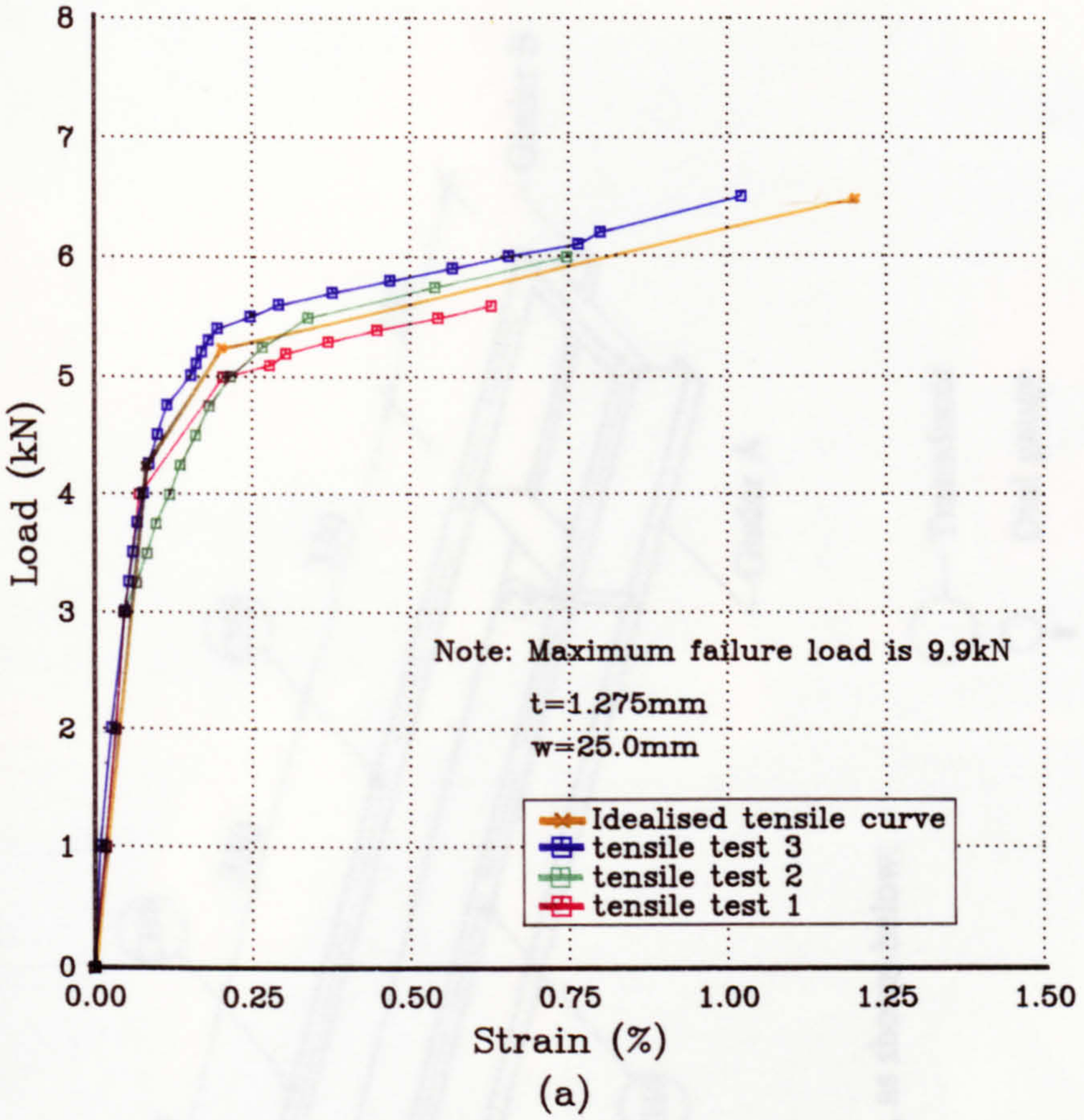

Figure 3.13 Tensile test results for material used in the Leeds tests

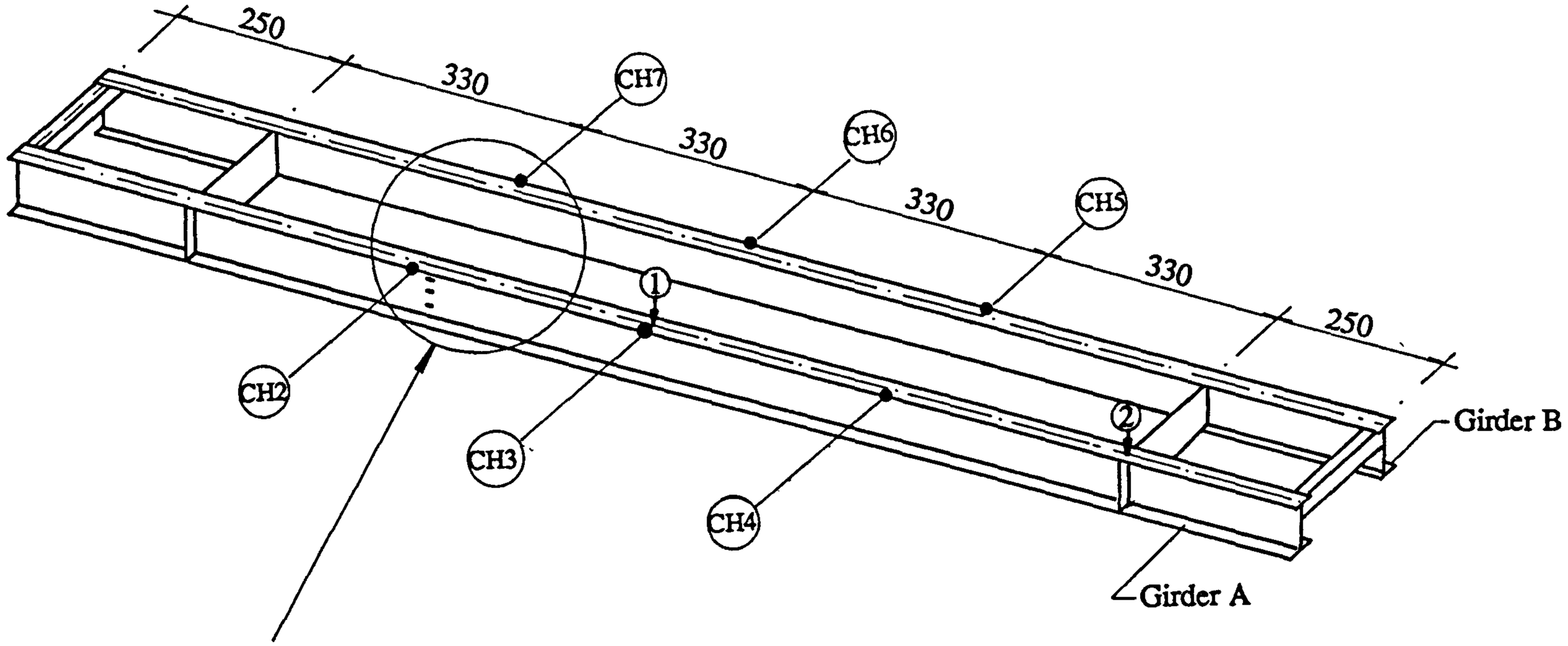

Strain gauges were only provided at this section, as shown below:

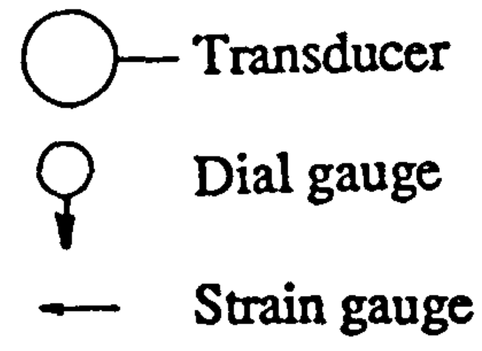

Figure 3.14 Transducers, dial gauges and strain gauges position for Leeds Test 1

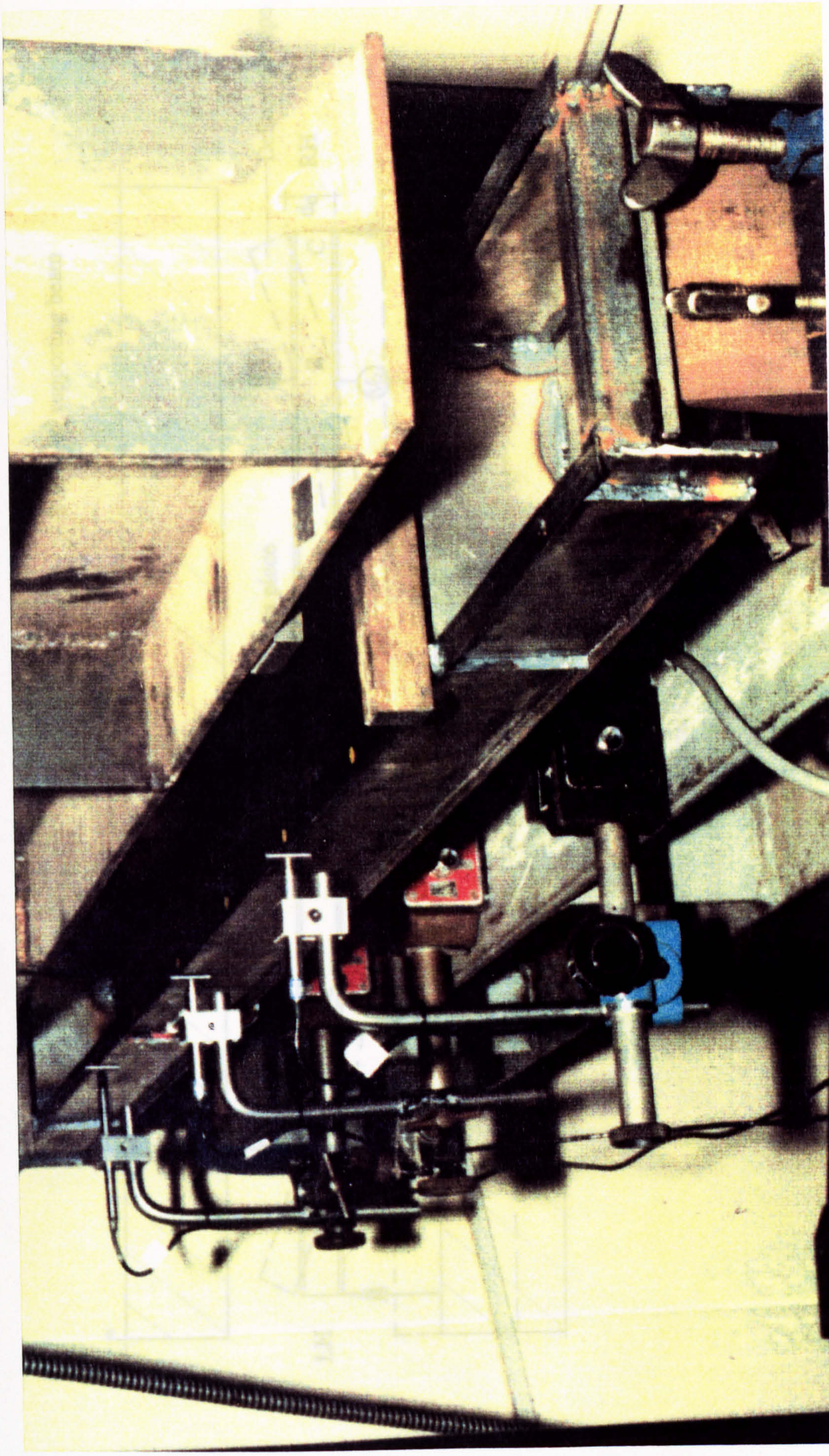

Figure 3.15 LVDT positions for Leeds Test 1

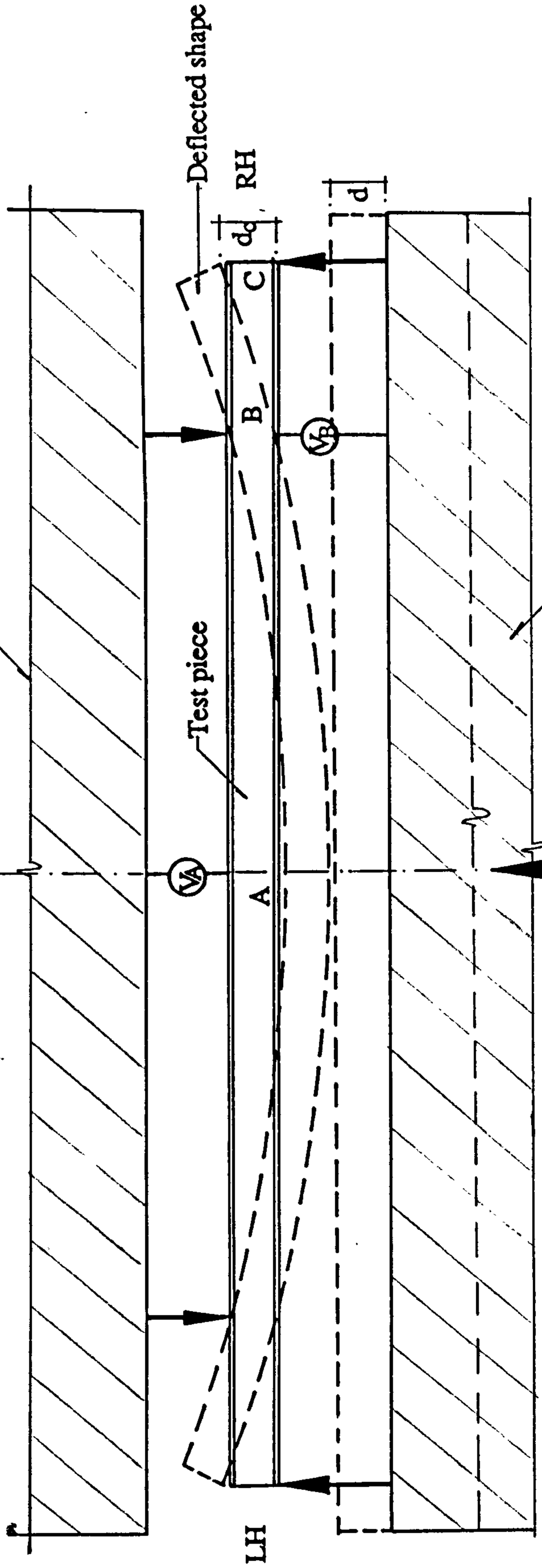

Dial gauge reading at A: vertical displacement at mid-span
Dial gauge reading at B: movement of loading beam d
Assuming loading beam is rigid, then $d_c = d$
where d_c = deflection at the loading point C (relative to B)

Figure 3.16 Measurement of vertical deflection for Leeds Test 1 Not drawn to scale

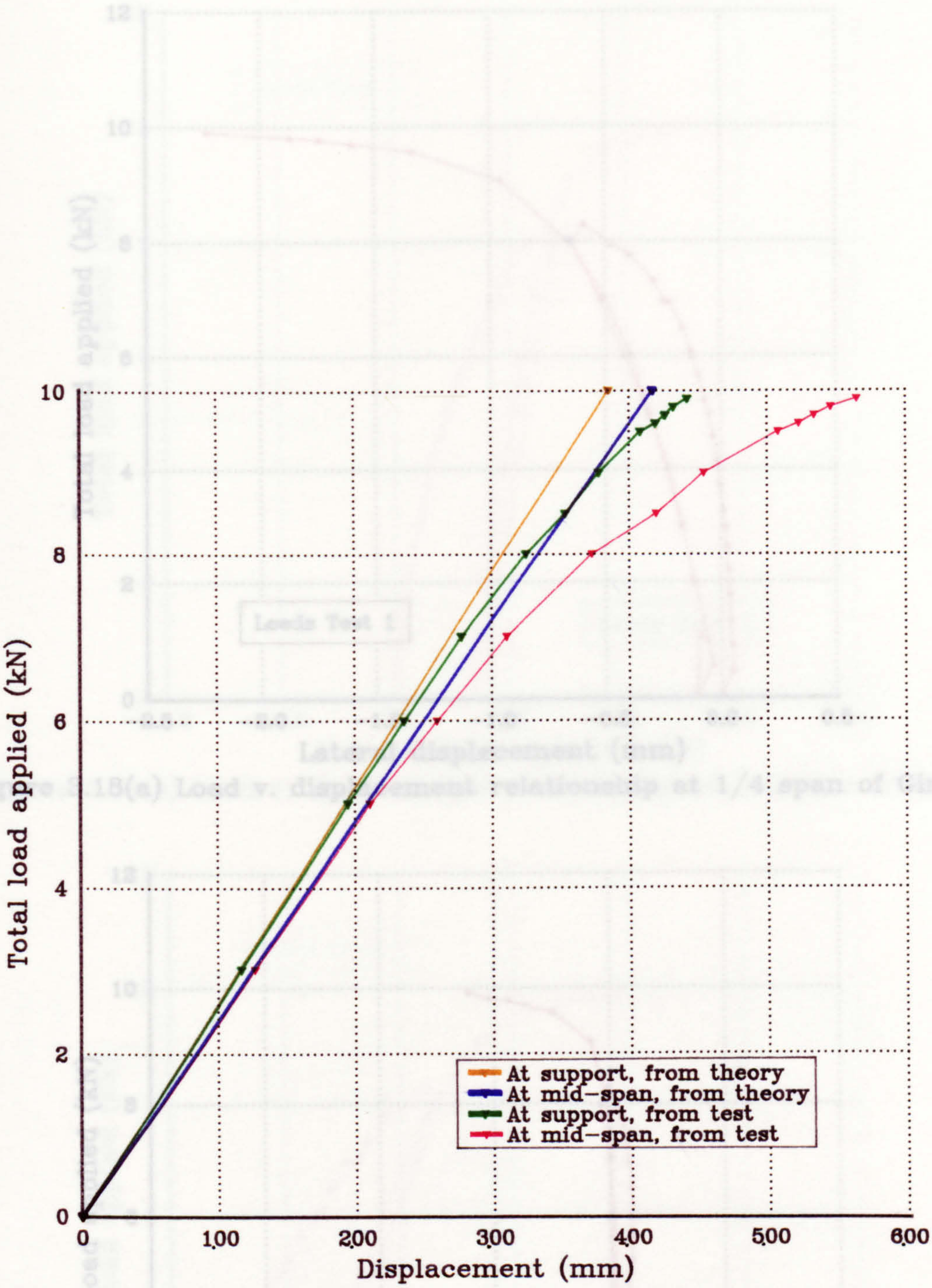

Figure 3.17 Load v. vertical displacement relationship for Leeds Test 1

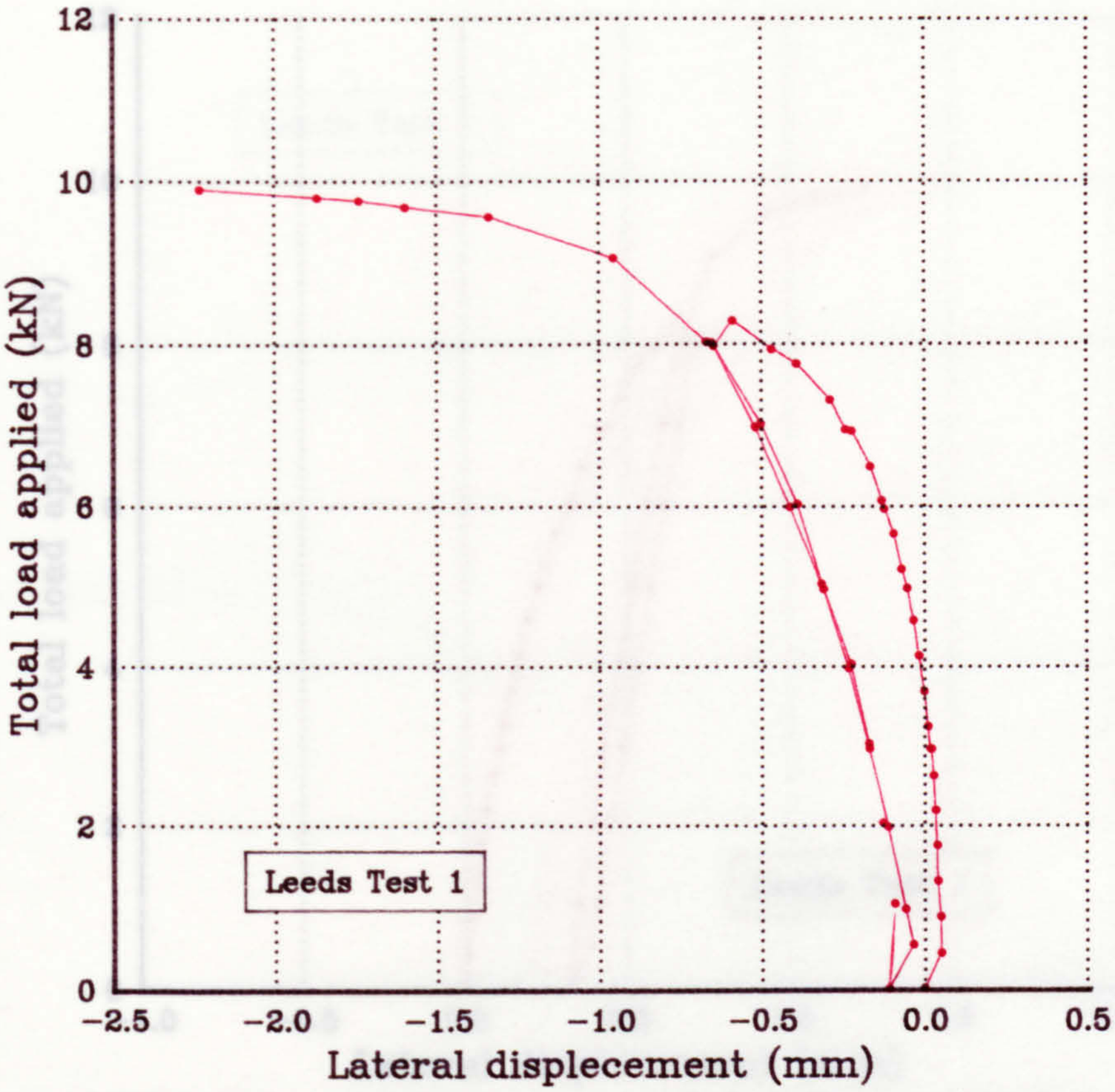

Figure 3.18(a) Load v. displacement relationship at 1/4 span of Girder A

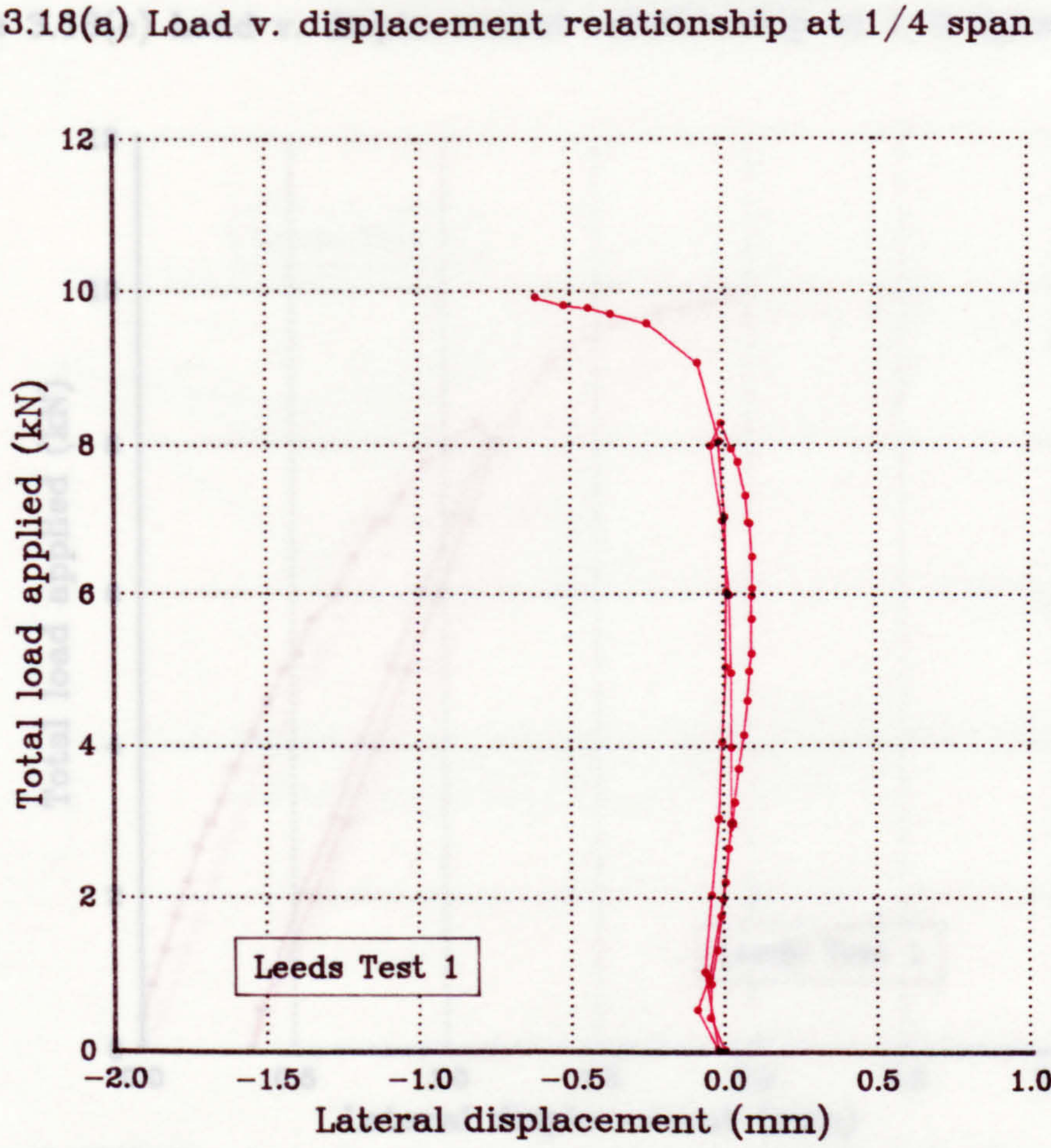

Figure 3.18(b) Load v. displacement relationship at 1/4 span of Girder B

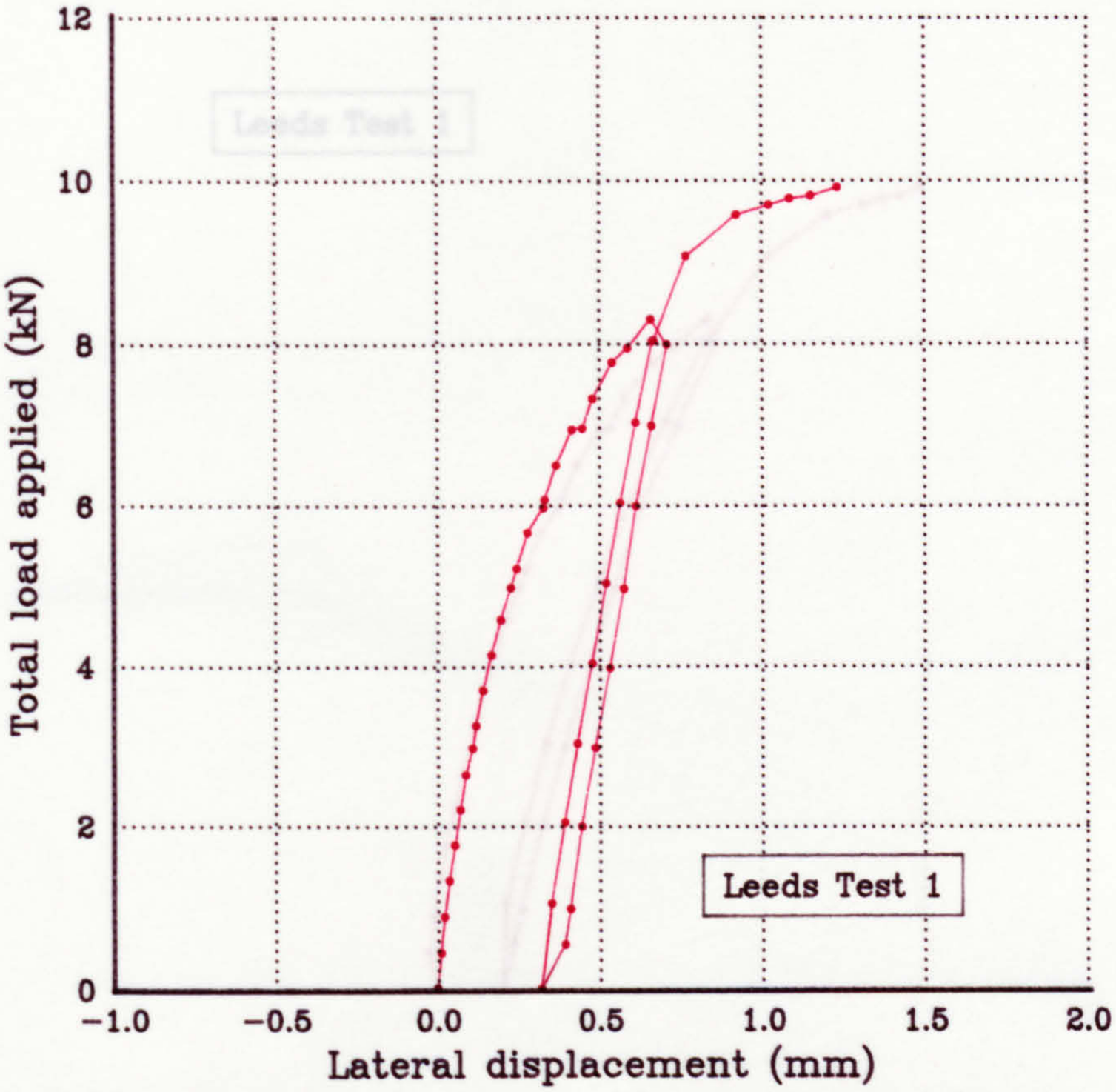

Figure 3.18(c) Load v. displacement relationship at 1/2 span of Girder A

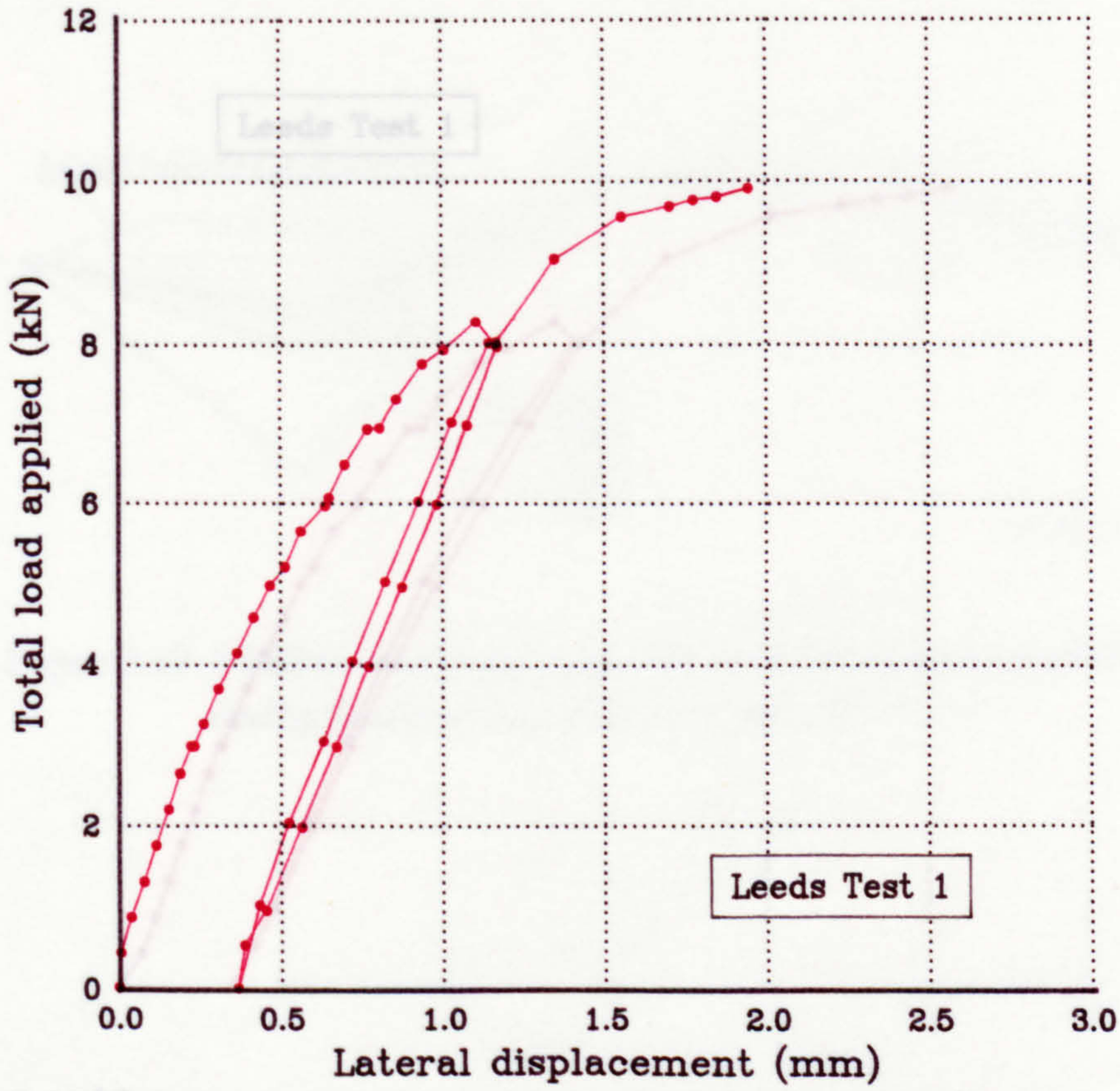

Figure 3.18(d) Load v. displacement relationship at 1/2 span of Girder B

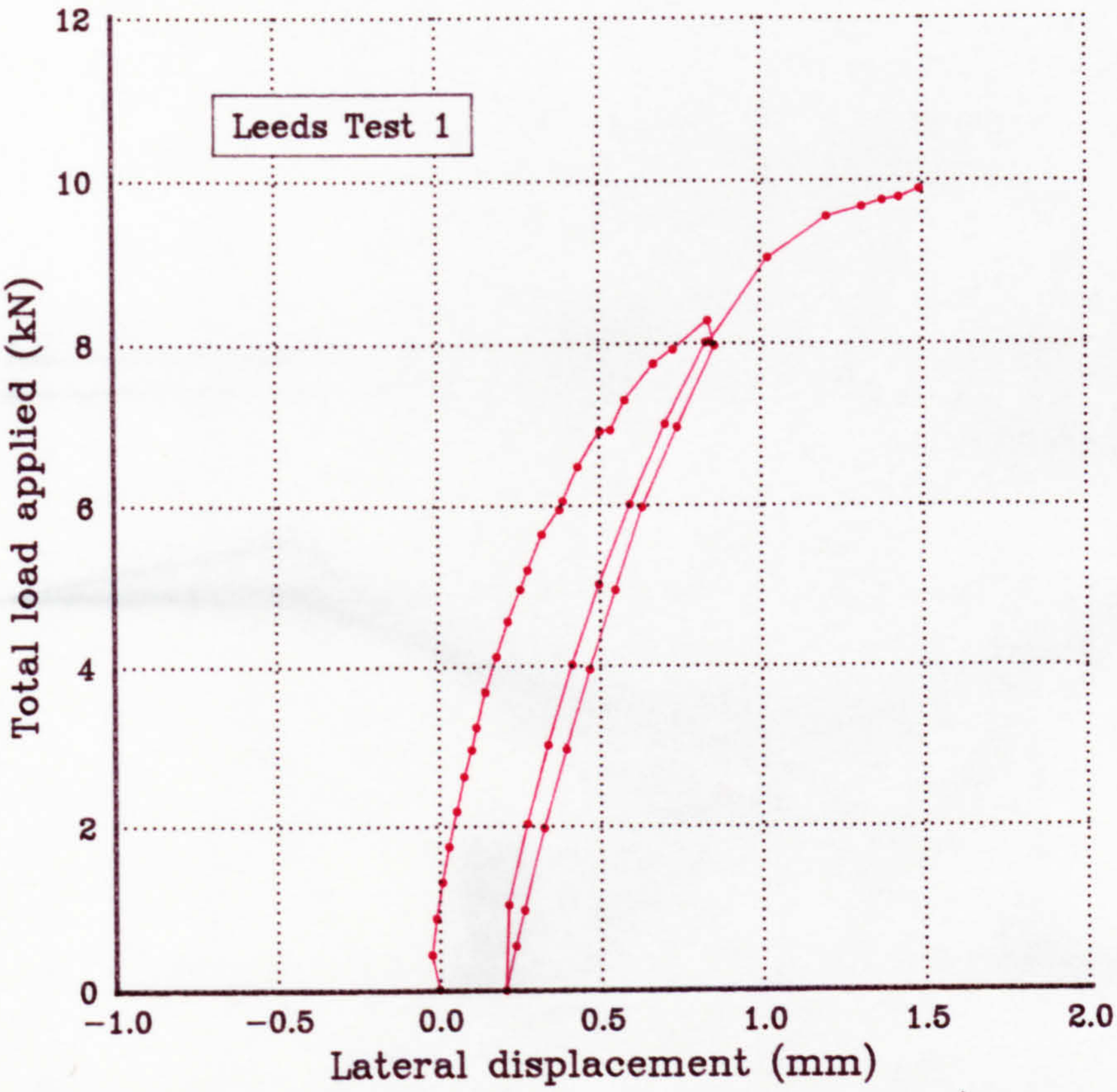

Figure 3.18(e) Load v. displacement relationship at 3/4 span of Girder A

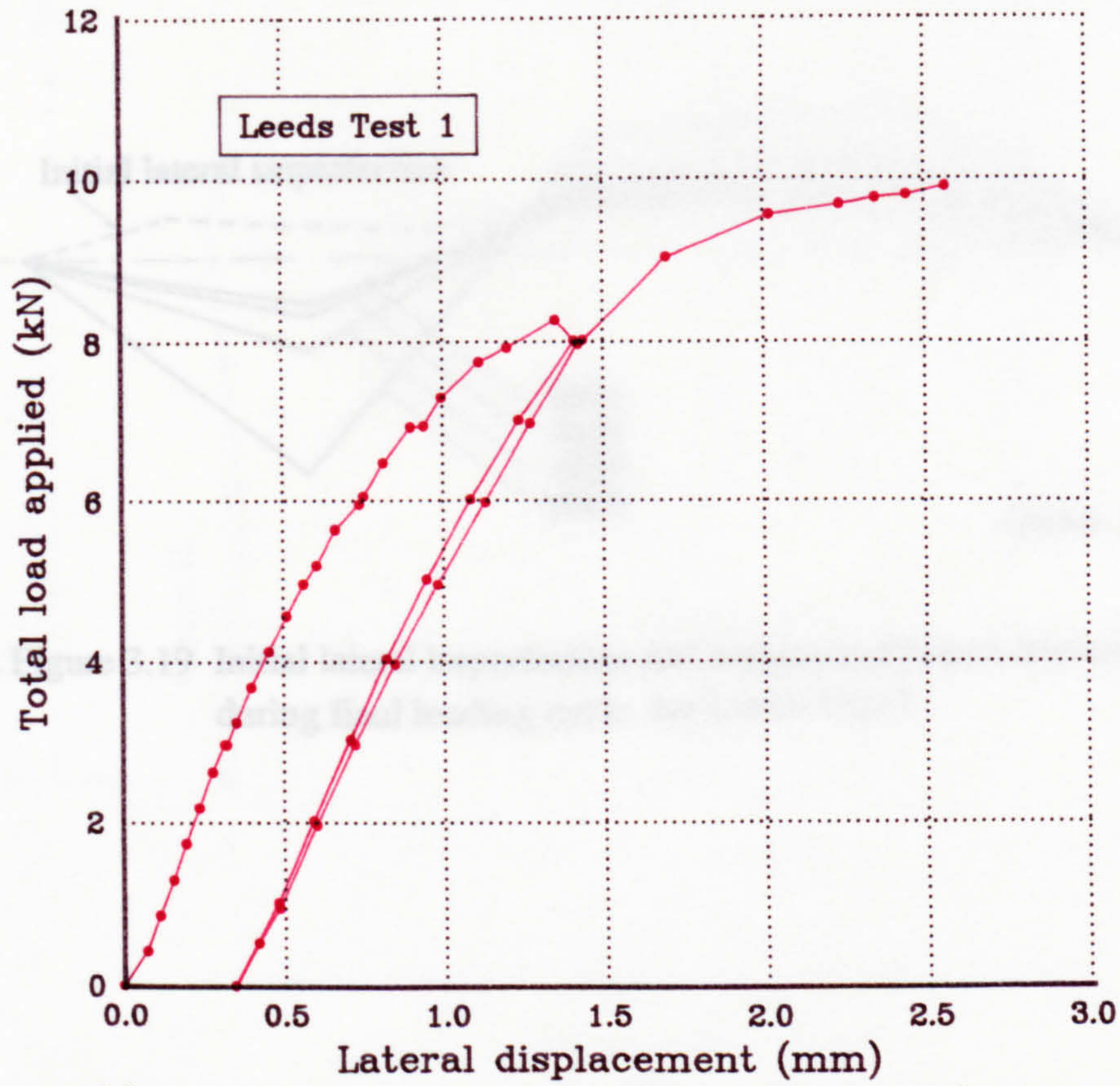

Figure 3.18(f) Load v. displacement relationship at 3/4 span of Girder B

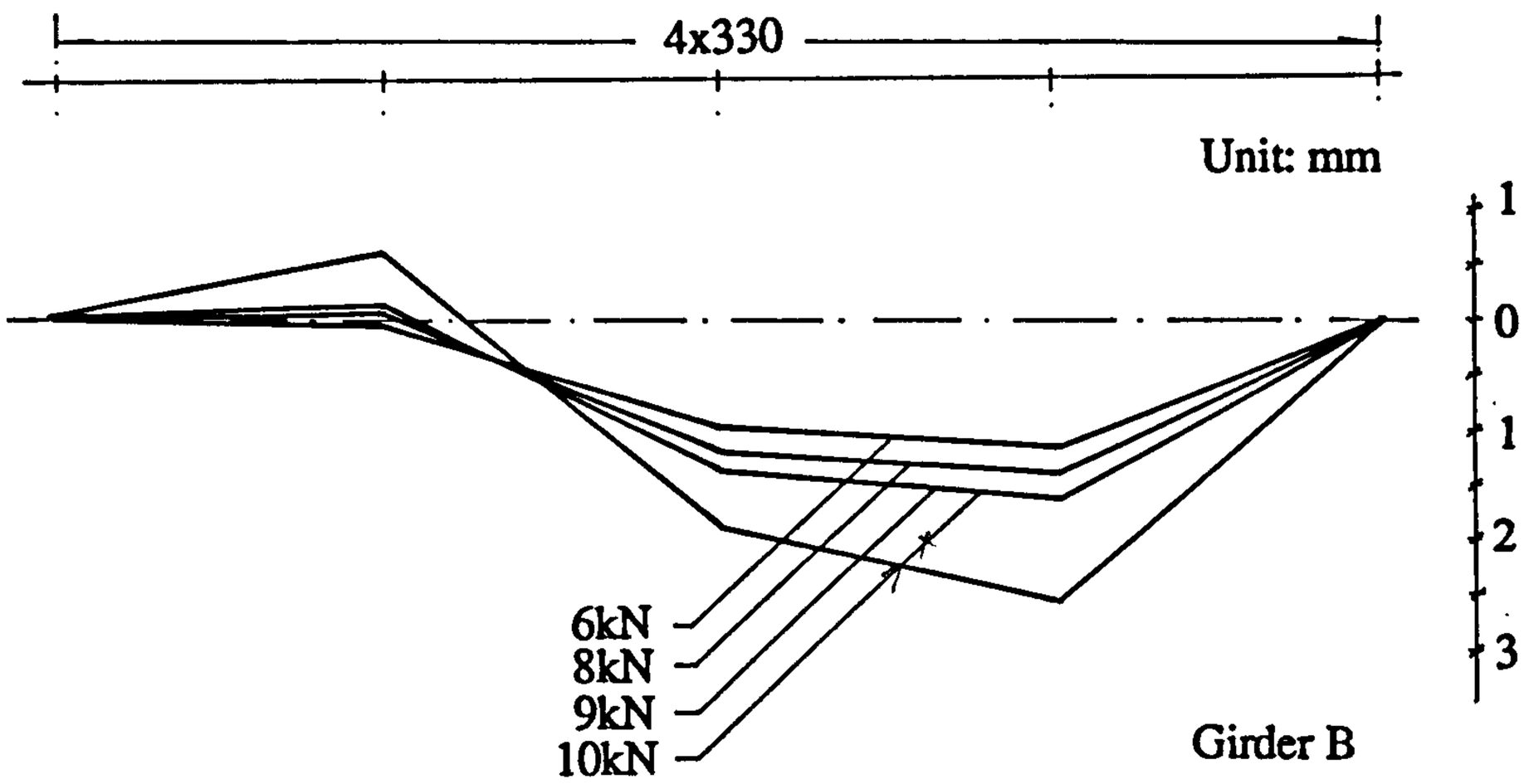

Figure 3.19 Initial lateral imperfection and variation of lateral displaced shapes during final loading cycle for Leeds Test 1

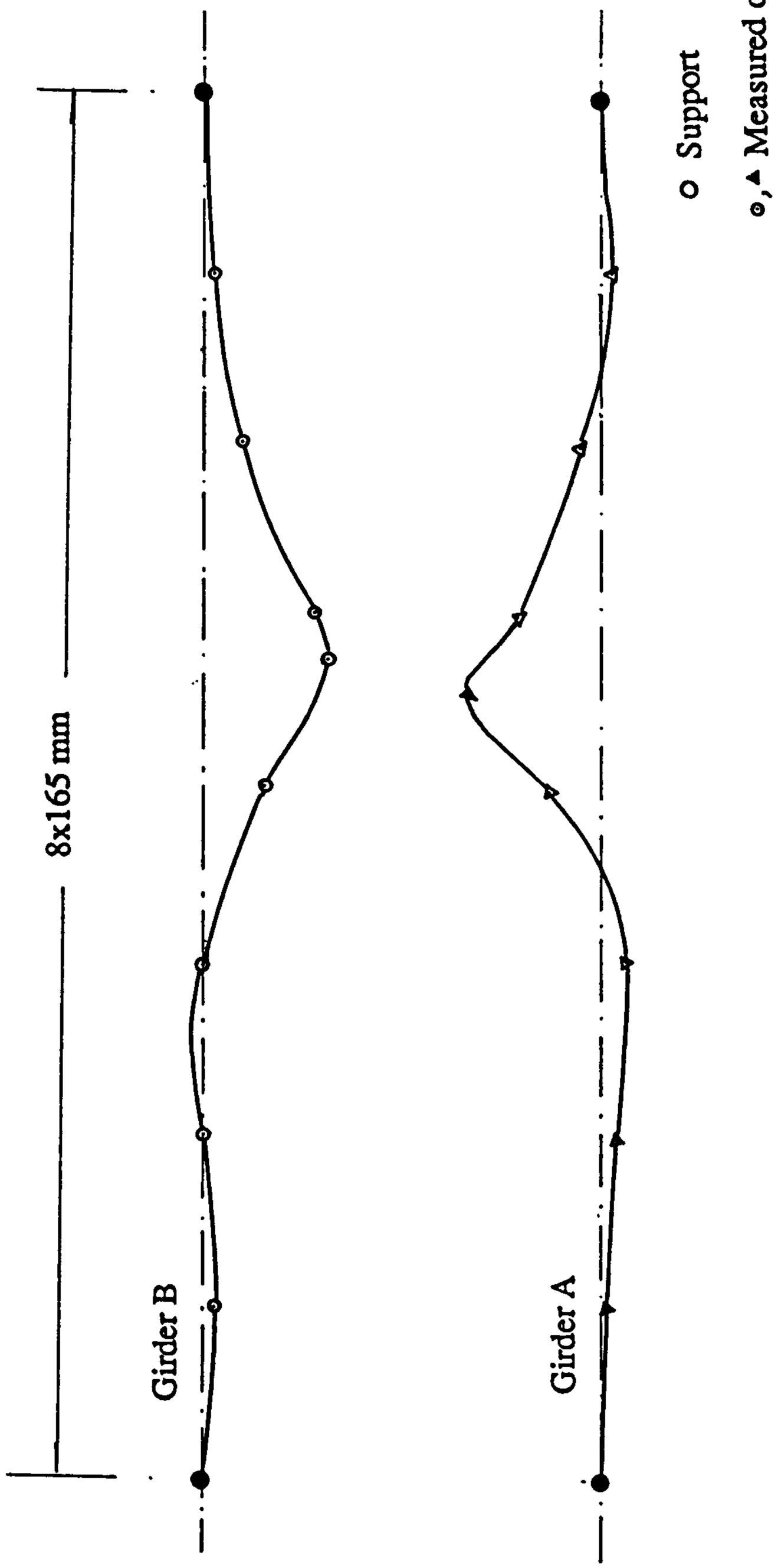

Figure 3.20. Measured final deformed compression flanges after unloading

Figure 3.21 Residual buckled shape of compression flange for Leeds Test 1

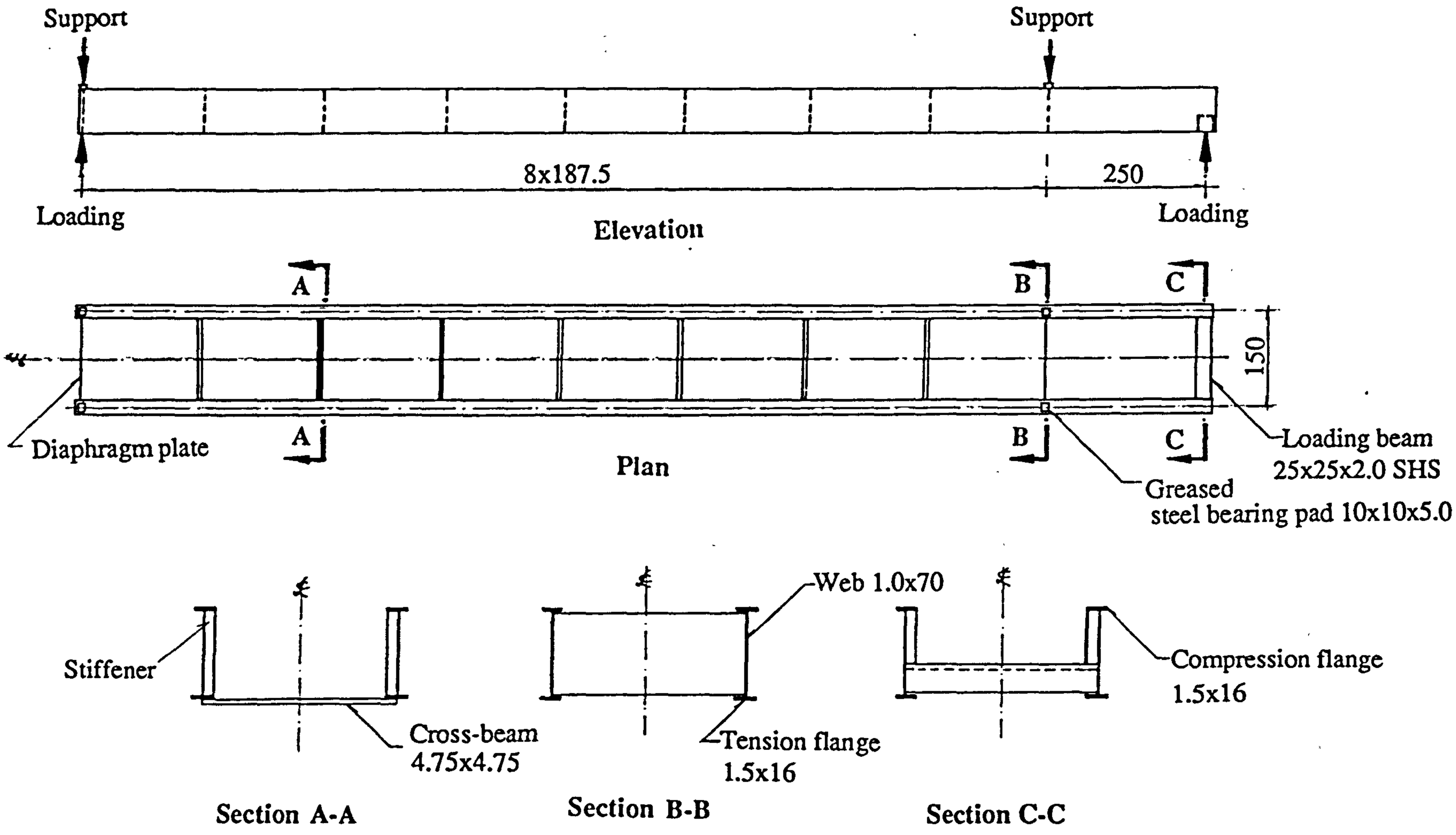

Figure 3.22 General arrangement of Leeds Test 2 Unit : mm

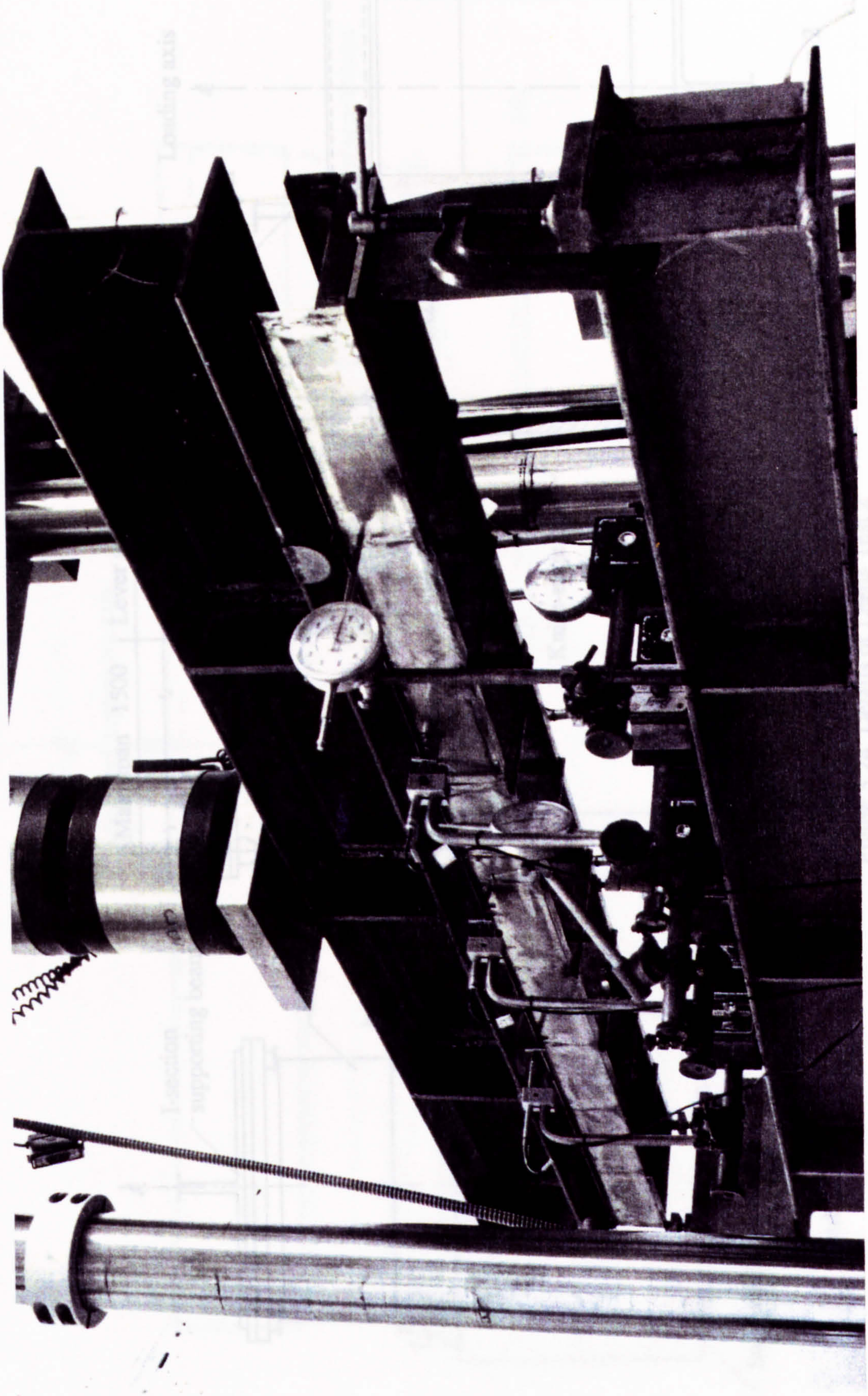

Figure 3.23 Loading arrangement and instrumentation for Leeds Test 2

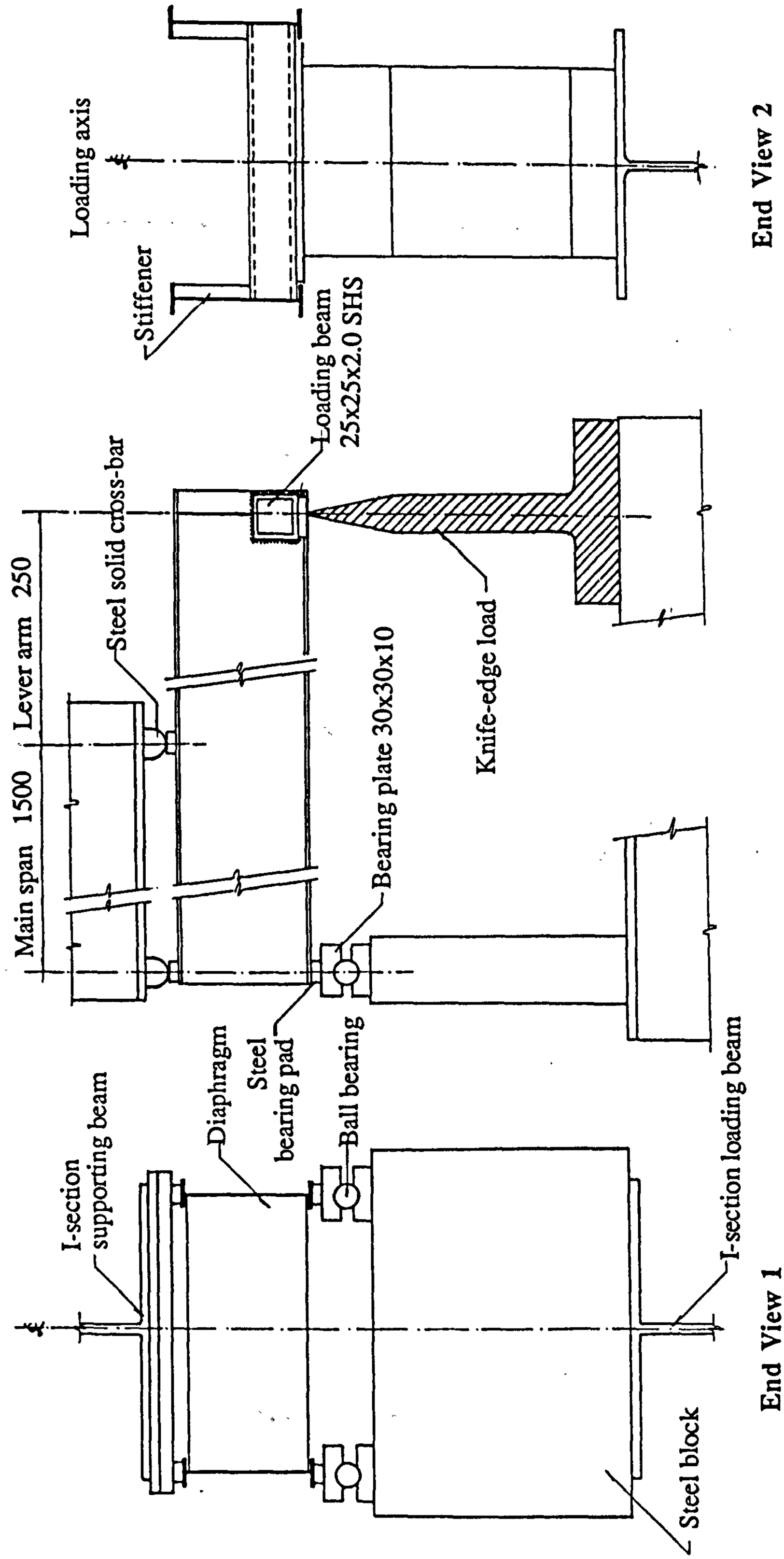

Figure 3.24 Details of Leeds Test 2

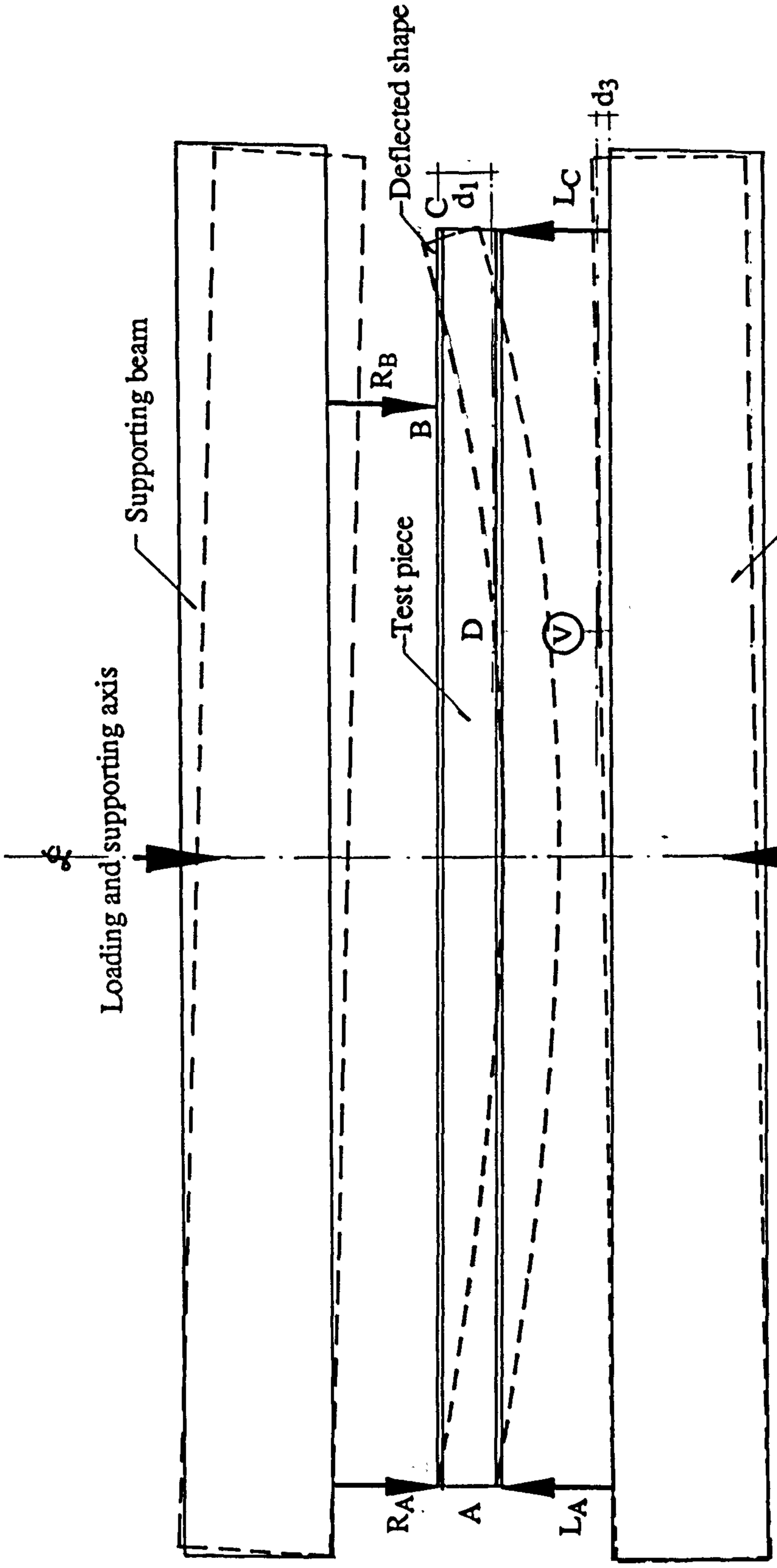

Dial gauge reading at point D: $d_1 - d_2 + d_3$, where d_1 is the true vertical deflection
d_2 is the movement of the test piece due to movement at C
d_3 is the vertical displacement of the moving beam at position D

$L_A = L_C$ $R_B = \frac{7}{6}L_C$ $R_A + R_C = L_A + L_C$

Figure 3.25 Measurement of vertical deflection for Leeds Test 2

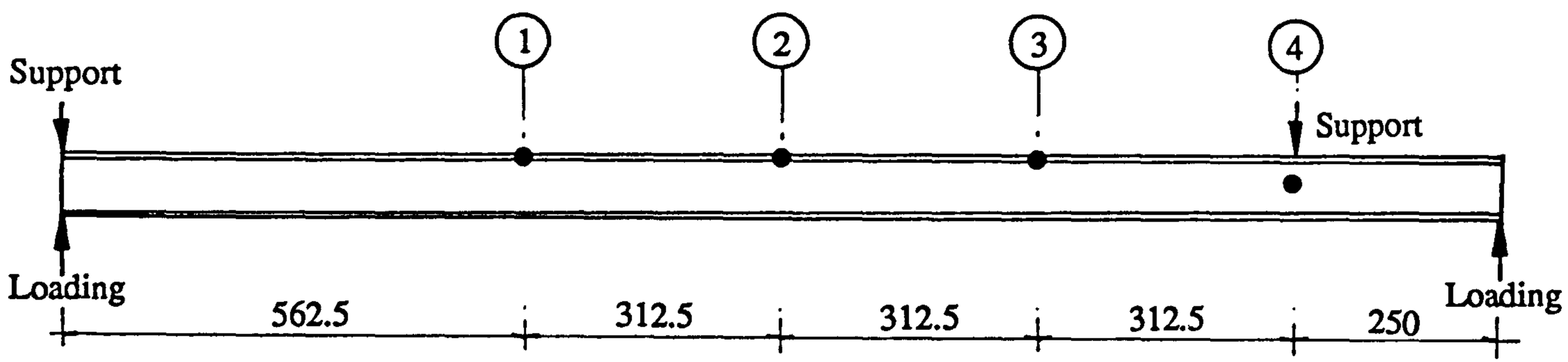

Lateral LVDT gauge at points 1, 2 and 3 (both girders)
Vertical dial gauges at point 3 (both girders)
Horizontal dial gauge at point 4

Figure 3.26 Gauge positions for Leeds Test 2

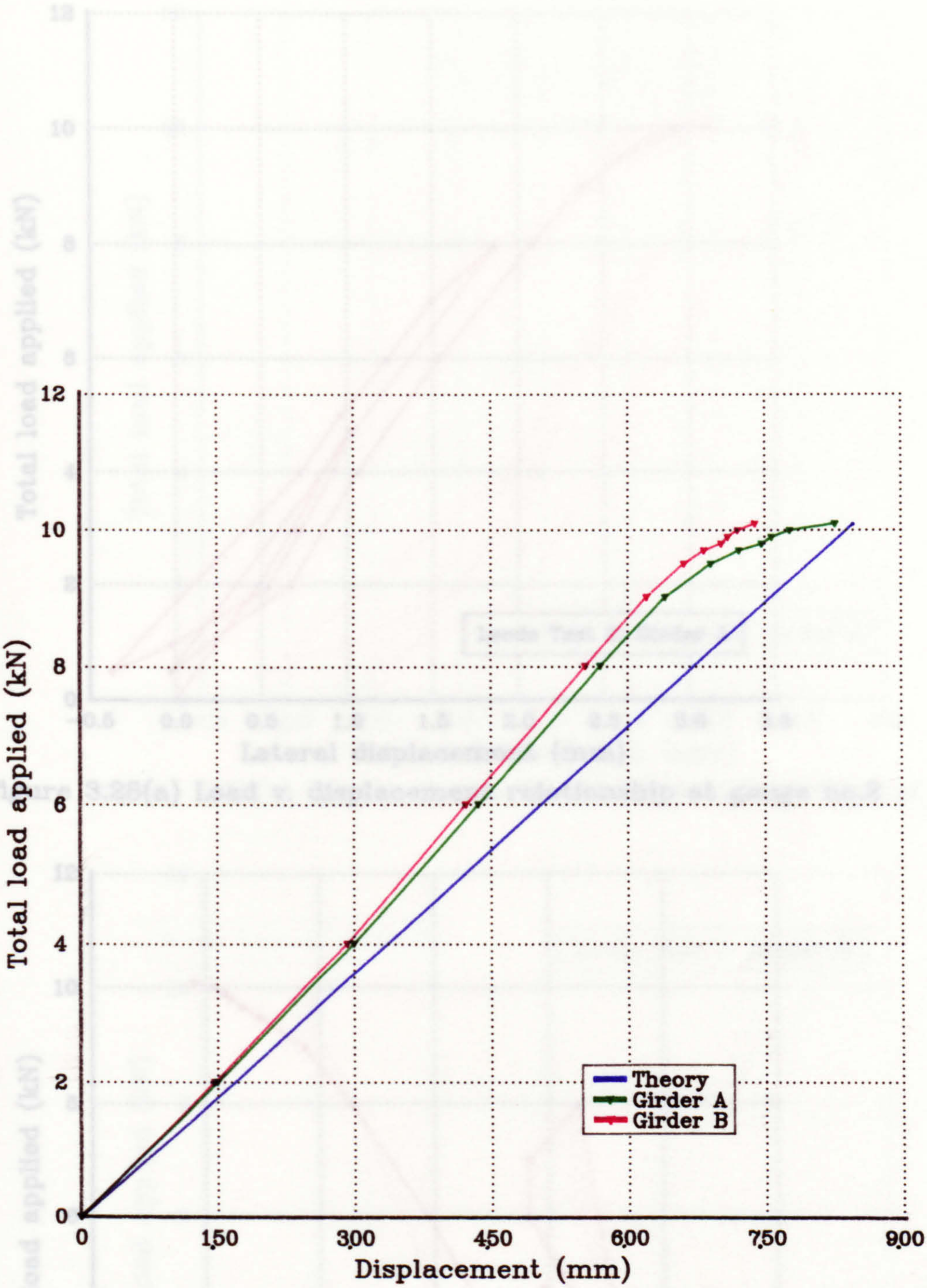

Figure 3.27 Load v. vertical displacement relationship for Leeds Test 2

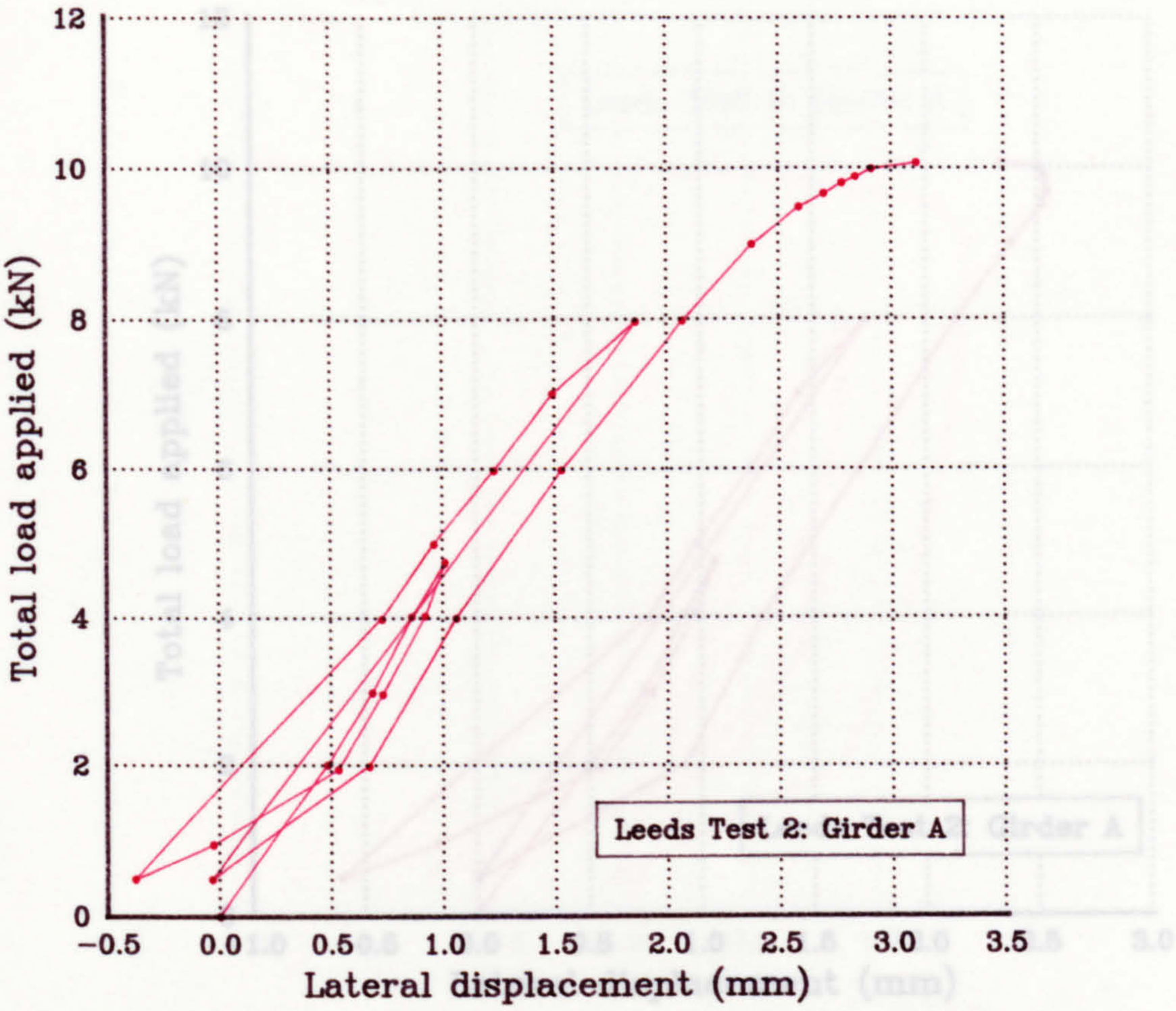

Figure 3.28(a) Load v. displacement relationship at gauge no.2

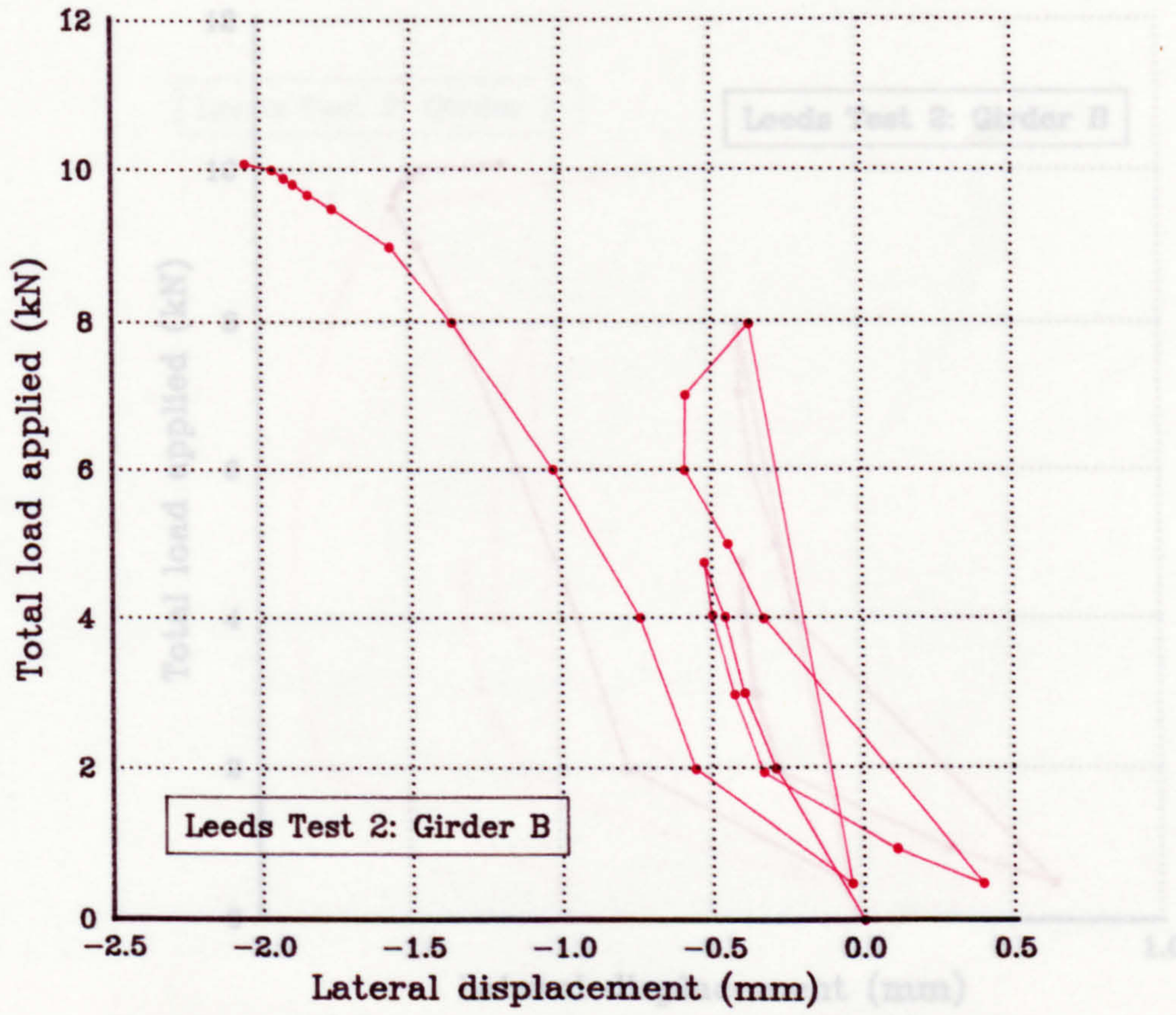

Figure 3.28(b) Load v. displacement relationship at gauge no.7

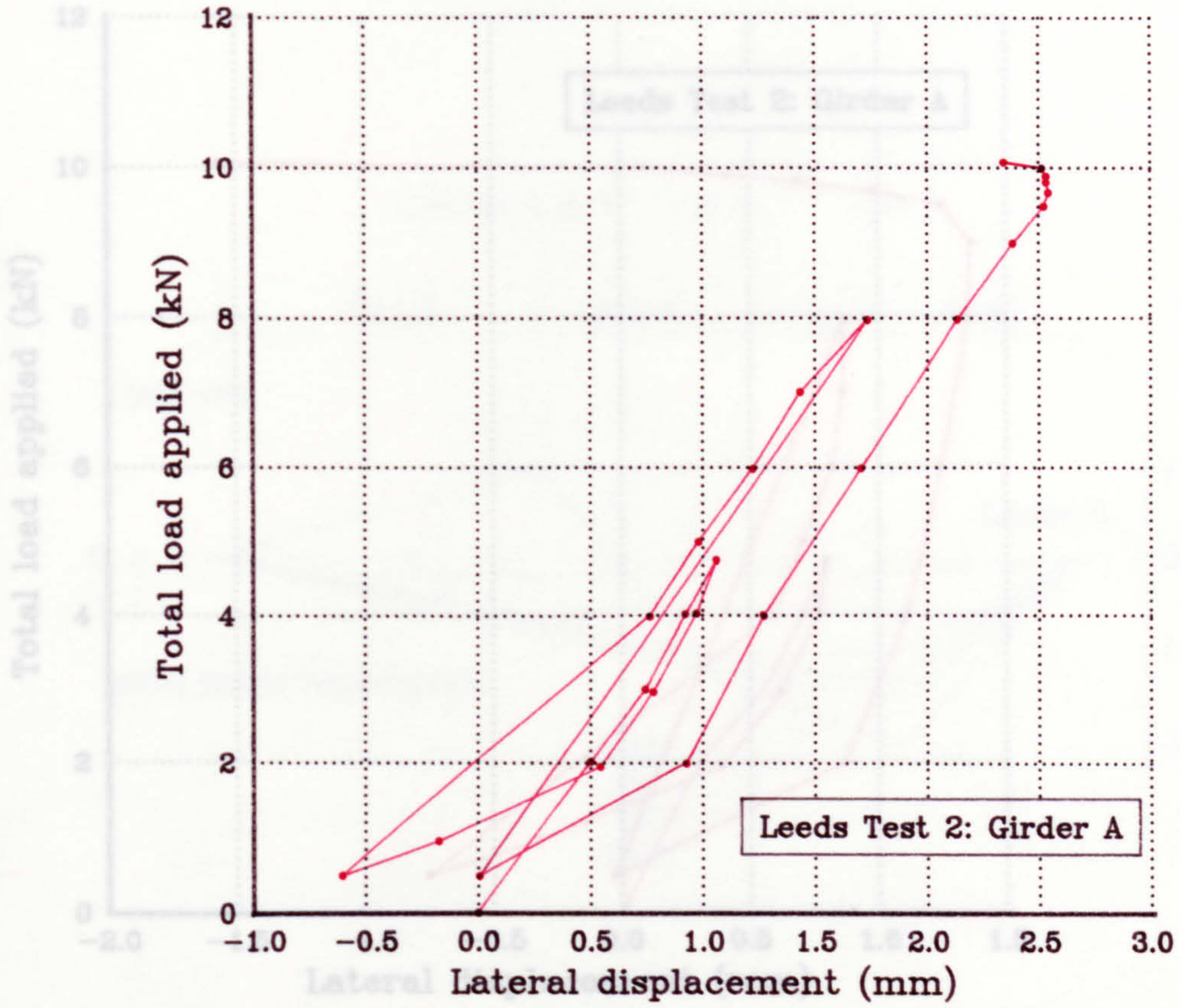

Figure 3.28(c) Load v. displacement relationship at gauge no.3

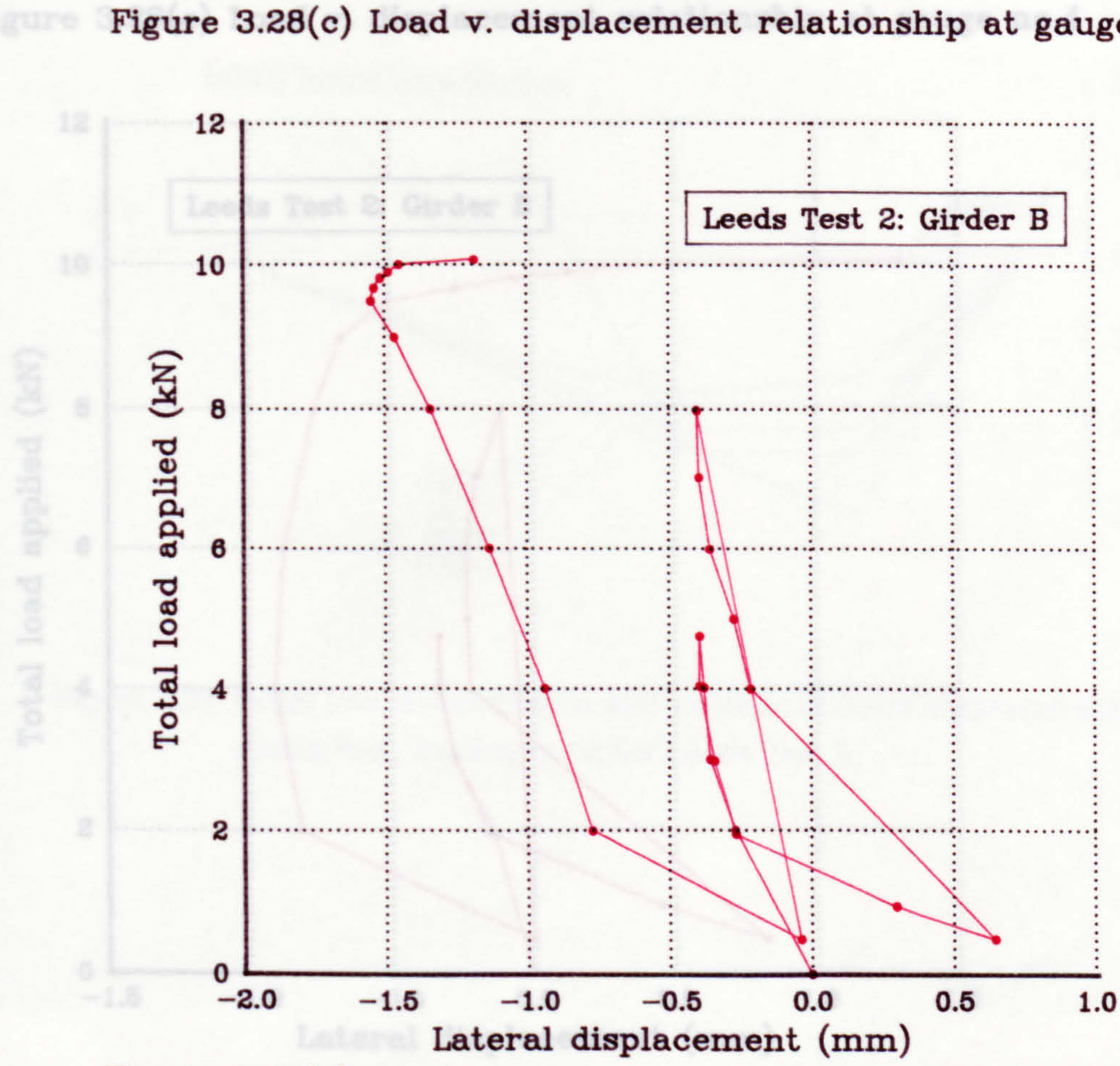

Figure 3.28(d) Load v. displacement relationship at gauge no.6

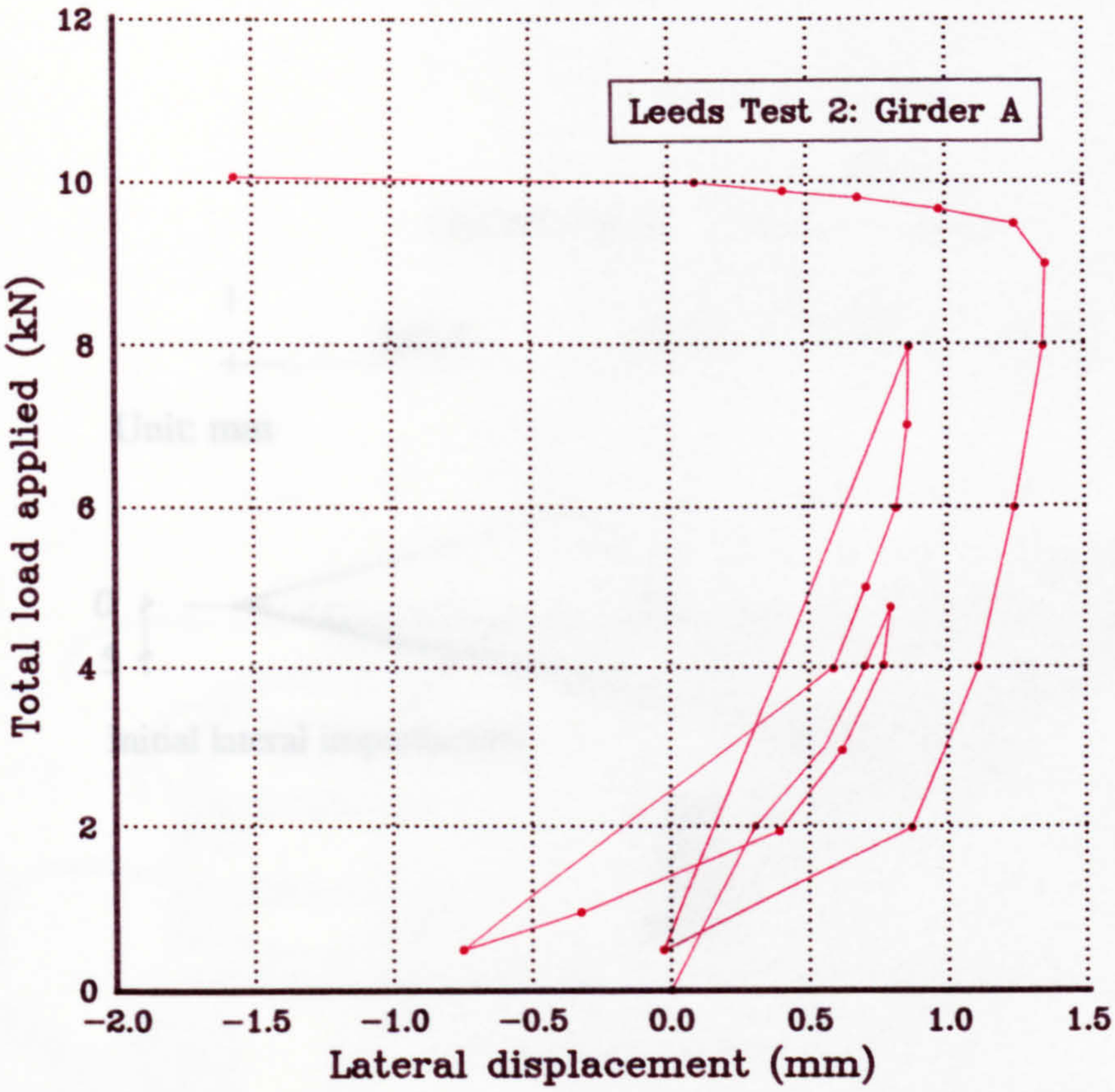

Figure 3.28(e) Load v. displacement relationship at gauge no.4

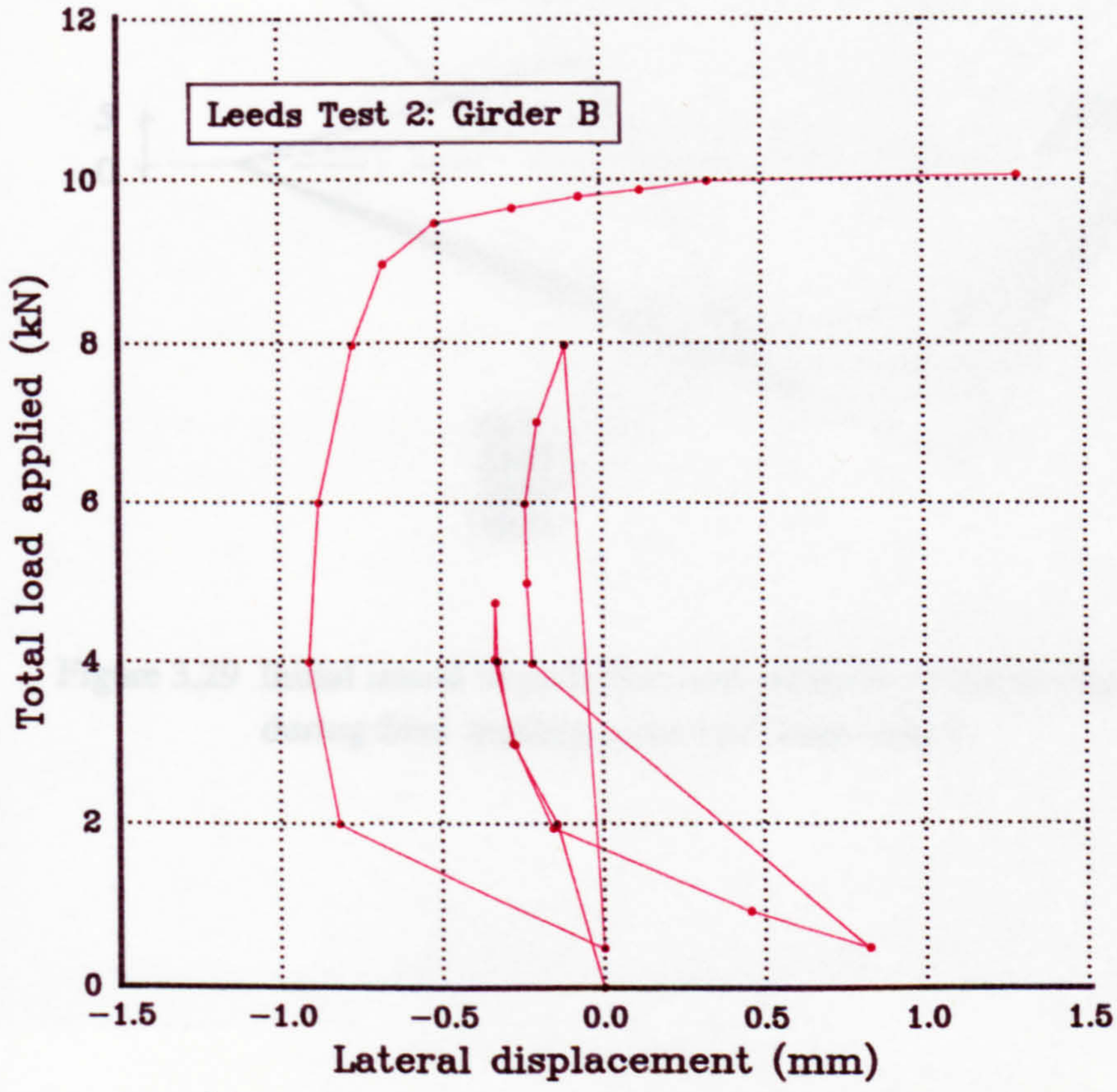

Figure 3.28(f) Load v. displacement relationship at gauge no.5

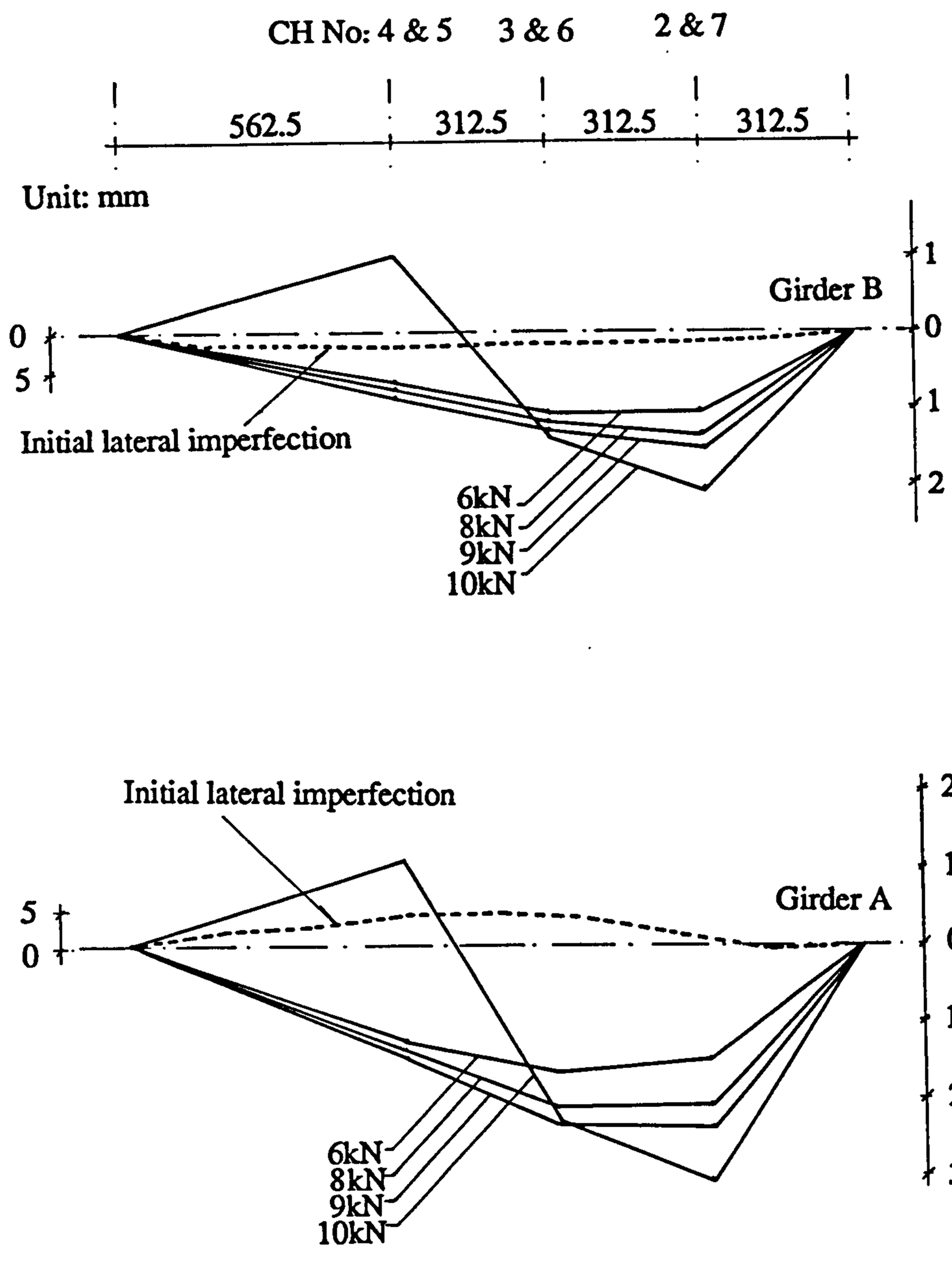

Figure 3.29 Initial lateral imperfection and variation of lateral displaced shapes during final loading cycle for Leeds Test 2

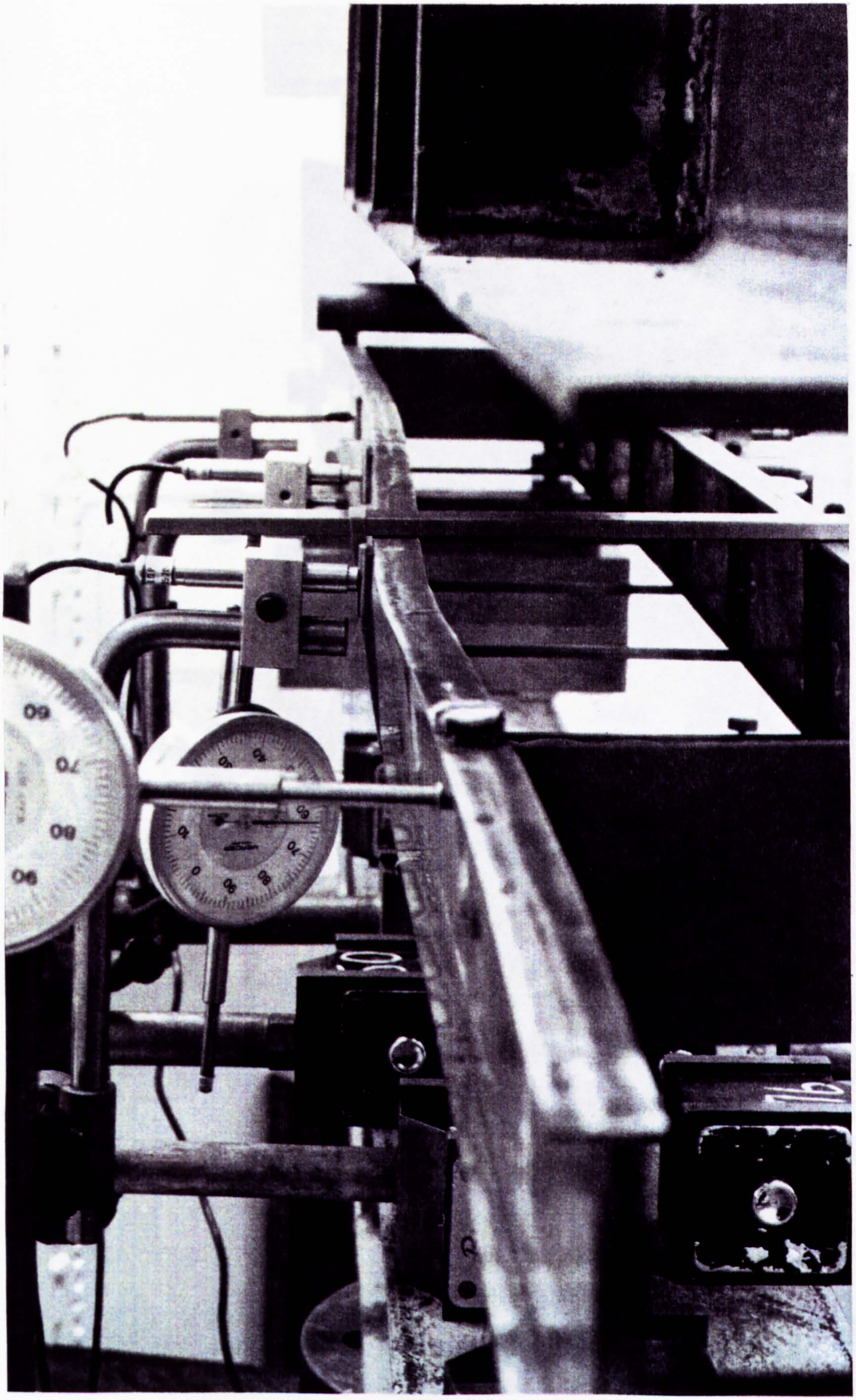

Figure 3.30 Onset of buckling for Leeds Test 2

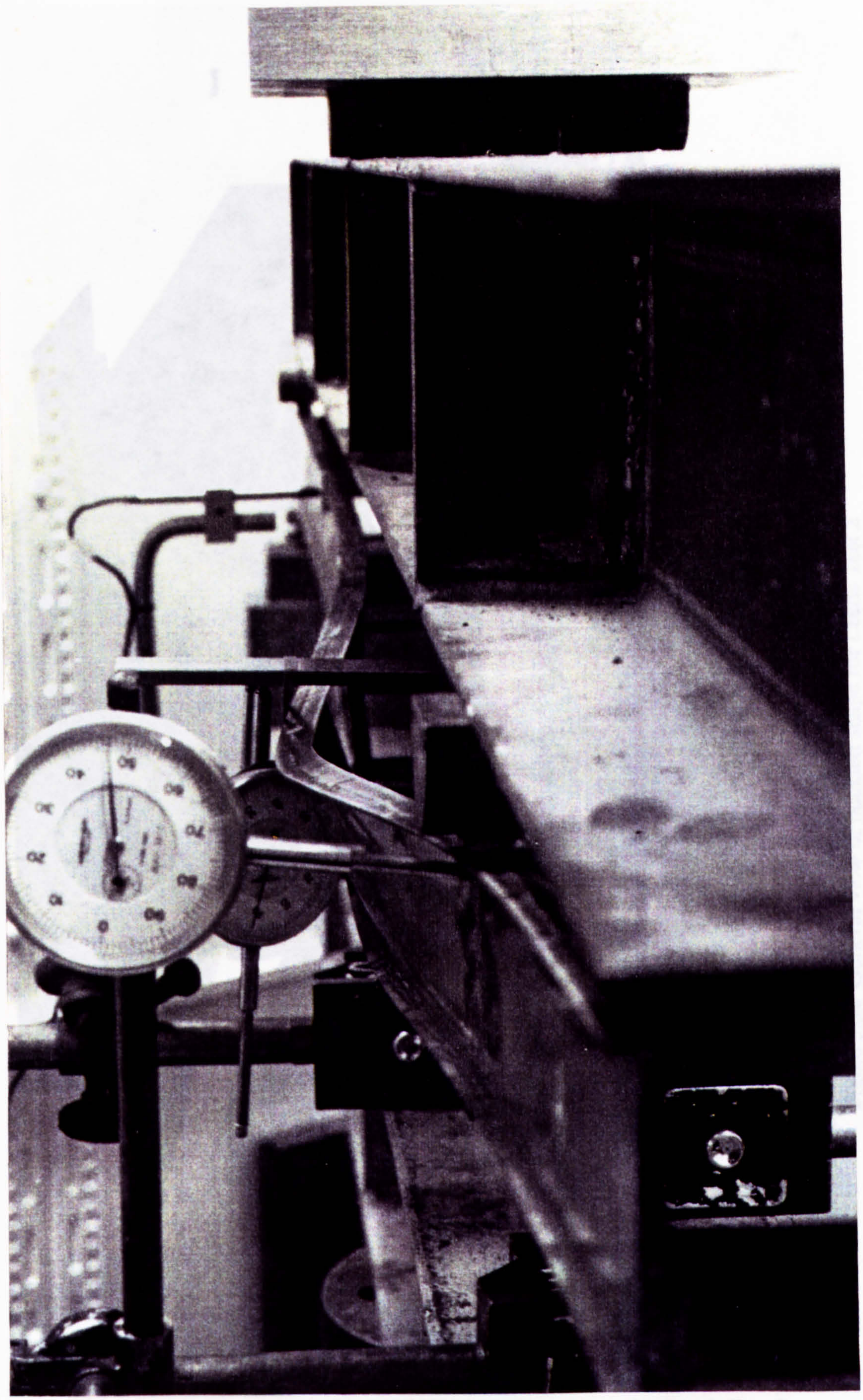

Figure 3.31 Final buckled shape of compression flange for Leeds Test 2

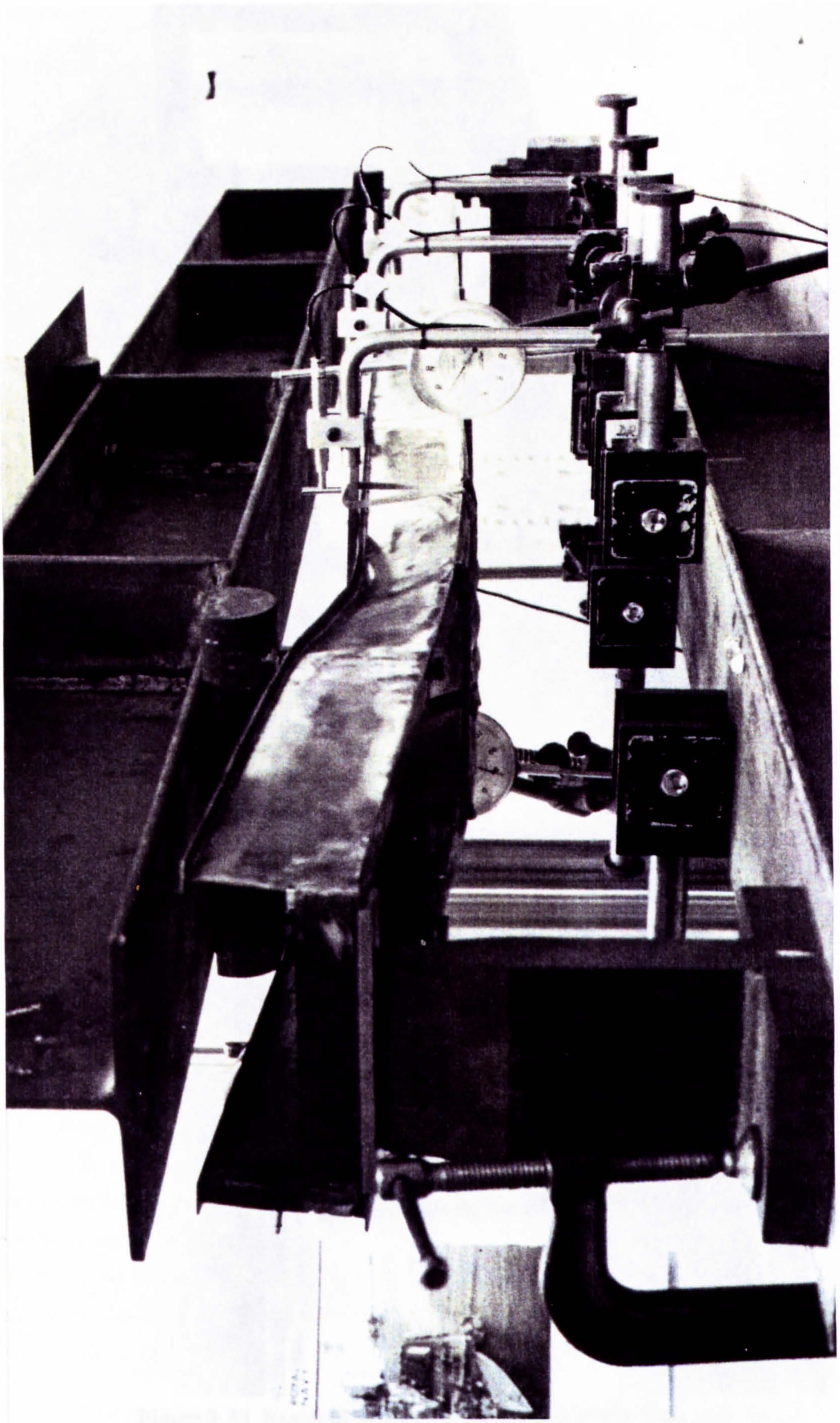

Figure 3.32 General view of buckled shape for Leeds Test 2

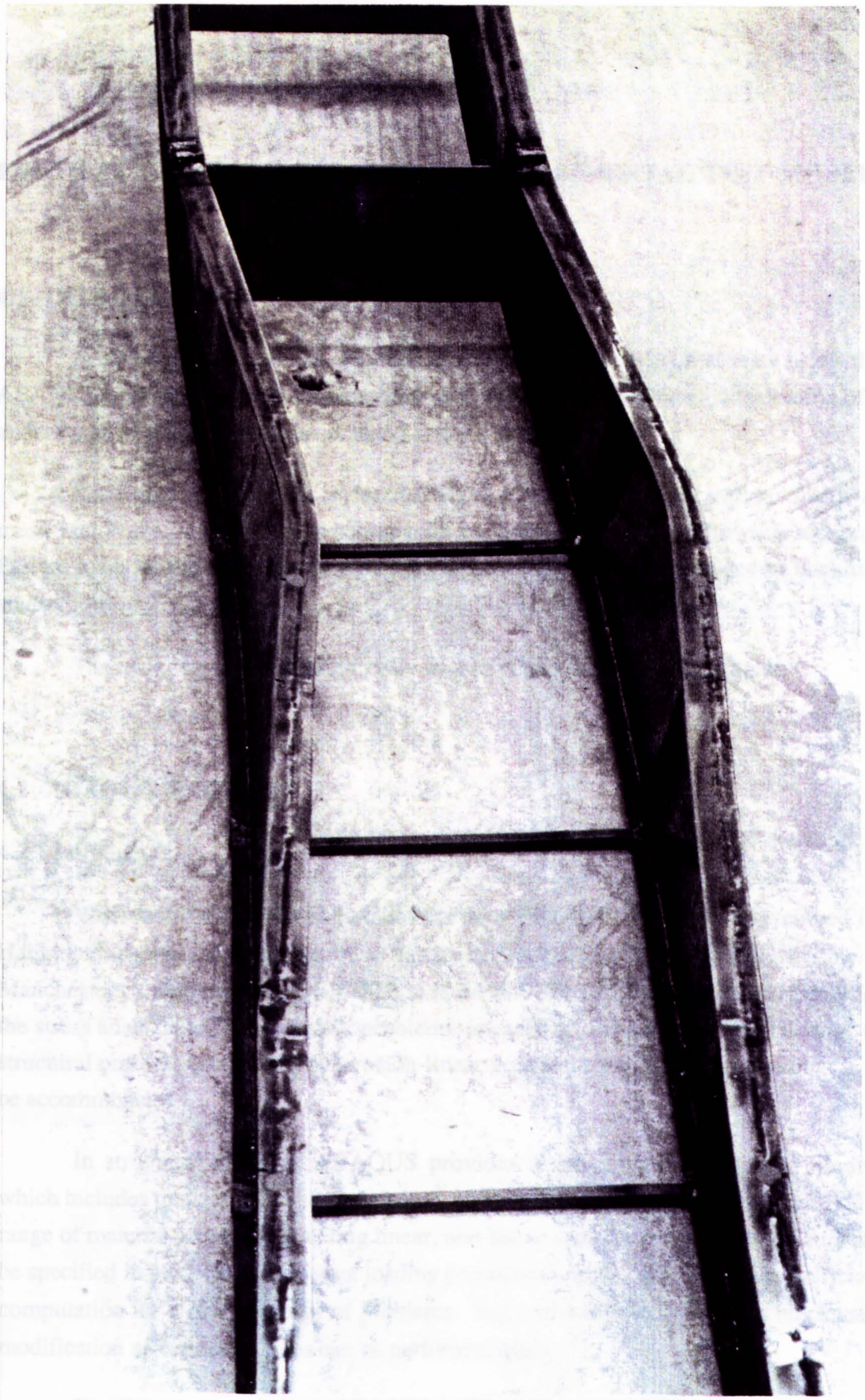

Figure 3.33 Residual shape of compression flange for Leeds Test 2

CHAPTER 4

FINITE ELEMENT IDEALISATION OF EXPERIMENTAL TEST MODELS

4.1 INTRODUCTION

Analytical finite element modelling of the three experimental tests using the ABAQUS package was primarily intended to validate the finite element idealisation of a wider range of practical U-frame braced I-section girder bridges.

Simulation of each test is described and the results of using various forms of mesh and types of elements are compared and discussed in the following sections. Failure loads of the three tests are summarised and corresponding modes of buckling studied.

The main features in ABAQUS are first briefly descrided in this chapter.

4.2 ABAQUS PACKAGE

4.2.1 Introduction

Version 4.7 of the finite element package ABAQUS[50,51,52,53] developed by Habbitt, Karlsson and Sorensen Inc., was installed on a vector processing machine at Manchester Computing Centre (MCC) in late 1989. The package, intended mainly for the stress analysis and heat transfer problems, is capable of dealing with a vast range of structural problems, especially where non-linear geometric and material behaviour is to be accommodated.

In structural analysis, ABAQUS provides a comprehensive element library, which includes thick and thin shell elements, solid elements, spring elements etc.. A full range of material properties covering linear, non-linear and elasto-plastic behaviours can be specified in modelling. Different loading procedures can be chosen to ensure efficient computation for a diverse range of problems. Input is controlled by option blocks and modification of various features can be performed easily.

The data structure for an ABAQUS job running at MCC[54] can be divided into three sections. The first section contains the job controlled card, which includes CPU

running time to be allocated and the required disk size for storage of job information during the execution of the analysis, which includes pre-analysis data checking and the main analysis phase after the pre-run. The second section, known as the 'data deck', is the main section dealing with the definition of the finite element model and the analysis to be undertaken. Finally, there is a 'graphical output control card', which controls conversion of the neutral plot files produced by the ABAQUS into Gino Savdra files, transferable to the Leeds CMS.

ABAQUS jobs can be sent to the vector processing machine either via the Leeds University Amdahl computer and Joint Academic Network (JANET)[55] or via the Amdahl system 5890-300E at MCC.

4.2.2 Data Preparation

The 'data deck' used to define a finite element problem to ABAQUS consists of two parts; model data and history data. The model data is a geometrical description of the model giving the node coordinates, element types, properties and locations, material definitions, boundary constraints and so on. History data defines the sequence of events for which the model's response is sought. Control of output files including restart files, printed outputs and plots is also included in the history data.

4.2.2.1 Model Data

(a) Node Definition

The options in ABAQUS allow the nodes of a finite element model to be defined either directly by giving the coordinates of the individual nodes or indirectly by generating them between already defined end nodes using various line shapes. Other options allow existing nodes sets to be copied. Space between two already defined nodes can be filled with nodes of defined regular spacing. However, for irregular meshes, most of the nodes have to be specified individually. A right-handed rectangular cartesian coordinate system is used mainly.

(b) Element Definition

Direct geometrical definition of a master element can be achieved by ordering the nodes in a specific pattern. Incremental generation of elements, which is of the same type as the master element, can then be achieved by specifying increment in node and element numbers between successive elements in the three directions. Groups of elements can also be copied to form new meshes elsewhere.

Each element is assigned to one type of element (shell, beam, spring elements etc). The two main types of element used in this research were quadrilateral shell elements and beam elements.

For shell elements the thickness, section properties (number of integration points through the thickness) and material properties have to be specified. In the case of beam elements, the cross-sectional dimensions and direction cosines of the sectional axes in cartesian coordinates have to be declared.

(c) Material Definition

Material properties are introduced by declaring either elastic or inelastic behaviour together with associated properties of the material.

(d) Kinematic Conditions

Constraints, either translational or rotational, can be imposed on the model, linearly or non-linearly. Prescribed movements at nodal points may be specified at supports or linear multi-point constraints may be applied to related nodes or node sets. Non-linear multi-point constraints (MPCs), both rotational or translational, between certain nodes can also be specified. These relationships can be directly selected from types of constraint available with ABAQUS or may be specified by the user.

4.2.2.2 History Data

The history data input defines the sequence of loading imposed on the model and the response variables (linear or non-linear) being sought. The data can be divided into several steps, each of which is a period or part of a loading input. The analysis procedure automatically provides the type of analysis defined. ABAQUS allows direct control of increment size or alternatively provides automatic control in which the programme selects its own increments according to success in achieving a convergent solution in the previous increment. Non-linear problems are therefore run with high efficiency without the need for considerable previous experience in handling the particular problem.

When non-linear analysis is required, both geometrical non-linearity, involving modification of geometry and the stiffness matrix during the loading, and the material non-linearity, which is introduced by the definition of inelastic or plastic material properties, may be accommodated. Geometrical non-linearity, with large displacement and rotation but small strains, is the basis for the formulation in ABAQUS.

The output request option is also defined in the history input data. Many output files, including plots, print-outs and restart files may be produced after an increment, but this can be controlled selectively by the user. Element variables can be specified for points of integration, centroids or nodal points; nodal displacements may also be specified. Graphical output from the analysis including deformation and stress contours may be generated also.

4.3 FINITE ELEMENT IDEALISATION OF THE WELDING INSTITUTE MODEL

Finite element idealisation of the test piece in three-dimensional form was represented by an assembly of two-dimensional thin plates and had the same configuration as the test model except for some simplification of the cantilever loading region. (A typical ABAQUS job is given in Appendix I.) Attempts to create uniform bending in the main span by applying equal opposite horizontal point loads along the centre and edges of the tension and compression flange at the supports were frustrated by severe local yielding at a relatively early stage of the loading process. Subsequently, loading arm extensions were included in the modelling as in the test.

Instead of modelling the actual initial lack of straightness in the two girders of the test piece, a lateral imperfection of $\frac{\text{Span}}{1000}$ was introduced into the compression flange only by displacing the flange nodes laterally to a parabolic single half-wave profile.

4.3.1 Finite Element Mesh

Sub-divisions of the elements in the plates were arranged carefully in order to obtain optimum results. In general, a refined mesh was used in regions of high stress gradient and a coarse mesh in other regions. The general mesh arrangement was as shown in Figure 4.1. Various types of element were tried and compared.

4.3.2 Choice of Element

Two-dimensional non-conforming eight-node or four-node quadrilateral shell elements[50,56] (namely S8R5 and S4R5 in ABAQUS system) were chosen. These elements were designed so that the shear locking problem usually encountered in thin shell elements, was circumvented by employing, firstly, reduced integration along the surface (2x2 points for the S8R5 elements and one point for the S4R5 elements) but exact integration through the thickness (with five points by default for both types of element) and secondly, the discrete Kirchoff assumption using the penalty method. Based on a kinematic formulation, variable displacement and strain within the boundary

of an element are allowed. For S8R5 elements, the displacements are quadratic over the surface and linear across the thickness whereas for S4R5 elements, the displacements are all linear.

Most of the nodes of an element have five degrees of freedom, including three translational and two rotational on their surfaces. If a rotational restraint in a direction perpendicular to the plane of the element is applied to a node, either the node is attached to a beam or shell element, both of which have six degrees of freedom, or it is involved in a MPC that includes the rotational degree of freedom, in which case this node will also have six degrees of freedom instead of five.

The two or three node beam elements (B31 or B32 in ABAQUS) were used as they allowed linear or quadratic variation of displacement along their length and appeared to be adequate for the modelling of cross members. The formulation of these two types of element is based on Timoshenko's beam theory where the effect of shear deformation is included. These elements have six degrees of freedom at each node so that the nodal compatibility will be satisfied at the junction nodes with S4R5 or S8R5 elements respectively. Rigid links between the beam and shell elements were provided by linking the corresponding nodes together with using the *MPC option.

4.3.3 Load Application

Since the cantilever loading arm was included in the finite element idealisation, a closer representation of the actual test was simulated. Vertically downward point loads were applied at the tips of the top flanges. The rigid cross-beams interconnecting the two girders at both ends, used to apply load in the test, were not modelled.

In order to reduce load concentration at a point and obtain the equivalent effect of a uniformly distributed knife-edge load, the point loads were divided into 1:4:1 ratio for the three nodes along the edge of each S8R5 element but simply 1:1 ratio for the two nodes in a S4R5 element.

Local stress concentration still occurred in the vicinity of the point load but in general, a uniform bending moment over the entire central span was obtained.

4.3.4 Material Modelling

The material was modelled as elasto-plastic and its yielding properties were obtained from a tensile test done by the Welding Institute. Plasticity in the plates was governed by the von Mises yield criterion since using this, in combination with integration through the thickness of shell elements or through the cross section of beam elements, gives an accurate procedure for tracing plasticity in a plate structure [57]. Strain hardening of material and residual stress were not taken into account in this analysis.

4.3.5 Type of Analysis

A non-linear large displacement static analysis was carried out. The loads were applied as a series of small increments, for each of which the programme sought to give a convergent solution with minimum computing time using an automatic convergence strategy based on tolerances given as input.

4.3.6 Boundary Conditions

Due to the double symmetry of the test model, it was only necessary to simulate one-quarter of the structure, provided that appropriate boundary conditions were adopted.

Owing to the complexity of the behaviour of the cross-section at mid-span, the development of lateral displacement of the compression flange into symmetrical or anti-symmetrical buckling mode was not predictable in spite of the symmetrical vertical displacements. However, by declaring either one set of the boundary conditions, the occurrence of the other would be suppressed. Therefore, it was decided that instead of one-quarter, one-half of the test model was used.

The boundary conditions used in modelling of the half structure were much simplified. No symmetrical or anti-symmetrical constraints, which usually induce unnecessary increase or decrease of the structure stiffness, were exerted onto the girders at the mid-span position. Assuming that there was a coupling effect from the U-frames, the symmetrical behaviour of the two girders about the plane perpendicular to the cross-beams was simulated by using the YSYMM parameter in the *BOUNDARY module. 'Simply supported' boundary conditions were applied to the girders (using vertical restraints to nodes at the supporting position and longitudinal restraints at mid-span). Lateral movement at the end of cantilever loading arms was also prevented, as in the test.

A full-span modelling of the test is also presented here for comparison purposes and as a check on boundary behaviour observed in the half-span modelling. No symmetrical conditions need to be declared for providing artificial constraints to the nodes in the plane(s) of symmetry. Two girders were simply supported with longitudinal constraints applied at one end of the model. The direction of initial bows in the twin girders was set to be convex outwards.

4.3.7 Finite Element Results

4.3.7.1 Half Structure with S8R5

The ultimate moment capacity obtained from the ABAQUS analysis was 36.0kNm, which was 24.1% higher than the experimental collapse load.

From the load versus lateral deflection curve plotted in Figure 4.2, it can be seen that collapse of the structure was sudden. Lateral deflection of the nodes at mid-span increased fairly slowly until the buckling load was approached.

First-yield in the analysis was encountered in the elements adjacent to the load points at an early stage (47% of failure load) mainly because of the high stress concentration. As the load increased further, the yielding zone developed and spread locally. This was followed by yielding at the support positions. No yielding in the remainder of the elements, including those in compression, was detected throughout the loading period. Since strains were not measured during the laboratory test, only displacements may be compared with those occurring in the finite element analysis. However, in both cases, the models were loaded to failure, which took the form of excessive lateral deflection of the compression flange.

The mode of buckling (three half-waves as shown in Figures 4.3(a) and 4.3(b)) did not develop until the final failure load was reached in the test. It was observed that lateral deflection of the compression flange was oscillatory and convergence was slow probably due to plasticity in the load bearing elements.

4.3.7.2 Half Structure with S4R5

Using the same finite element mesh and boundary conditions, the change from S8R5 to S4R5 type elements caused a 3.8% increase in failure load relative to the test result and a 16% decrease in comparison with the modelling using S8R5 elements. The ultimate moment capacity reached was 30.096kNm and the relationship between load and lateral deflection of the node at mid-span is plotted in Figure 4.2.

The progress of lateral displacement of the compression flange and the twist of the web is clearly shown in Figures 4.4(a), 4.4(b) and 4.4(c). The final mode of buckling, illustrated in Figure 4.5, consisted of three half-waves, which was in accordance with the buckled shape obtained in the WI test.

Yielding in the elements subjected to direct applied load was not observed until 94% of the failure load was reached, while the rest of the model remained elastic throughout. The yielding in these elements was detected at an early stage when S8R5

elements were used, and thus, the sensitivity of S8R5 and S4R5 elements differed. When buckling in the compression flange took place, a few elements in compression at mid-span yielded because of the large lateral displacements developed locally.

Changes in lateral deflection of the compression flange caused by the presence of thickened bearing stiffeners (two times the original thickness) or the general reduction of yield stress to $355N/m^2$ are shown in Figure 4.6.

4.3.7.3 Full structure with S4R5

To verify the boundary conditions used in modelling the half structures, a whole finite element model (shown in Figure 4.7), was simulated. The same mesh system as before was adopted. S4R5 shell elements were used together with B31 beam elements. (A more accurate model could have been simulated using eight-noded shell elements and three-noded beam elements but the data storage limit in the ABAQUS system would have been exceeded.) The ultimate moment capacity of the whole model was 28.6kNm, which was slightly lower than the values obtained in modelling one-half of the structure but was very close to the experimental value. The load-deflection curve is also shown in Figure 4.2.

However, the difference in buckling behaviour between the whole finite element model and the actual test was very pronounced. Instead of forming three half-waves in the final lateral buckling shape of the compression flange, two half-waves of different wavelengths were formed, as shown in Figures 4.8 and 4.9. The overall buckling mode is depicted in Figure 4.10. The difference in magnitude of the two half-waves may have been caused by the longitudinal restraint applied at one end of the girder rather than at mid-span. The coupling effect of the U-frames was obvious, together with the concave and convex bowing in the deflected cross-beams, as shown in Figure 4.10, which were also observed in the test.

4.4 FINITE ELEMENT IDEALISATION OF LEEDS TEST 1

4.4.1 Finite Element Mesh

In a similar manner to idealisation of the Welding Institute test, the finite element analysis of the Leeds Test 1 was performed by modelling the three-dimensional test piece as an assemblage of two-dimensional thin plates. To simplify the test arrangement, the loading cross-beams attached to the ends of the girders were again not included. Two models, one forming one-quarter of the test piece using a coarse mesh with S8R5 elements and the other forming one-half of the structure using more refined mesh with S4R5 elements (as shown in Figure 4.11) were created. An initial lateral displacement

of $\frac{\text{Span}}{1000}$ at mid-span was imposed on nodes situated along the longitudinal centre line of the compression flange.

4.4.2 Choice of Element.

There was no clear indication from the finite element modelling of the Welding Institute test of any benefit of using S8R5 as opposed to S4R5 in the presence of MPCs. Nevertheless, both types of element were employed again in modelling Leeds Test 1. As no cross-beam was used in the test, the top flange (which included steel deck), web, bottom flange, diaphragm(s) (if modelled) and stiffeners were all represented by two-dimensional shell elements. As a result, MPCs were not used in the idealisation of Leeds Test 1.

Symmetric geometry and loading of the girders about longitudinal and transverse planes of symmetry was exploited to save computer time and storage.

4.4.3 Load Application

In modelling one-quarter of the structure, the extension of the main span to form the cantilever loading arm was omitted and instead, a series of horizontal concentrated loads at the edge of the end cross-section of the girder were applied in order to create uniform bending moment over the main span. Although a ratio of 1:4:1 for loading on three adjacent nodes was used, local disturbances in the vicinity of the load were expected.

However, for the half structure, the cantilever loading arm was modelled and point loads were applied at the end of the cantilever to create uniform bending moment over the main span.

4.4.4 Material Modelling

From the results of actual tensile tests of the tin-plates used, the material properties employed in the finite element modelling was idealised as shown in Figure 3.13.

The stress-strain relationship could be described as tri-linear. The first yield stress was approximated as 142.73Nmm^{-2}. Followed by the effect of strain hardening, the second yield point reached 165.35Nmm^{-2}. The final ultimate yield stress was taken as 283.46Nmm^{-2}. Young's Modulus was estimated as 1.72×10^5Nmm^{-2} and Poisson's ratio of 0.26 approximately.

4.4.5 Type of Analysis

As in the case of the Welding Institute model, a non-linear large displacement analysis was carried out with automatic convergence control.

4.4.6 Boundary Conditions

In the modelling of one-half of the structure using S4R5 element, 'symmetrical' conditions about the longitudinal plane of the top deck plate were declared along the edges of the deck plate and two supporting diaphragms. Lateral movement of the girder at the loading positions was also restrained. Support positions were restrained against vertical displacement. Longitudinal movement was prevented for the nodes at mid-span to stop floating of the structure.

Boundary conditions used in the modelling of one-quarter of the structure were complicated because of the simulation of mid-span. If the final buckled shape is symmetrical, lateral movement of web and compression flange are permitted. As section warping would not develop for the symmetrical buckling mode, the only restraints applied was longitudinal restraints. Rotation of the nodes at mid-span about the transverse axis was limited to ensure zero slope of the vertical deflection at mid-span. However, if anti-symmetrical buckling occurred, the lateral and longitudinal movements of the nodes along the depth of the section at the mid-span were restricted. Vertically, nodes at the mid-span section were left free to displace although the slope of deflection was kept to zero. The possibility of warping of the section at compression flange level was also considered. A series of linear equations were set to enforce the nodes of the compression flange at mid-span to be in line with each other.

4.4.7 Finite Element Results

4.4.7.1 Quarter Model with S8R5

In the case of simulation of symmetrical buckling mode, the ultimate load obtained from finite element analysis was only 439.25Nm which was 29% lower than the test result. The load-deflection curve is plotted in Figure 4.12. Severe yielding in edge elements due to load concentration developed and no further loading could be absorbed.

A simple single quarter-wave formed gradually in the half-span of the girder modelled based on a half parabola with amplitude $\frac{1.32}{1000}$ m at mid-span declared initially for lack of straightness of the girder. Therefore, in terms of the whole span, a symmetrically deflected shape of one single half-wave about mid-span is implied.

The mode of buckling which developed was strongly affected by the boundary conditions declared for mid-span. When constraint at mid-span was altered to promote the formation of a anti-symmetrical buckling mode, a single half-wave was formed despite of the fact that the same initial lack of lateral straightness was adapted. The ultimate load achieved was much reduced to 343.20Nm which was only approximately half of the ultimate moment reached in the test.

Although the magnitude of the final or total displacement (which was comparable to the lateral displacement measured during the test) was small, the load-displacement curves plotted showed that lateral buckling had occurred in the compression flange.

4.4.7.2 Half Model with S4R5

The ultimate failure load reached by the finite element analysis model was 669.8Nm which was 8% higher than the test failure load. Load-deflection curve is plotted in Figure 4.13. Lateral buckling in the compression flange was not clearly demonstrated until the model could no longer take any perceptible increase of load. Large spread of yield and thus distortion of web at mid-span led to an irregular buckled shape in the compression flange as shown in Figure 4.14.

At the initial stage of the loading process, the lateral displacement of the central line of the compression flange (see Figure 4.15(a)) followed the initial lack of straightness of a single parabola with amplitude $\frac{1.32}{1000}$ m at mid-span. During the increase of load, the analysis results indicated that some ripples had appeared in the compression flange (see Figure 4.15(b)). As the buckling load approached, a general single half-wave (still with the presence of the ripples) with maximum amplitudes of 1.06mm at mid-span was formed. However, the development of this formation was checked by an increased rate of displacement at other nodal points. Eventually, at failure, a seriously distorted mode was obtained as shown in Figures 4.14.

4.5 FINITE ELEMENT IDEALISATION OF LEEDS TEST 2

4.5.1 Finite Element Mesh

Treating the top and bottom flanges of the test girders as rigid beams and the webs as thin shells, a relatively coarse finite element model was generated for idealisation of Leeds Test 2 as shown in Figure 4.16. However, a more detailed mesh (see Figure 4.17, with mesh refinement) was also prepared for analysis. The mesh adopted in the modelling of half of the Test 1 structure was modified and used because of the geometric similarity of the two test pieces. In both of the Test 2 simulations, the mesh

was arranged in such a way that the point load was located at a nodal point. The difference in results was compared and discussed.

An initial lateral displacement of $\frac{\text{Span}}{1000}$ was introduced into the compression flanges before load was applied.

4.5.2 Choice of Elements

In both cases of modelling, four-node shell elements, in conjunction with two-node beam elements, were employed. By representing the flanges as beam segments and the webs as thin shells, the modelling was much simplified. As in the modelling of cross-beams, transverse web stiffeners were also formed using beam elements. On the other hand, in the refined mesh, only cross-beams were considered as beam elements, while all other components of the girder were modelled using S4R5 shell elements.

4.5.3 Load Application

Two point loads were applied at a distance of $\frac{6}{7}$ span from the LH side support, which was the exact position of the point loads in Test 2, to generate a triangular bending moment diagram in the full model. In the actual test, point loads were applied at two positions of the span, one coinciding with an end support (See Chapter 3). This reduced the eccentricity of the loading beam. One point load, divided in the ratio of 1:2:1, was exerted on three nodes of two top flange elements to produce the same bending moment distribution in the finite element model of the one-half structure.

To simulate the test load conditions more precisely, another point load coinciding with the supporting point at the far end was added in the one-half structure model. This additional load point should not alter the pattern of bending moment diagram as it was originally intended. The effect, owing to the difference between these two loading cases, will be discussed later.

4.5.4 Material Modelling

Since the type of plate used in Leeds Test 1 was also employed in Leeds Test 2, the material properties used in the modelling of Leeds Test 2 were taken to be identical to those used in the modelling of Leeds Test 1.

Material properties of cross-beams were not tested. A yield stress of $275 Nmm^{-2}$, which is the typical yield stress for mild steel was taken for the entry of material card for these cross-beams.

4.5.5 Boundary Conditions

In both models, in order to simulate the supporting conditions in the laboratory, nodes at support positions were simply supported and laterally restrained whereas at the loading positions, only lateral restraints were imposed.

4.5.6 Type of Analysis

The same type of non-linear large displacement analysis, as used in the modelling of the WI test and Leeds Test 1, was employed with automatic convergence control.

4.5.7 Finite Element Results

4.5.7.1 Full Model with Flanges Modelled by Beam Elements

The maximum load achieved was 356.98Nm. This was significantly lower in comparison with the 631.25Nm ultimate load capacity of the test girder. The load-displacement relationship is plotted in Figure 4.18. The difficulty in obtaining a convergent solution is clearly evident in the curve when the buckling load was approached.

The sudden large increase in lateral displacement of the node 0.125m away from the load point is also illustrated in the load-displacement relationship. The changing lateral displacement at the centre line of the compression flange, is traced in Figure 4.19 and the final deformed shape is shown in Figure 4.20.

It was observed from the plots and the node outputs that the lateral displacement of the two compression flanges were virtually equal in magnitude but opposite in direction. Thus, the coupling effect of the U-frame bracing was clearly demonstrated in the finite element analysis, although this effect was not observed in the laboratory testing. In the latter, the two compression flanges basically deflected in the same direction (probably owing to uneven seating, initial distortion of the test piece or other unaccountable errors which occurred in the testing process as discussed in Chapter 3).

4.5.7.2 Half Model with S4R5 Elements

(a) With a more detailed mesh and one loading point at $\frac{1}{7}$ from RH support, the ultimate load capacity of the structure improved to 472.50Nm which was now 25% lower than the experimental test value of 631.25Nm. The load-deflection curves are shown in Figure 4.21. No convergence problem was encountered. The failure load was reached fairly rapidly. There was no yielding in any of the elements throughout the loading process, even after buckling.

The section at which the buckling occurred was different to that in the full model using beam elements and in the test. The maximum amplitude was approximately 0.3m from the load points, ie, between the first cross-beam and the second and the direction of buckling was opposite to the full model. The overall buckled shape is illustrated in Figure 4.22 and the lateral displacement of the nodes on the longitudinal central line of the compression flange and the out-of-plane deflection of the web nodes in Figure 4.23.

The reactions at the supports, were found to agree with the expected ratio of 1:6 as a consequence of the loading position.

(b) When the loading conditions were altered to simulate the laboratory test more accurately, ie, with two load points, there was not much increase in the load capacity of the structure. The ultimate moment achieved was 473.14Nm. However, the final buckled shape was a reverse of the buckled shape obtained from the modelling with only one point load. This sudden change of direction of deflection is clearly shown in the load-deflection curve plotted in Figure 4.21. Despite the same initial imperfection (in terms of magnitude and direction) set out before loading commenced, the difference in the buckled shapes showed the difficulty in prediction of the buckled mode of girders.

4.6 DISCUSSION

The results from finite element analysis of the three laboratory tests are summarised in Table 4.1.

4.6.1 Modelling of the Welding Institute Test

Notwithstanding the fact that, as one of the earliest models formed for the modelling of experimental testing, rather coarse meshes were generated, the bending stiffness of the test piece had been represented fairly accurately by the finite element models. Therefore, it led to agreeable results with the laboratory findings despite the difference in the initial imperfection of the structures.

From the modelling of one-half of the WI test and by adopting the same mesh used in one-half modelling but with different types of element, it was felt that the disadvantage of applying larger number of MPCs for the interconnection between shell and beam elements overwhelmed the advantage of using higher order elements such as S8R5 and B32, which is theoretically, supposed to produce more accurate results. The use of MPCs might enhance the stiffness of the structure and result in a much higher value of the ultimate load capacity of the model. Otherwise, the failure load of the experimental test piece was reached at an earlier stage than it was supposed to be.

When the full model (using the same mesh as for the half structure model) was employed, there was close agreement in the ultimate load capacity of the structure in spite of disagreement in the ultimate buckled modes.

Table 4.1 Summary of ABAQUS modelling results of experimental tests in comparison with design and tests values

JOB	Element used	ABAQUS M_{ABQ} (Nm)	BS5400 M_D (Nm)	Experiments M_{exp} (Nm)	$\frac{(M_{ABQ}-M_{exp})}{M_{exp}}$ %
WI-HALF	S8R5	$36.0x10^3$			+24.1
WI-HALF	S4R5	$30.1x10^3$	$14.98x10^3$	$29.0x10^3$	+3.8
WI-FULL	S4R5	$28.6x10^3$			-1.3
LT1-QRT*	S8R5	439.25	363.74	618.75	-29.0
LT1-HALF	S4R5	669.8			+8.3
LT2-FULL	B31	356.98	340.42	631.25	-43.4
LT2-HALF	S4R5	472.5			-25.1

*With symmetrical boundary condition declared at mid-span

Thus, comparison between results from the half model and the full model indicated that additional constraints might have been applied to the half model. In the full model, the end nodes of the cross-beams in the longitudinal plane of symmetry displaced very little while in the case of half model, no displacement was allowed for these nodes because of the declaration of boundary conditions enforcing the symmetrical behaviour of the twin girders.

Other factors, which could have a significant effect on the load capacity of the structure are the presence of residual welding stresses and local strain hardening. However the latter factor should increase the ultimate load capacity of the test piece. Also, the large initial displacement in one of the girders may have promoted earlier collapse. Further investigation is required to study the effect of unequal initial lateral displacements in the compression flanges of the girders.

4.6.2 Modelling of the Leeds Test 1

Fairly good correlation between experimental and finite element buckling loads was obtained in modelling of one-half of the test piece, using the actual material properties obtained from tensile tests. No MPCs were used in the simulation.

However, the difference in final buckled modes may well have been caused by the difference in initial lack of straightness of the two compression flanges. The initial distortion of the test piece due to stresses built-in during manufacture (which was comparatively significant because of the thinness of plate used) was not considered in the finite element simulation.

The modelling of one-quarter of the structure was not successful because of the occurrence of local force concentration and distortion which prevented the structure from achieving its buckling load capacity.

4.6.3 Modelling of the Leeds Test 2

The modelling of one-half structure using S4R5 elements was considered as satisfactory even though ultimate load capacity was rather low in comparison with the test result (the possibilities of causing the unexpectedly high load capacity of the test piece were discussed in Chapter 3). The mode of buckling was similar to the failure mode of the compression flanges in the test except that the coupling effect of the U-frames was not demonstrated clearly in the actual test as a consequence of initial distortion or uneven seating at the supports.

Although the coarse mesh in the full model using beam elements as flanges and stiffeners did not produce a value of buckling load close to that of the test piece, the analysis gave clear evidence of the influence of U-frame bracing.

As in the case of Leeds Test 1, the presence of residual stresses and actual initial imperfection of the structures were not taken into account in these finite element modelling.

4.6.4 Conclusion

Finite element modelling of the three experimental tests using the ABAQUS package has been presented. It is clear that the package can produce valid analyses of the test models with first order elements (S4R5 and B31). Therefore, it will be used in the study of a range of practical steel girder bridges in which the instability of compression flanges and load capacity of girders braced by U-frames will be the focus point of this study. Although the effect of actual initial imperfection and presence of residual welding stresses may not be included in the finite element modelling, the buckling behaviour of the girders and the function of U-frames will be revealed through the numerical modelling.

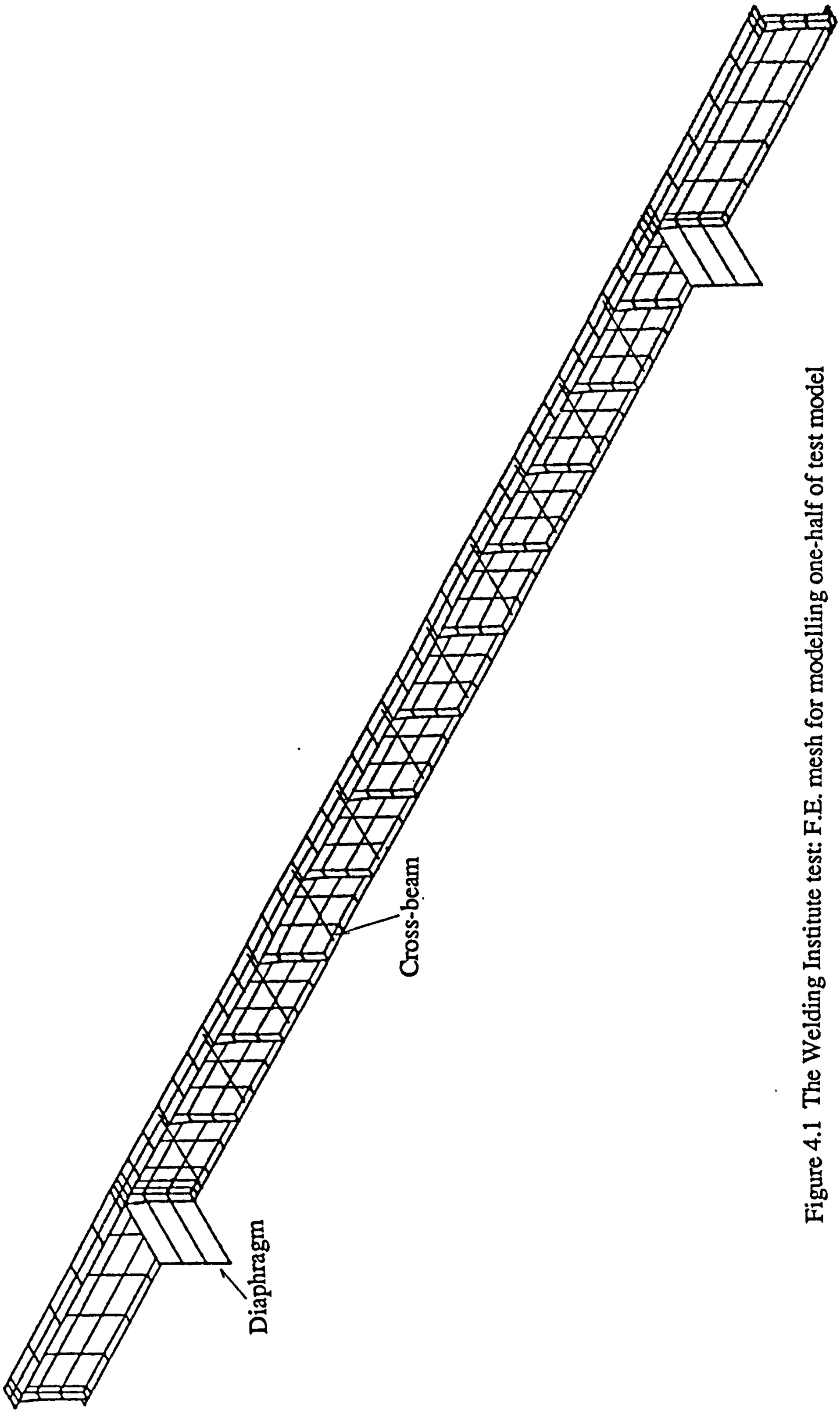

Figure 4.1 The Welding Institute test: F.E. mesh for modelling one-half of test model

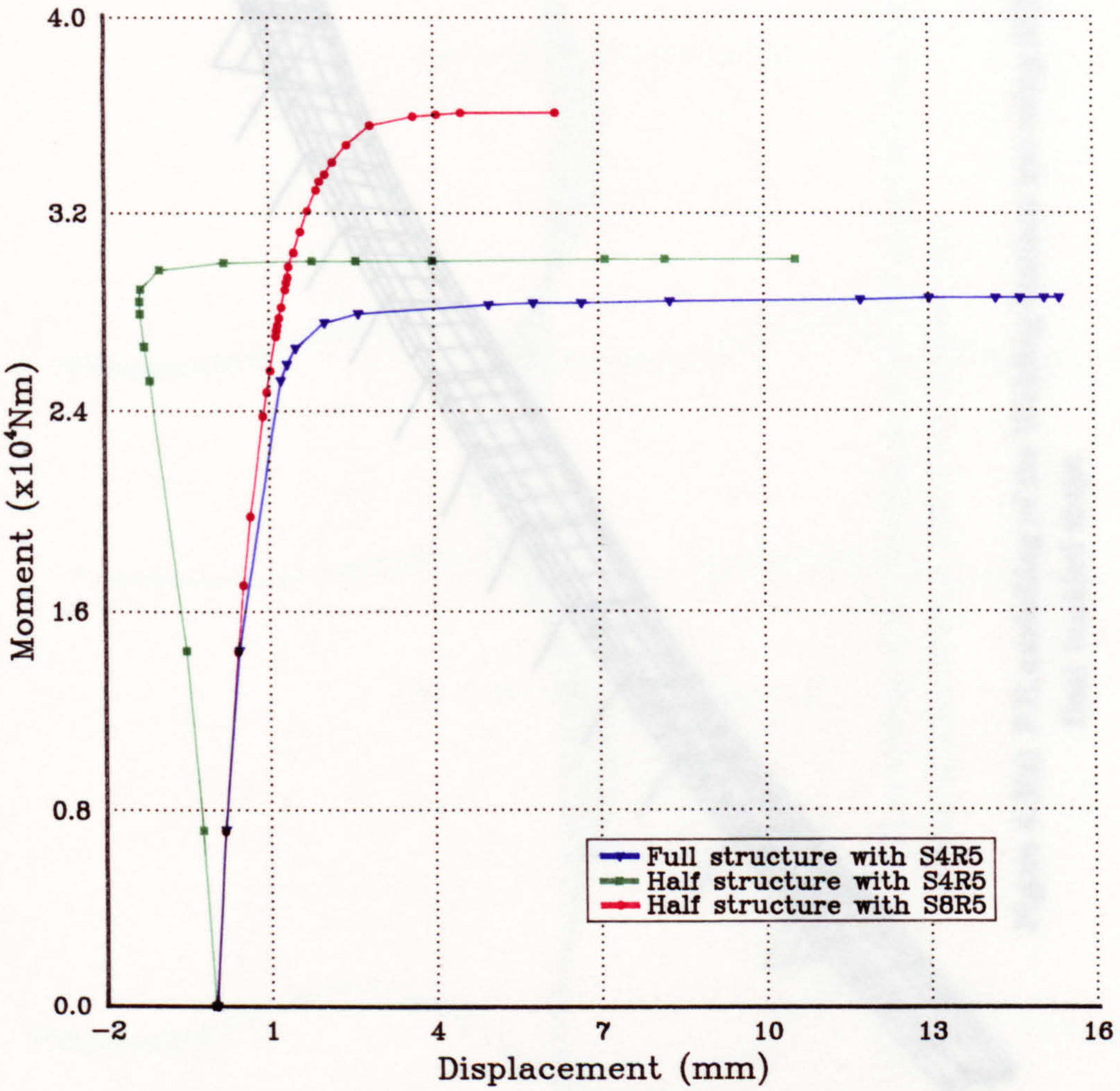

FIgure 4.2 F.E. modelling of the Welding Institute test: load v. lateral displacement relationship using different elements

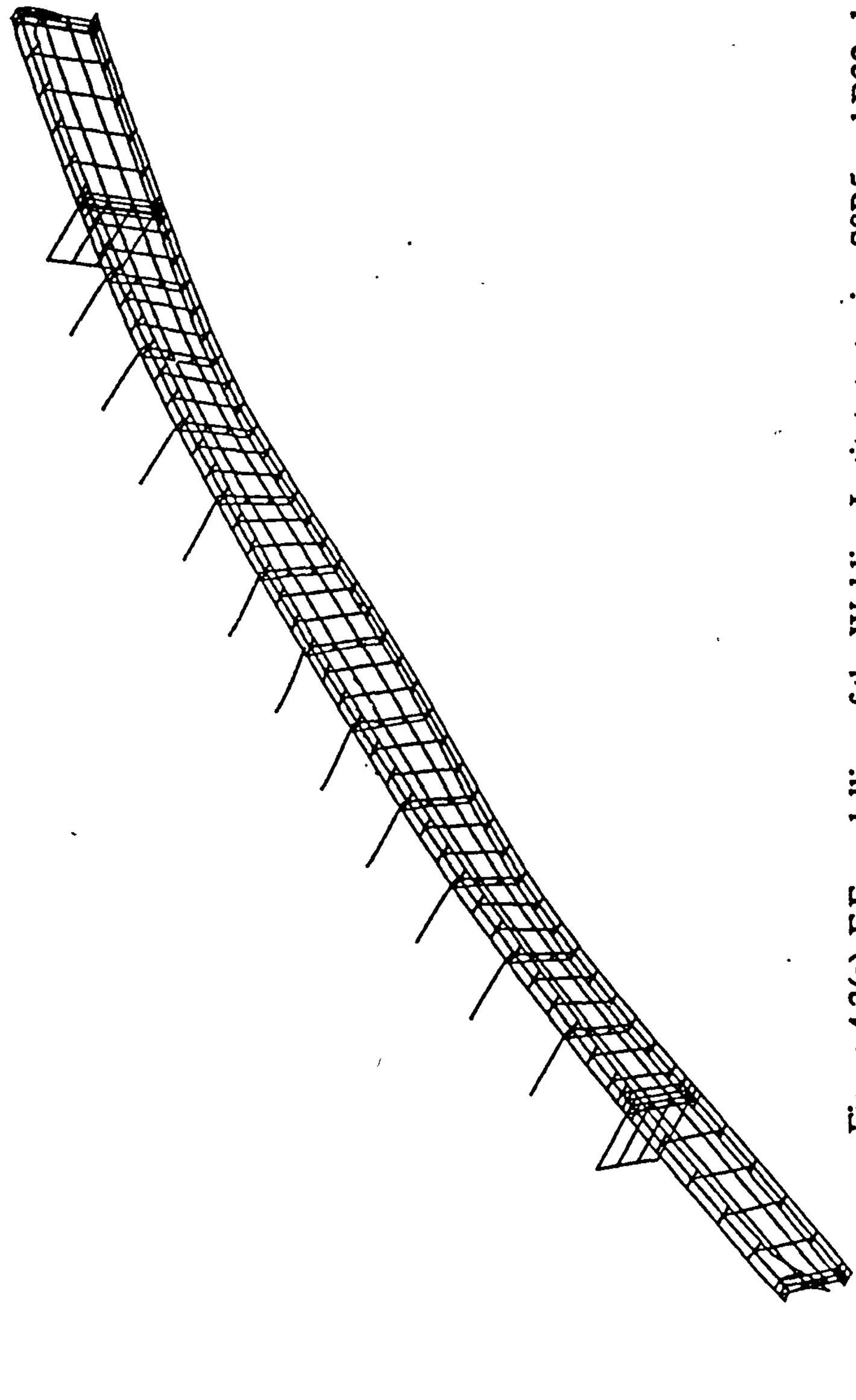

Figure 4.3(a) F.E.modelling of the Welding Institute test using S8R5 and B32 elements: final buckled shape

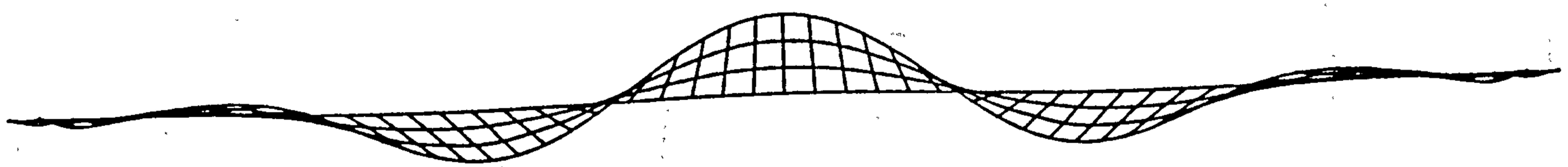

Figure 4.3(b) F.E.modelling of the Welding Institute test using S8R5 and B32 elements: final buckled shape of girder web in plan view

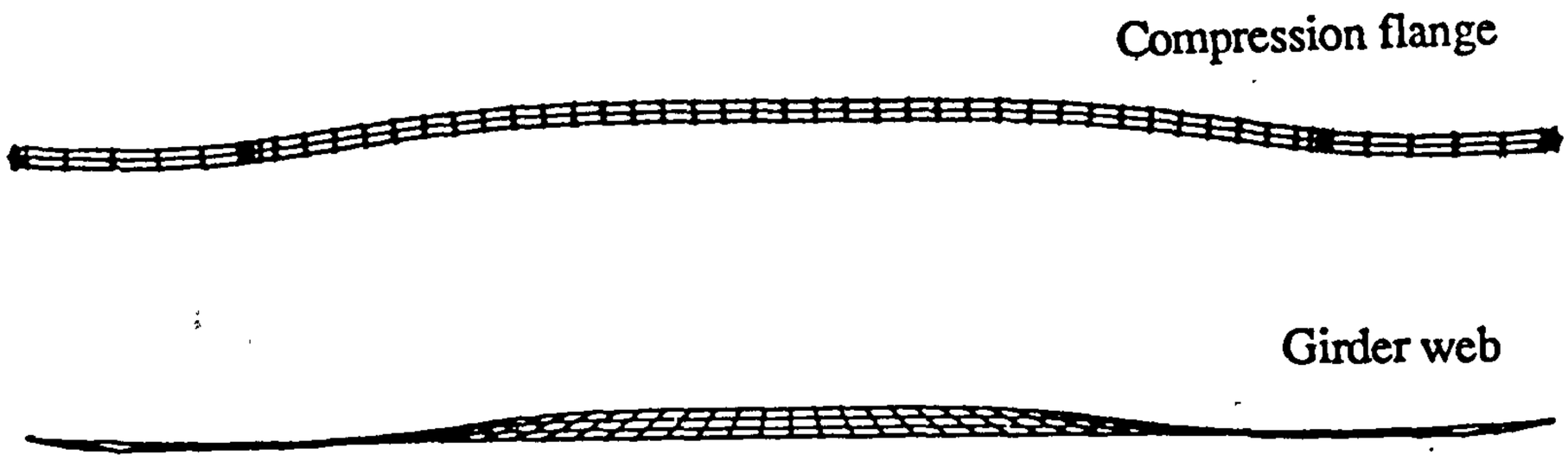

(a) At 95% of buckling load

(b) At 99.5% of buckling load

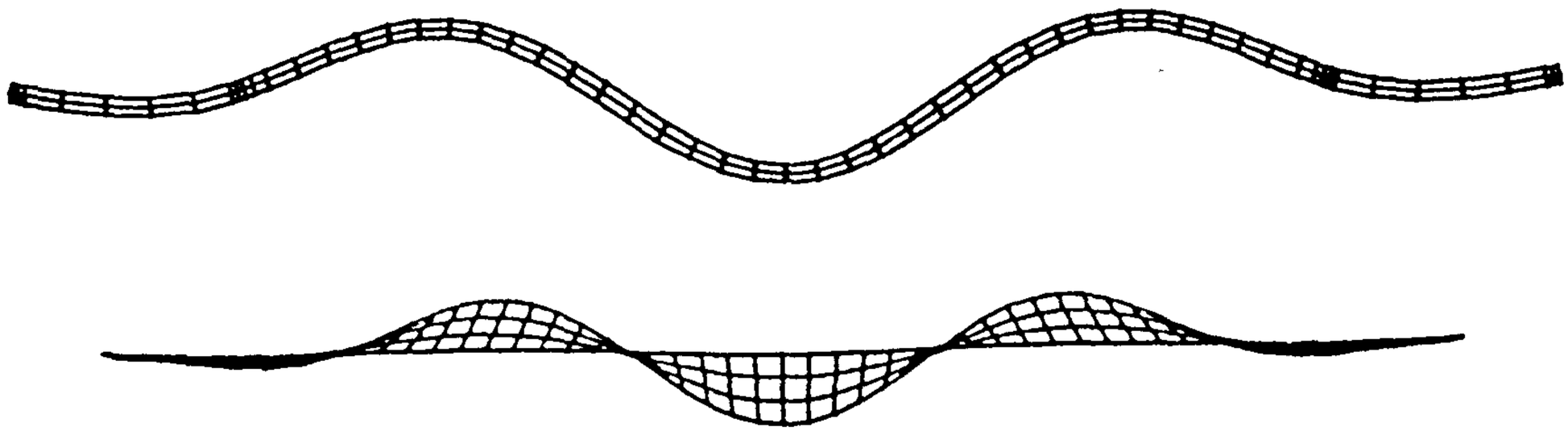

(c) At buckling load

Figure 4.4 F.E.modelling of the Welding Institute test using S4R5 and B31 elements: variation of lateral displaced shapes

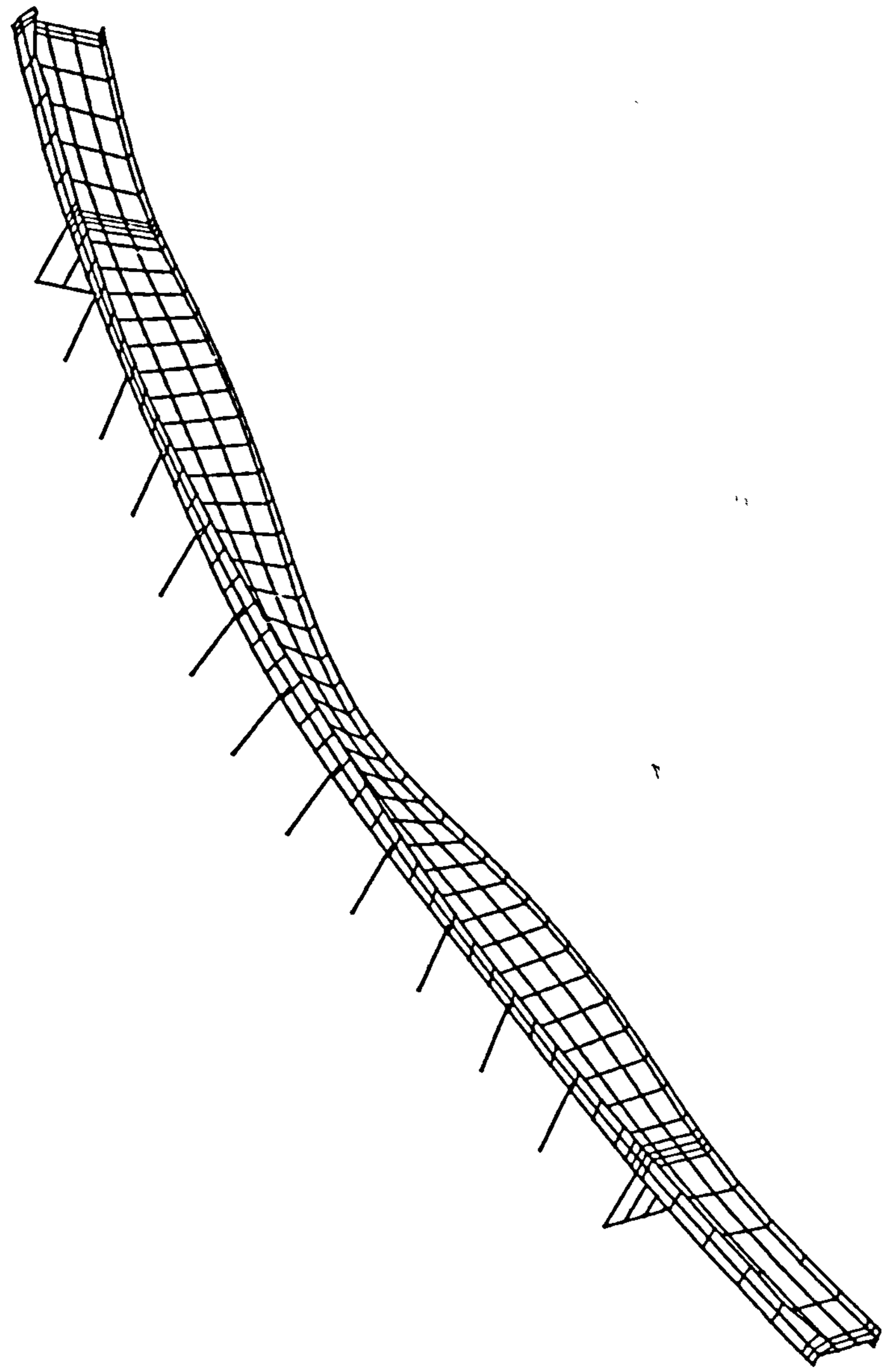

Figure 4.5 F.E.modelling of the Welding Institute test using S4R5 and B31 elements: final buckled shape

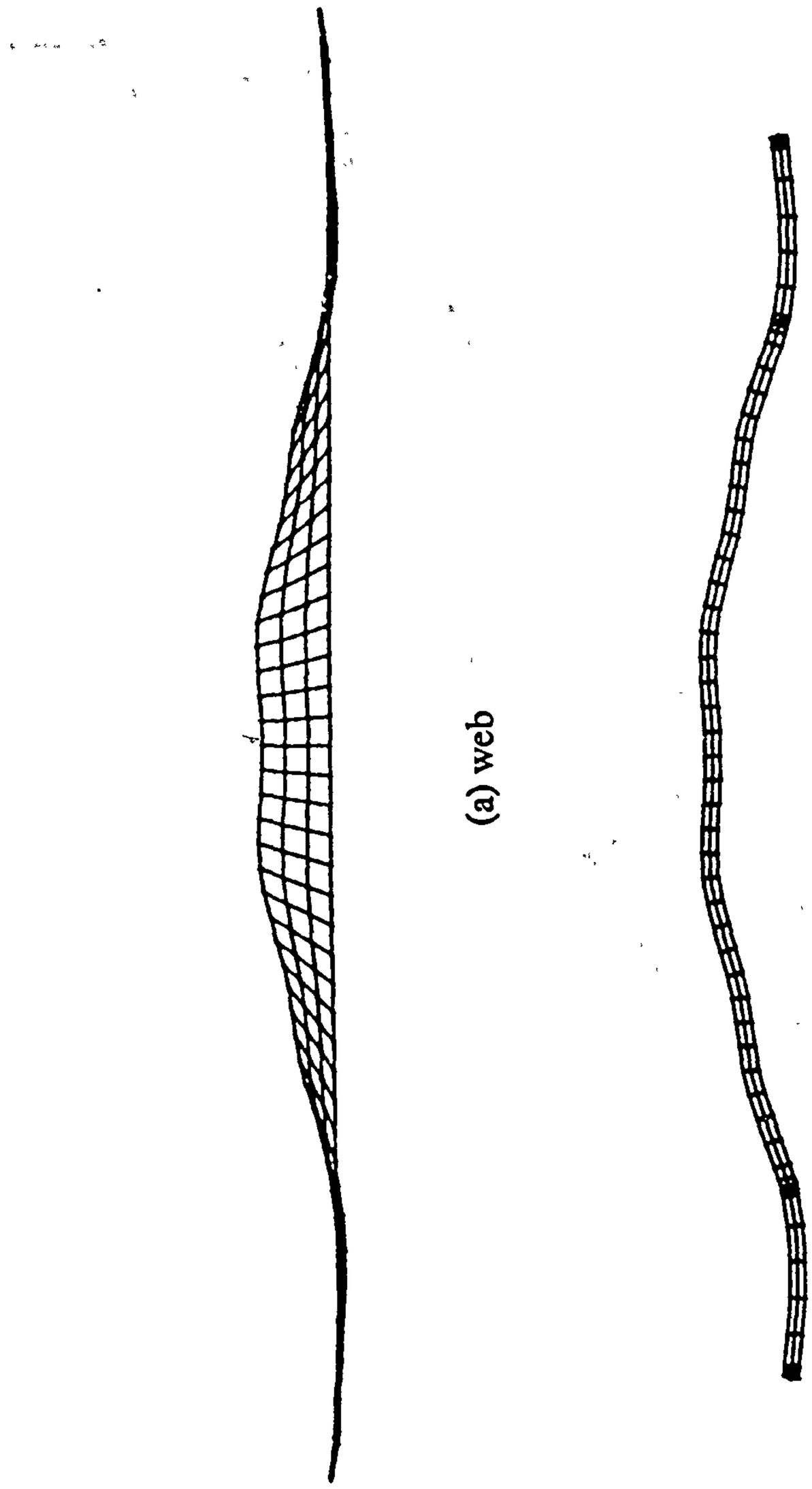

(a) web

(b) compression flange

Figure 4.6 F.E.modelling of the Welding Institute test using S8R5 and B32 elements with thickened bearing stiffeners: final buckled shape in plan view

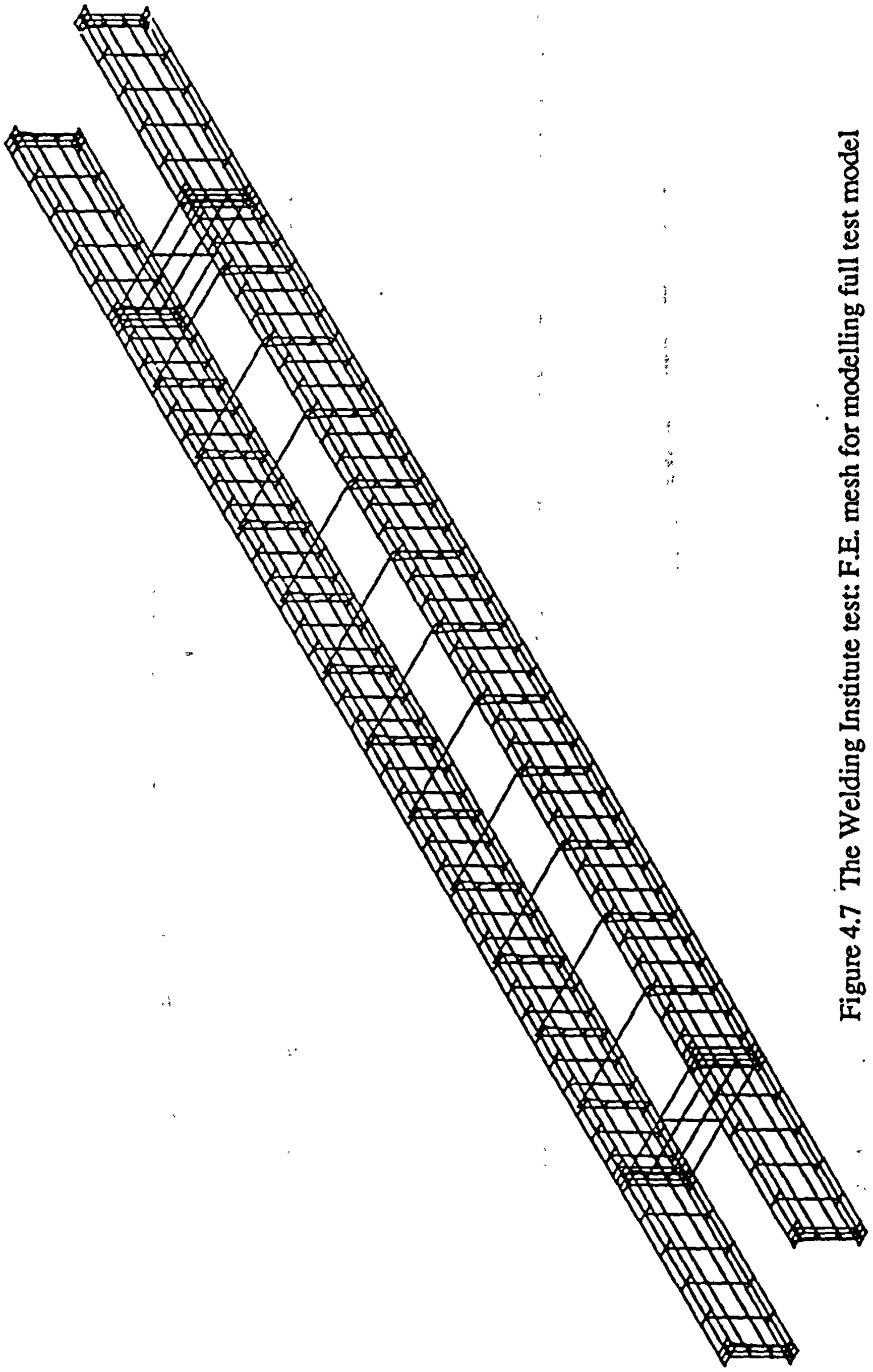

Figure 4.7 The Welding Institute test: F.E. mesh for modelling full test model

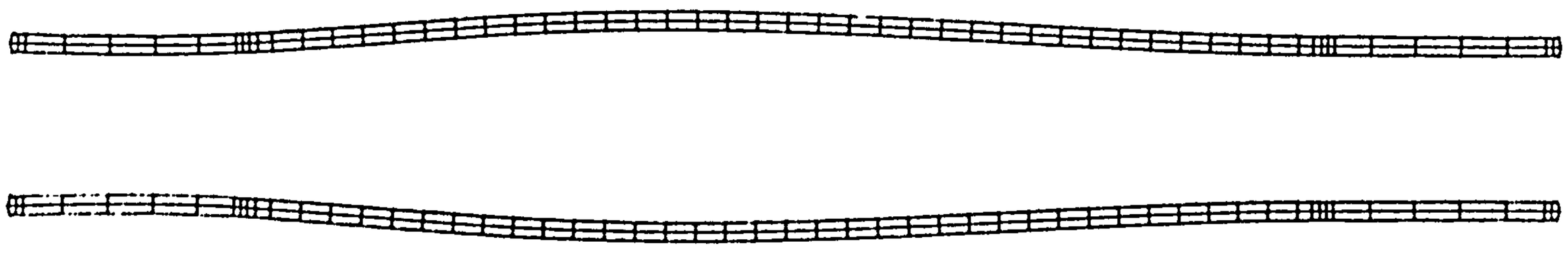

(a) compression flange

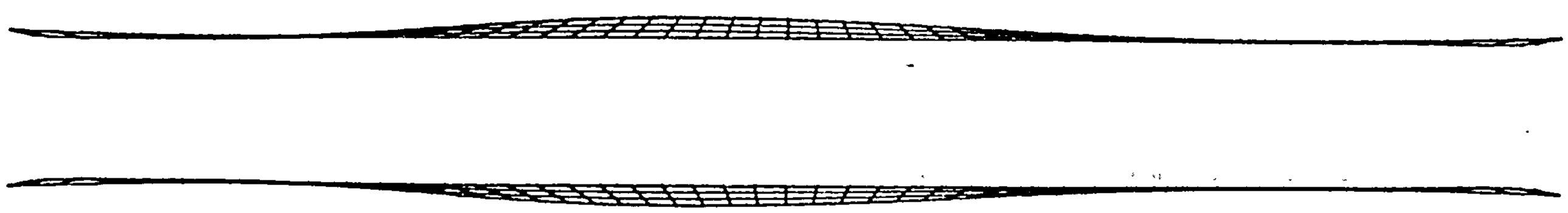

(b) girder web

Figure 4.8 F.E.modelling of the Welding Institute test (full model using S4R5 and B32 elements): lateral displaced shape at 90% of buckling load

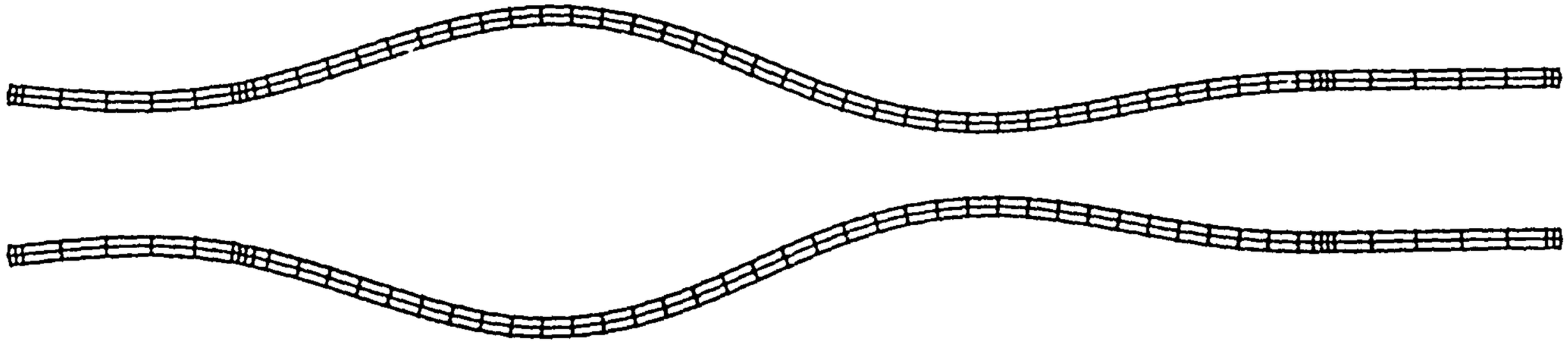

(a) compression flange

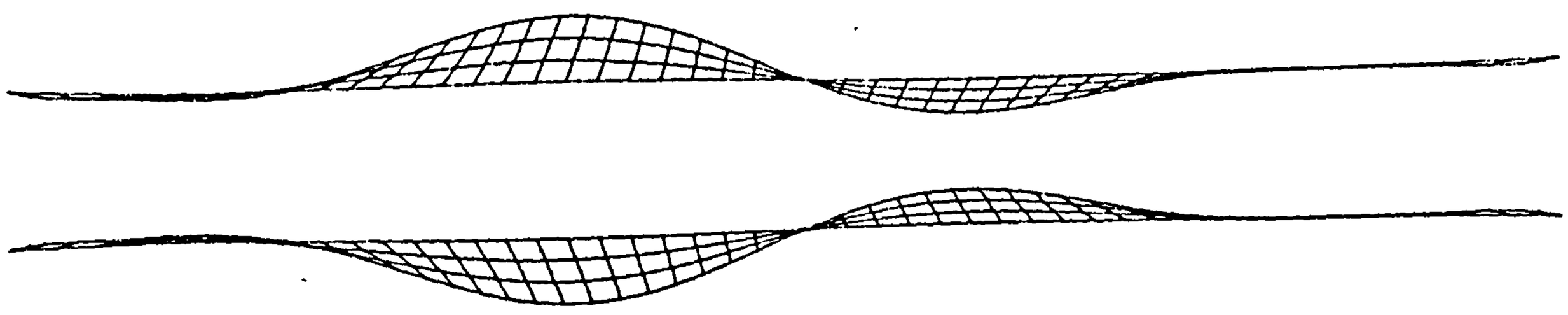

(b) girder web

Figure 4.9 F.E.modelling of the Welding Institute test (full model using S4R5 and B32 elements): final displaced shape in plan view

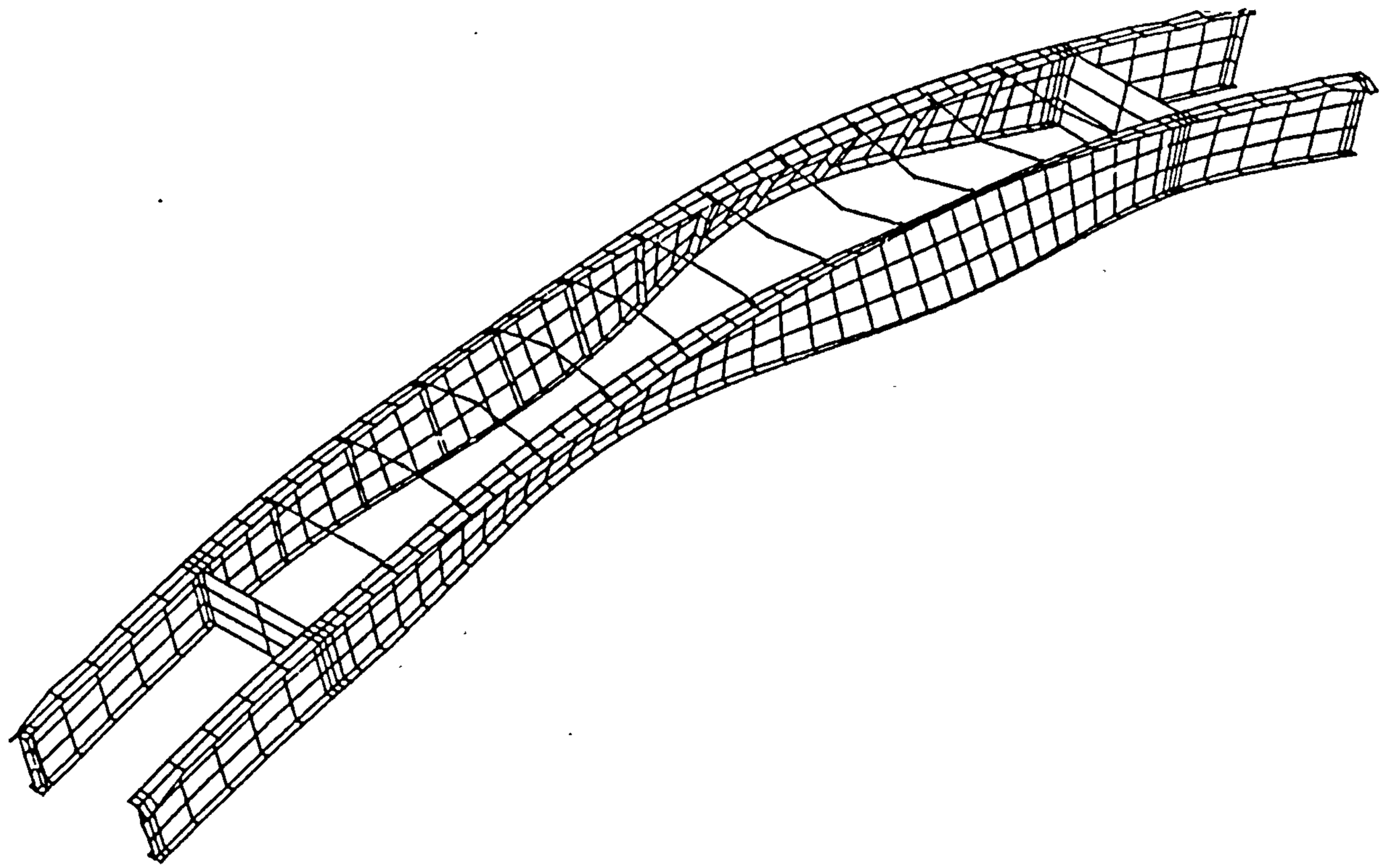

Figure 4.10 F.E.modelling of the Welding Institute test (full model using S4R5 and B32 elements): final buckled shape

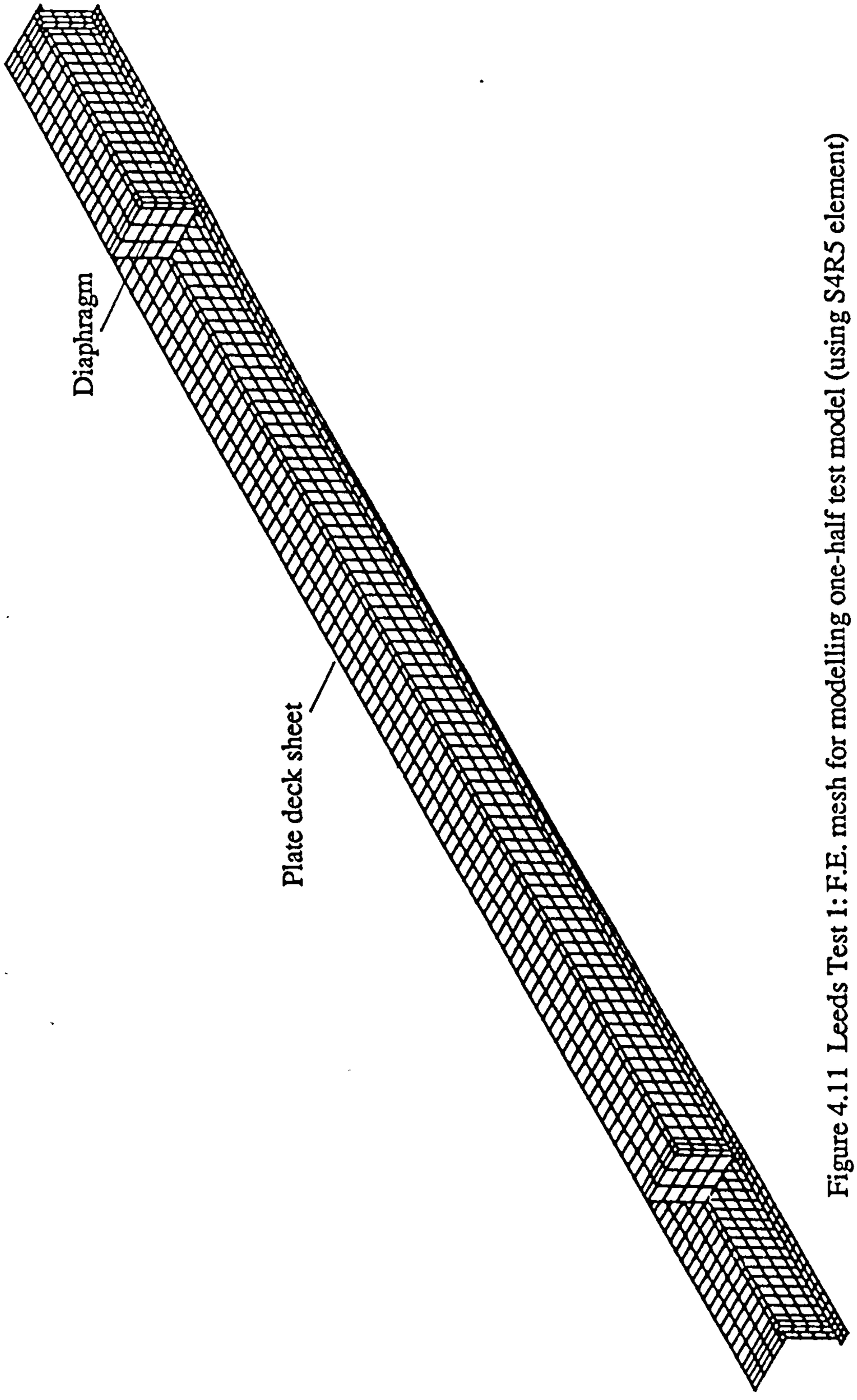

Figure 4.11 Leeds Test 1: F.E. mesh for modelling one-half test model (using S4R5 element)

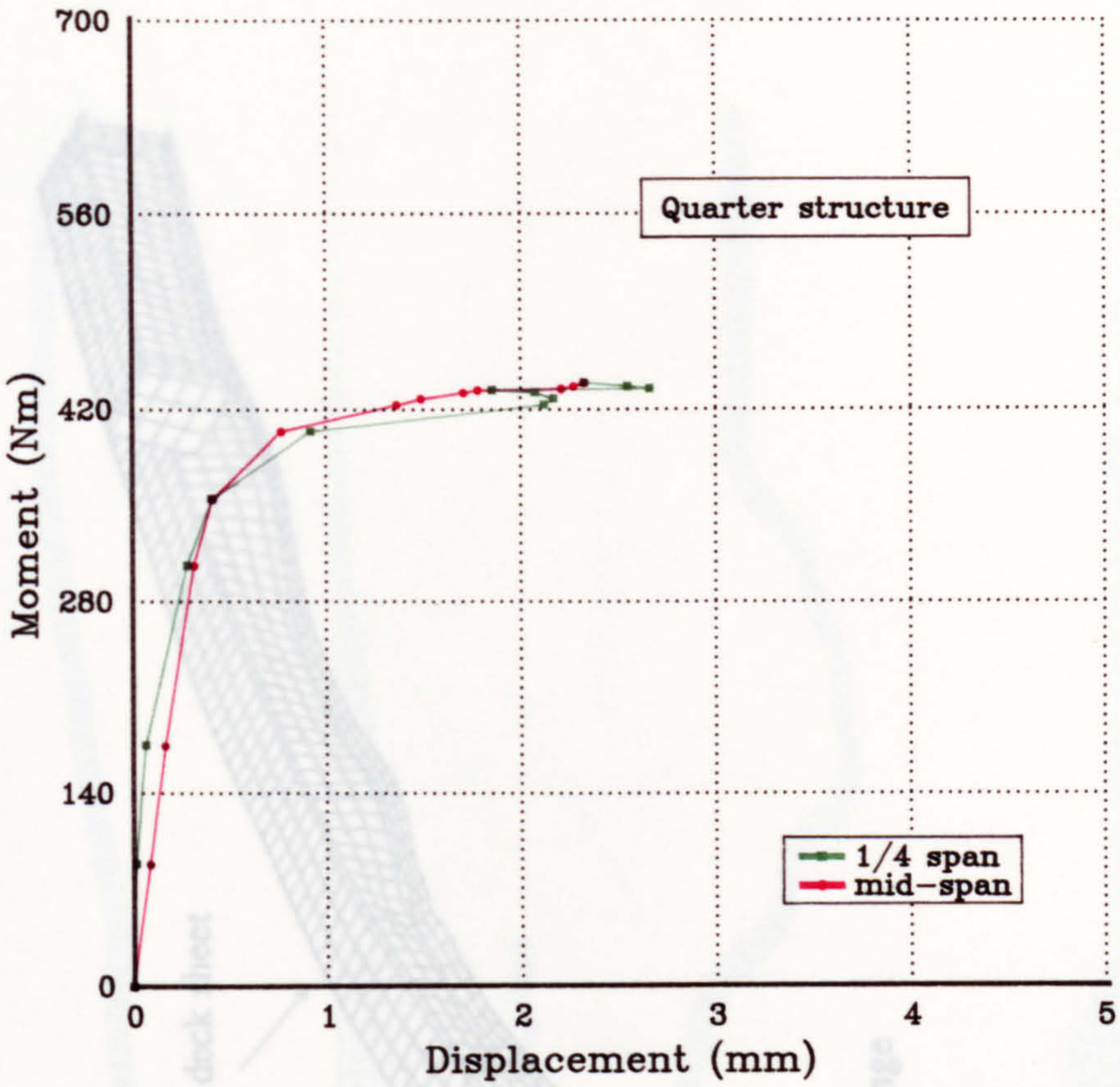

Figure 4.12 F.E. modelling of Leeds Test 1: Load v. lateral displacement relationship using S8R5 elements

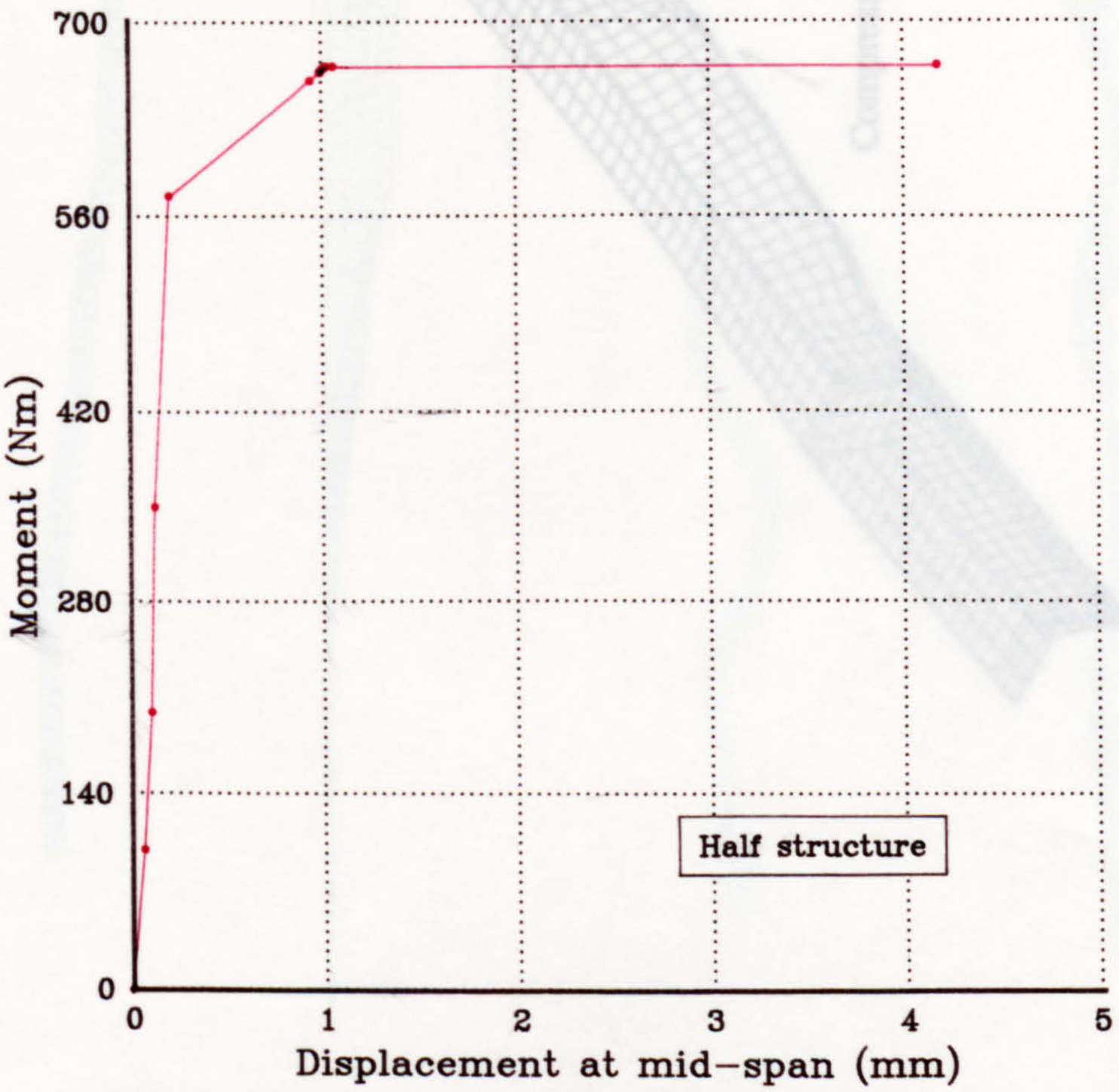

Figure 4.13 F.E. modelling of Leeds Test 1: load v. lateral displacement relationship using S4R5 elements

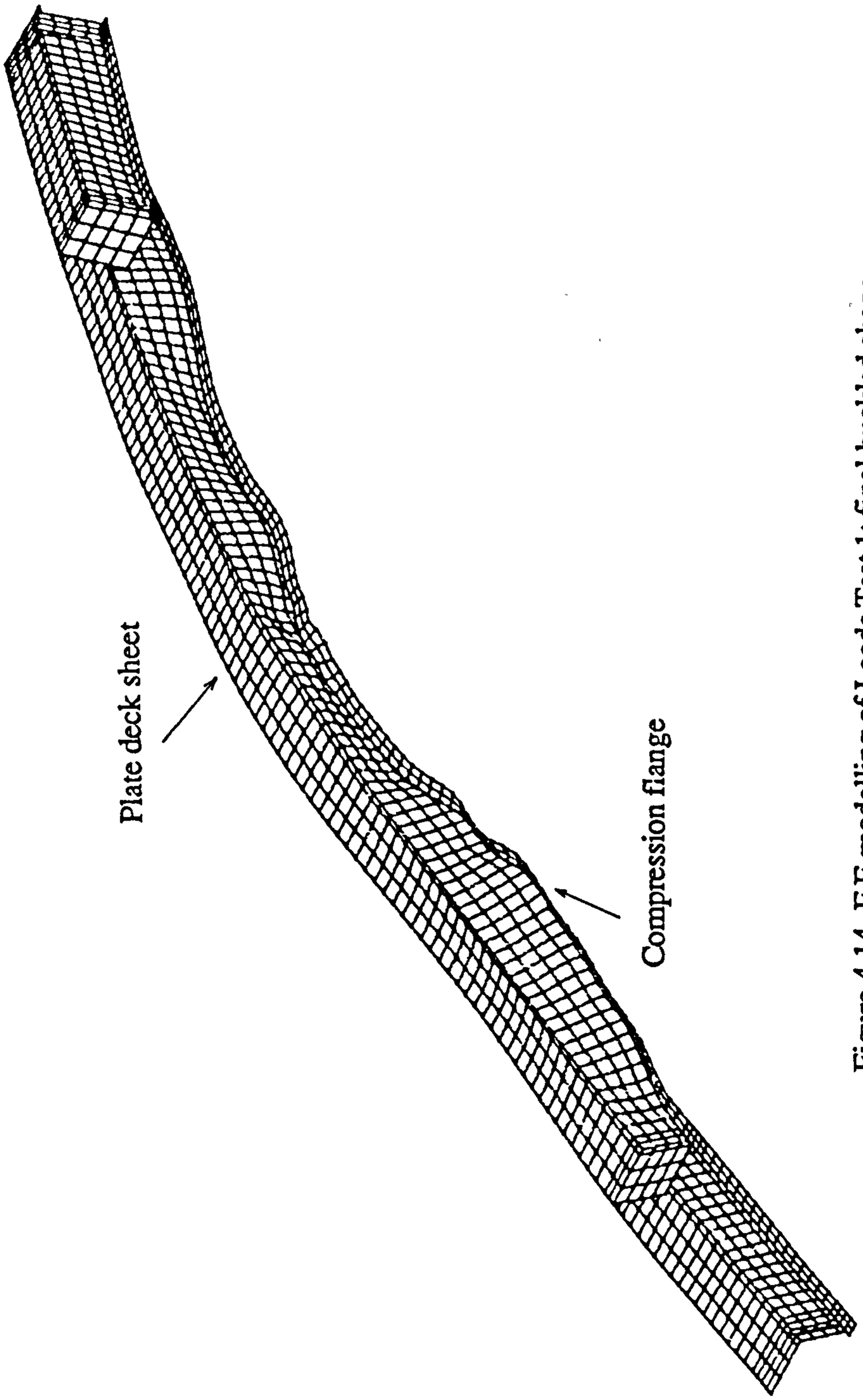

Figure 4.14 F.E.modelling of Leeds Test 1: final buckled shape

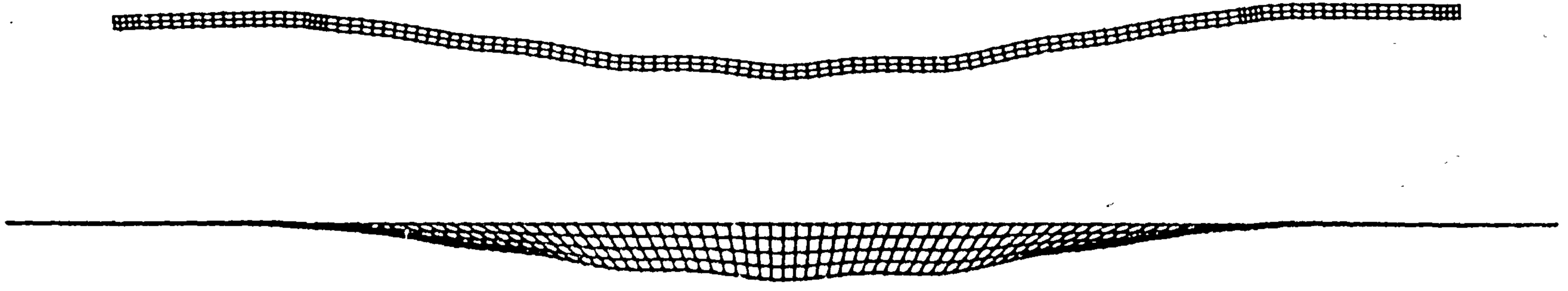

(a) 99.9% of buckling load

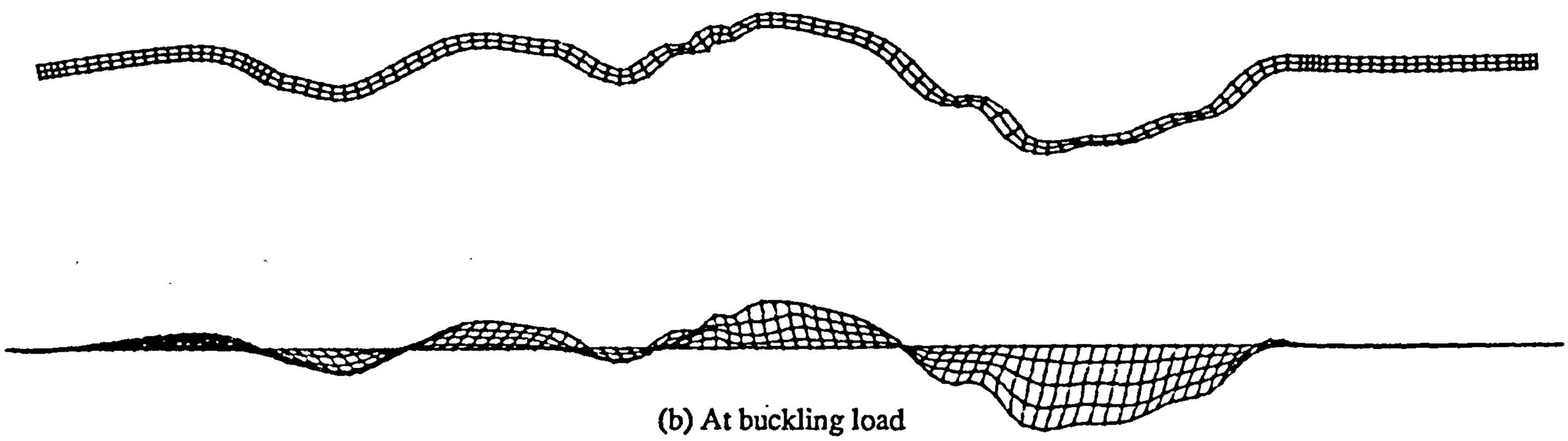

(b) At buckling load

Figure 4.15 F.E.modelling of Leeds Test 1: variation of lateral displaced shapes in plan view

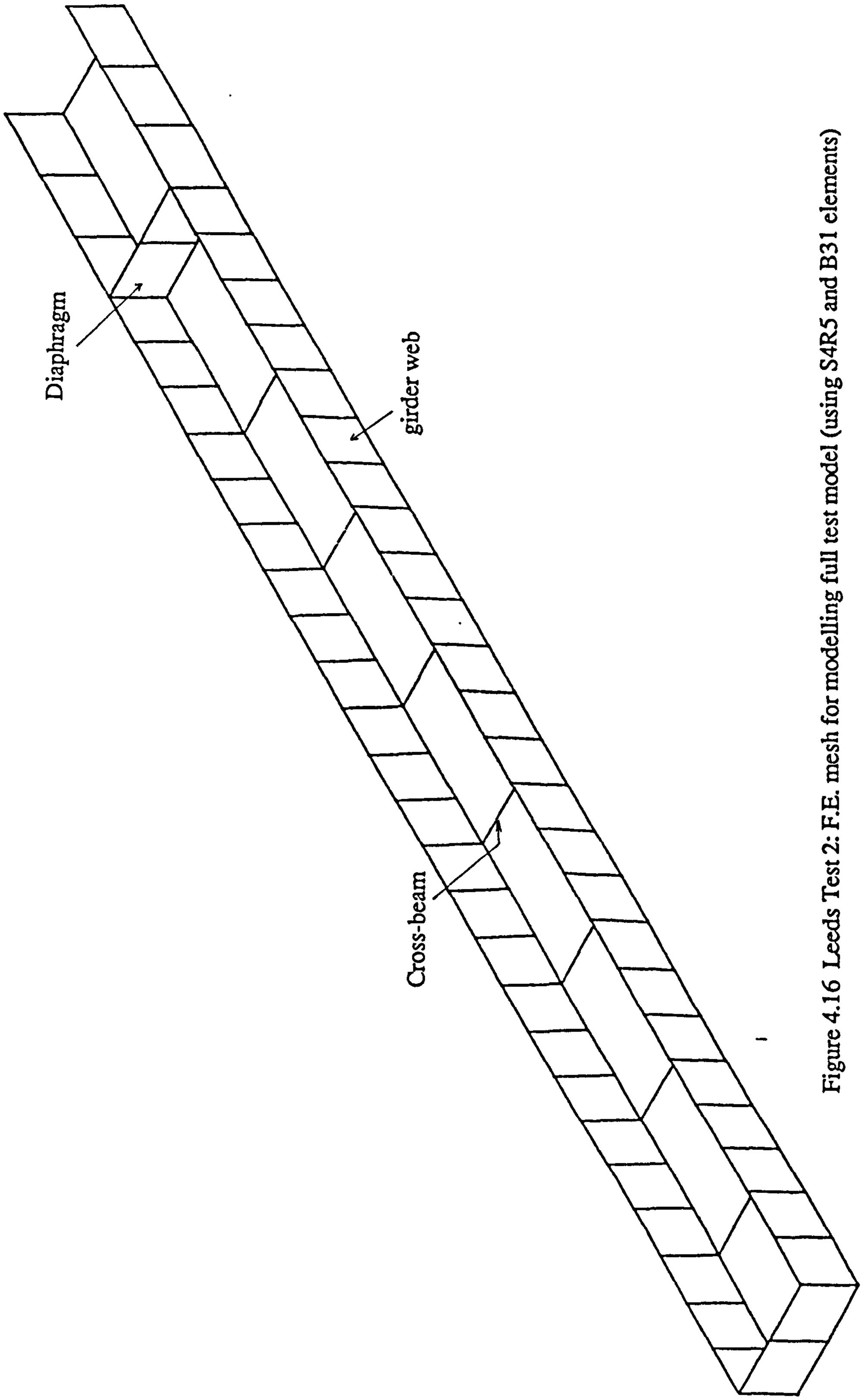

Figure 4.16 Leeds Test 2: F.E. mesh for modelling full test model (using S4R5 and B31 elements)

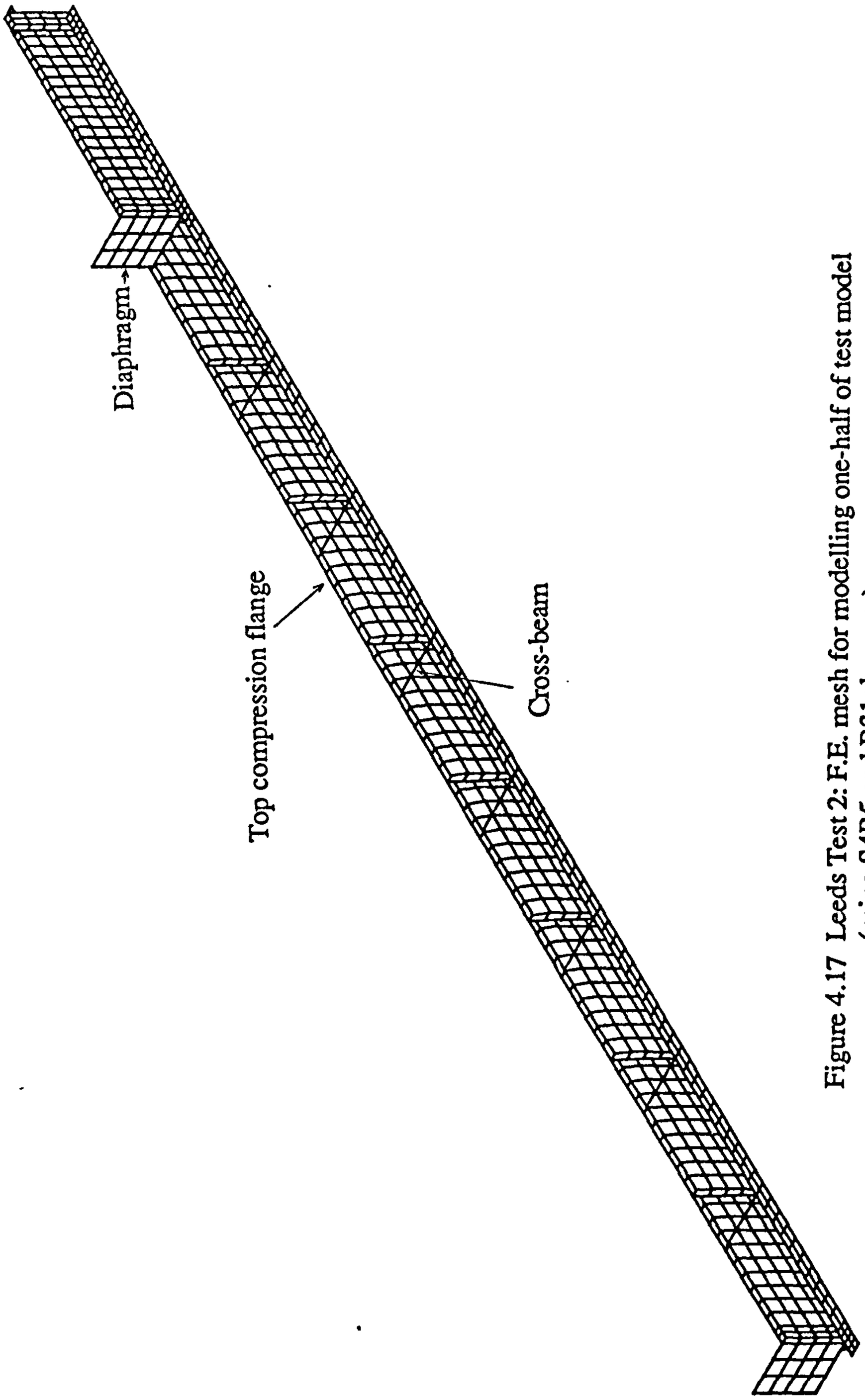

Figure 4.17 Leeds Test 2: F.E. mesh for modelling one-half of test model (using S4R5 and B31elements)

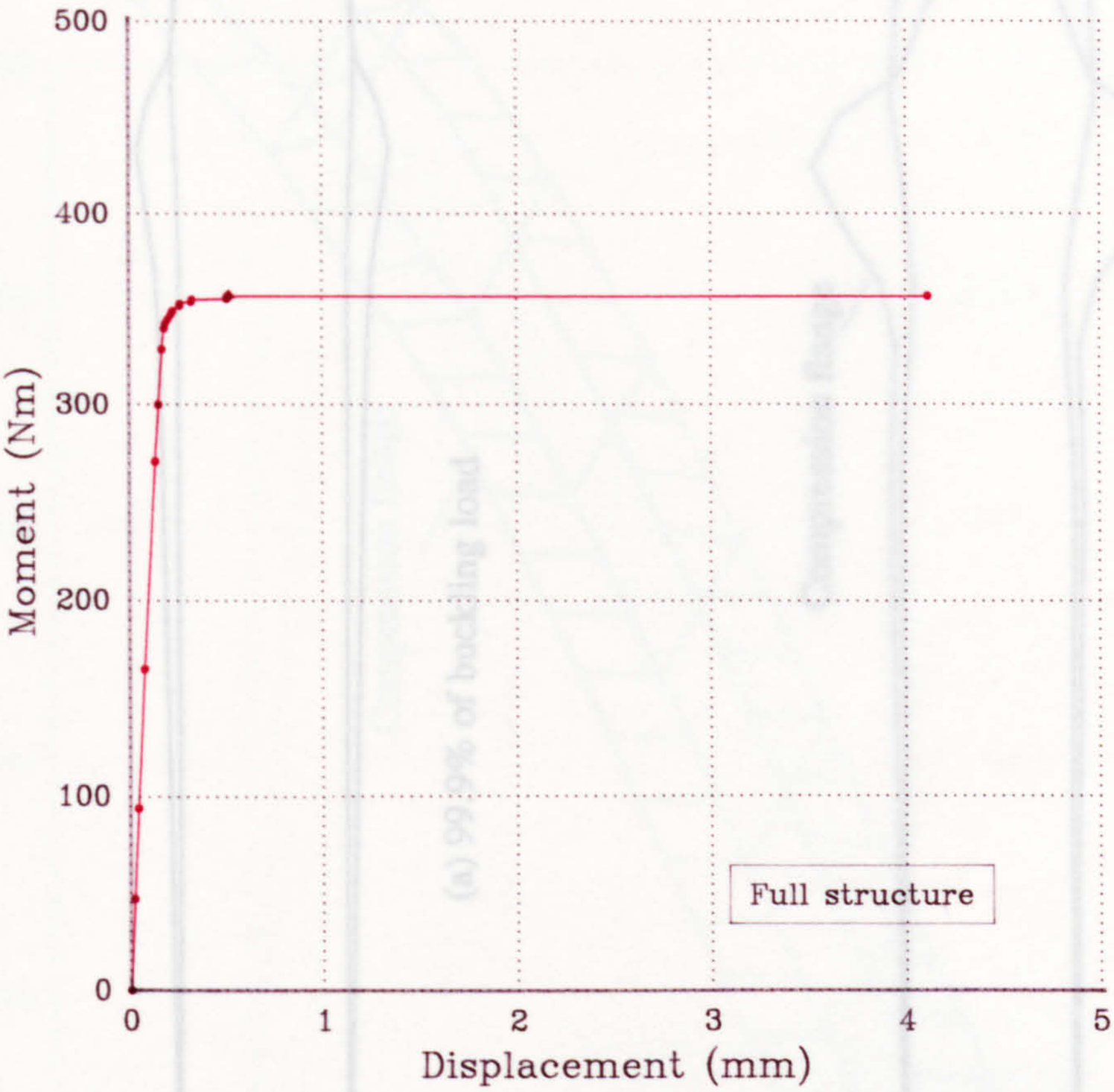

Figure 4.18 F.E. modelling of Leeds Test 2: load v. lateral displacement relationship using B31 elements

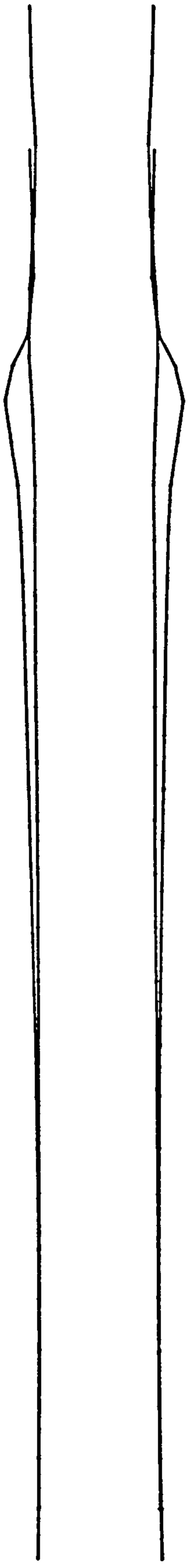

(a) 99.9% of buckling load

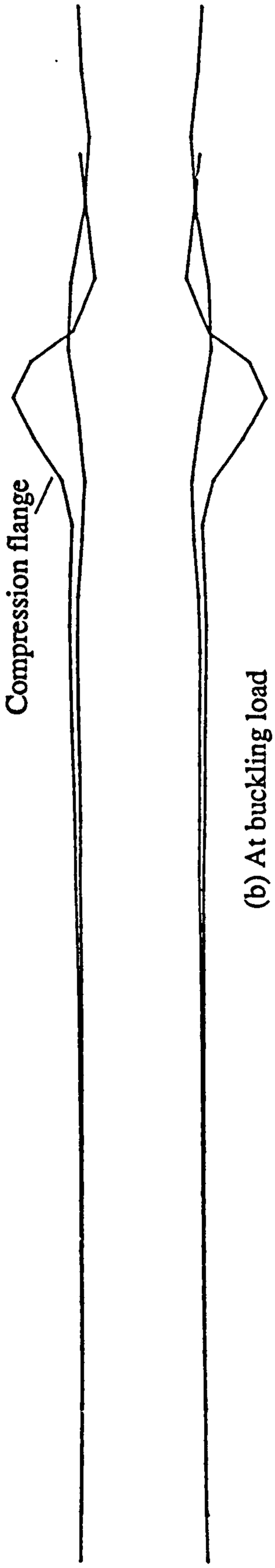

(b) At buckling load

Figure 4.19 F.E.modelling of Leeds Test 2 :
variation of lateral displaced shapes in plan view

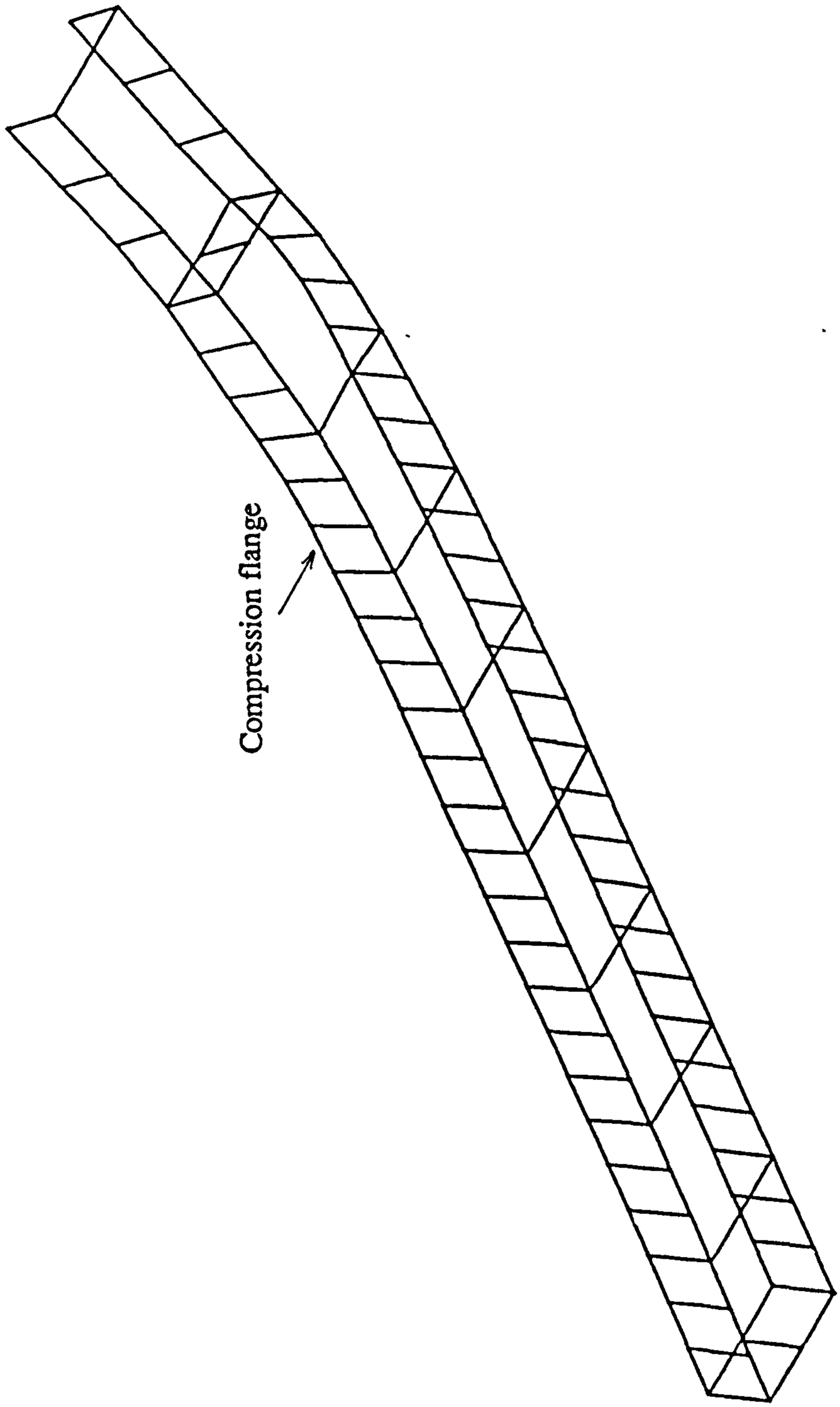

Figure 4.20 F.E.modelling of Leeds Test 2 (full model using S4R5 and B31 elements): final buckled shape

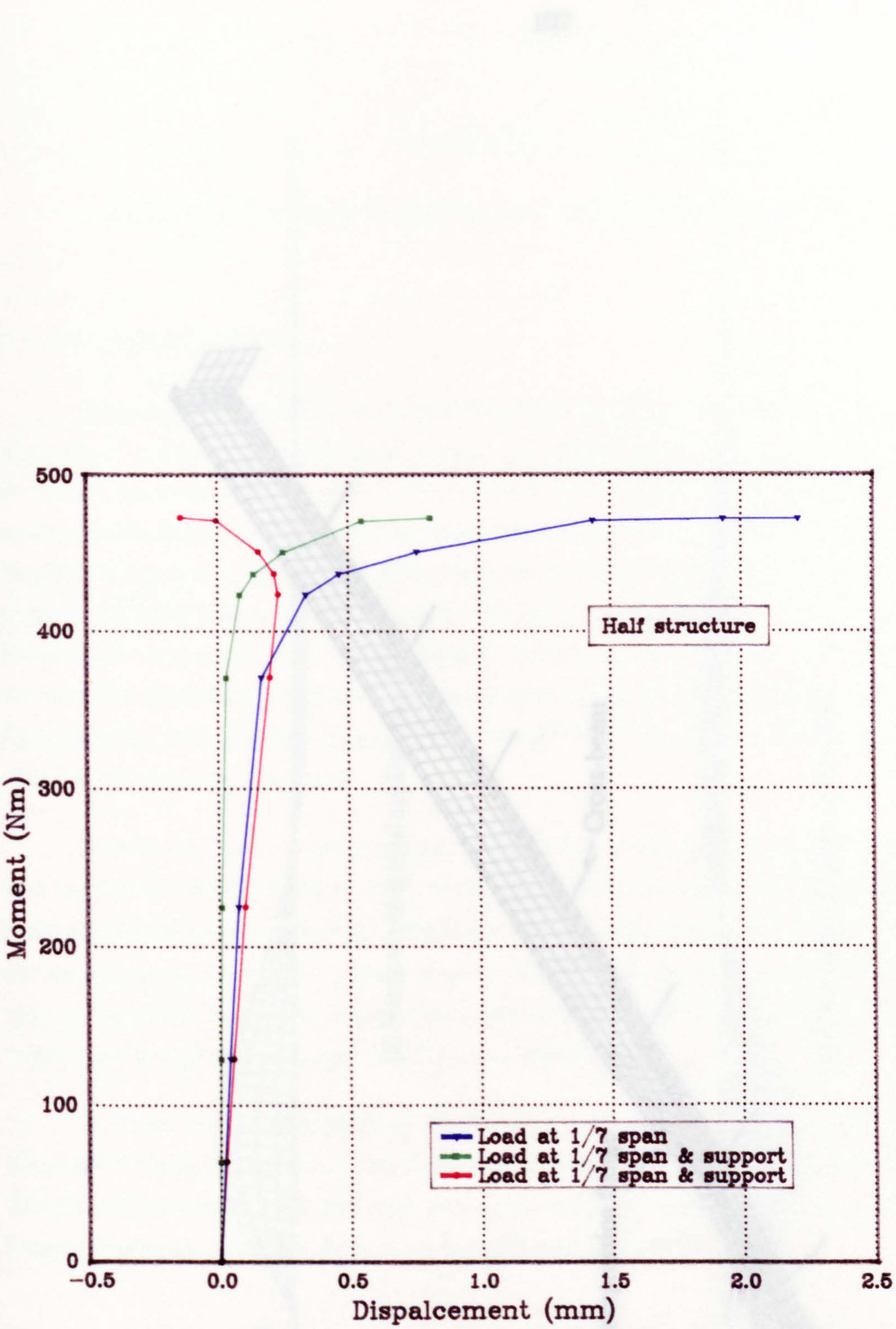

Figure 4.21 F.E. modelling of Leeds Test 2: Load v. lateral displacement relationships using S4R5 elements

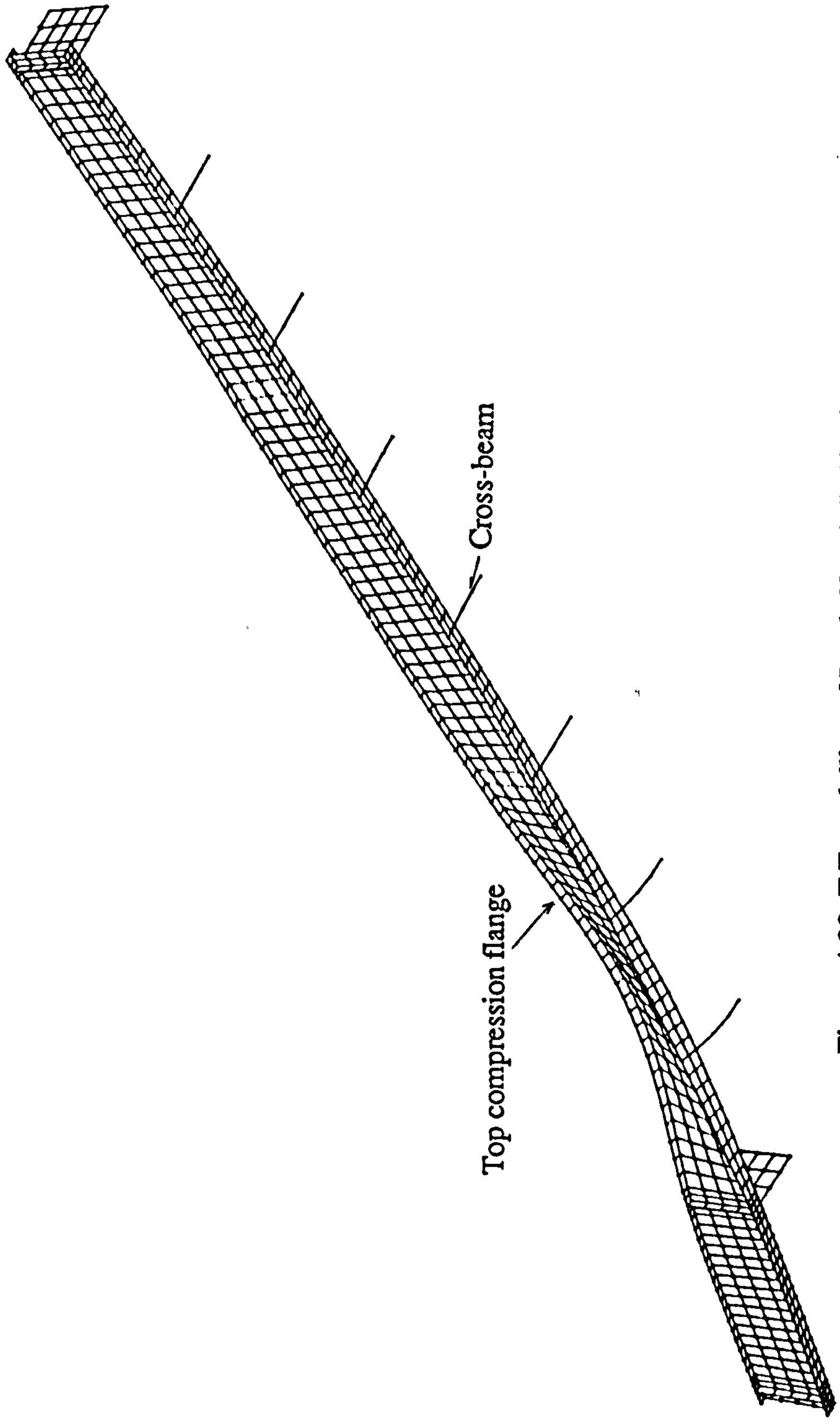

Figure 4.22 F.E.modelling of Leeds Test 2 (half using S4R5 and B31 elements): final buckled shape

(a) Vertical point load applied at point A

(b) Vertival point loads at A and B

Figure 4.23 F.E.modelling of Leeds Test 2 (half using S4R5 and B31 elements):
final lateral displaced shapes of girder web with two different loading conditions

CHAPTER 5

FINITE ELEMENT MODELLING OF BRIDGE GIRDERS

5.1 INTRODUCTION

Although the use of finite element techniques in large displacement elasto-plastic analysis of collapse or buckling of plates was described by Crisfield[29,30,58] in the seventies, analysis of steel plate girders braced by U-frames using the finite element method with shell elements had not been attempted until the work of Johnson and Bradford early in the eighties, in which elastic distortional lateral buckling of girders was studied. Perhaps due to limited computer storage or the limitations of the finite element programme used at the time, only one single rectangular element was used to represent the web of a plate steel girder and two rectangular elements to represent the compression flange on the tension side. The edge of the web was fully restrained to represent the effect of the rigid concrete deck.

Non-linear finite element analysis of an existing bridge, consisting of two girders, was carried out by Duffield et al[10] using ABAQUS, the finite element programme employed in the present research. A full three-dimensional model was used to investigate the behaviour of the bridge. Linear four-noded shell elements were used to model the web of the girder and linear two-noded beam elements were used for the modelling of tension and compression flanges and the cross-beams.

A more recent simulation of U-frame braced plate girders was carried out by Weston[26], using a large deflection finite element programme developed by Crisfield[29]. The plate girders were modelled with web subdivided into rectangular shell elements and flanges into beam segments, as in the work of Duffield et al[10].

5.2 FINITE ELEMENT IDEALISATION OF TYPICAL U-FRAME CONFIGURATIONS

5.2.1 Introduction

Two typical bridge configurations within the practical range of compression flange size and effective slenderness were selected[59] for study. The dimensions of the girders are shown in Figure 5.1. Deck Form 1 consists of two or more unstiffened

universal beams with plain concrete slab attached to the top flange. A span of 25m appropriate to this type of bridge was used for the analysis. Deck Form 2 comprises twin plate girders with vertical web stiffeners at a spacing of 3.0m and a corresponding span of 54m was adopted. A concrete slab provided interconnection between the two girders.

In order to study the basic formulation in BS5400: Part 3 for calculating the critical moment of resistance based on simply supported beams subjected to uniform bending moment, both types were loaded under uniform bending moment. The effect of moment gradient was investigated using two-span continuous girders for each deck form with UDL applied at the top flange level. This is a typical (or the most critical in continuous span bridges) practical loading case, in which critical moment evaluated according to BS5400 was found by other investigators to be extremely conservative.

For all the cases studied, an initial lateral displacement of $\frac{\text{Span}}{1000}$ in the bottom flange was introduced by displacing the flange nodes laterally to a parabolic single half-wave profile to initiate the occurrence of lateral buckling in the flange.

The resulting ultimate moment capacities under different constraints were compared with the BS5400 values.

5.2.2 Finite Element Mesh and Choice of Elements

The element meshes adopted are shown in Figure 5.2. A relatively coarse mesh was used for the modelling of Deck Form 1 and a refined mesh for Deck Form 2.

From the modelling of the experimental work in Chapter 4, it was found that use of thin shell element S4R5 would be sufficient for the two deck forms, provided the meshes were reasonably refined. Although the element thicknesses in the universal beam and the plate girder varied from 20mm to 70mm, thin shell elements were still chosen rather than thick shell elements because these thicknesses were small compared to other dimensions of the plates.

5.2.3 Discussion of Modelling of Concrete Deck

With the introduction of ABAQUS Version 4.8 in June 1991 and Version 4.9 in March 1992, modelling of concrete eventually became possible. However, because of the complexity of modelling the concrete material properties including cracking under tension, and involvement of the deck reinforcement, the analysis could not converge once cracks had formed in the concrete. Such solutions that were obtained required prolonged CPU time beyond available resources. Since the main theme of this study was to investigate the behaviour of steel plate girders under the U-frame action, modelling of the concrete deck was thought to be of minor importance and was abandoned.

Under a uniform bending moment or in the hogging region near a continuous support, the concrete deck which is at the level of the tension flange of a girder, together with the tension flange and part of the web, are in tension whereas the other parts of the girder will be in compression. Because concrete has little resistance to tension, the cracked concrete section will not contribute to the load capacity of the girder, as assumed in BS5400. Since the direction of cracks in the concrete are perpendicular to the longitudinal girder axes, the bending stiffness of the concrete about the major axis of the bridge cross-section is assumed to be lost completely. However, the effect of U-frame action still exists because the axial stiffness of the cracked concrete in the transverse direction and the bending stiffness about the longitudinal axis of the concrete deck should not vanish, thus the tension flanges will still be restrained by the deck slab.

From the calculation of δ values, as shown in Appendix II, it was observed, in the case of Deck Form 1, that the second term in the δ expression, which represents the bending stiffness of the concrete (which in turn is the torsional restraint to the tension flange), may be small in comparison with the first term representing the flexibility of the girder web. Increase in the thickness of the concrete or even an increase in the distance between the two girders will not influence the value of δ very much. Due to the presence of rigid concrete slab, the extremely high axial stiffness of the concrete prevents the tension flange from moving sideways and thus, there is no contribution to δ value from the axial stiffness of the concrete slab. Thus, the axial stiffness of the concrete was not taken into account in the calculation of δ value. However, with the presence of transverse web stiffeners as in Deck Form 2, the second term can be dominant. The existence of transverse web stiffeners reduces the flexibility of the web and first term in the expression becomes insignificant.

With the intention of simulating the effect of U-frame bracing which is mainly caused by (a) flexibility of the girder web and (b) torsional and translational restraints from the concrete deck, the presence of the concrete deck was replaced by equivalent boundary restraints in analysing the two deck forms. (Torsional stiffness of a composite cross-section may be reduced by the omission of the deck slab, but the effect on the ultimate capacity was found to be negligible[26].) The details of modelling are reported in the following sections.

5.2.4 Load Application and Boundary Conditions

Uniform bending moment for the single span case was originally generated by applying appropriate distributed horizontal loads to the nodes in the end cross-section of the steel beams. However, this method induced excessive local stress concentration and was abandoned. Instead, therefore, two loading cantilever arms were extended from both end supports of the girders. Point loads were applied vertically downwards at the

ends of the cantilevers to generate uniform bending moment in the main span. In the case of girder under UDL, a series of evenly spaced equal vertical point loads were placed on all mid-flange nodes of the tension flange.

One-quarter of the plan form for the full bridge could be modelled in both the single and double span cases in order to reduce computing time. Nevertheless, boundary conditions had to be set appropriately according to the anticipated mode of buckling.

For example, in the single span situation, buckling modes involving an odd number of half-waves could be achieved by constraining the nodes of the mid-span section to have zero rotation in the vertical and transverse directions (ie, z- and y- axes) and zero longitudinal displacement. ABAQUS facilitates an en bloc declaration of restraints at such a plane of symmetry. However, anti-symmetrical buckling modes of the compression flange, involving an even number of half-waves entail a mixture of symmetry of vertical displacement and anti-symmetry in the lateral displacement of the compression flange at mid-span. Warping of the cross-section also occurs at mid-span further complicating the boundary conditions at this position. Convergence of the finite element analysis for one-quarter of the whole structure, with complex boundary restraints imposed, was difficult to achieve (see Chapter 4). Lengthened CPU time was required in solving the problem. Thus, for the case of a single span, one girder of full span was modelled.

When double span girders with UDL were studied, only one-quarter of the structure could be modelled. Otherwise, the large number of degrees of freedom involved would exceed the limitation of the ABAQUS package. Rigid restraints were assumed at the middle support, which means zero displacement in both transverse and longitudinal directions (x- and y- axes) for all the nodes along the web of the girder. Rotational restraints about the x- and y- axes were also provided to enforce zero slope at all nodes over the central support both in longitudinal elevation and the transverse cross-section.

Owing to complexity of the boundary conditions at the inner support, the compression flange of beams/girders at this position may be restrained differently. Warping of the cross-section pivoting about the minor axis of the section due to the continuity of the spans may be allowable. Otherwise, it will not be permitted when rigid conditions are imposed. Therefore, there are two different sets of restraints applicable to the compression flange at the central support, ie, restraints:

(a) allowing for the occurrence of warping of the cross-section in which case a series of linear multi-point restraints were applied to the edge nodes of the compression flange to keep them pivoting about the minor axis and in line with each other; and

(b) not allowing the occurrence of warping and thereby the longitudinal movement of the compression flange is not permitted

Vertical stiffeners (with the same thickness as the web) were introduced at loading and support positions to absorb the concentrated action or reaction. Lateral movement was prevented at these positions as shown in Figure 5.3.

The boundary conditions that ought to be employed in the tension flange were as follows:

(a) It was thought to be appropriate that the lateral restraint of the concrete deck on the tension flange, which prevents translational movement of the flange, was replaced by lateral restraints applied on the longitudinal centre line of the flanges.

(b) Torsional restraints were imposed onto the nodes on the centre line of the tension flange to represent the reinforced concrete slab.

To observe the combined effect of both restraints, finite element analyses of the same girders under both restraints were carried out and results are presented.

5.2.5 Deck Form 1

U-frame action is provided in this case by the use of continuous support from an unstiffened web. The evaluation of the critical moment capacity of the girder according to BS5400 is given in Appendix II.

5.2.5.1 Uniform Bending Moment

With no restraints to the tension flange, the ultimate load obtained by ABAQUS was $2.1\text{x}10^6$Nm, which is 27% higher than the elastic critical value of $1.6\text{x}10^6$Nm based on a simply supported beam subject to uniform bending moment. In the derivation of the theoretical formula[8], the effect of major axis deflection is neglected[4]. If the effect is included, the expression:

$$M_{E1} = \frac{\pi}{L}(EI_yGJ)\sqrt{(1+\frac{\pi^2EI_w}{L^2GJ})} \quad \ldots\ldots\ldots (5.1)$$

will become:

$$M_{E2} = \frac{\pi}{L}\frac{(EI_yGJ)\sqrt{(1+\frac{\pi^2EI_w}{L^2GJ})}}{\sqrt{a\cdot b}} \quad \ldots\ldots\ldots (5.2)$$

where $a = (1-\frac{EI_x}{EI_y})$ and $b = (1-\frac{GJ}{EI_x}(1+\frac{\pi^2EI_w}{L^2GJ}))$

When EI_y becomes very large, the expression (5.2) reduces to (5.1). Allowing for the effect of major axis deflection increases M_E by 5% to 23%. The principal effect of monosymmetry is to cause the beam's effective torsional rigidity to increase when the larger flange is in compression (or decrease when the smaller flange is in compression). Therefore, although a relatively coarse mesh was used in the analysis, it was believed that reasonable results were generated.

As discussed in Section 5.2.4, three types of restraints as shown in Figure 5.3 were applied to the tension flange, namely:

(a) torsional;
(b) translational; and
(c) torsional and translational.

(a) Torsional Restraints Only

When the tension flange was only restrained torsionally in the longitudinal axis of the girder in Deck Form 1, an ultimate moment of failure of 6.50×10^6Nm was obtained. In comparison with design value of 4.22×10^6Nm, this is 54% higher. However, there was no sudden increase in the lateral deflection as the maximum load was approached in ABAQUS, as indicated in the load-deflection curve in Figure 5.4.

Re-examining the calculation of the above-mentioned design value, δ was obtained by the expression suggested by BS5400. However, in the case of purely torsional restrained tension flange, the torsion of the whole cross-section is more influential than the distortion of the section. The contribution due to the flexibility of the web, ie, the first term of the δ expression is insignificant. Therefore, δ would be reduced to 1.38×10^{-4}mm/N. Using of the moment of inertia of the whole section about the minor axis instead of the moment of interia of the compression flange only, the moment of resistance would be 6.57×10^6Nm which is much closer to the ABAQUS result.

Because of the high bending moment reached, the tension flange had gone completely plastic. Yielding had developed in a number of elements in the compression flange while the web of the girder still remained elastic. The section used was a non-compact section according to the classification in BS5400. The code classification seems therefore reasonable.

As the load increased, the lateral displacement of the compression flange grew to 80mm at mid-span. A single parabolic profile as shown in Figure 5.5(a), was developed. A plan view of the web at this stage is given in Figure 5.5(b). It implies that there might be some web distortion. In addition, the lateral movement of the tension

flange was obvious. Such large movement of the tension flange is impossible in a practical bridge. Thus, provision of lateral restraints to tension flange is essential.

(b) Translational Restraints Only

From the finite element analysis of Deck Form 1 with pure lateral restraint to the tension flange, the ultimate load capacity reached in the analysis was only 3.9×10^6Nm. Although this value is incomparable with the design value because of the difference in restraints, it was of interest to note the great difference in the resultant moment capacities between this case and case (a). If a similar re-calculation of the design value of moment of resistance as in the case (a) is done, δ should be taken as 3.45×10^{-3}mm/N due to the absence of torsional restraint and both the presence of the translational restraints and the flexibility of the web. Using the ratio of web thickness to the web depth instead of $\frac{t_f}{D}$ ratio in the λ_{LT} expression in BS5400, an evaluated moment of resistance of 4.3×10^6Nm is found closer to the ABAQUS result.

Nevertheless, the slope of the load-deflection curve, which is plotted in Figure 5.6, dropped fairly rapidly. It indicated a rapid increase in lateral displacement at mid-span as the buckling load was approached. The lateral displacement of the compression flange, following the assumed initial imperfection, gradually increased in magnitude. The final buckling mode was a single half-wave (shown in Figure 5.7, together with the overall displaced girder in Figure 5.8).

There was no yielding throughout the loading process.

(c) Translational and Torsional Restraints

When both restraints were applied at the same time to the nodes on the centre line of the tension flange, an ultimate moment capacity of 7.34×10^6Nm was obtained. This was a significant improvement in the load capacity of the girder.

Furthermore, the lateral displacement at mid-span was reduced considerably. The occurrence of buckling with a swift increase in lateral displacement, as the buckling load is approached, is clearly discernible in the load-deflection curve plotted in Figure 5.9. The final buckled shape of the compression flange and the displaced profile of the web in plan view are illustrated in Figure 5.10

(d) Restraint Imposed by the Presence of the Cross-Beams

When the cracked concrete deck was replaced by equivalent cross-beams (taken to be 180x180mm spaced at one metre centres), the ultimate capacity of the same girder using the same mesh system was 8.1×10^6Nm which was higher than the case of a girder with either translational or torsional restraints only but comparable to a girder with both

translational and rotational restraints. This increase in capacity might be attributed to the axial and flexural stiffness of the cross-beams, which functioned as lateral and torsional restraints to the entire tension flange, instead of restraints to the nodes on the longitudinal centre line of the flange, only (see Figure 5.3).

(e) Summary

(a) From the three cases studied, it can be seen that torsional restraints continuously applied to the top flange are much more influential on the load capacity of the girder than translational restraints. Nevertheless, the presence of the translational restraints is essential in bridge structures. This will inevitably cause distortion in girder web (see Figure 5.7(c)). The neglect of the axial stiffness of concrete in the coded design procedure appears to be reasonable, ie, no allowance for the lateral movement of tension flange is given in δ expression. The advantage of combining torsional and translational restraints is clear.

(b) However, although factors taken into consideration in the expression of δ appear to be appropriate, the current design value which is due to the combination of both restraints, still seems to be over conservative.

(c) The load-deflection relationships for the compression flange were summarised in Figure 5.11. The influences of each type of restraints can easily be seen.

5.2.5.2 Moment Distribution due to UDL

In calculations for girders of continuous span, the concrete deck in the hogging moment region is disregarded in BS5400: Part 3 Clause 9.4.2.7. Thus, the elastic or plastic moduli are based on the bare steel section. Although the concrete in the sagging region does contribute to the moment capacity of the composite beam, yet the deciding factor for the bending resistance of the beam is the stability of the compression flange in the hogging region. Consequently, concrete deck in the sagging region was excluded in the following analyses.

As discussed in Section 5.2.4 two types of restraints applied to the compression flange at the inner support were studied and the results are discussed below.

5.2.5.2.1 Without Allowance for the Occurrence of Warping

(a) Torsional Restraints only

With torsional restraints only, the girder reached a maximum moment of 7.50×10^6Nm. The design value was 6.57×10^6Nm. During the loading, lateral deflection in the compression flange progressed as shown in Figure 5.12. The node at which

maximum lateral displacement occurred was not in the compression zone because non-warping restraints were applied to the edge of the flange at mid-span. The distortion in the web was also noticed from the plan view shown in Figure 5.13.

(b)Translational Restraints only

The ultimate moment capacity achieved was 8.35×10^6Nm. The load and lateral deflection relationship is plotted in Figure 5.14. It is obvious that lateral buckling had occurred in the bottom flange. Yielding, and thus some distortion of elements in the compression zone, was detected towards the end of loading.

The deformed shape of the web in plan view is shown in Figure 5.15; the maximum lateral deflection was just outside the compression region. (Overall deflection is shown in Figure 5.16.)

(c) Translational Restraints and Torsional Restraints

With the combination of restraints applied along the longitudinal centre line of the tension flange, it could be said that the effect of additional translational restraint on the moment capacity of a girder with purely torsional restraints was much greater than the effect of additional torsional restraints on a girder with purely translational restraints. The final failure moment reached was 8.59×10^6Nm, only a 2.8% increase in comparison with the previous case.

From the relationship of load versus lateral displacement at a node near mid-span, which became the maximum displacement, in Figure 5.17, a large increase in the deflection at approximately two thirds of the failure load was followed by an increase in slope until another further increase in the lateral deflection. (For comparison, load-deflection curves for cases with different restraints were shown in Figure 5.18.) Lateral deflection of the entire bottom flange is as shown in Figure 5.19. It can be seen that the lateral displacement did not follow the initial imperfection and serious distortion due to excessive yielding was clearly seen in the compression flange on the plots produced. An abrupt vertical drop of a node disabled the girder and prevented further loading from being resisted. This local failure also caused a change in the failure mode of the bottom flange.

5.2.5.2.2 With Allowance for the Occurrence of Warping

The load-deflection relationship was similar to that in the previous cases. It is surprising that the local yielding only reduced the ultimate loading capacity by a small fraction. Severe distortion of the elements in compression was observed as well. The final failure shape of the compression flange was shown in Figure 5.20.

5.2.6 Deck Form 2

Though the continuous concrete deck was also present as in Deck Form 1, U-frame action was also enhanced further by the presence of vertical web stiffeners equally spaced along the span. Element mesh adopted is shown in Figure 5.21.

5.2.6.1 Uniform Bending Moment

(a) Torsional Restraints only

With pure torsional restraints, the ultimate moment of resistance was 5.21×10^7Nm, in comparison with the design value of 4.65×10^7Nm. The finite element result was just 12% higher, therefore it appeared that BS5400 was not as conservative as it was originally thought to be for this type of deck form. It is because the second term in the δ expression becomes significant when the presence of the transverse web stiffeners reduces the flexibility of the web. The first term can then be neglected.

Lateral displacement at mid-span was plotted against load in Figure 5.22.

(b) Translational Restraints only

An ultimate moment of 4.35×10^7Nm was obtained compared to design value of 4.65×10^7Nm if δ is taken as 8.40×10^{-5} m/N (ie, ignoring the effect of torsional restraint). The maximum lateral deflection was in excess of 250mm at mid-span. The relationship between the load applied and the lateral displacement occurred at mid-span was shown in Figure 5.23. It is similar to the load-deflection curve obtained in case of Deck Form 1.

A gradual increase rather than a sudden jump in the displacement was observed. The displaced profile of the web in plan view and in sectional elevation from one end of the beam remained the same, as illustrated in Figure 5.7. The final buckled shape of the compression flange was a single parabolic curve (see Figure 5.8). Distortion of the web at mid-span and rotational movement of the tension flange in the absence of the torsional restraints were clearly pictured in the plots produced by ABAQUS.

Local yielding occurred in the compression flange elements adjacent to the support positions.

(c) Translational and Rotational Restraints

The ultimate buckling moment was 5.67×10^7Nm, which was only greater than the design value by 22%. Unlike the finding in the analysis of Deck Form 1, the

additional effect of torsional restraint on a purely laterally restrained girder or that of lateral restraint on a purely torsionally restrained girder seemed to be insignificant.

The load-deflection curve is shown in Figure 5.24. It is clear from the rapid growth in lateral displacement at mid-span that lateral buckling of the compression flange has occurred.

Both the flanges and the web were yielded at failure load. The entire cross-section became plastic. The classification of the section as non-compact according to BS5400, seems to be inappropriate in this case.

(Another finite element model of Deck Form 2 was generated. The element size used was twice that used in the above model, ie, a relative coarse mesh was employed. However the ultimate moment capacity reached was 5.71×10^7Nm, only 0.7% higher than the result from the refined mesh. In retrospect, a less refined mesh should have been used in the idealisation of Deck form 2.)

(d) Summary

From the finite element analyses of the girder of Deck Form 2, it can be seen that in all three cases the failure moment capacity produced by ABAQUS was close to the design value according to BS5400. Thus, the Code seems to give a reasonable safety margin for the case of the girder subject to uniform bending moment. The influence of torsional restraint on the ultimate load capacity of a girder was still found to be greater than that of the translational restraints (see Figure 5.25)

5.2.6.2 Moment Distribution due to UDL

From the study of double span of Deck Form 1 under UDL, it can be seen that the difference between restraints (a) allowing warping of the compression flange and (b) preventing warping of the compression flange at the mid-span section, does not have much effect on ultimate moment capacity of a girder. The only influence is the final failure mode.

Since the difference in restraints does not affect much of the moment capacity of a girder (see section 5.2.5.2.2), restraints not permitting warping were applied for compression flange at mid-span in the following study of Deck Form 2.

(a) Torsional Restraints Only

The failure moment achieved was 5.44×10^7Nm. It was not much higher than the moment capacity of the girder under uniform bending moment. The interest of modelling

this case was merely to compare the effect of purely torsional restraints with that of purely translational restraints.

The large increase in lateral displacement in Figure 5.26 marked the lateral buckling in the flange.

(b) Translational Restraints Only

With the presence of translational restraints only, the ultimate moment capacity of the girder reached 6.60×10^7Nm. This was approximately 42% higher than the design value.

The lateral displacement of the node at the final maximum displacement point is plotted against applied load in Figure 5.27. The curve shows no sign of lateral buckling of the flange in compression. From ABAQUS plot shown in Figure 5.28, it can be seen that, ripples had developed in the web. An elastic bending moment of 3.89×10^7Nm at which these ripples would occurred was obtained by considering the elastic buckling of a thin plate under combined bending and compression[8].

(c) Torsional and Translational Restraints

The ultimate moment of resistance of the girder under both torsional and translational restraints was 6.63×10^7Nm. Similar to the study in Deck Form 1, this value was very close to that of the girder under translational restraints only.

There was, however, a major difference in the lateral displacement of the bottom flanges. The flange in compression deflected in the opposite direction to that of the flange in tension. Therefore, a deformed shape with 2 unequal half-waves was produced. However, from the load-deflection curves shown in Figure 5.29, it can be seen that no lateral buckling had occurred. Effects of restraints are summarised in Figure 5.30.

5.3 CONCLUSION

Two configurations of typical I-section girder bridges braced by U-frames were analysed under two loading situations, namely, (a) single span under uniform bending and (b) double span under UDL. The results of the analysis are summarized in Table 5.1.

Since concrete modelling was not included, various types of restraint were imposed at tension flange level. The results are summarised in the following table.

Table 5.1 Summary of the ultimate bending resistances of Deck Form 1 and 2 by ABAQUS

Bending Moment Distribution	Boundary Conditions to the Tension flange	Deck Form 1 ($x10^6$Nm)	Deck Form 2 ($x10^7$Nm)
Uniform	Torsional only	6.50	5.21
	Translational only	3.90	4.35
	Translational and Rotational	7.34	5.67
From UDL on two equal spans	Torsional only	7.50	5.44
	Translational only	8.35	6.60
	Translational and Rotational	8.40	6.63

In the case of a single span with uniform bending moment, the influence of translational restraint at tension flange level on the moment capacity of the girder was minimal. The design values according to BS5400 appear to be reasonable.

However, the same may not be said for girders of double span under UDL. In this case, translational restraints were very effective. In the presence of a high moment gradient, failure moments obtained in the finite element analyses were much higher than the corresponding design values.

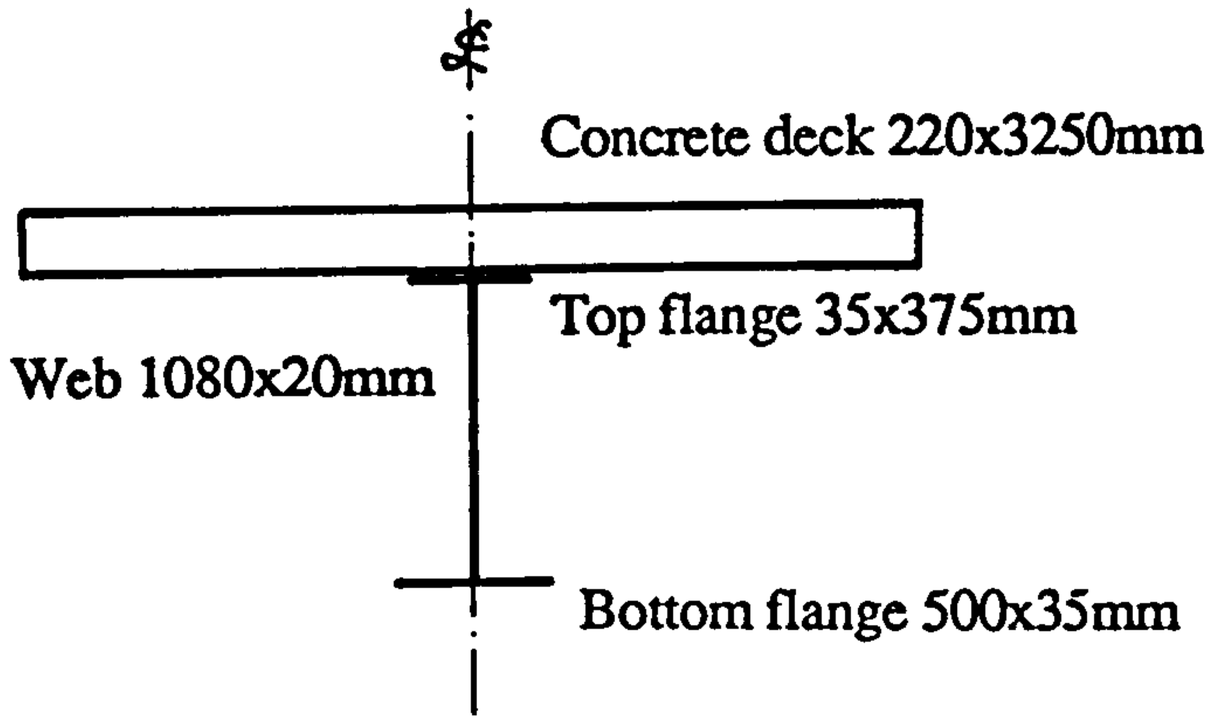

(a) Deck Form 1 : Non-compact section
Span 25m

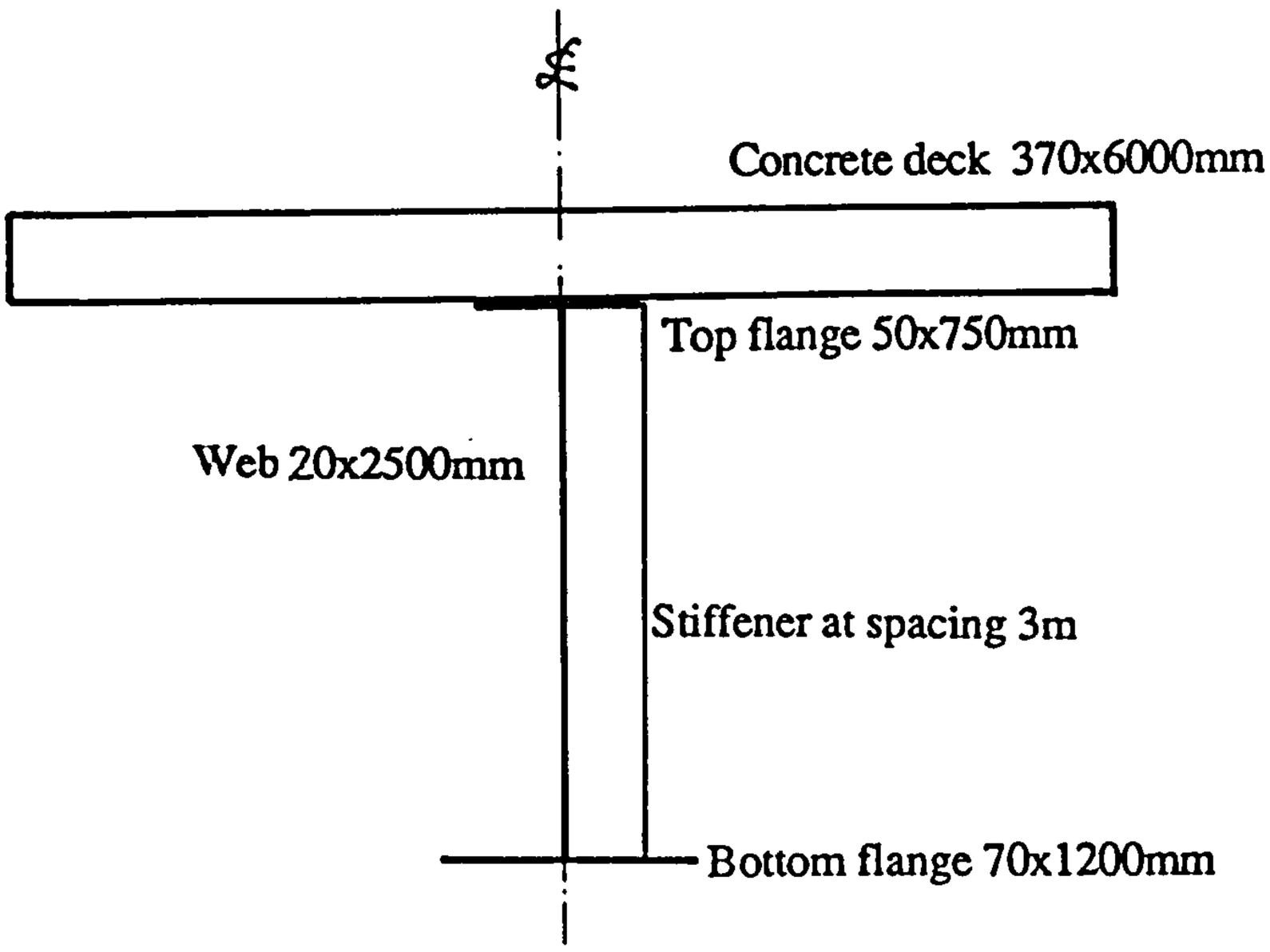

(b) Deck Form 2 : Non-compact section
Span 54m

Figure 5.1 Typical bridge configurations

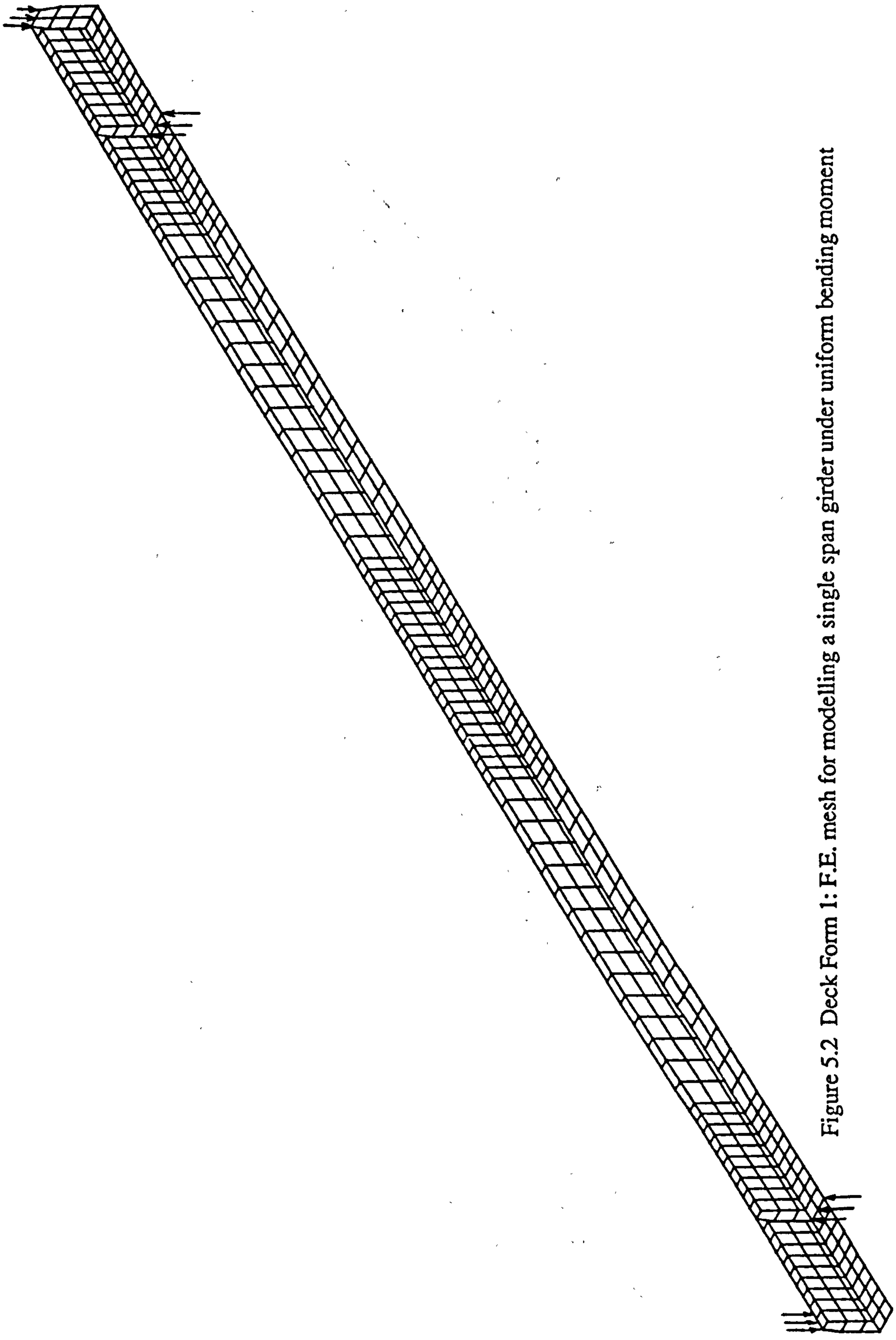

Figure 5.2 Deck Form 1: F.E. mesh for modelling a single span girder under uniform bending moment

Translationally restrained tension flange

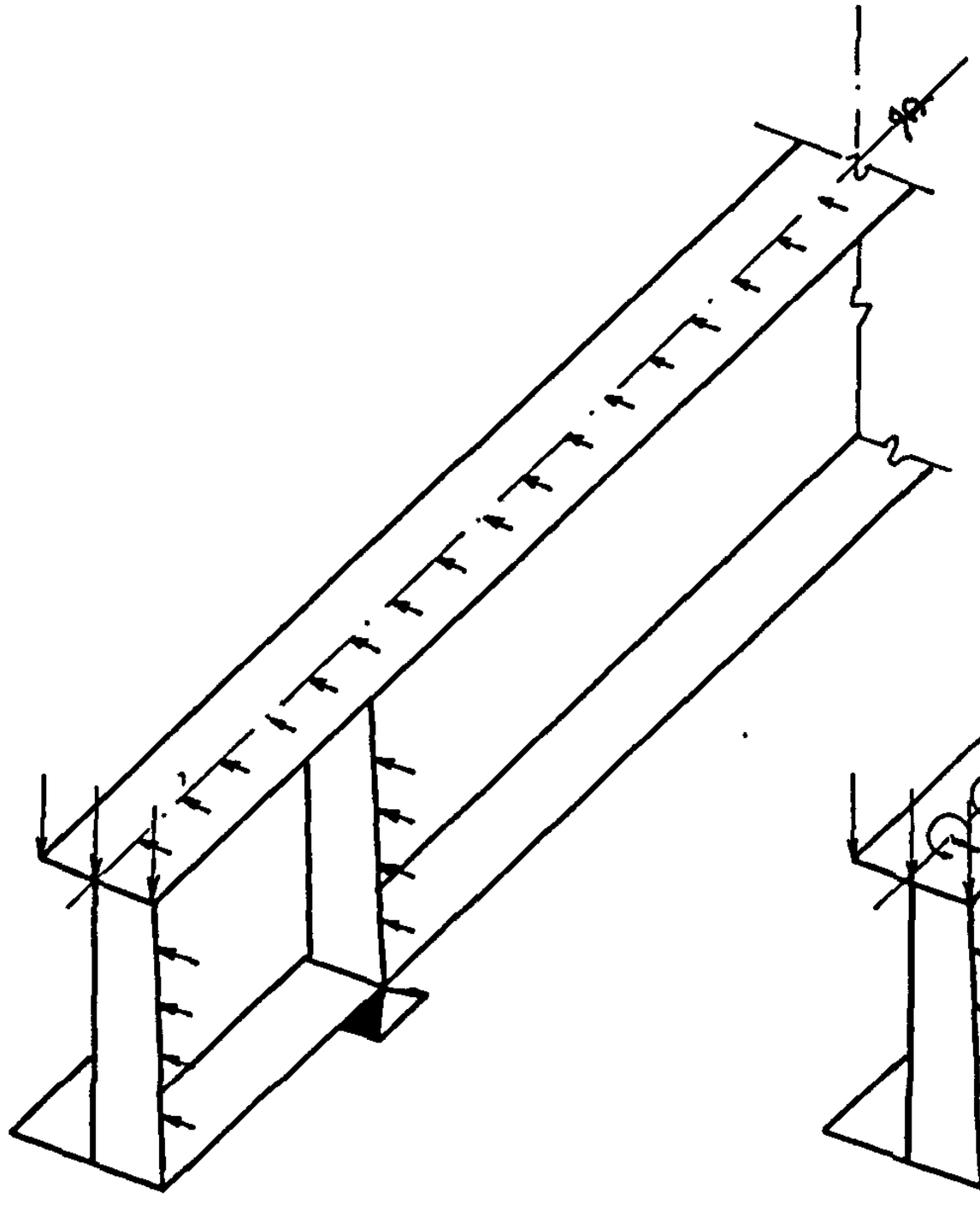

3.90x10^{6}Nm

Translationally and torsionally restrained tension flange

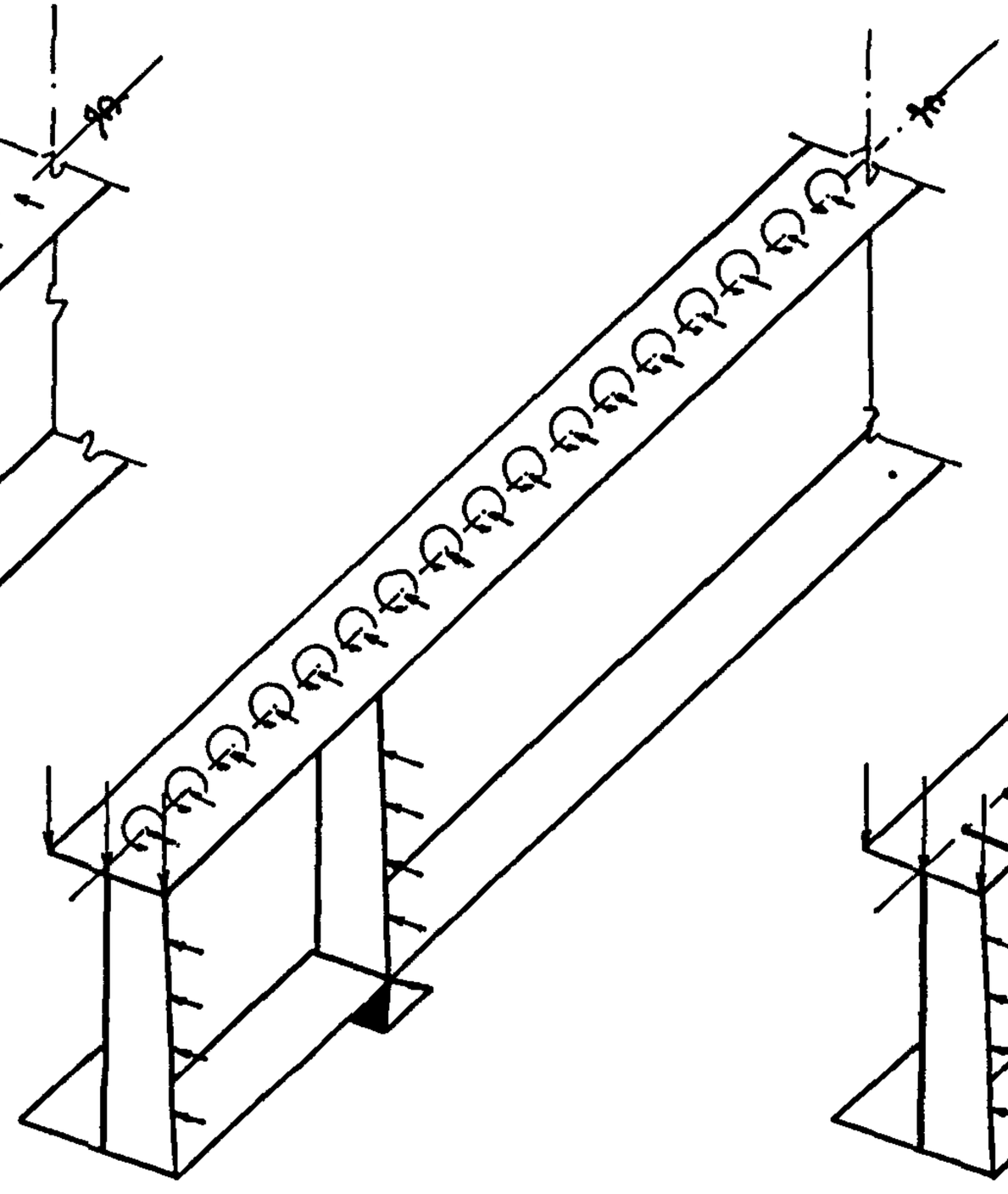

7.34x10^{6}Nm

Tension flange restrained by cross-beams

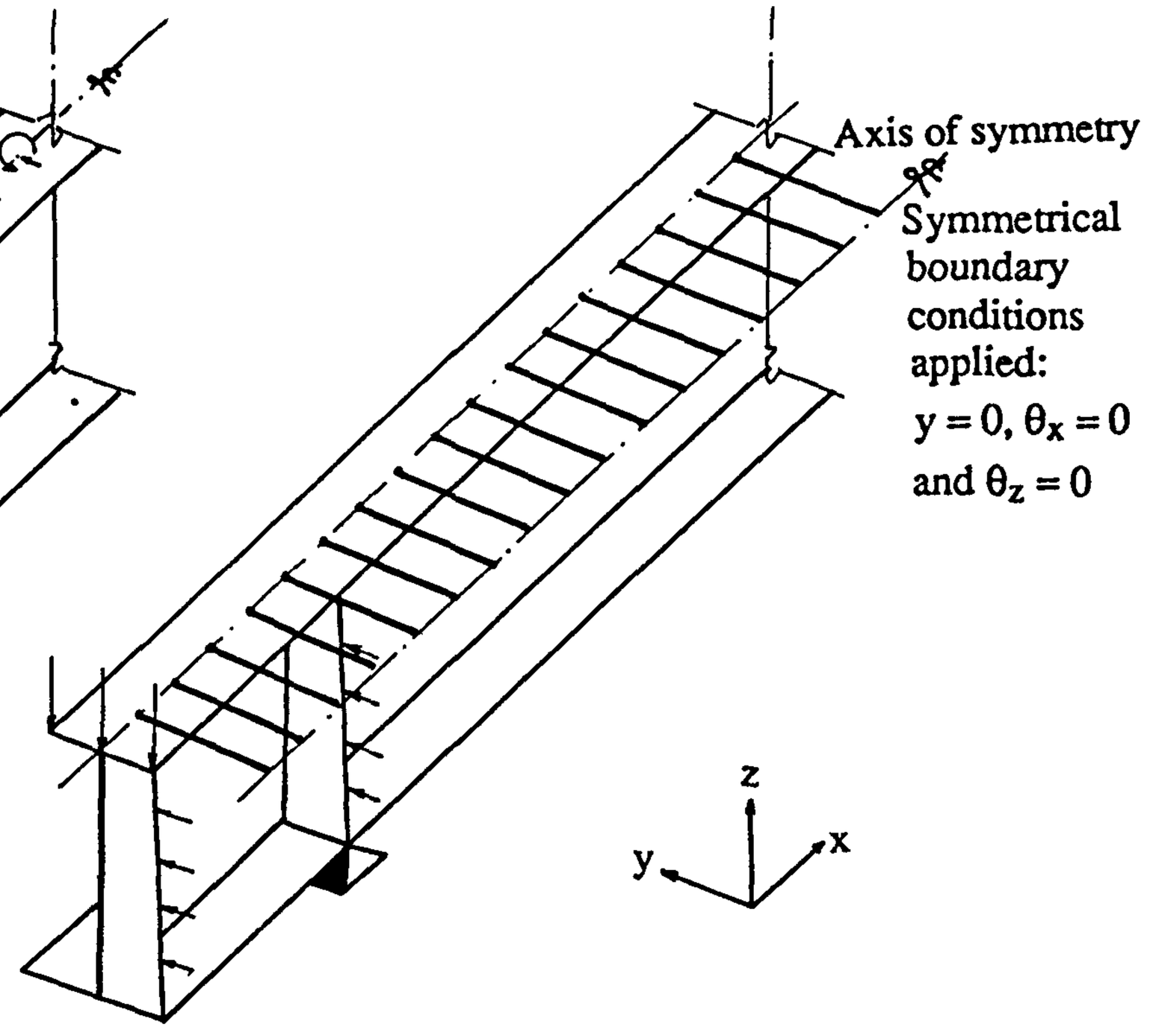

8.10x10^{6}Nm

Design bending resistance to BS 5400 4.22x10^{6}Nm

Figure 5.3 Effect of boundary conditions on the buckling moment of a single span girder

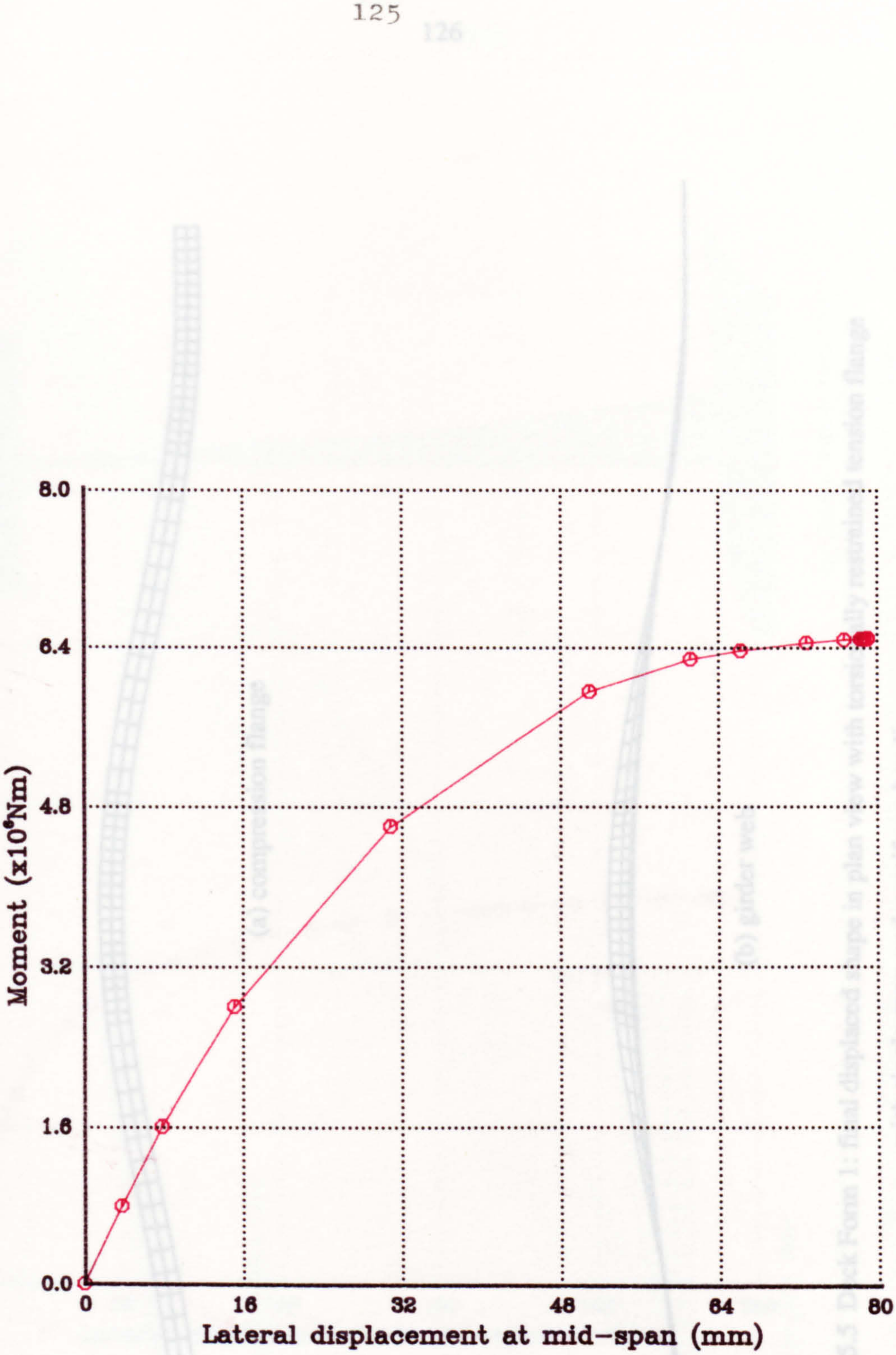

Figure 5.4 Load v. displacement relationship for Deck Form 1 with torsionally restrained tension flange under uniform bending moment

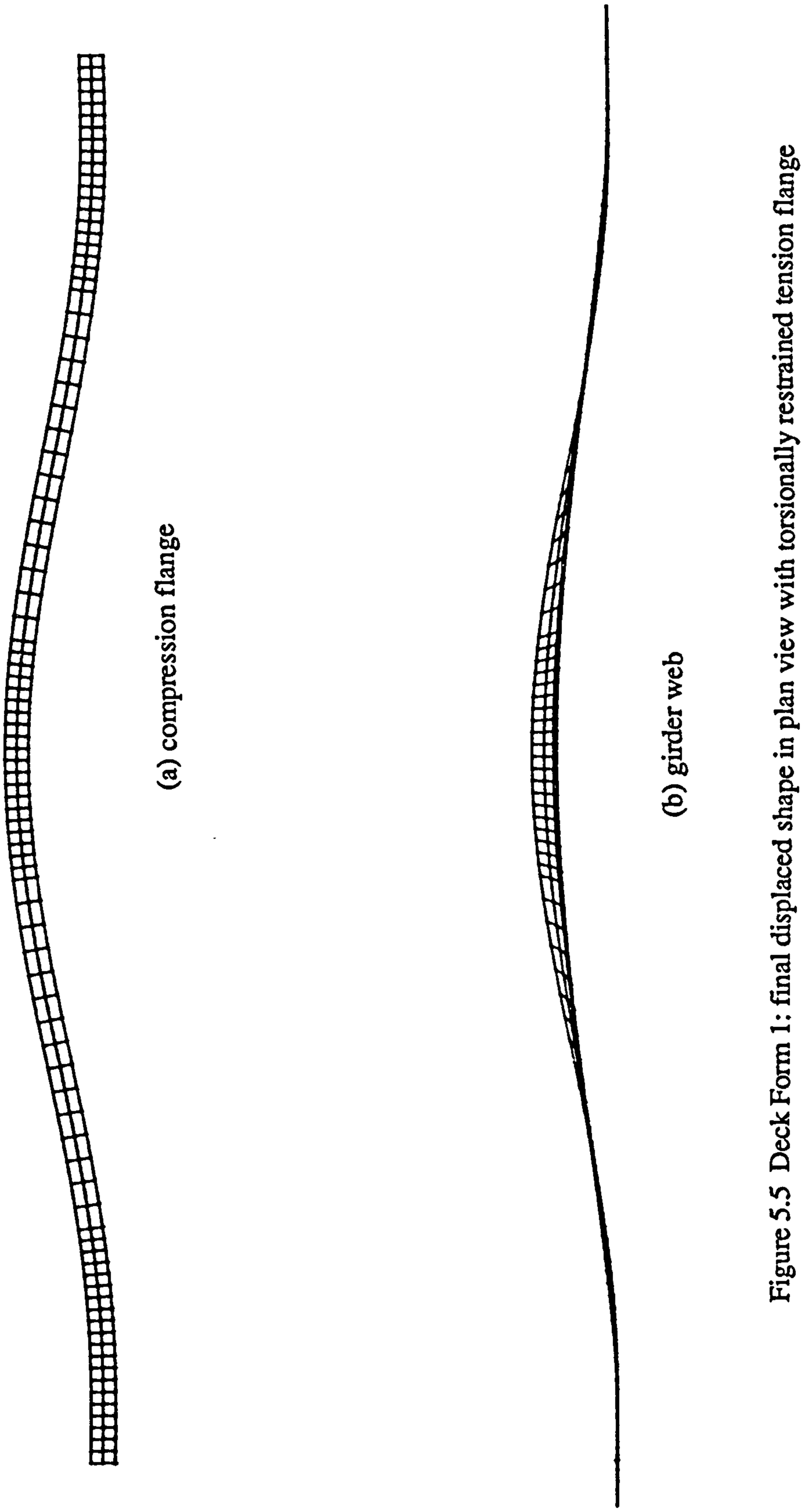

(a) compression flange

(b) girder web

Figure 5.5 Deck Form 1: final displaced shape in plan view with torsionally restrained tension flange with single span under uniform bending moment

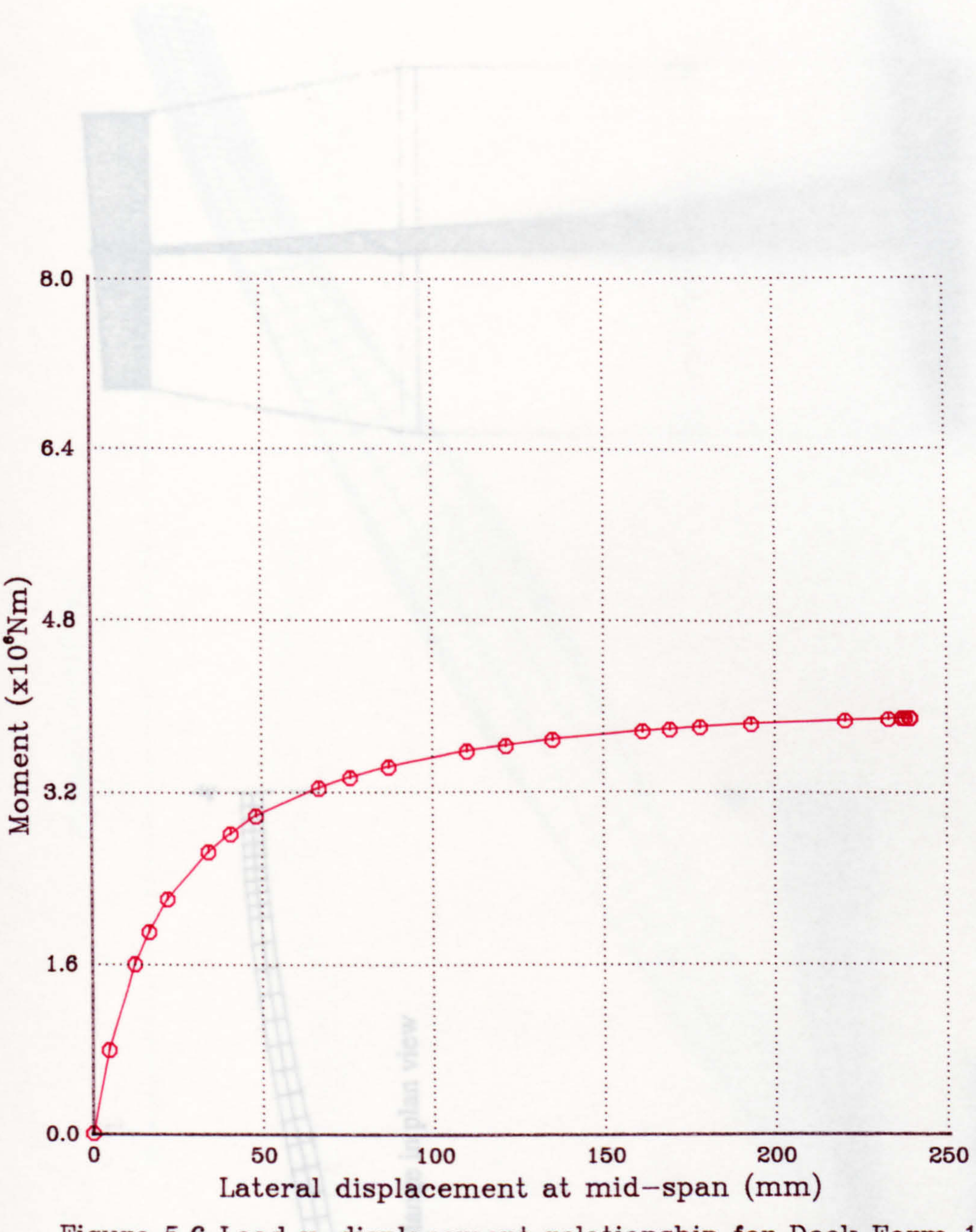

Figure 5.6 Load v. displacement relationship for Deck Form 1
with laterally restrained tension flange
under uniform bending moment

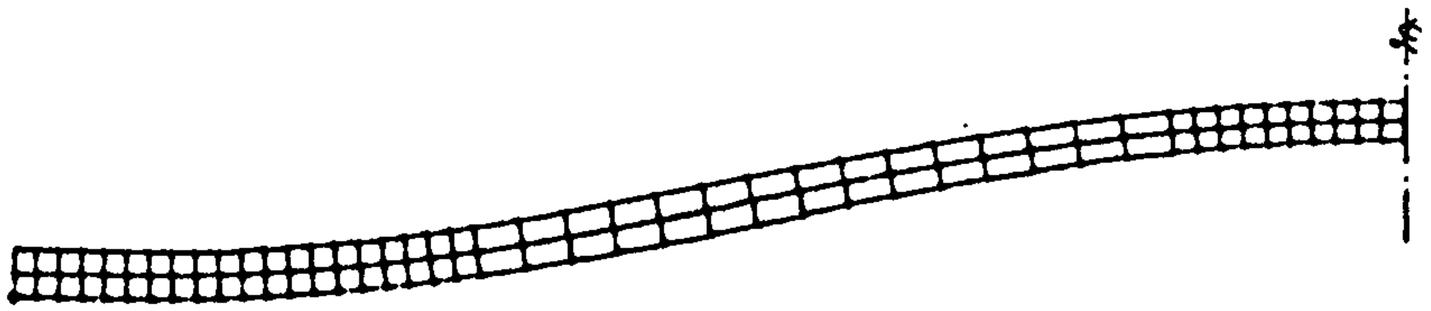

(a) compression flange in plan view

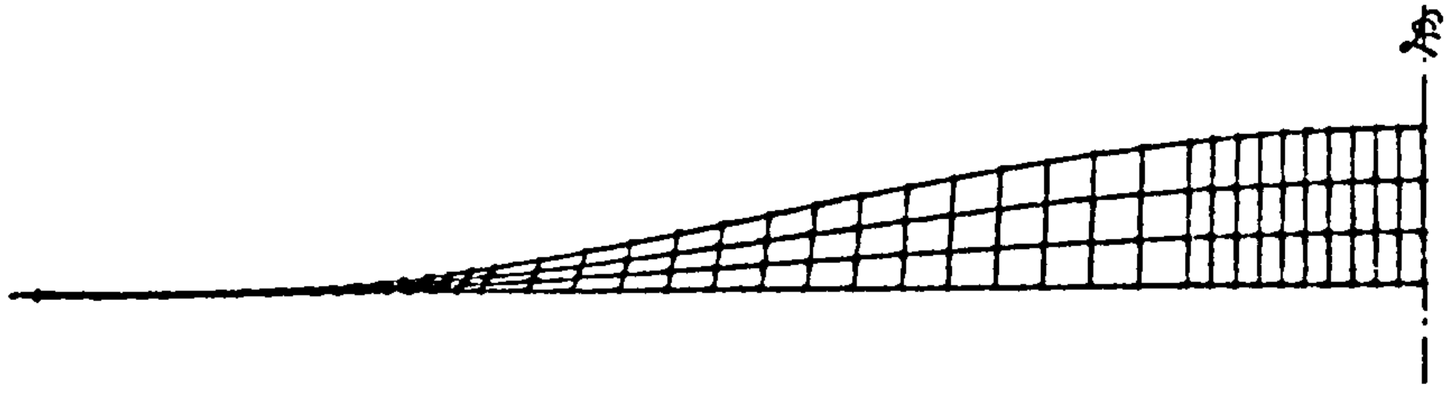

(b) girder web in plan view

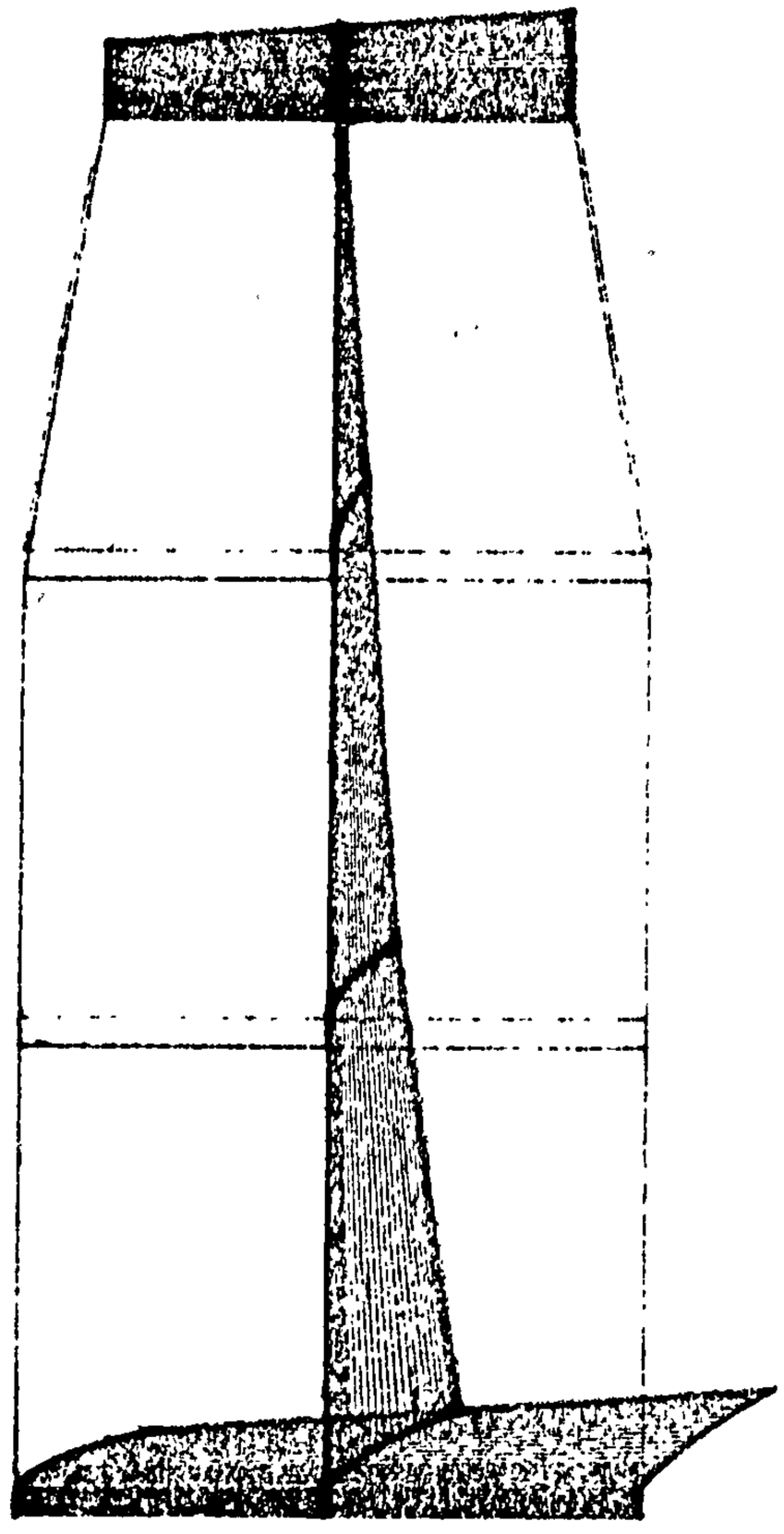

(c) girder web in end view

Figure 5.7 Deck Form 1: final displaced shape with laterally restrained tension flange with single span under uniform bending moment

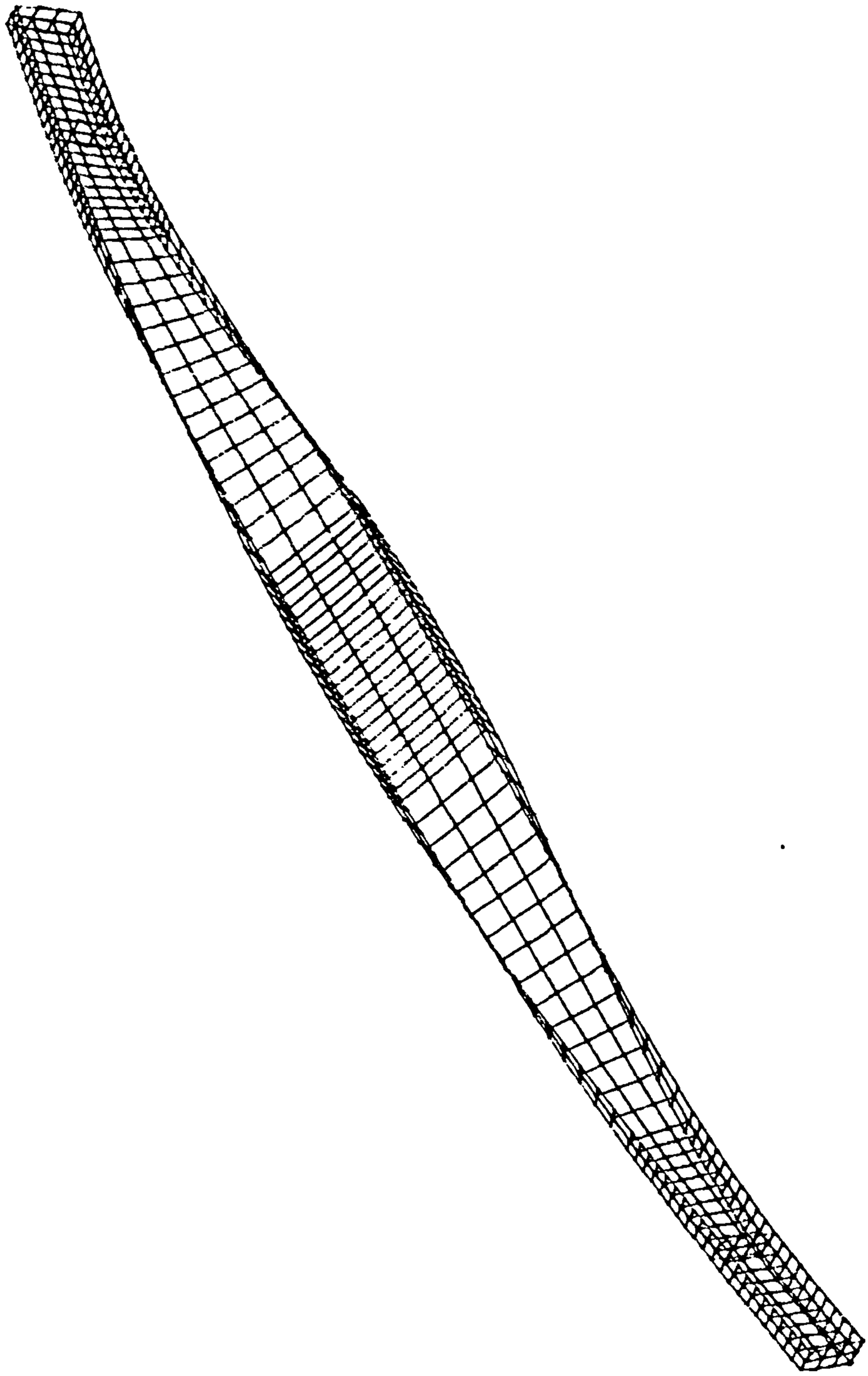

Figure 5.8 Deck Form 1: final displaced shape with laterally restrained tension flange w
span under uniform bending m

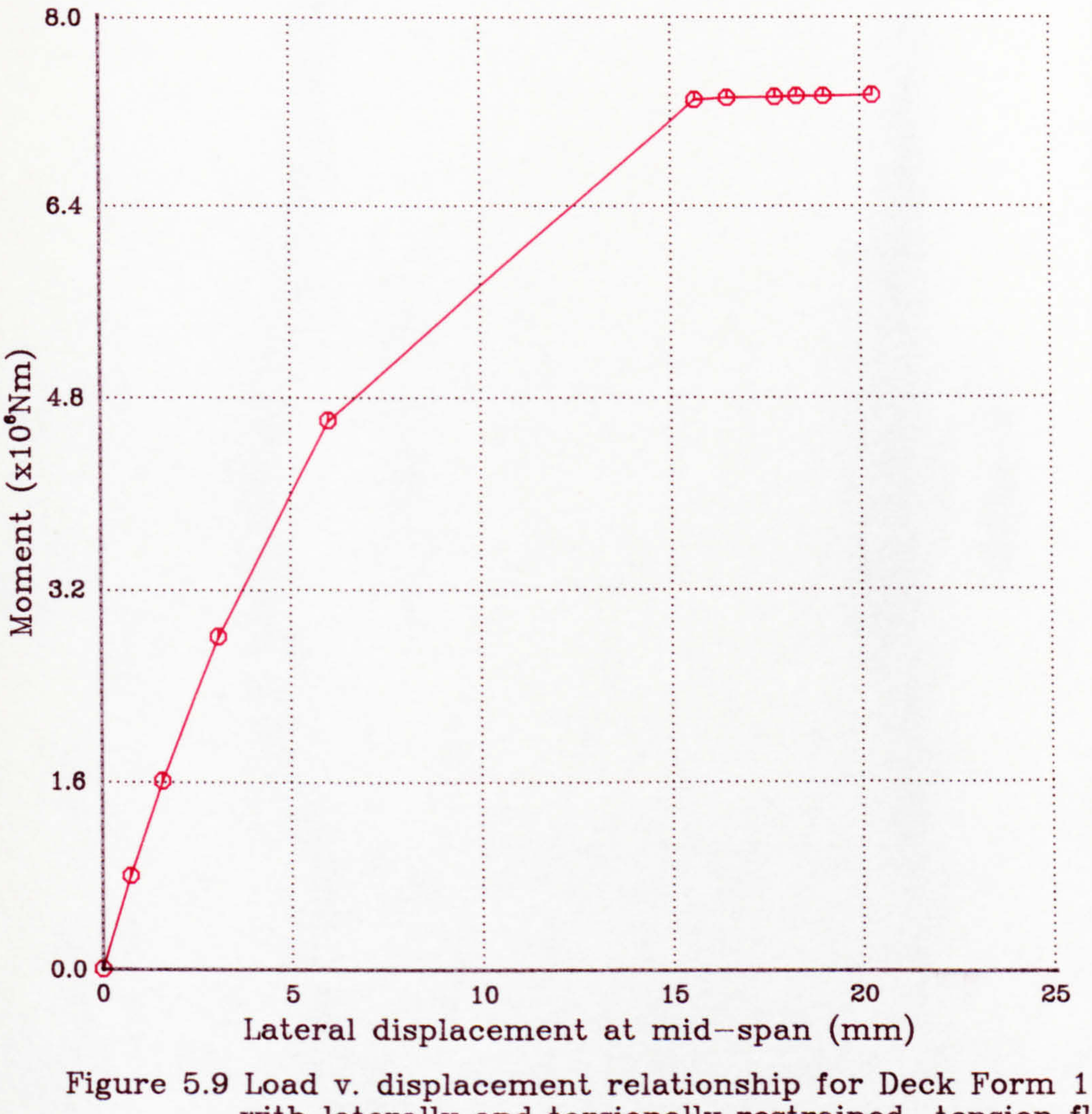

Figure 5.9 Load v. displacement relationship for Deck Form 1 with laterally and torsionally restrained tension flange under uniform bending moment

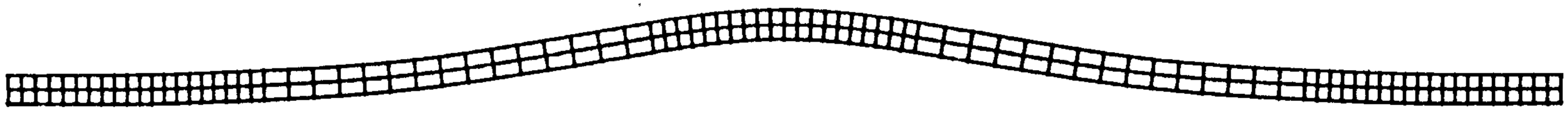

(a) compression flange

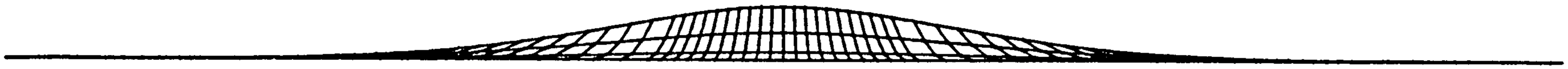

(b) girder web

Figure 5.10 Deck Form 1: final displaced shape in plan view with torsionally and laterally restrained tension flange with single span under uniform bending moment

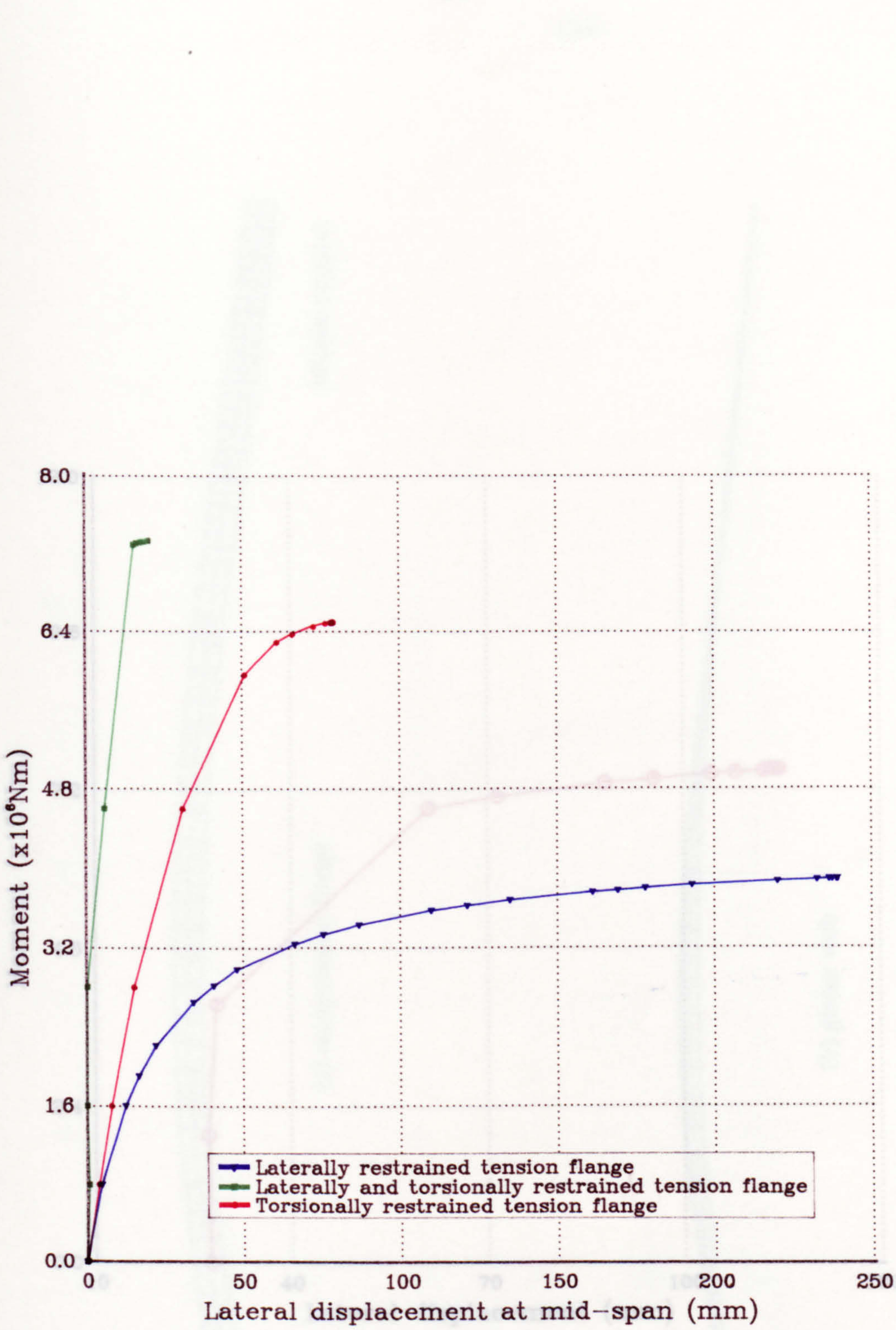

Figure 5.11 Effect of restraints on bending resistance of Deck Form 1 under uniform bending moment

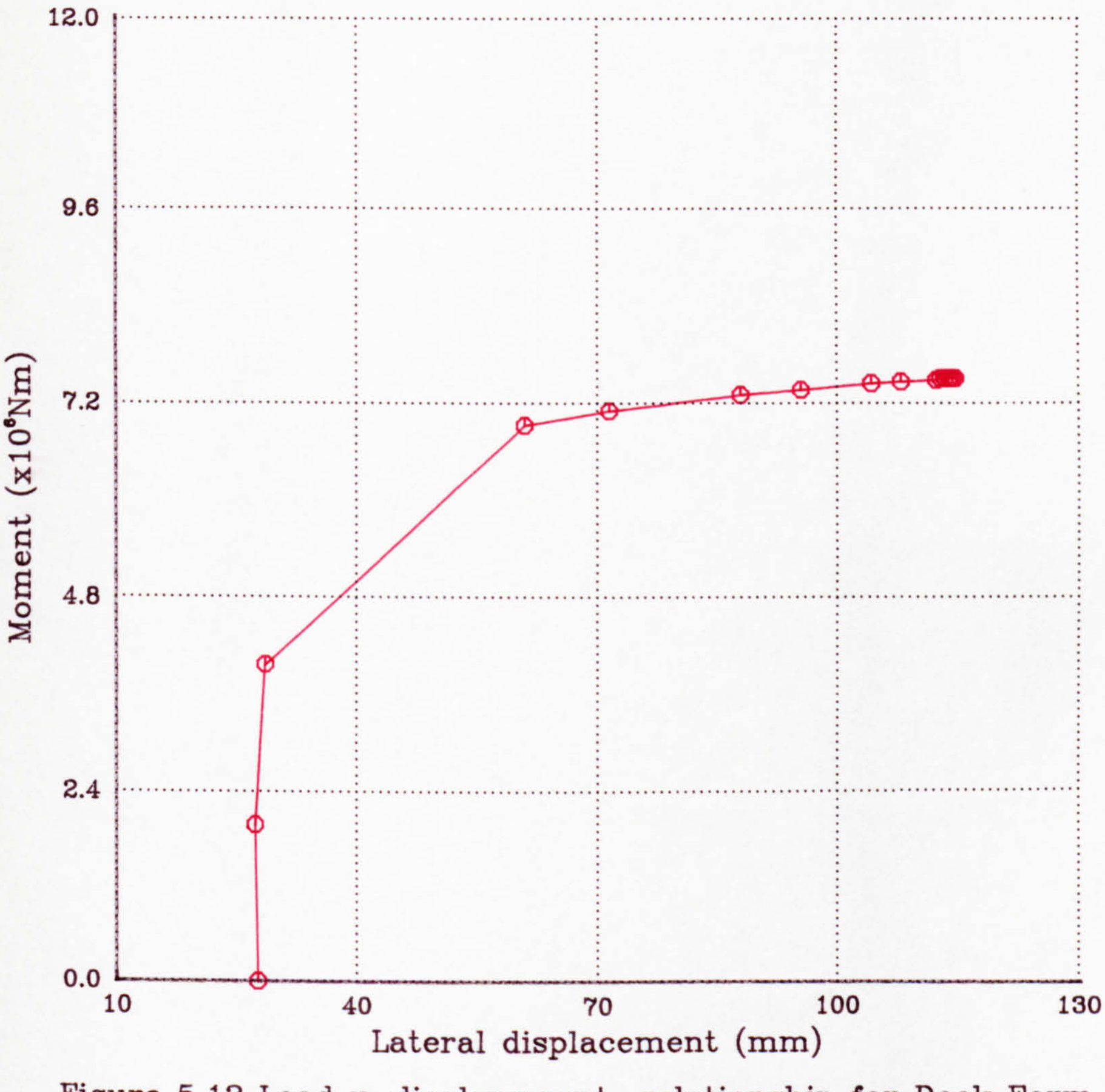

Figure 5.12 Load v. displacement relationship for Deck Form 1 with torsionally restrained tension flange under UDL on double span

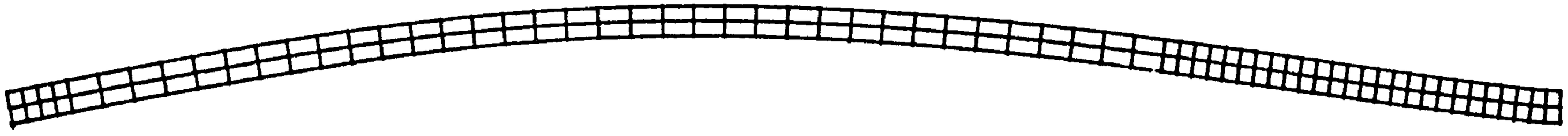

End support (a) compression flange Middle support

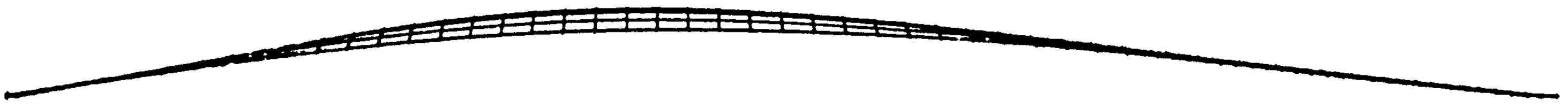

(b) girder web

Figure 5.13 Deck Form 1: final displaced shape in plan view with torsionally restrained tension flange with double span under UDL

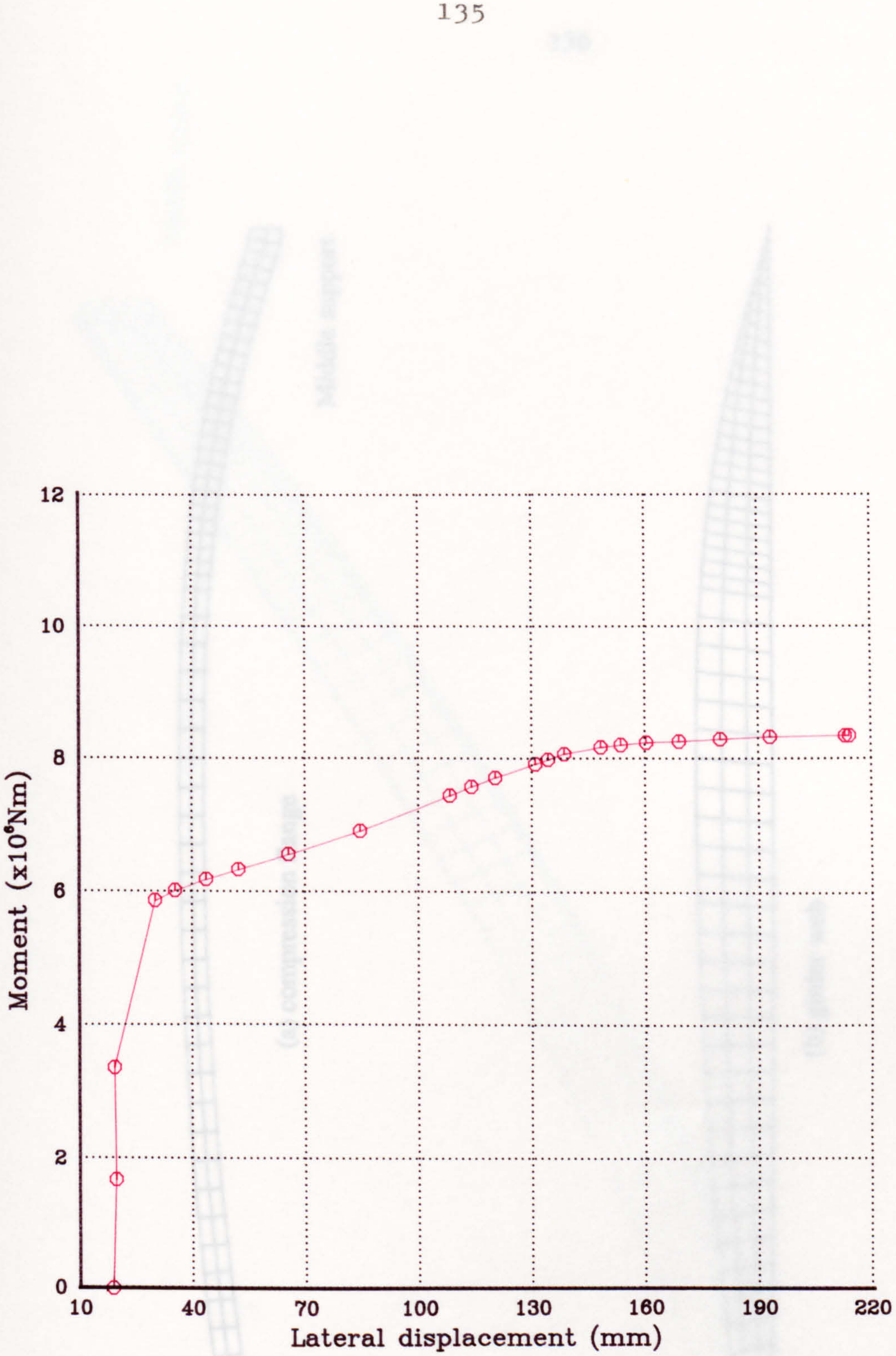

Figure 5.14 Load v. displacement relationship for Deck Form 1 with laterally restrained tension flange under UDL on double span

(a) compression flange

End support

Middle support

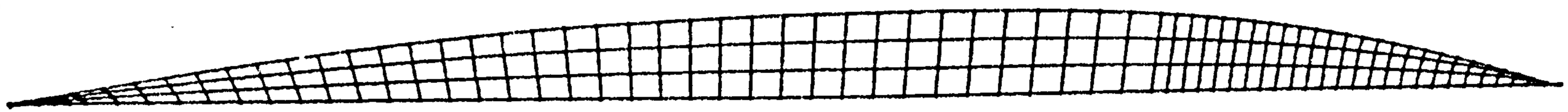

(b) girder web

Figure 5.15 Deck Form 1: final displaced shape in plan view with laterally restrained tension flange with double span under UDL

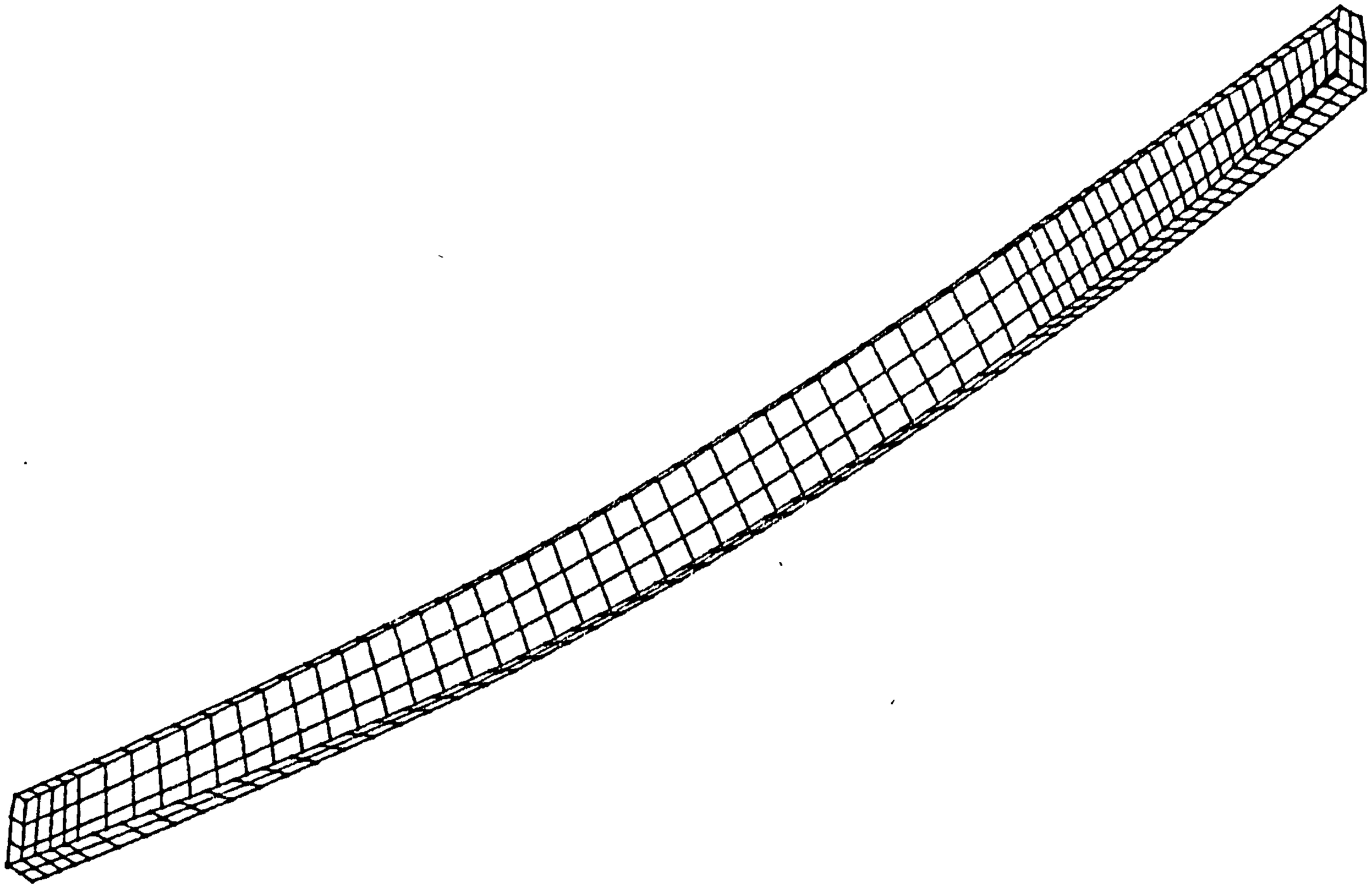

Figure 5.16 Deck Form 1: final displaced shape with laterally restrained tension flange with double span under UDL

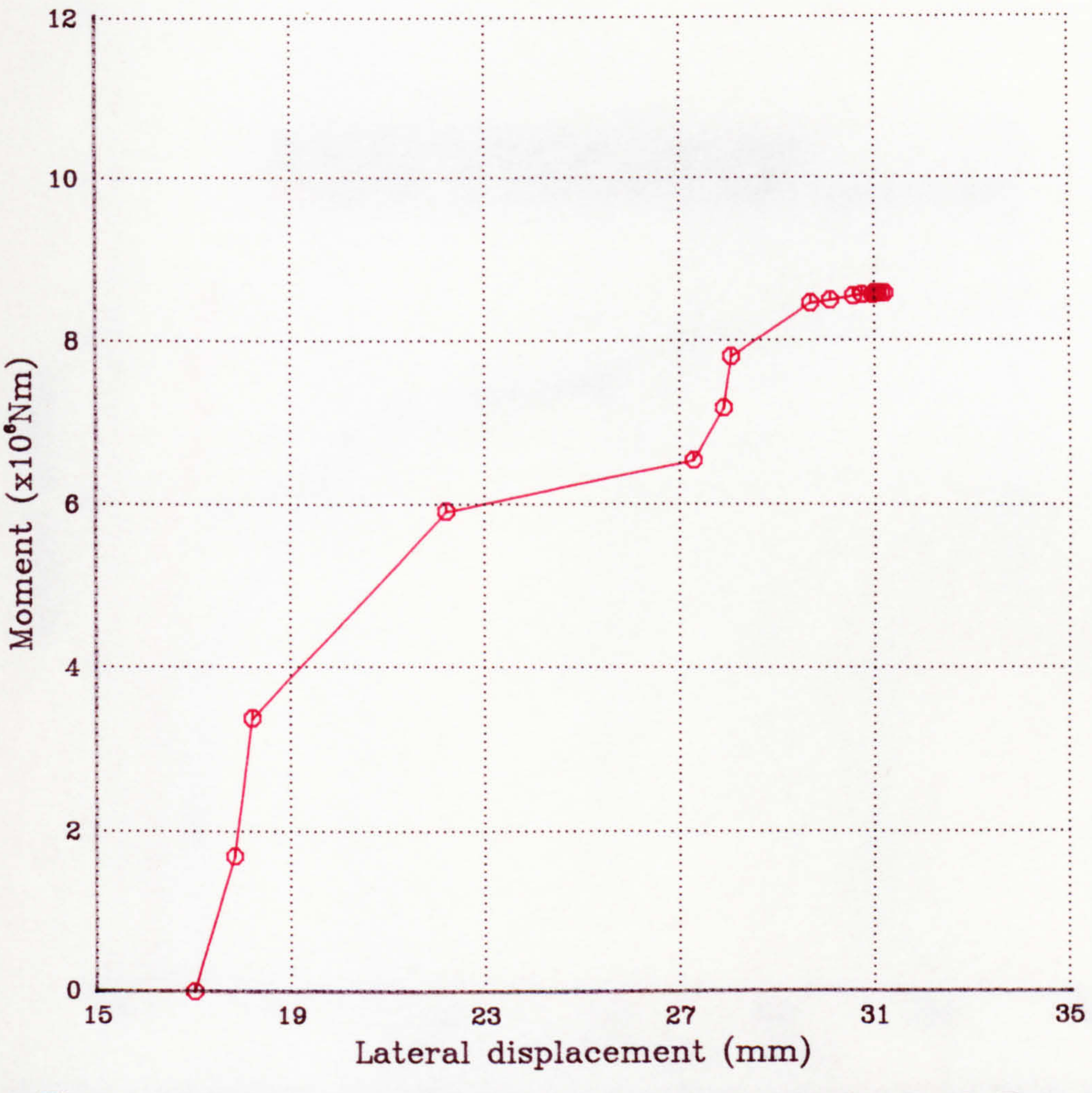

Figure 5.17 Load v. displacement relationship for Deck Form 1 with laterally and torsionally restrained tension flange under UDL on double span

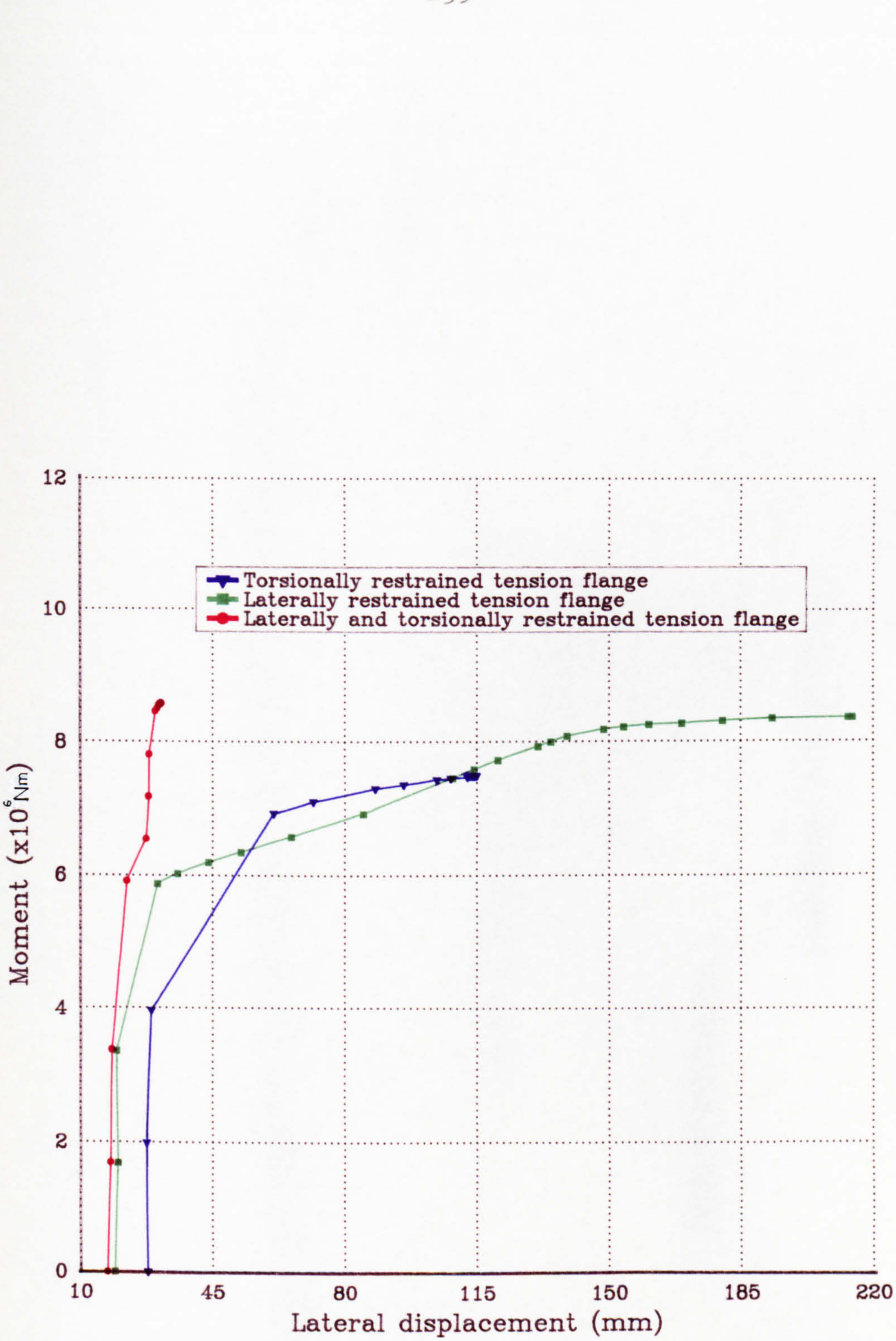

Figure 5.18 Effect of restraints on bending resistance of Deck Form 1 with two span under UDL

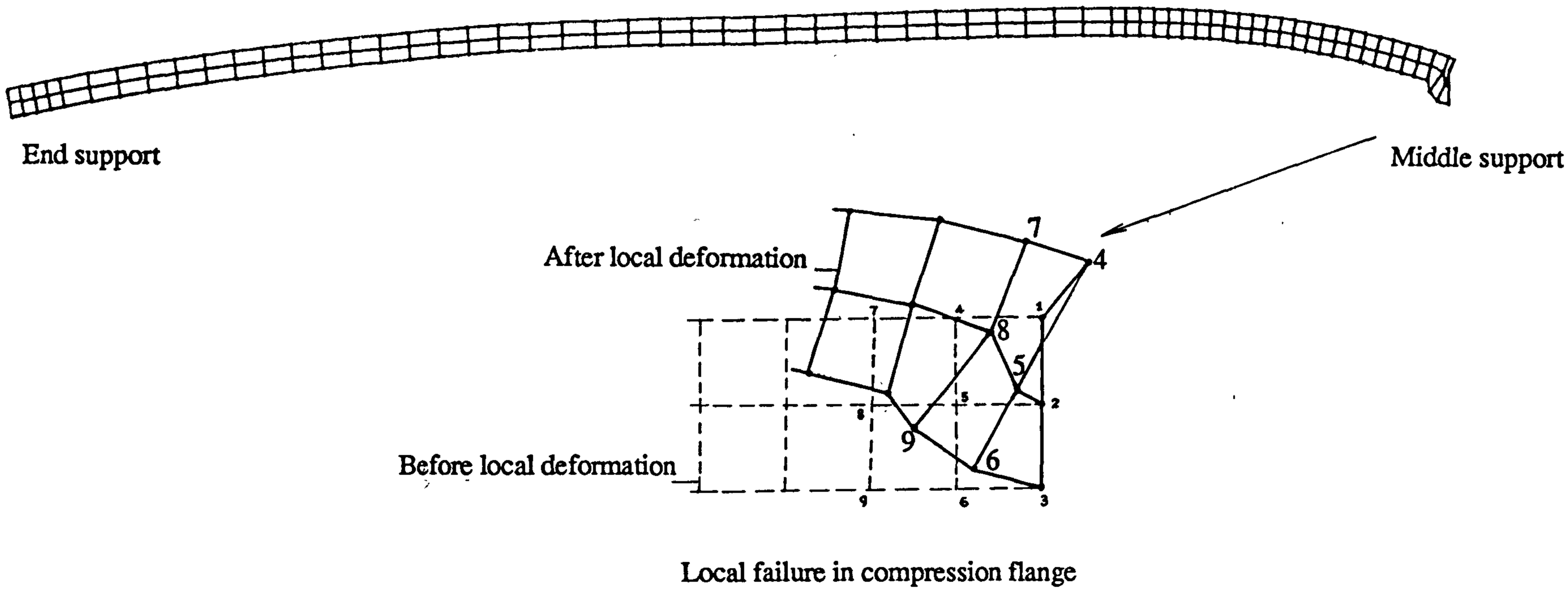

Figure 5.19 Deck Form 1: final displaced shape in plan view with torsionally and laterally restrained tension flange with double span under UDL (no sectional warping at middle support)

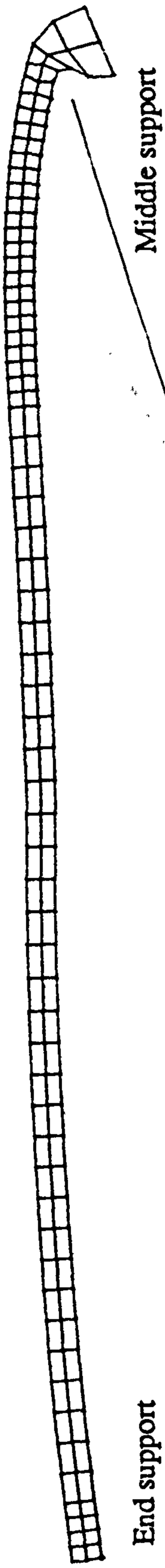

Figure 5.20 Deck Form 1: final displaced shape in plan view with torsionally and laterally restrained tension flange with double span under UDL (allowing for sectional warping at middle support)

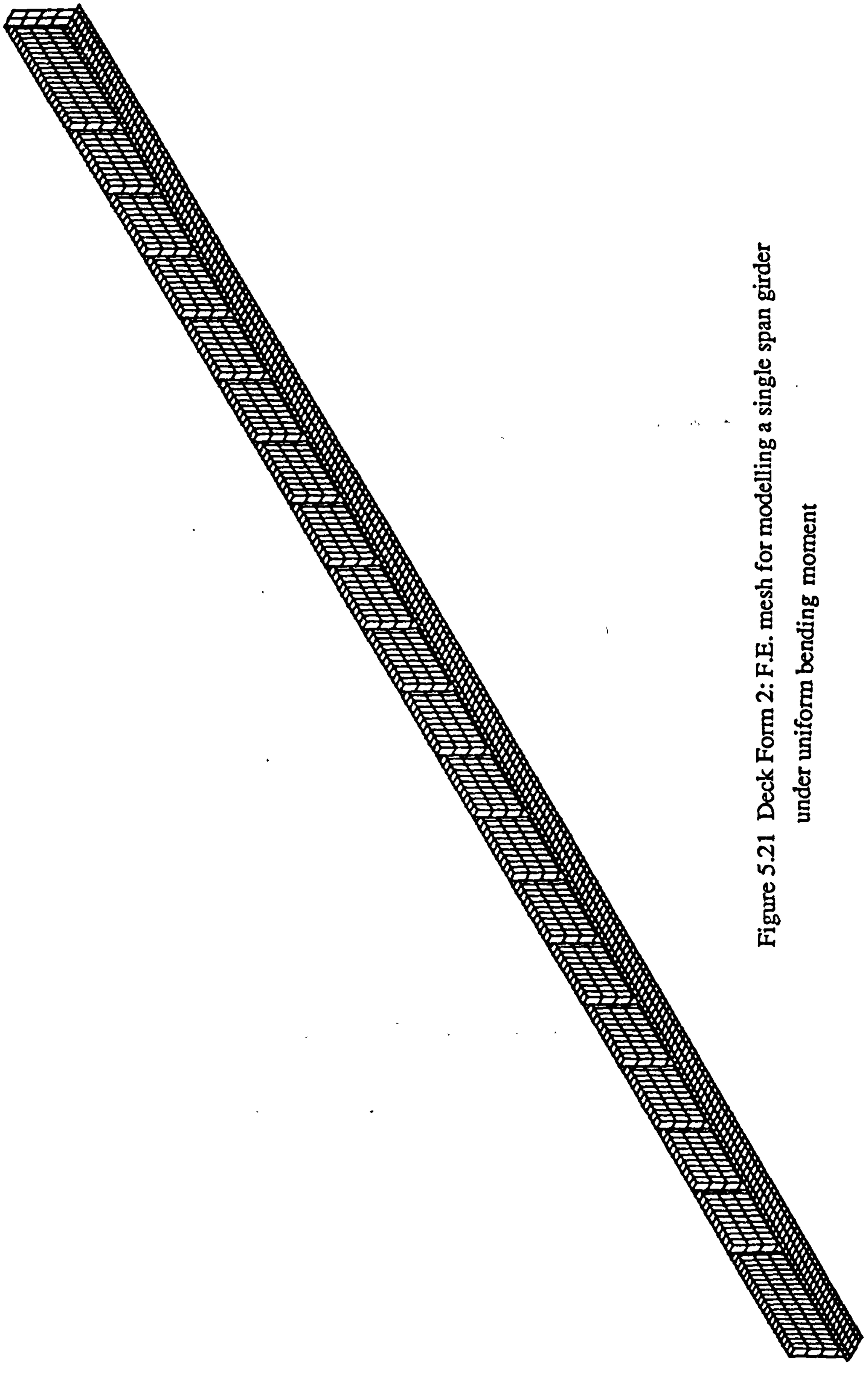

Figure 5.21 Deck Form 2: F.E. mesh for modelling a single span girder under uniform bending moment

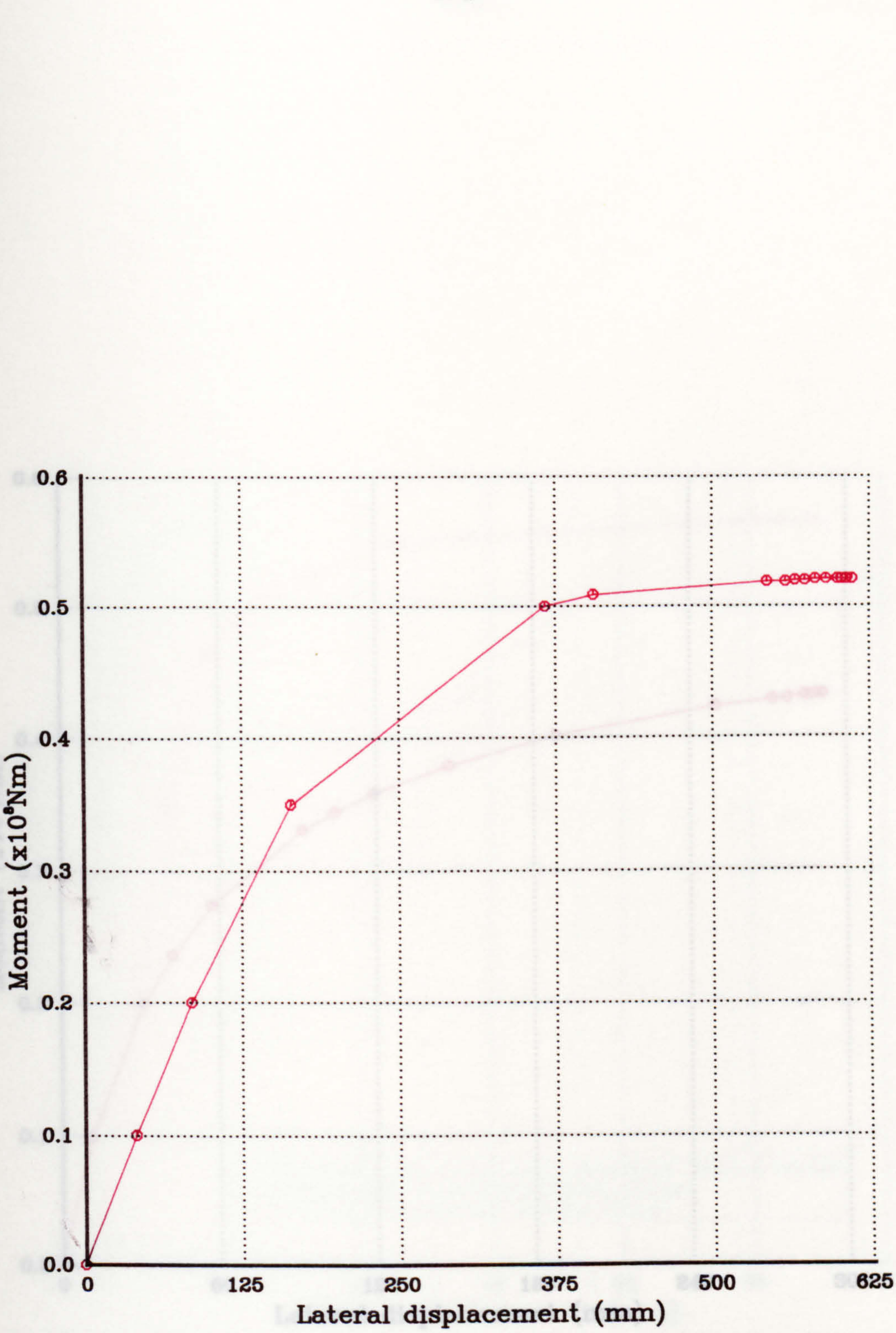

Figure 5.22 Load v. displacement relationship for Deck Form 2 with torsionally restrained tension flange under uniform bending moment

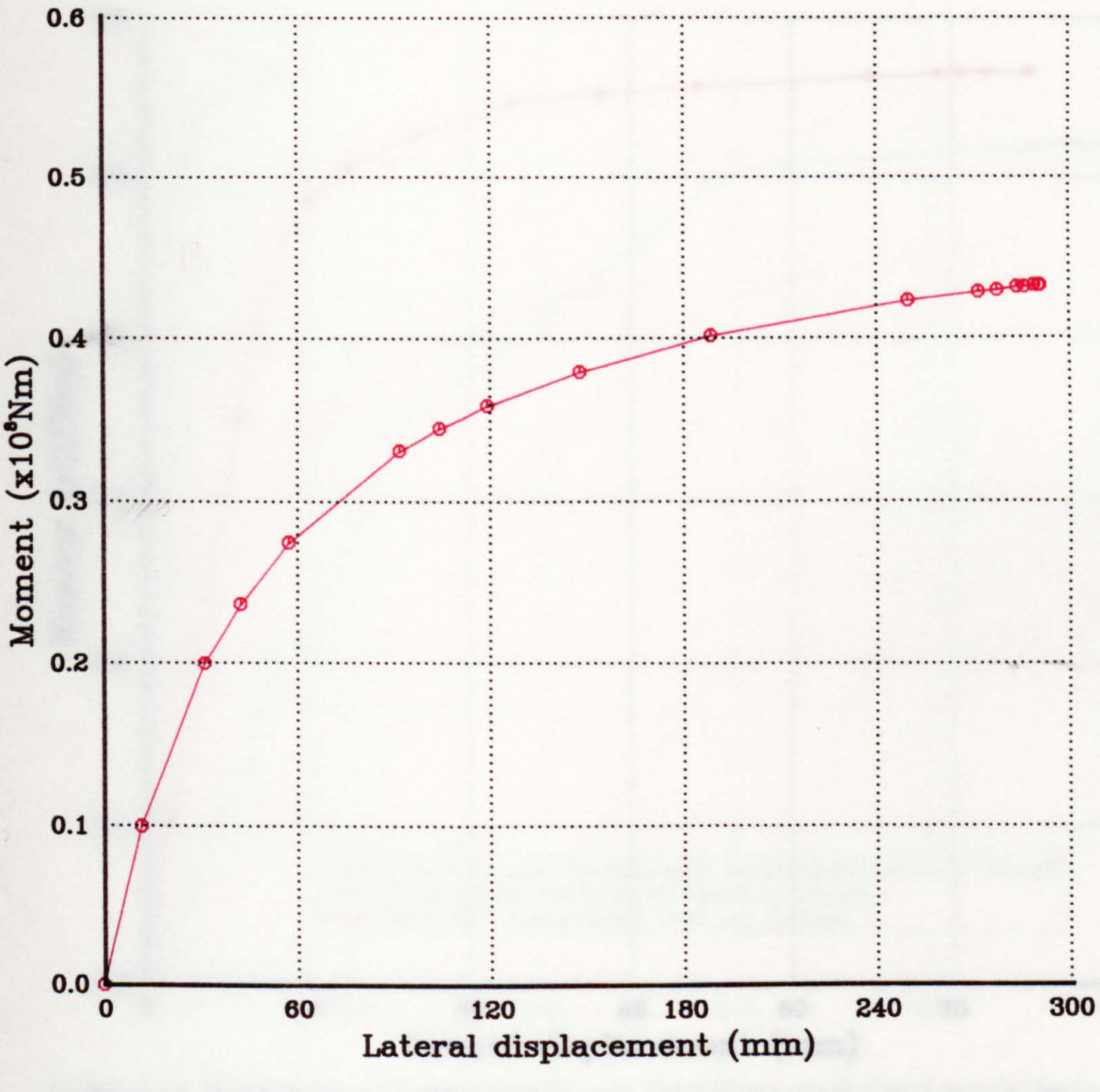

Figure 5.23 Load v. displacement relationship for Deck Form 2 with laterally restrained tension flange under uniform bending moment

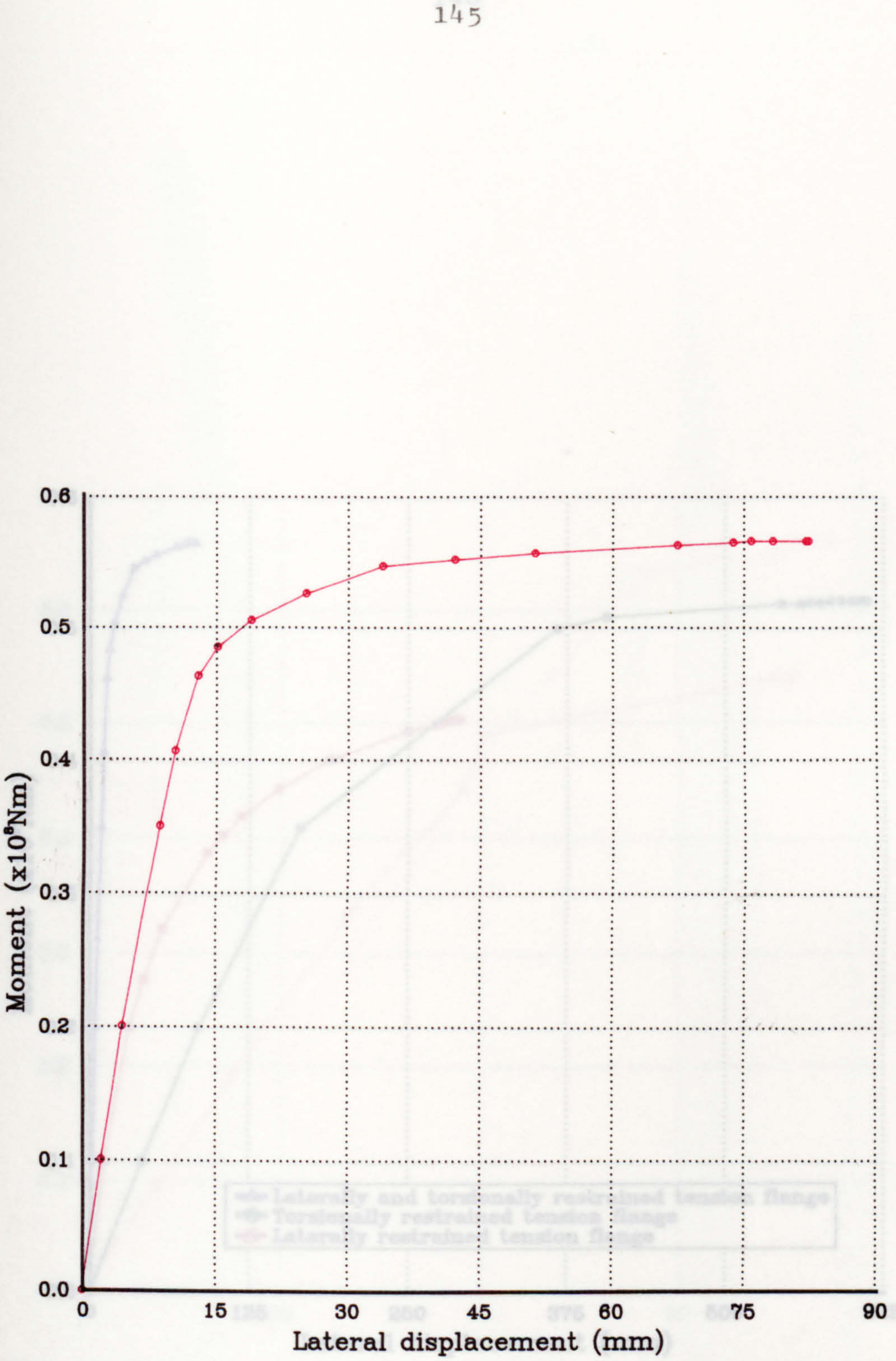

Figure 5.24 Load v. displacement relationship for Deck Form 2 with laterally and torsionally restrained tension flange under uniform bending moment

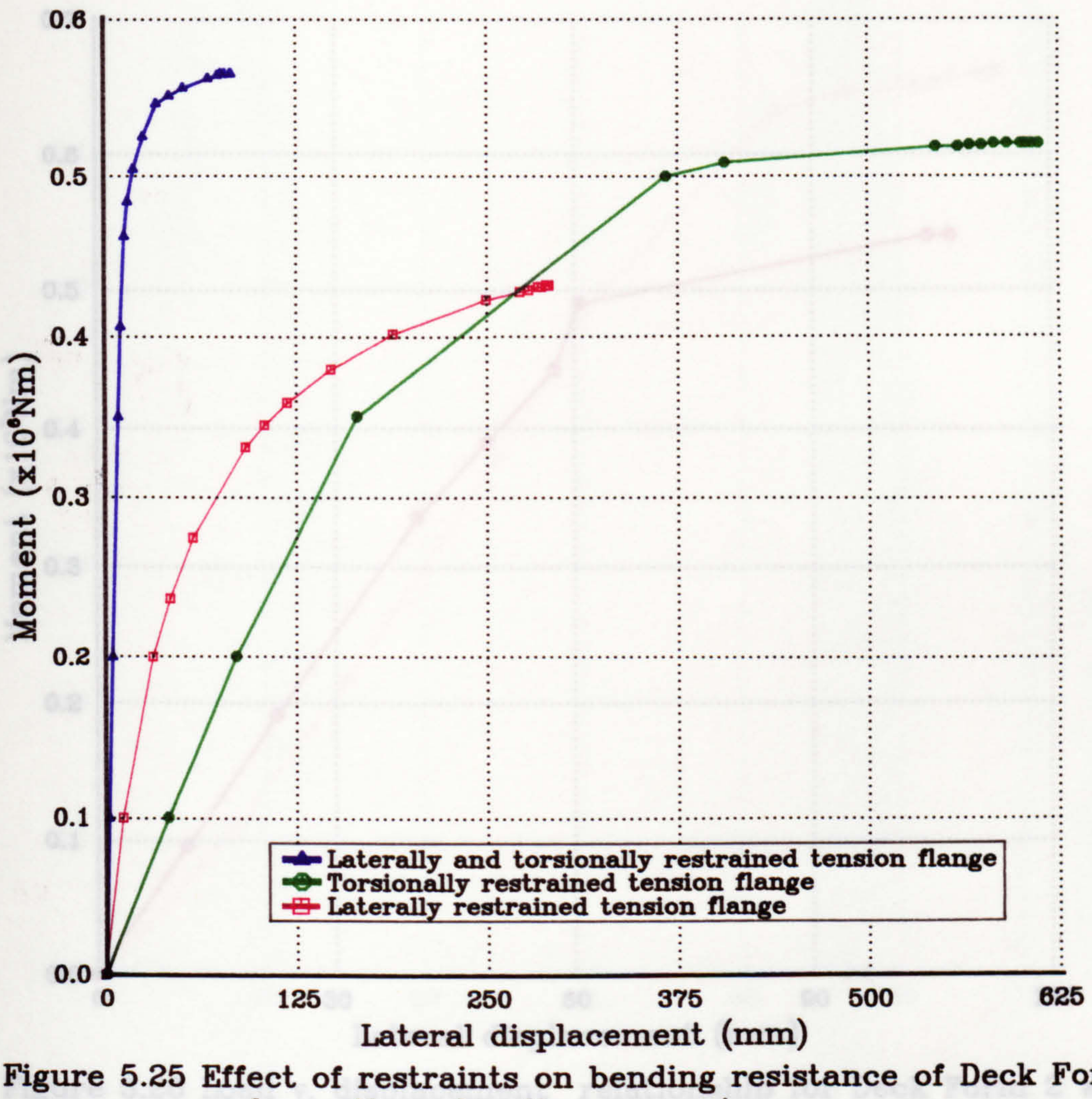

Figure 5.25 Effect of restraints on bending resistance of Deck Form 2 under uniform bending moment

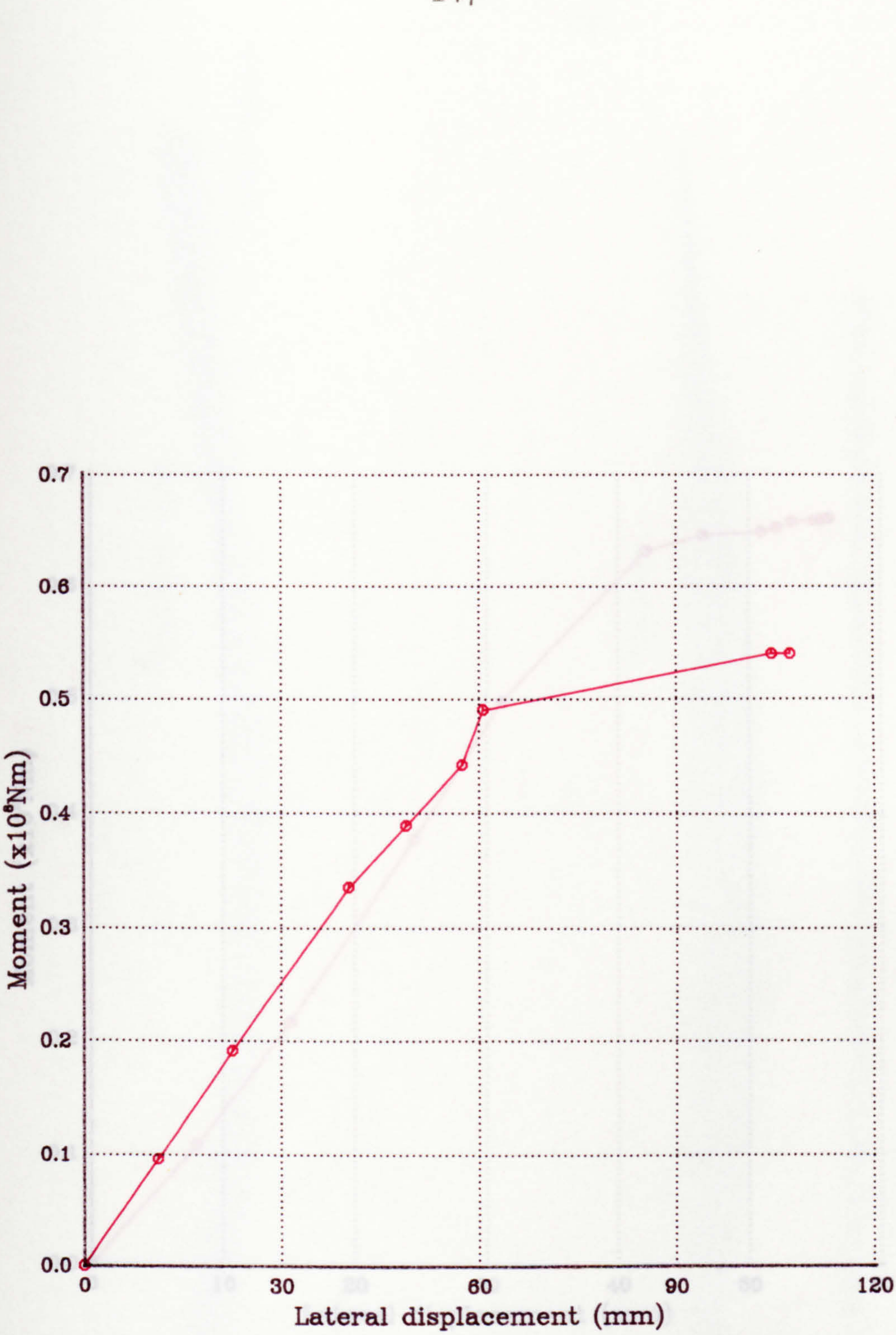

Figure 5.26 Load v. displacement relationship for Deck Form 2 with torsionally restrained top flange under UDL on double span

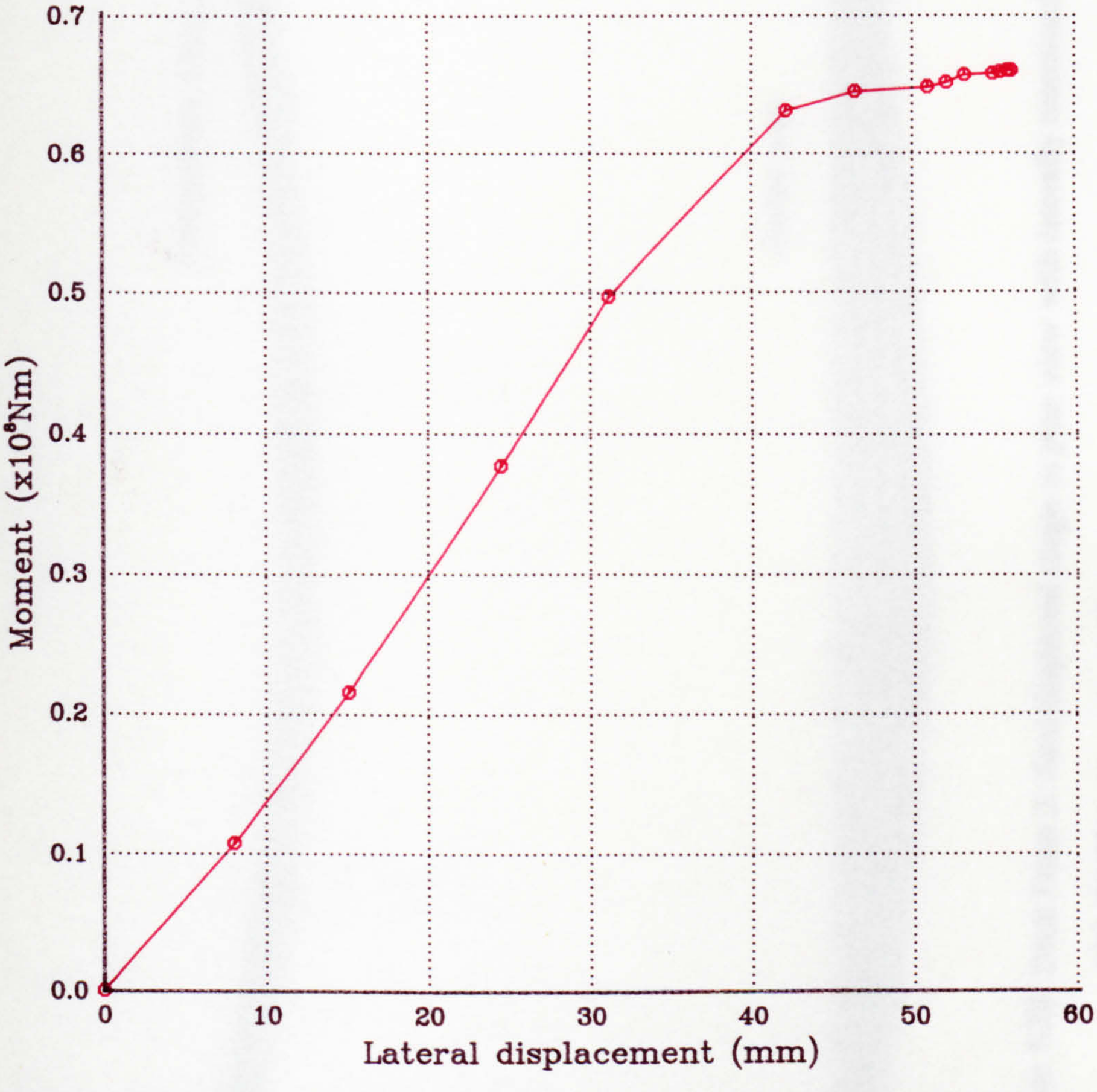

Figure 5.27 Load v. displacement relationship for Deck Form 2 with laterally restrained top flange under UDL on double span

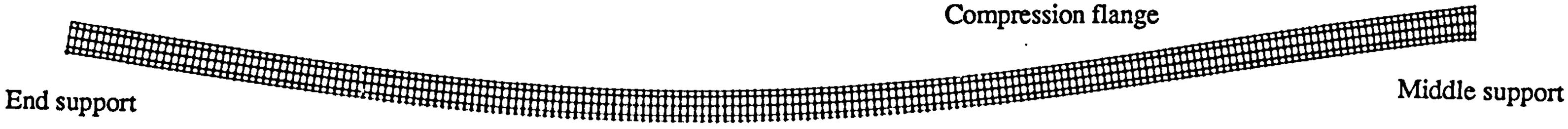

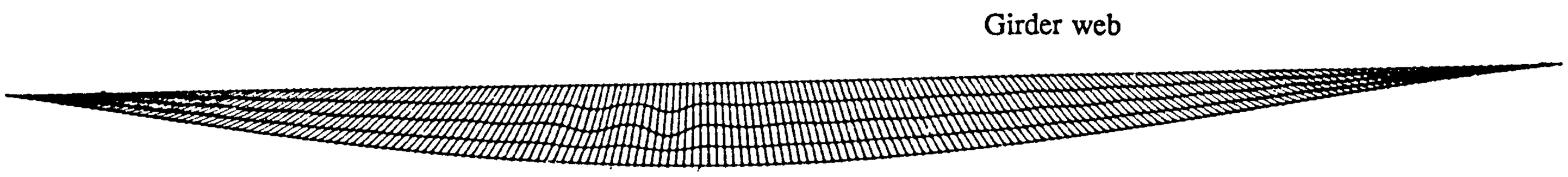

Figure 5.28 Deck Form 2: final displaced shape in plan view with laterally restrained tension flange with double span under UDL

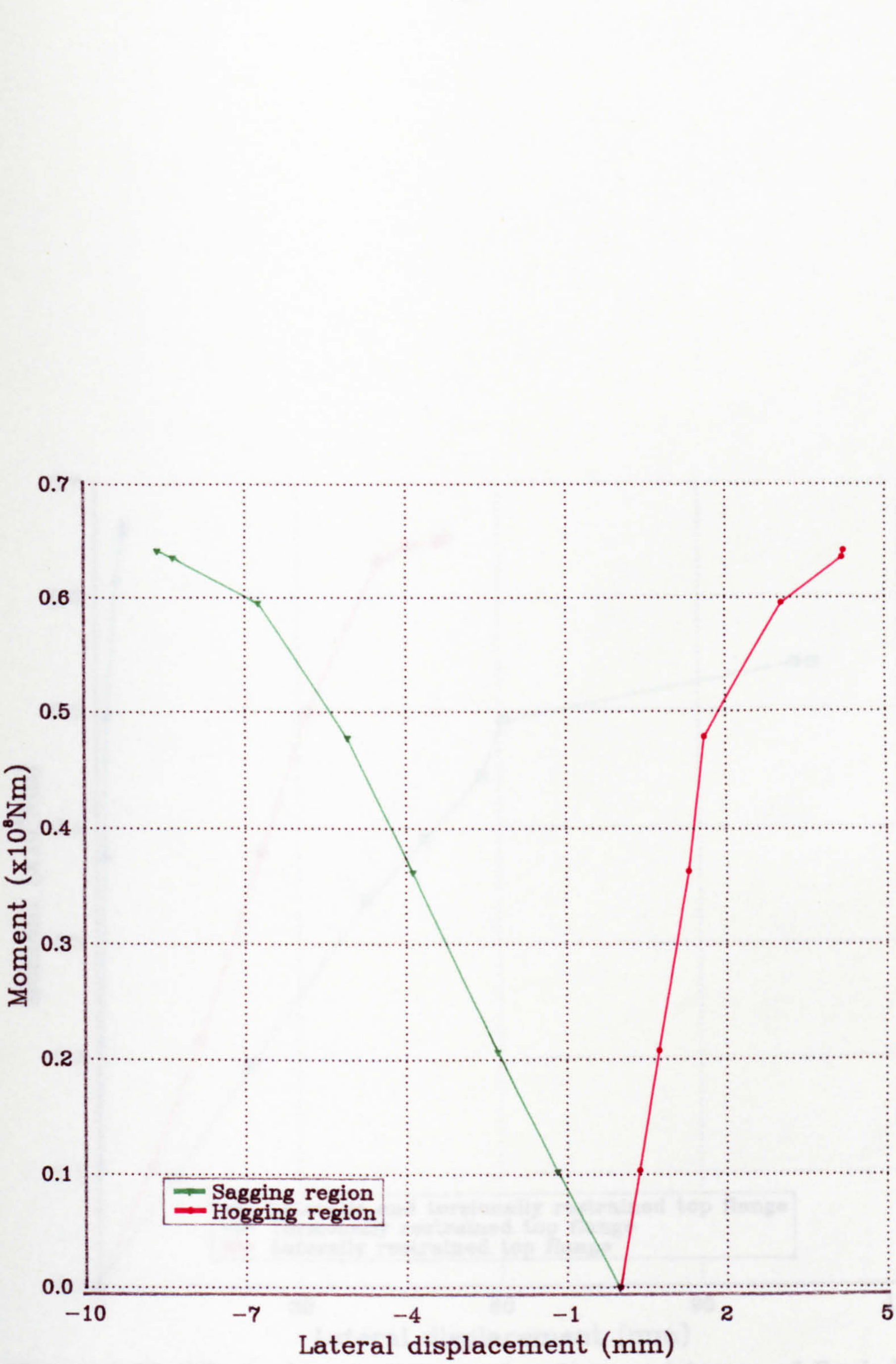

Figure 5.29 Load v. displacement relationship for Deck Form 2 with laterally and torsionally restrained top flange under UDL on double span

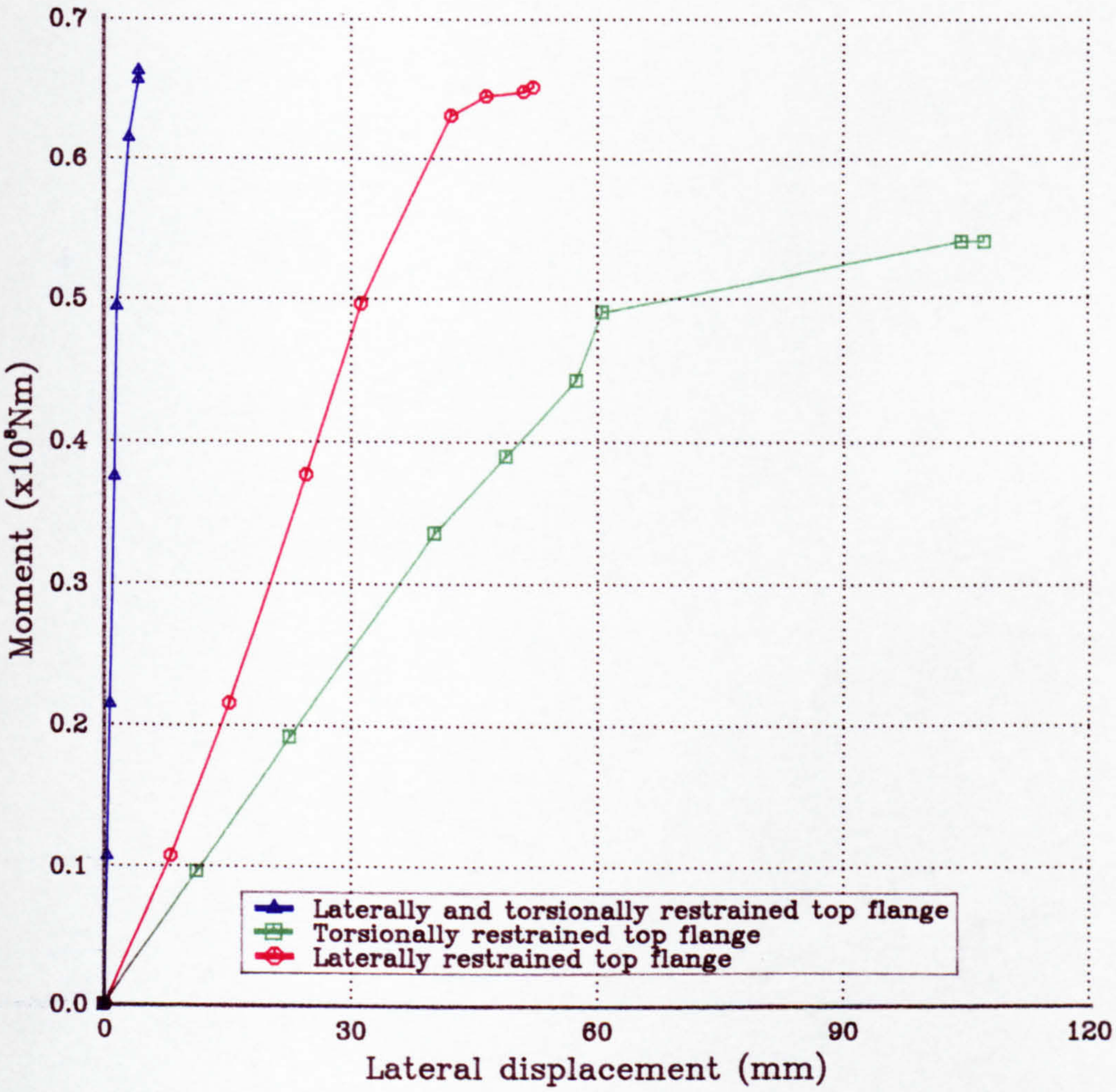

Figure 5.30 Effect of restraints on bending resistance of Deck Form 2 with double span under UDL

CHAPTER 6

FINITE ELEMENT IDEALISATION OF DISCRETE U-FRAMES

6.1 INTRODUCTION

Although studies on lateral buckling of compression flanges braced by a concrete deck are relatively limited, research into the behaviour of compressive flanges under discrete U-frame bracing is even less. In particular, the effect of cross member bracing has not, to author's knowledge been examined.

The stiffness of U-frame bracing depends on the flexual rigidity of the cross members per metre run. For a discrete U-frame situation, the stiffness is mainly related to the stiffness of cross members and spacing between them.

Hence, a series of finite element analyses of plate girders, under discrete U-frame bracing action, were carried out using various parameters, including:

(a) size of cross-beams;

(b) distance between cross-beams;

(c) $\frac{D}{t_f}$ ratio; and

(d) moment variation due to UDL.

In the past, the ratio of overall depth D to the thickness of the flange t_f (in the case of flanges with equal thickness or, otherwise, the mean thickness of the flanges), which is an approximation of the torsional index of a section, had been taken as a parameter in the study of lateral torsional buckling of steel I-section girders. Its effect on the load capacity of a bare steel girder was shown clearly [20]. The Perry-Robertson curve is based on a special case where this ratio is approaching infinity. In the situation of I-section girders braced by U-frames, this so-called torsional index $\frac{D}{t_f}$ has not been considered by previous researchers, perhaps because distortion in the girder web overshadowed its importance. Instead, the web slenderness has been found to be a more critical parameter [22,26] in continuous U-frames. The only case of moment variation studied numerically thus far is the single fixed-end span situation.

The influence of these parameters, or rather, their combined effects on the ultimate load carrying capacities of girders, and the behaviour of compression flanges under U-frame restraint have been investigated in the present study. The effectiveness of

discrete U-frames has been compared with that of continuous U-frames. The differences between design values according to BS5400 and computed results are discussed here. The suitability of the formulae proposed recently is also considered.

Based on the dimensions of the girders in Deck Form 1 (see Chapter 5) and the corresponding stiffness of one meter run concrete deck, an approximately equivalent cross-beam of size 180x180mm was used to interconnect girders, instead of a concrete deck. To study the effect of size of cross members in general, three beam sizes, namely, 50x50mm, 100x100mm and 150x150mm were selected.

As a result of limitations on computer storage and computation time, four-node thin shell elements (S4R5) accommodating five degrees of freedom per node were used rather than eight-node elements for top and bottom flanges, web and transverse web stiffeners. Linear beam elements (B31) were used to simulate the cross-beams.

To connect the beams to the tension flange of the girder, MPC elements were used so that a rigid connection was provided between corresponding nodes.

Material employed for the series was assumed to have the following properties: $E = 2.05 \times 10^{11} Nm^{-2}$, $\upsilon = 0.3$ and the yield stress σ_{yc} was assumed to be $3.55 \times 10^{8} Nm^{-2}$ for all thicknesses of steel plates. The stress-strain relationship for the material was assumed to be perfectly elasto-plastic and the strain hardening effect was ignored.

Three sets of girders based on three different $\frac{D}{t_f}$ ratios were studied. Within each set, cross members of three different dimensions were placed at spacings of 1.0m, 2.5m, and 5.0m. The transverse web stiffeners were positioned at cross-beams positions. The initial imperfection adopted was a single parabola of maximum initial bow $\frac{L}{1000}$ at mid-span.

The study is divided into two parts. The first concerns girders under uniform bending moment and the second, girders under non-uniform moment.

6.2 UNIFORM BENDING MOMENT

The basic configuration of the models, as shown in Figure 6.1, consists of a pair of simply supported steel plate girders interconnected by cross-beams at tension flange level to form clear discrete U-frame bracings. Bearing stiffeners were provided on both sides of the web at supports and vertical stiffeners were placed only on the inner web faces at U-frame positions. For all models, the overall span was 25.0m. Due to the symmetry of the U-frames, only one girder of a pair was modelled. To accommodate the force concentration at the supports, the mesh was refined in that region.

Concentrated loads were applied at the ends of the cantilever extensions to the girder to create uniform bending over the girder span. The thickness of the bearing stiffeners was twice that of the vertical web stiffeners.

6.2.1 $\frac{D}{t_f}$ ratio of 31

6.2.1.1 Load Capacity

It was clear that the ultimate load capacity of the girders was influenced by the size of cross-beams and this was investigated.

When the cross-beams were placed 1.0m apart, the ultimate capacity of the girder with cross-beam size 50x50mm was 5.94×10^6Nm. This increased by 25.7% with the beam size doubled. However, a further increase of only 1% occurred when the beam size changed to 150x150mm. When the spacing between the members was 2.5m, an increase of 54% of ultimate load was achieved as a result of doubling the cross-beam size. Again, just a slight increase of 2% in the failure load was observed after a further increase of 50% in beam size. This effect was more marked when the spacing was increased to 5.0m. A considerable jump of 65% of the ultimate load capacity followed by only another 5% increase were shown when the cross-beam size changed from 50x50mm to 100x100mm and then to 150x150mm.

Therefore, an increase in the size of the cross-beam beyond a certain critical value did not increase the ultimate load capacity of the girders very much. A summary of the results is given in Table 6.1. The relationship between the two is plotted in Figure 6.2.

In contrast to the effect of cross-beam size, an increase in the spacing reduced the ultimate load capacity of the girders. However, the influence of spacing was only dominant when cross-beams with the smaller dimension of 50x50mm were used. A loss of 25% of the failure load was noticed when spacing increased from 1.0m to 2.5m. A further reduction of 10% occurred when the beams were spaced at 5.0m. For cross-beams of sizes 100x100mm and 150x150mm, the reduction was only between 1% to 4%. Hence, the influence of spacing was insignificant.

6.2.1.2 Load-Deflection History

During the loading process, attention was focussed on the lateral movement of the compression flanges, the rate of change of movement and the development of plasticity in elements. Load versus deflections of the compression flange at mid-span were plotted in Figure 6.3.

(a) Spacing=1.0m

It was observed that for a cross-beam size of 50x50mm, localised yielding in the extreme fibre of a few main girder elements was detected when the applied load was 99% of the failure load. Compression flange elements at mid-span and elements in the vicinity of the support region had yielded completely by the end of loading.

When cross-beam size increased to 100x100mm, yield occurred in the same region as mentioned above but at a slightly earlier stage. Yielding in the web elements at the mid-span section were also noticed.

Table 6.1 Comparison between BS5400 design values of bending resistances and ABAQUS results for girders with $\frac{D}{t_f}$ ratio of 31 under uniform bending

Cross-beam spacing (m)	Cros-beam size (mm)	l_e (m)	λ_{LT}	$M_{D(1)}$ BS5400 ($x10^6$Nm)	σ_{li} BS5400 (Nmm^{-2})	$M_{D(2)}$ ABAQUS ($x10^6$Nm)	σ_{li} ABAQUS (Nmm^{-2})	$\frac{M_{D(2)}}{M_{D(1)}}$
1.0	50	15.62	118.56	2.29	105.08	5.95	273.06	2.60
	100	7.90	66.61	6.07	259.42	7.48	343.28	1.23
	150	5.36	46.36	7.08	325.09	7.55	346.49	1.07
2.5	50	19.64	140.67	1.72	78.81	4.75	217.99	2.76
	100	9.94	81.78	4.33	198.67	7.31	335.47	1.69
	150	6.74	57.58	6.30	288.97	7.45	341.96	1.18
5.0	50	23.35	159.03	1.36	62.39	4.27	195.96	3.14
	100	11.82	94.77	4.08	157.62	7.03	322.63	1.72
	150	8.01	67.46	5.51	252.85	7.38	338.68	1.34

The plasticity in the elements near the support region was developed at 94% of the failure load when 150x150mm cross beams were used. When the applied load reached 98% of ultimate failure load, the elements in the compression flange at mid-span started

yielding. This was followed by yield in the web elements in the support region and mid-span.

(b) Spacing =2.5m

There is no plasticity throughout the entire loading process for the case of using 50x50mm cross-beams since the load capacity of girders was decreased by 25% due to the change of spacing from 1.0m to 2.5m

The severity of plasticity reduced when the other two cross-beam sizes were employed. This is also attributable to the fact of loss in ultimate load capacity of the girders.

(c) Spacing=5.0m

When the spacing was further increased to 5.0m, the occurrence of the plasticity in the structures was similar to the situations with spacing of 2.5m.

From the load-deflection relationships of all the girders studied so far (see Figure 6.3), the rates of increase of displacement were significantly affected by the size of the cross-beams. For the small cross-beams, the increase in lateral deflection at mid-span was gradual with the increase in the magnitude of the load until a certain threshold whereby the rate of increase of lateral deflection accelerated producing an excessive total deflection at the completion of loading.

6.2.1.3 Buckling Mode

(a) Spacing =1.0m

When the beam size was 50x50mm, a single half-wave was developed as the final deflected shape of the compression flange. However, when the cross-beam size increased to 100x100mm, the lateral deflection of the compression flange near the supports became relatively small, compared with the same pair of girders with 50x50mm cross-beams. A deformed shape consisting of three half-waves developed in the final loading stage. The amplitude of the half-waves was dramatically reduced. When the size increased to 150x150mm, a buckling mode of multiple half-waves was clearly developed in the compression flange between the supports at the failure stage. The three resultant buckling shapes associated with the three cross-beams are illustrated in Figure 6.4. Thus, increase in cross-beam size altered the number of half-waves of the final buckled shape. The magnitude of deflection was also affected. When the size of the cross-beams was 50x50mm, the maximum deflection was approximately 110.0mm, while, for a size of 150x150mm, the maximum deflection was only about 16mm.

(b) Spacing = 2.5m

The buckled shape only consisted of one single half-wave for cross-beams of sizes of 50x50mm and 100x100mm. A three half-wave curve, similar to that shown in Figure 6.4(b), was developed when the size was 150x150mm. There was a dramatic reduction in the magnitude of the final displacement as the cross-beam size increased.

(c) Spacing=5.0m

Only one single half-wave was generated despite the change in the size of cross-bracing. The overall deformed structure with one single half-wave as the buckled shape of compression flange is depicted in Figure 6.5.

6.2.1.4 Effect of Transverse Web Stiffeners

With the presence of transverse web stiffeners, the model resembles that of twin girders with discrete U-frames. If these stiffeners are removed and the cross-beams placed very closely, continuous U-frame action is simulated. With this in mind, twin girders of the same dimensions and components as the previous ones minus web stiffeners were modelled and analysed under uniform bending.

With a cross-beam size of 150x150mm and spacing between bracings of 1.0m, the result showed that the effect of the stiffeners on load capacity was not crucial. This agrees with the findings of Kerensky[20] and Bradford[16]. The maximum load reached was 7.29×10^6Nm, a reduction of 3.4% only. Nevertheless, the deflected shapes in the two cases are, however, very different. Instead of forming multiple half-waves, only one half-wave was formed in the absence of stiffeners. Considering the relationship between load capacity and the number of half-waves, it is quite clear that there is no simple connection between the two.

The displacements along the depth of the cross-section with or without the stiffeners were observed. The reduction in the flexibility of the web was obvious with the presence of the transverse web stiffeners. Thus, the role of transverse web stiffeners was not so much enhancement of the ultimate load capacity of the girders but prevention of any excessive displacement.

6.2.2 $\frac{D}{t_f}$ ratio of 41

A second set of girders with a higher value of $\frac{D}{t_f}$ ratio was analysed. The cross-section was classified as a non-compact section according to BS5400.

6.2.2.1 Load capacity

As shown in the Table 6.2 below, there were, in general, substantial increases in ultimate load capacity in response to change of cross-beam size from 50x50mm to 100x100mm (46% increase for the set with spacing of 1.0m and more than 70% for the sets with spacing of 2.5m and 5.0m). However, the percentage of increase declined when the size of the cross-beams was further increased to 150x150mm (as summarized in Figure 6.6).

Table 6.2 Comparison between BS5400 design values of bending resistances and ABAQUS results for girders with $\frac{D}{t_f}$ ratio of 41 under uniform bending

Cross-beam spacing (m)	Cross-beam size (mm)	l_e (m)	λ_{LT}	$M_{D(1)}$ BS5400 ($x10^6$Nm)	σ_{li} BS5400 (Nmm^{-2})	$M_{D(2)}$ ABAQUS ($x10^6$Nm)	σ_{li} ABAQUS (Nmm^{-2})	$\frac{M_{D(2)}}{M_{D(1)}}$
1.0	50	17.64	144.11	2.25	76.10	6.83	232.63	2.49
	100	8.19	80.18	6.07	205.10	9.97	339.58	1.42
	150	6.04	55.59	8.72	294.47	10.32	351.50	1.09
2.5	50	22.18	171.67	1.67	56.25	5.55	189.03	2.76
	100	11.21	98.57	4.41	148.89	9.69	330.04	1.85
	150	7.59	69.13	7.35	248.15	10.01	340.94	1.24
5.0	50	26.38	194.33	1.27	43.01	5.12	174.39	3.26
	100	13.33	114.56	3.48	117.46	8.83	300.75	2.15
	150	9.03	81.14	5.97	201.82	9.89	336.85	1.44

The change in ultimate load was not very sensitive towards the spacing of the cross-beams, especially in the case of larger cross-beams of 150x150mm. A maximum loss in ultimate load of about 25% occurred when the spacing changed from 1.0m to 5.0m when 50x50mm cross-beams were used. For strong cross-beams, ie, 150x150mm, the reduction in failure load, due to an increase in spacing from 1.0m to

2.5m and then to 5.0m was 3% and 1% respectively. Thus, the effect of spacing was insignificant.

6.2.2.2 Load-Deflection History

As shown in Figure 6.7, applied load was plotted against lateral deflection of that point on the compression flange associated with maximum lateral displacement at failure load.

(a) Spacing =1.0m

When the cross-beam size was 50x50mm, yield in the compression flange elements and cross-beam elements at mid-span position were detected at the very end of the loading stage. At failure, a few cross-beams near mid-span had completely yielded. No local yielding in the vicinity of the supports was found.

For the cases in which 100x100mm or 150x150mm cross-beams were provided for bracing action, there was no yielding detected in the cross-members. Yield in web elements at the supports and compression flange elements at mid-span was not significant until 99% of the failure load was reached. Accompanying this yield was a sudden increase in lateral deflection of the compression flange at mid-span.

(b) Spacing=2.5m

The use of 100x100mm and 150x150mm cross-beams produced a similar load-deflection history to the situation mentioned above. A sudden increase in lateral displacement of the compression flange occurred when yield developed in the elements near the supports and at mid-span. However, decreasing the size of cross-beams to 50x50mm generated a much smoother increase in the lateral displacement of the compression flange. As the ultimate load carrying capacity fell considerably, no yielding and thus, no plasticity was detected throughout the whole loading procedure.

The load-deflection history in the cases of 100x100mm and 150x150mm was similar to the situation of 1.0m spacing mentioned above.

(c) Spacing =5.0m

The yield of compression flange at mid-span and the elements near the support region towards the end of the loading stage caused a sharp increase in the deflection of the compression flange of the girders braced by 150x150mm cross-beams. When the size of cross-beams was reduced to 100x100mm, yield in the support regions was found to develop earlier than the yielding in the compression flange. There was no sudden increase in lateral displacement, and comparatively speaking, the displacement was much greater than for other cases with the same size of cross-beam but reduced spacing. The observation was also true for the case of girders braced by 50x50mm cross-beams. The

compression flange at mid-span did not yield until the very end of loading. This yielding may have been caused by the excessive deformation at mid-span.

The load-deflection curves for the girders with $\frac{D}{t_f}$ ratio of 41 followed the same trend as those for $\frac{D}{t_f}$ ratio of 31.

6.2.2.3 Buckling Mode

A single half-wave was generated for most of the combinations of cross-beams and spacings between them. Although these combinations, in turn, resulted in values of λ_{LT} ranging from 60 to 170, they seemed to be irrelevant to the deformed shapes of the compression flange braced by the U-frames. The amplitude of these half-waves, in general, reduced with increase in cross-beam size.

There was a special buckled shape, as shown in Figure 6.8, when the value of λ_{LT} was 55.59 for the girder braced by 150x150mm spaced at 1.0m. This buckled shape consisted of an odd number of unequal half-waves. It is interesting to note that the maximum lateral deflection did not occurred at mid-span.

6.2.3 $\frac{D}{t_f}$ ratio of 61

Following the study of girders with two variations of depth of web, it can be seen that these two groups of girders exhibited similar buckling behaviour (in terms of load-deflection history of the girders and buckling mode of the compression flanges) under the systematic changes of cross-beam size and spacing. The effect of the stiffness of the U-frames obtained from the cross-beam size and cross-beam spacing on much more slender section with $\frac{D}{t_f}$ ratio of 61 was investigated as follows.

6.2.3.1 Load Capacity

For a fixed value of spacing, the ultimate load capacity of the girders (as tabulated in Table 6.3) increased with increase in size of cross-beam. It was worth noting from Table 6.3 that, as the spacing increased from 1.0m to 5.0m, the effect of increasing the size from 50x50mm to 100x100mm on the ultimate load capacities fell from 91% to 50% but increased from 4% to 48% for the change of size from 100x100mm to 150x150mm. This led to a situation in which, when the spacing was 5.0m, a rise in the ultimate moment capacity of 50% was achieved for every increase in cross-beams size, ie, from 50x50mm to 100x100mm and then to 150x150mm. These are summarized in Figure 6.9.

The observation differed from the results obtained from the two groups of girders studied previously in which the ultimate load capacity was less influenced by the change

of size of cross-beams from 100x100mm to 150x150mm than that from 50x50mm to 100x100mm.

6.2.3.2 Load-Deflection History

The relationships between load and lateral deflection at mid-span of the compression flange for all the cases are plotted in Figure 6.10. Similar to the two groups studied before, it can be seen that the huge lateral deflection of the compression flange of the girders braced by 50x50mm cross-beams was considerably reduced as the sizes of cross-beam increased and the smooth load-displacement curves drastically changed when cross-beams of 150x150mm were used.

Table 6.3 Comparison between BS5400 design values of bending resistances and ABAQUS results for girders with $\frac{D}{t_f}$ ratio of 61 under uniform bending

Cross beam spacing (m)	Cross beam size (mm)	l_e (m)	λ_{LT}	$M_{D(1)}$ BS5400 ($x10^6$Nm)	σ_{li} BS5400 (Nmm^{-2})	$M_{D(2)}$ ABAQUS ($x10^6$Nm)	σ_{li} ABAQUS (Nmm^{-2})	$\frac{M_{D(2)}}{M_{D(1)}}$
1.0	50	21.42	197.22	2.14	43.01	8.33	170.52	3.89
	100	10.80	95.40	7.82	157.16	15.91	325.69	2.03
	150	7.37	75.29	11.20	224.98	16.57	339.20	1.48
2.5	50	26.93	236.00	1.48	29.78	7.47	152.92	5.04
	100	13.58	133.44	3.54	71.13	13.70	280.45	3.87
	150	9.26	93.69	8.15	163.78	16.18	331.22	1.99
5.0	50	32.03	268.11	1.15	23.16	7.05	144.32	6.13
	100	16.15	155.67	3.29	66.17	10.55	215.97	3.21
	150	11.02	110.29	6.09	122.42	15.6	319.34	2.56

(a) Spacing =1.0m

For cross-beams of 50x50mm, yield in the cross-beams near mid-span developed first, and was then followed by yield in cross-beams further away from mid-span. Elements in the compression flange at mid-span and the support region did not yield until the end of the loading. When the cross-beams increased to 100x100mm, no yielding in the cross-beams was detected. However, yield in web and bottom flange over the supports region occurred at 95% of the failure load. Elements in the compression flange at mid-span yielded at failure. When 150x150mm cross-beams were used, elements in the vicinity of the supports started yielding at a relatively early stage. Again, no yielding in the compression flange was noticed until failure.

(b) Spacing = 2.5m

No yielding in the cross-beams was detected. Elements remained elastic as the load increased. A slight yield over the supports was found at the ultimate load. When the cross-beam size changed to 100x100mm, yield of the elements over the support developed at a much earlier stage.

(c) Spacing = 5.0m

Apparently, there was no yielding throughout the whole loading process when girders were braced by 50x50mm and 100x100mm cross-beams. When 150x150mm were employed, however, yield occurred over the support region at the end of the loading.

The load-deflection curves plotted for case of spacing of 1.0m were similar to those plotted for torsional indices $\frac{D}{t_f}$ of 31 and 41 but when spacings between cross-beams became greater, the increase in slope of the curve was more gradual.

6.2.3.3 Buckling Mode

In general, a single half-wave, as shown in Figure 6.11, was the final displaced shape for the group of girders . The only exceptional case was in the case of using 150x150mm cross-beams with 1.0m spacing. The final buckled mode in the compression flange, together with the overall deformed structure is shown in Figure 6.12

6.2.4 Comparison of Finite Element Results with BS5400

The ultimate bending resistance of the girders obtained from ABAQUS was compared with the design values in accordance with BS5400 and the maximum compressive stresses estimated from the ABAQUS results were plotted on the limiting

stress curve, ie, Figure 10 of BS5400: Part 3, as shown in Figure 6.13 for comparison purpose.

In spite of the differences in their $\frac{D}{t_f}$ ratios most of the points plotted could be represented on a single curve, whereas in the tests done for lateral torsional buckling of I-girders without U-frame action, the stress curve was dominated by the factor $\frac{D}{t_f}$. This shows that the $\frac{D}{t_f}$ ratio has little influence in the bending resistance of girders braced by U-frames.

At lower values of slenderness parameter λ_{LT}, stresses obtained were kept at only small margins above the limiting stress curve. However, as the λ_{LT} value increased, the stresses achieved from ABAQUS were always higher than those designed according to the Code and the difference between the two grew wider as λ_{LT} became greater. (When the λ_{LT} was greater than 100, the difference was kept almost constant.)

Consistently, as the failure moment values in Tables 6.1, 6.2 and 6.3 have shown, the finite element analysis of the 27 girders braced by U-frames of various stiffnesses proves that, for near compact and non-compact sections, the design values of BS5400 could be regarded as very conservative.

6.3 BENDING DUE TO UDL

Having studied the behaviour of girders under uniform bending in the section above, the effect of the moment variation due to a UDL on double-span twin girders is examined in the following section.

In practical girder bridges of continuous span, instability of steel girders, braced by a concrete deck or cross-beams is most likely to occur adjacent to an intermediate support, where the bottom flange and part of the web are in compression. In the design of such structures, the method given in BS5400, which ignores the effect of steep moment gradient, ie, the variation of longitudinal stress in the hogging region, has been shown to be unduly conservative in the case of continuous U-frames.

Double-span twin girders under UDL were considered as a representative case for assessing the stability of the compression flange in a negative bending moment zone.

The general arrangement of the model was almost the same as that studied for uniform bending. A refined mesh was used for the flanges and webs within a distance of one-quarter of the span from the middle support as that was the length of the hogging region.

A full model was a waste of computing resources and even modelling one of the double-span twin girders was considered uneconomic in terms of CPU time. Consequently, only a quarter of the full model, consisting of a girder of a 25.0m single span with one end simply supported and the other represented as an intermediate support, was used. The intermediate support was simulated by declaring several boundary conditions as shown in Figure 6.14. The *EQUATION module was used to ensure that the grid line across the compression flange (ABC) at the support remained straight yet pivoted about point B during the loading process. As the web was involved, rotation about the transverse axis of the structure, ie, the y-axis, was also suppressed. Lateral movement of the section over the support was not permitted. Vertical movement of nodes in contact with the support was naturally restricted.

To introduce some initial imperfection, the lower flange was loaded by a set of evenly spaced transverse point loads equivalent to an initial bow of $\frac{L}{1000}$ at mid-span.

Vertically downwards point loads were applied uniformly along the longitudinal centre line of the tension flange in order to create the bending moment distribution due to UDL.

6.3.1 $\frac{D}{t_f}$ ratio of 31

6.3.1.1 Load capacity

From the ABAQUS results tabulated in Table 6.4, it was shown that the ultimate load capacity of the girders, generally, remained approximately constant (or a slight increase which was insignificant when the size of cross-beams changed from 50x50mm to 100x100mm when the spacing was 1.0m) irrespective of the various combinations of size and spacing of cross-beams, which resulted in different U-frame stiffness. The difference in the failure loads of girders with cross-beam of 150x150mm spaced at 1.0m and those with cross-beams of 50x50mm spaced at 5.0m was only 1.7×10^5Nm whereas their slenderness ratio λ_{LT} values were 30.96 and 106.21 respectively.

The observation, to a large extent, differed from the situations with U-frames under uniform bending moment, in which the change in stiffness of U-frames was influential to the ultimate load carrying capacity of the girders. Thus, the effect of the moment variation outweighed all other effects and enhanced the bending resistance of the girders.

It was also quite noticeable that, except for the cases of spacing of 1.0m, the failure loads did not increase or decrease monotonically with increase or decrease in stiffness of the U-frames or the slenderness ratio λ_{LT}, particularly, when the spacings were 2.5m and 5.0m.

Table 6.4 Comparison between BS5400 design valuesof bending resistances and ABAQUS results for girders with $\frac{D}{t_f}$ ratio of 31

(double span under UDL)

Cross beam spacing (m)	Cross beam size (mm)	λ_{LT}	$M_{D(1)}$ BS5400 (x10^6Nm)	$M_{D(2)}$ ABAQUS (x10^6Nm)	$\frac{M_{D(2)}}{M_{D(1)}}$
1.0	50	79.18	4.89	8.43	1.72
	100	44.89	7.74	8.58	1.11
	150	30.96	7.74	8.60	1.11
2.5	50	93.95	3.79	8.19	2.16
	100	54.62	7.12	8.11	1.14
	150	38.45	7.74	8.16	1.05
5.0	50	106.21	2.90	7.70	2.66
	100	63.29	6.38	8.16	1.28
	150	45.05	7.72	8.12	1.05

*Not including $\frac{D}{2y_t}$

6.3.1.2 Load-Deflection History

The load-deflection relationships for all the girders analysed by ABAQUS are plotted in Figure 6.15.

When 50x50mm cross-beams were employed, the lateral deflection of the bottom flange increased gradually and became relatively large towards the end of load. When the size of cross-beams changed to 100x100mm, the slope of the load-deflection curve showed a sudden increase in the stiffness of U-frame bracing and much reduced lateral deflections of the bottom flange. When cross-beams of 150x150mm were used, there was a further slight increase in the stiffness and the lateral displacement was even smaller.

The common feature of the three curves was that there was an unexpected increase in the slopes of the curve followed by a decrease when the applied load was 80% of the total failure load.

6.3.1.3 Failure Mode

For girders with cross-beams of 50x50mm and 100x100mm spaced at 1.0m, 2.5m and 5.0m, the point with maximum lateral deflection always occurred approximately 8.5m away from the middle support, where the bottom flange was not in compression but tension. When cross-beams of 150x150mm were used, the position of the maximum lateral deflection shifted to 4.0m from the support with close spacing of cross-beams at 1.0m. Then, as the spacing increased to 2.5m and subsequently to 5.0m, the point of maximum lateral deflection drifted to 6.5m and 7.5m away from the support. Nevertheless, the overall failure modes of all the girders in this series were generally the same as shown in Figure 6.16. There were no half-waves formed in the compression zone and localised yields in the compression flange adjacent to the middle support were observed.

In the case of cross-beams of 150x150mm spaced at 1.0m, local yield in the compression flange was severe. Necking in elements in the tension region was also detected as shown in Figure 6.17.

6.3.2 $\frac{D}{t_f}$ ratio of 41

6.3.2.1 Load Capacity

Generally speaking, the ultimate load carrying capacity (tabulated in Table 6.5) increased with increase in size of cross-beam and decrease in spacing (with some exceptions). However, the effect of these parameters was still not significant, particularly when the cross-beams were closely spaced. The ultimate bending resistance of the girders was increased by just 3% when the size of cross-beams varied from 50x50mm to 150x150mm with spacing of 1.0m and the corresponding λ_{LT} values from 37.13 to 96.24. When the cross-beams were placed at 5.0m, the change of cross-beam size from 50x50mm to 150x150mm gave a 9.5% increase in ultimate load capacity, although the λ_{LT} value, including the effect of moment gradient, was reduced from 129.78 to 54.19, a drop of 58%. The influence of spacing of cross-bracing was also not influential. For cross-beams of 150x150mm, there was only a 7% reduction when spacing increased from 1.0m to 5.0m.

Table 6.5 Comparison between BS5400 design values of bending resistances and ABAQUS results for girders with $\frac{D}{t_f}$ ratio of 41

(double span under UDL)

Cross-beam spacing (m)	Cross-beam size (mm)	λ_{LT}	$M_{D(1)}$ BS5400 (x10^6Nm)	$M_{D(2)}$ ABAQUS (x10^6Nm)	$\frac{M_{D(1)}}{M_{D(2)}}$
1.0	50	96.24	4.94	11.73	2.37
	100	53.55	10.52	12.09	1.15
	150	37.13	10.52	12.11	1.15
2.5	50	114.65	3.73	11.55	3.10
	100	65.83	8.20	10.91	2.73
	150	46.17	10.46	11.74	1.12
5.0	50	129.78	2.94	10.33	3.51
	100	76.51	6.94	11.45	1.65
	150	54.19	9.68	11.31	1.17

*Not including $\frac{D}{2y_t}$

6.3.2.2 Load-Deflection History

The lateral deflection of the compression flange at the point of maximum displacement at failure load is plotted against load in Figure 6.18.

Similar to the load-deflection curves for girders with $\frac{D}{t_f}$ ratio of 31, there was a substantial increase in the slope of the curves when 100x100mm cross-beams were used instead of 50x50mm. A further slight increase was achieved when 150x150mm cross-beams were employed instead of 100x100mm. In most of the load-deflection curves, change in the rate of increase in deflection seemed to be inevitable.

The magnitude of the lateral deflection fell with increase in the cross-beam size and decrease in the cross-beam spacing. The position of maximum deflection moved towards the middle support as the size of cross-beam increased.

Similar buckling modes for the compression flange occurred (shown in Figure 6.19) to those described for the group with $\frac{D}{t_f}$ of ratio of 31. In addition, deformation in the top flange and web in sagging region were observed (as shown in Figures 6.20 and 6.21), when cross-beams were placed 2.5m and 5.0m apart.

6.3.3 $\frac{D}{t_f}$ ratio of 61

6.3.3.1 Load capacity

Table 6.6 Comparison between BS5400 design values of bending resistances and ABAQUS results for girders with $\frac{D}{t_f}$ ratio of 61

(double span under UDL)

Cross-beam spacing (m)	Cross-beam size (mm)	λ_{LT}	$M_{D(1)}$ BS5400 ($x10^6$Nm)	$M_{D(2)}$ ABAQUS ($x10^6$Nm)	$\frac{M_{D(2)}}{M_{D(1)}}$
1.0	50	131.67	4.86	17.71	3.64
	100	63.71	14.66	17.82	1.22
	150	50.35	16.78	17.87	1.06
2.5	50	157.61	3.44	14.80	4.30
	100	89.20	9.37	16.91	1.80
	150	62.57	14.66	17.25	1.18
5.0	50	179.06	2.73	12.66	4.64
	100	103.96	7.24	14.24	1.97
	150	73.66	12.36	16.55	1.34

*Not including $\frac{D}{2y_t}$

From Table 6.6, it can be seen that the ultimate bending resistance of the girders was constantly increasing with the increase in size and decrease in spacing of cross-beams, though the amount of increase was, in the case in which the spacing between cross-beams was 1.0m, negligible. When the cross-beams were further apart, an almost equal increase was achieved for every 50mm increase in cross-beam size.

6.3.3.2 Load-deflection History

(a) Spacing = 1.0m

As shown in Figure 6.22(a) when 50x50mm cross-beams were used, there was a progressive increase in lateral deflection with increase of load. However, at 70% of failure load, the rate of increase in lateral deflection reduced and this was followed shortly by a change of direction in the lateral movement. Therefore, it can be seen that at a point approximately 8m from the middle support, the direction of deflection reversed. At the next loading increment, there was no deflection and subsequent loading caused further deflection in the original direction.

When larger cross-beams were used (ie, sizes 100x100mm and 150x150mm), the load-deflection curves were of higher gradient. The phenomenon observed before did not recur. Lateral deflection was in general small and no sudden large displacement was observed in the case of 150x150mm cross-beams.

(b) Spacing = 2.5m

In all the three curves plotted in Figure 6.22(b), there was no sudden increase in lateral deflection during the loading process, ie, no buckling of compression flange was detected even though large lateral displacement of the compression flange was developed in the case of 50x50mm cross-beams.

(c) Spacing = 5.0m

It can be seen from Figure 6.22(c) that, although the rate of increase in lateral deflection as applied load increased differed, there was a rather gradual increase in the rate for every 50mm increase in cross-beam size. Sudden increase in lateral deflection was only developed at the completion of a loading process.

6.3.3.3 Failure Mode

With cross-beams of 50x50mm, the general failure mode of the compression flange was almost the same, as shown in Figures 6.23, 6.25 and 6.27. This case was not repeated with larger size cross-beams because of local yield and severe distortion of the flange elements adjacent to the middle support (except in the case of 100x100mm and 150x150mm spaced at 5m). Owing to the slenderness of the web in this set of girders, the distortion of web next to the middle support was seen clearly from the ABAQUS plot, as shown in Figures 6.24, 6.26 and 6.28. Large displacement in the region of the top compression flange together with bulging of the girder web at that position were also observed.

6.3.4 Comparison of finite element analysis with BS5400

For the three sections studied here, the ultimate bending resistance computed by ABAQUS was much higher than the design values of BS5400. Despite the wide range of λ_{LT} values in each group, the ultimate load capacity of the girders varied little, especially in the case of girders with a $\frac{D}{t_f}$ ratio of 31.

Local yield in the elements adjacent to the internal support seemed to dominate the failure modes of the girders analysed so far. Therefore, local distortion of the girder web or flanges over the internal support prevented lateral buckling of the compression flange in the hogging region.

6.4 DISCUSSION ON THE APPLICATION OF RECENTLY PROPOSED DESIGN METHODS

It seems that there is no direct comparison between the finite element analysis of the three groups of girders and other previous research results or proposed new design methods. This is mainly because the emphasis of the other investigations was, firstly, on continuous U-frame action in composite beams without transverse web stiffeners, and secondly, the moment distribution on a fixed-end span under UDL.

If web stiffeners are present, the flexibility of the shear connection between steel top flange and the restraining slab might not be negligible[2] and thus it is not acceptable to ignore the contribution of the joint flexibility in the δ expression. Weston showed[26] that it could be extremely small in comparison with other terms but might become significant when very large stiffeners were used.

Even though MPCs were employed in the finite element modelling presented here, and the flexibility between the connections of the cross-beams and the top flanges were considered as rigid, the newly proposed methods for continuous U-frames are still not applicable to the situations in which actions of discrete U-frames were clearly demonstrated (See section 6.2.1.4) in the presence of the transverse web stiffeners at the positions of cross bracings.

The simplified method (based on a strut on elastic foundation) developed by Goltermann and Svensson, including various loading cases, could well be used for cases with continuous U-frame action. However, the expression for evaluation of torsional restraints, especially in discrete U-frames with the presence of stiffeners has to be modified. This modification may bring some alteration to the two proposed parameters, which are in terms of torsional and lateral restraint (see equation (2.8)) to compression flanges.

6.5 CONCLUSION

6.5.1 Uniform Bending Moment

The moment capacities of the girders braced by discrete U-frames under uniform bending moment, obtained by ABAQUS analysis, were greater than the design values given by BS5400. The difference was dependent on the λ_{LT} values of the girders.

The change of cross-beams from 50x50mm to 100x100mm increased the bending resistance rapidly, especially when the spacing between cross-beams was relatively small. The influence of further increase in cross-beam size to 150x150mm on the ultimate bending resistance was insignificant.

Excessive lateral displacement of the compression flange was produced using small cross-beams but the displacement reduced drastically with use of larger cross-beams and sudden increase in the deflection indicated lateral buckling of the compression flanges. It was also noticed that when the spacing of cross beams was 1.0m, the maximum lateral displacement of the compression flange was always smaller in the cases using 100x100mm than those using 150x150mm.

Buckling shapes for the girders with lower values of λ_{LT} consisted of a number of half-waves, otherwise one single half-wave was the usual form of buckling in compression flanges. All the buckling modes were symmetrical about mid-span.

Yielding in the elements at mid-span or adjacent to the support region was only developed at a late stage of the loading process.

The transverse web stiffeners could be seen clearly as a factor for the alteration of the buckled shapes of the compression flanges and they sharply reduced the lateral deflection of the flanges. The absence of these stiffeners would not apparently reduce the bending resistance of the girder.

6.5.2 Moment due to UDL

The ultimate load capacities of the girders were increased in the presence of non-uniform bending moment distribution. The design method according to BS5400, even including the slenderness factor η for the variation of the bending moment between points of full restraints was proven to be over conservative.

Because of the dominating effect of non-uniform moment distribution, the influence of other factors on bending resistance of girders, in most cases studied, became negligible.

Relatively large lateral displacement in the bottom flange developed when small cross-beams were used. For girders with larger cross-beams, changes in displacement were very subtle.

Localised yield and distortion in the compression flange elements in the vicinity of an internal support were far more obvious than any lateral 'buckling' of the flange in the hogging moment region for both near compact and non-compact sections and they were more likely to occur when larger size cross-beams were placed closely, ie, with low λ_{LT} values.

The beneficial effect of moment gradient on load-carrying capacity was clearly demostrated. The behaviour of girders, particularly the lateral displacement of flanges in compression, was much affected by variation in bending moment. Even if lateral buckling was the critical mode of compression flange failure for a girder with uniform bending moment, local failure was still dominant when the same girder was under moment variation.

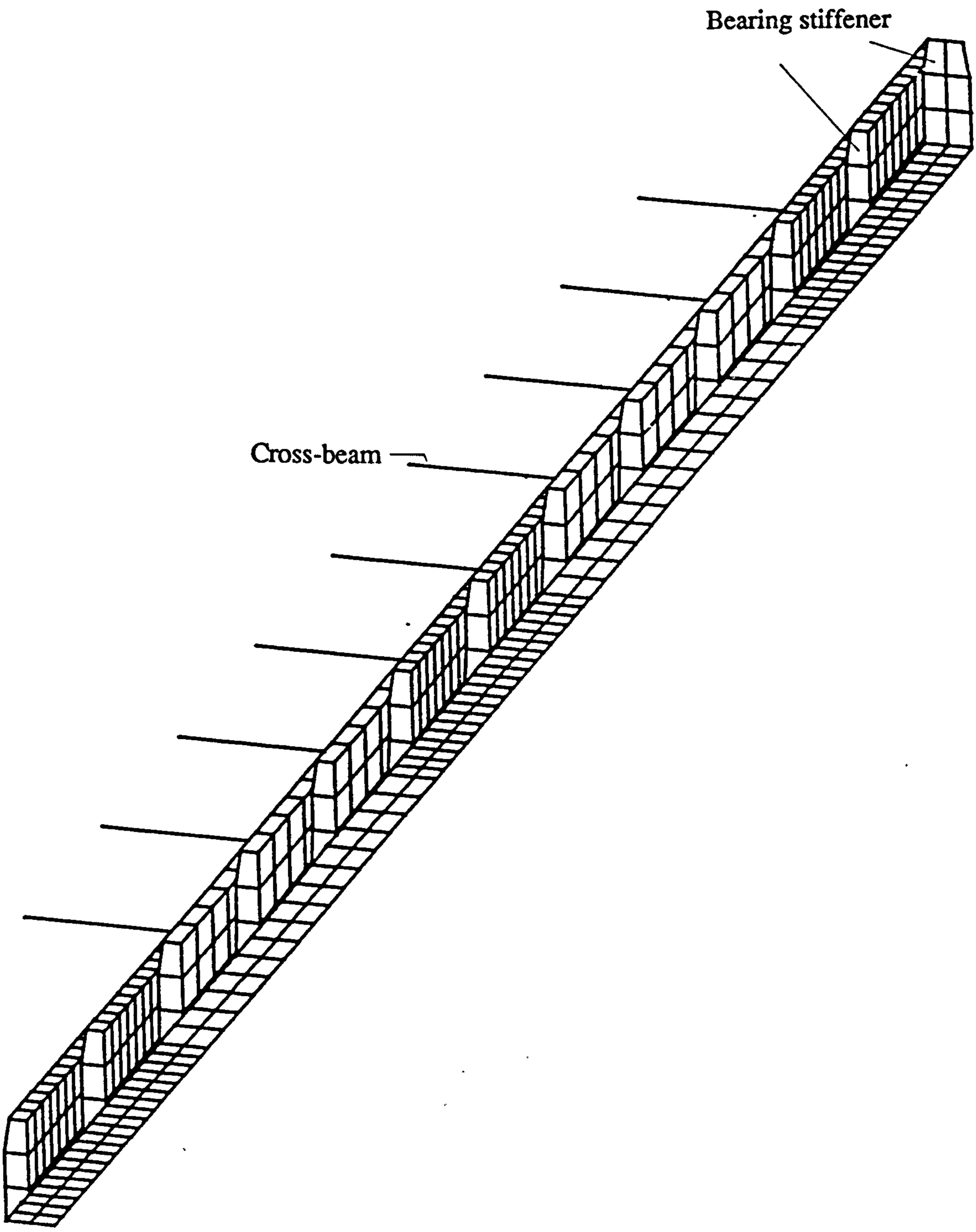

Figure 6.1 F.E. mesh for modelling discrete U-frames

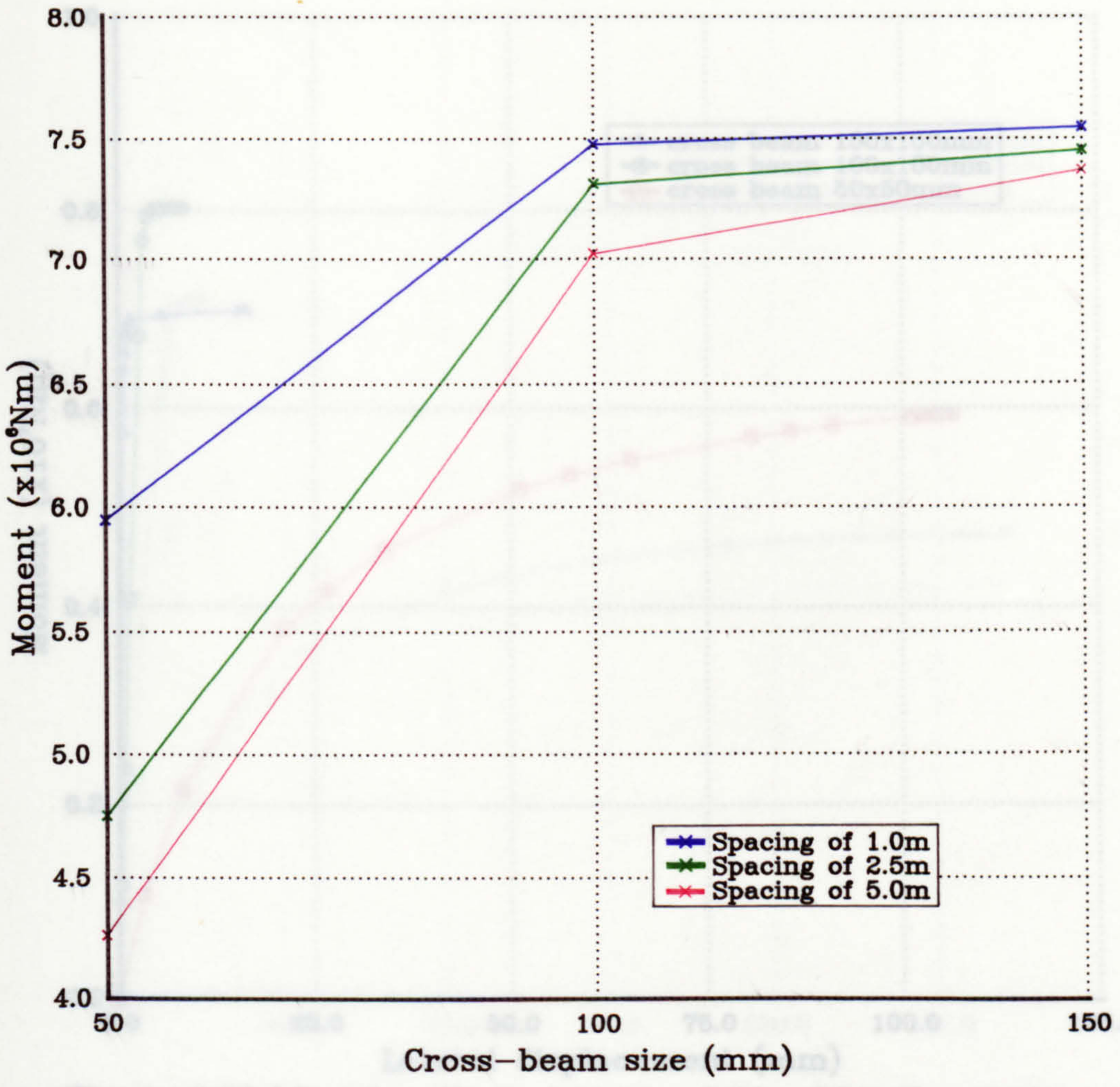

Figure 6.2 Effect of cross-beam size and spacing on bending resistance of girders with D/t, ratio of 31

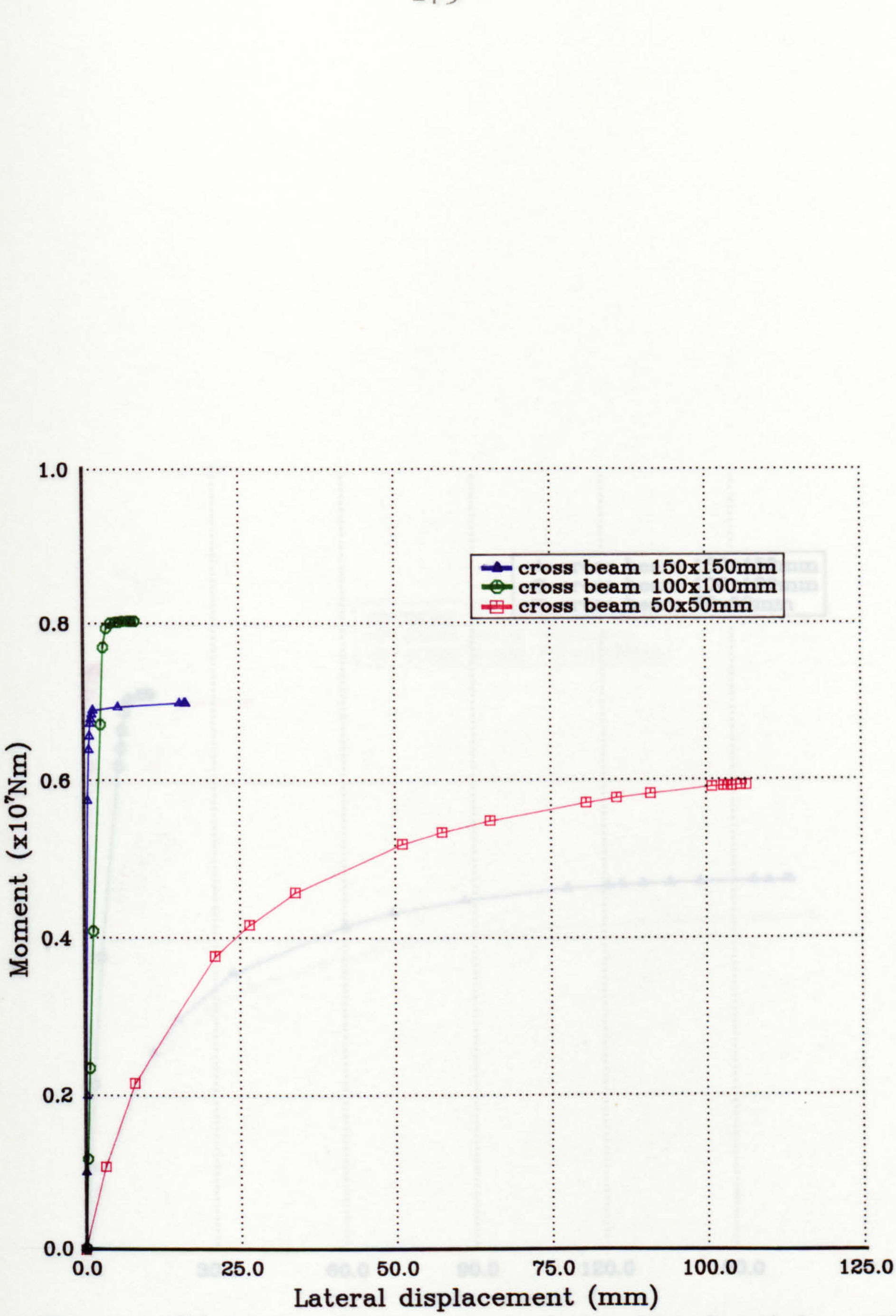

Figure 6.3(a) Load v. displacement relationships for girders with D/t_f ratio of 31 and cross-beam spacing of 1m under uniform bending moment

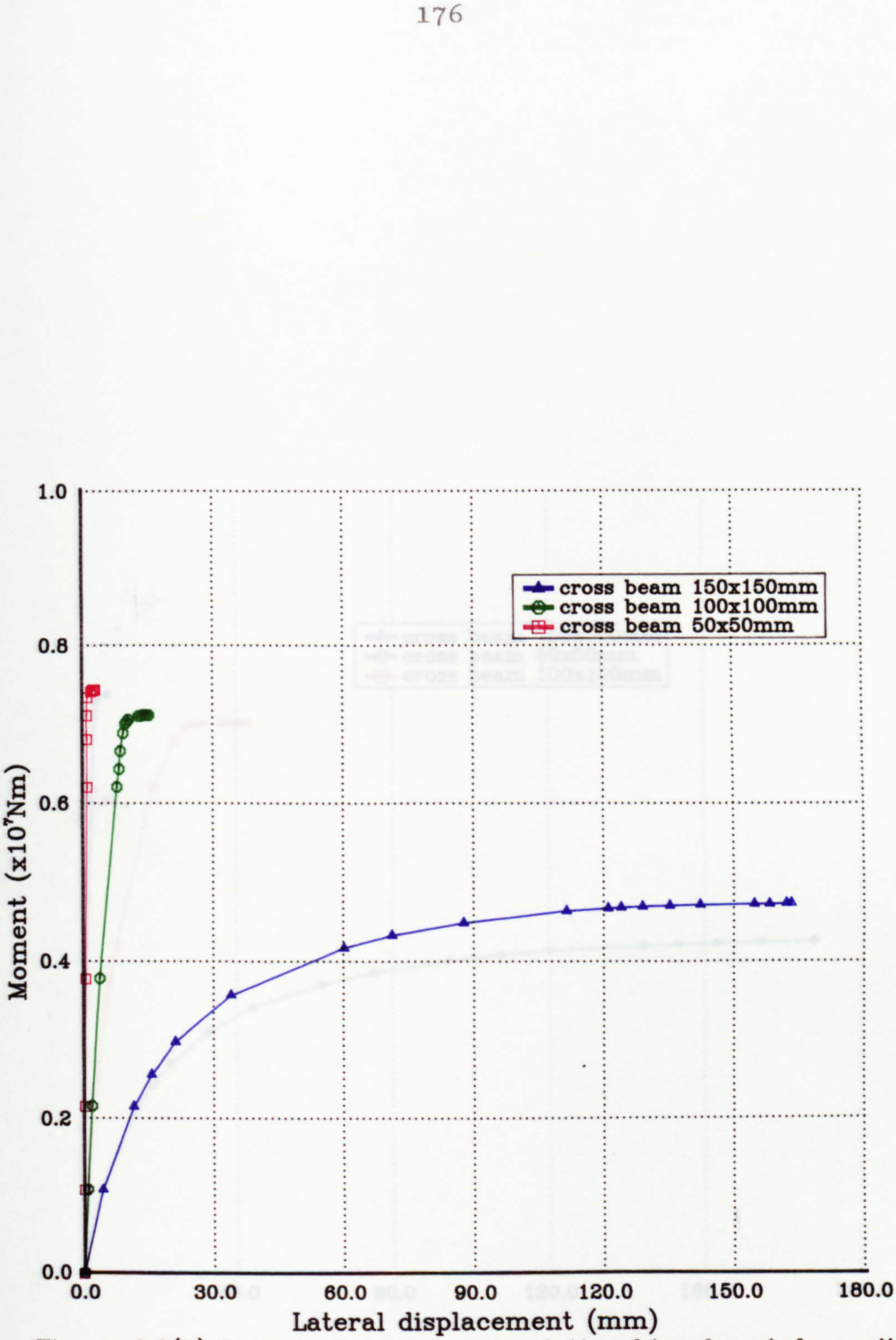

Figure 6.3(b) Load v. displacement relationships for girders with D/t_f ratio of 31 and cross-beam spacing of 2.5m under uniform bending moment

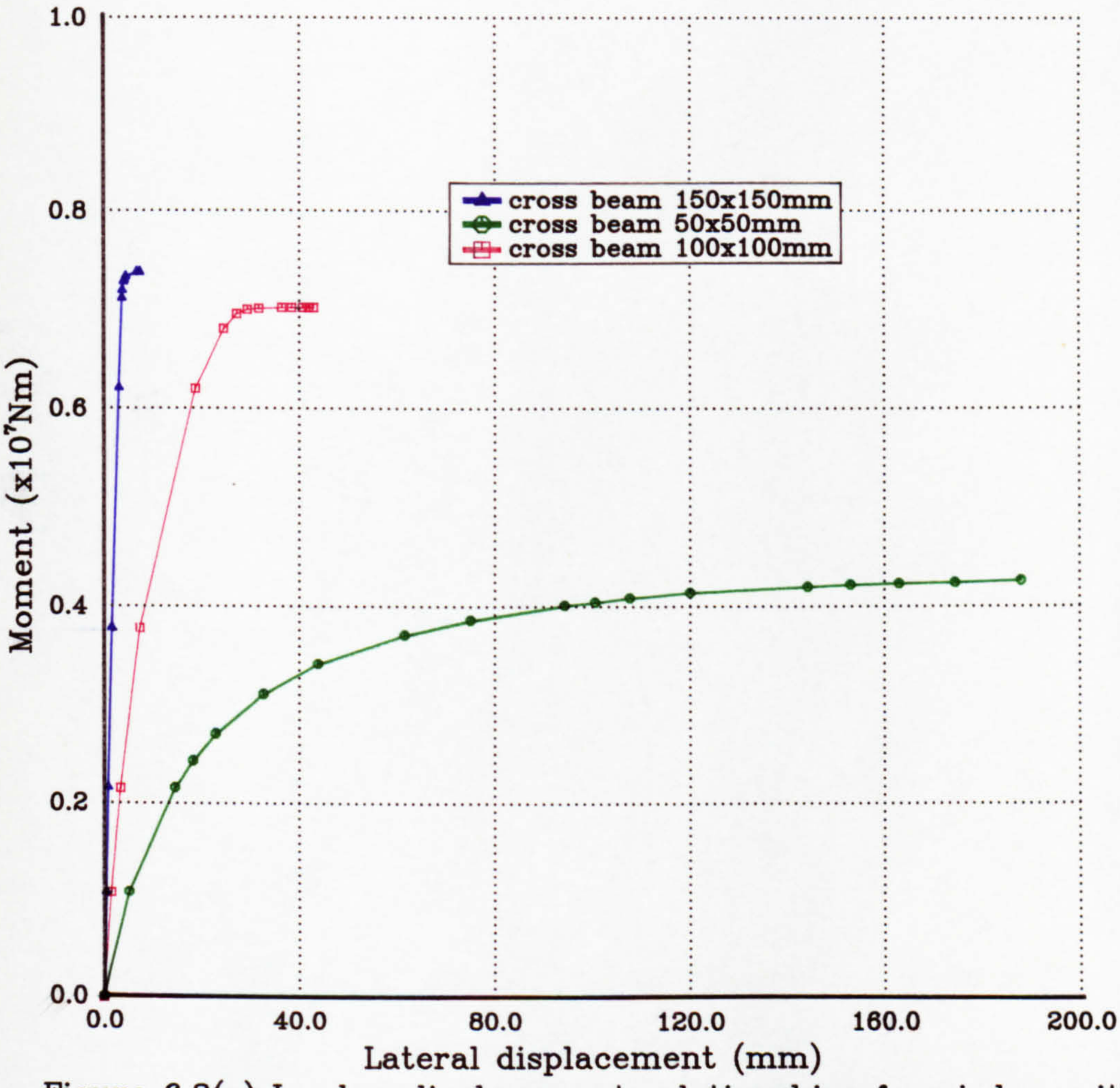

Figure 6.3(c) Load v. displacement relationships for girders with D/t_f ratio of 31 and cross-beam spacing of 5m under uniform bending moment

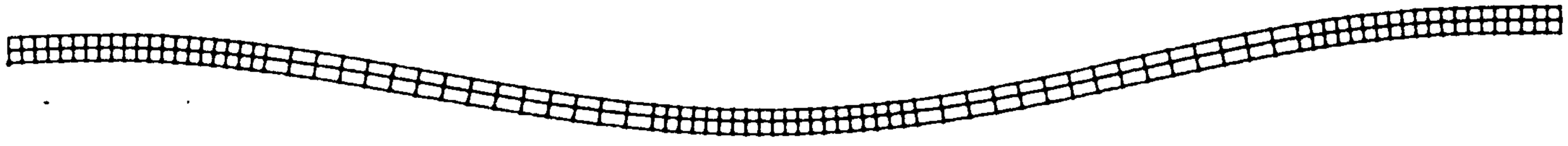

(a) cross-beam size: 50x50mm

(b) cross-beam size: 100x100mm

(c) cross-beam size: 150x150mm

Figure 6.4 Buckled shapes of compression flange for girders with $\frac{D}{t_f}$ ratio of 31 and cross-beam spacing 1m, under uniform bending moment

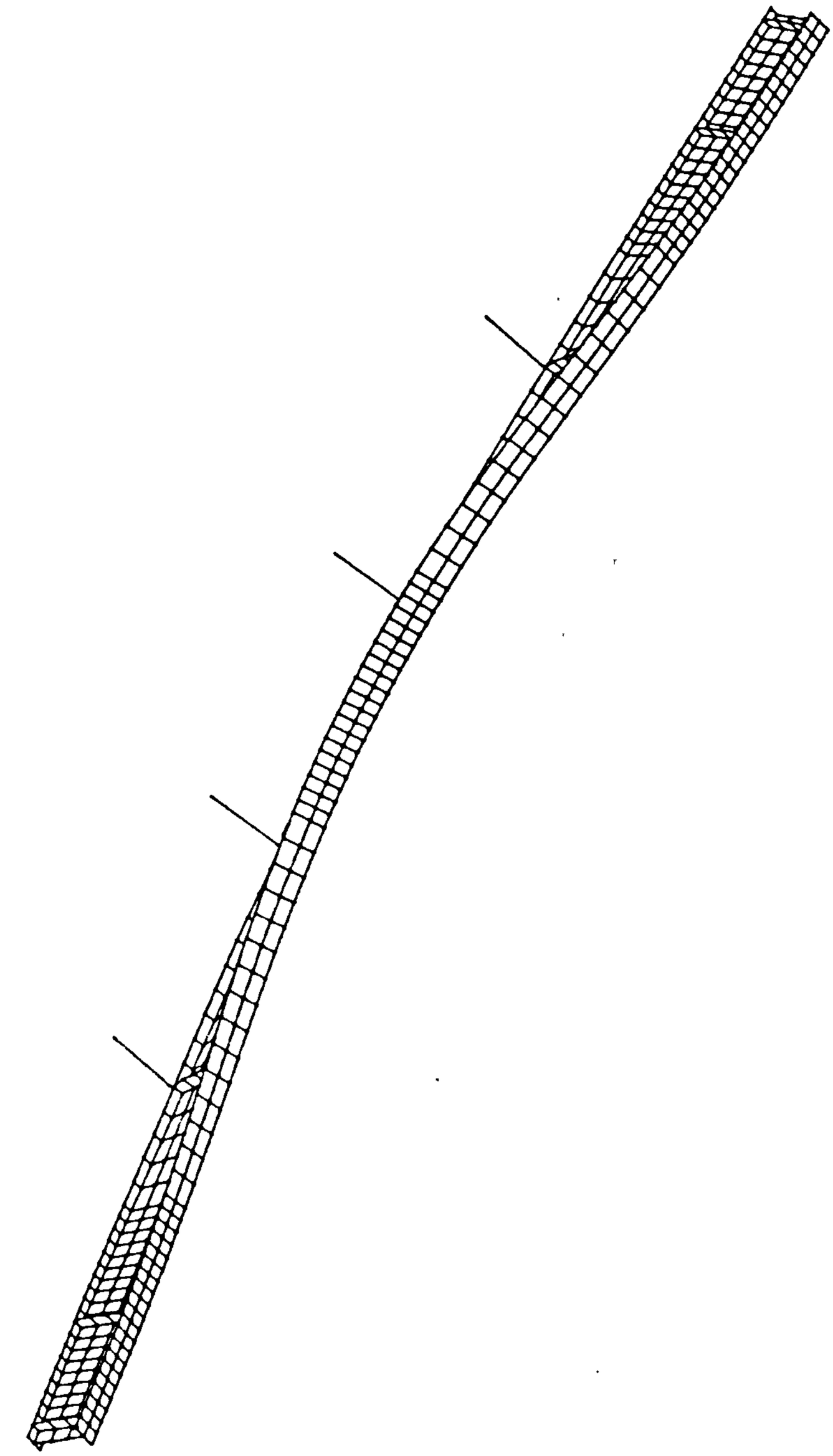

Figure 6.5(a) General buckled shape for girders with $\frac{D}{t_f}$ ratio of 31, view (1)

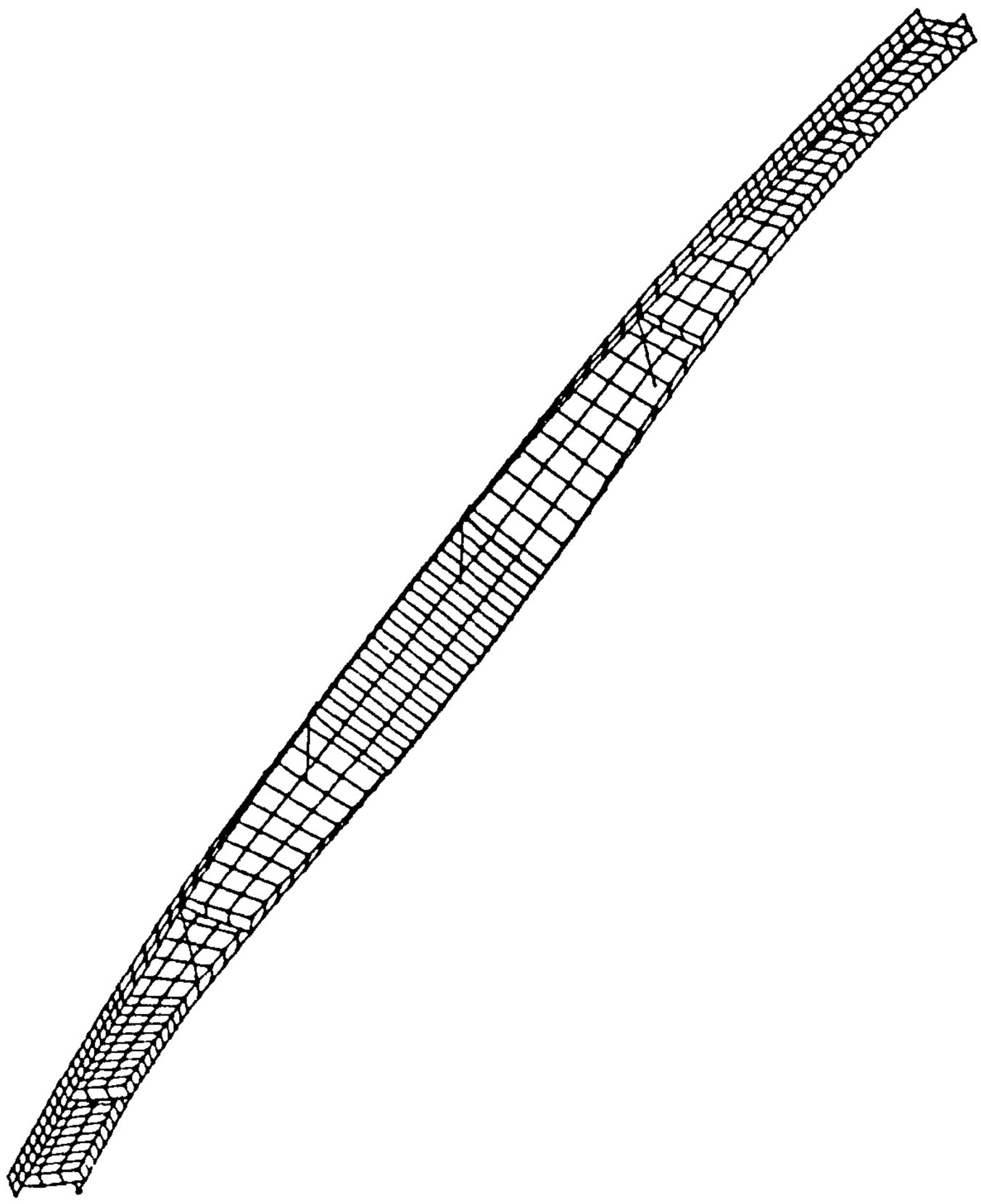

Figure 6.5(b) General buckled shape for girders with $\frac{D}{t_f}$ ratio of 31, view (II)

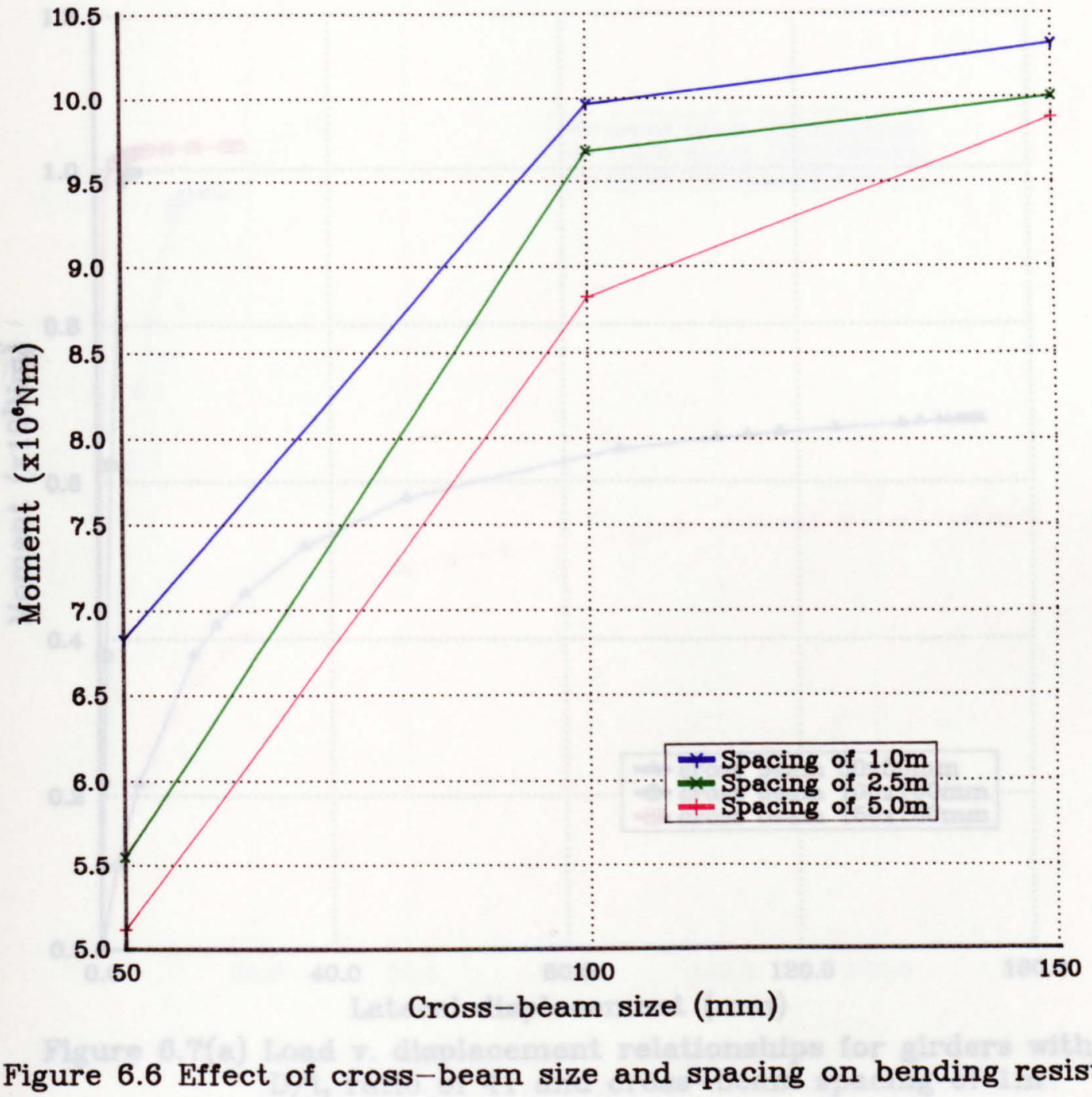

Figure 6.6 Effect of cross-beam size and spacing on bending resistance of girders with D/t_f ratio of 41

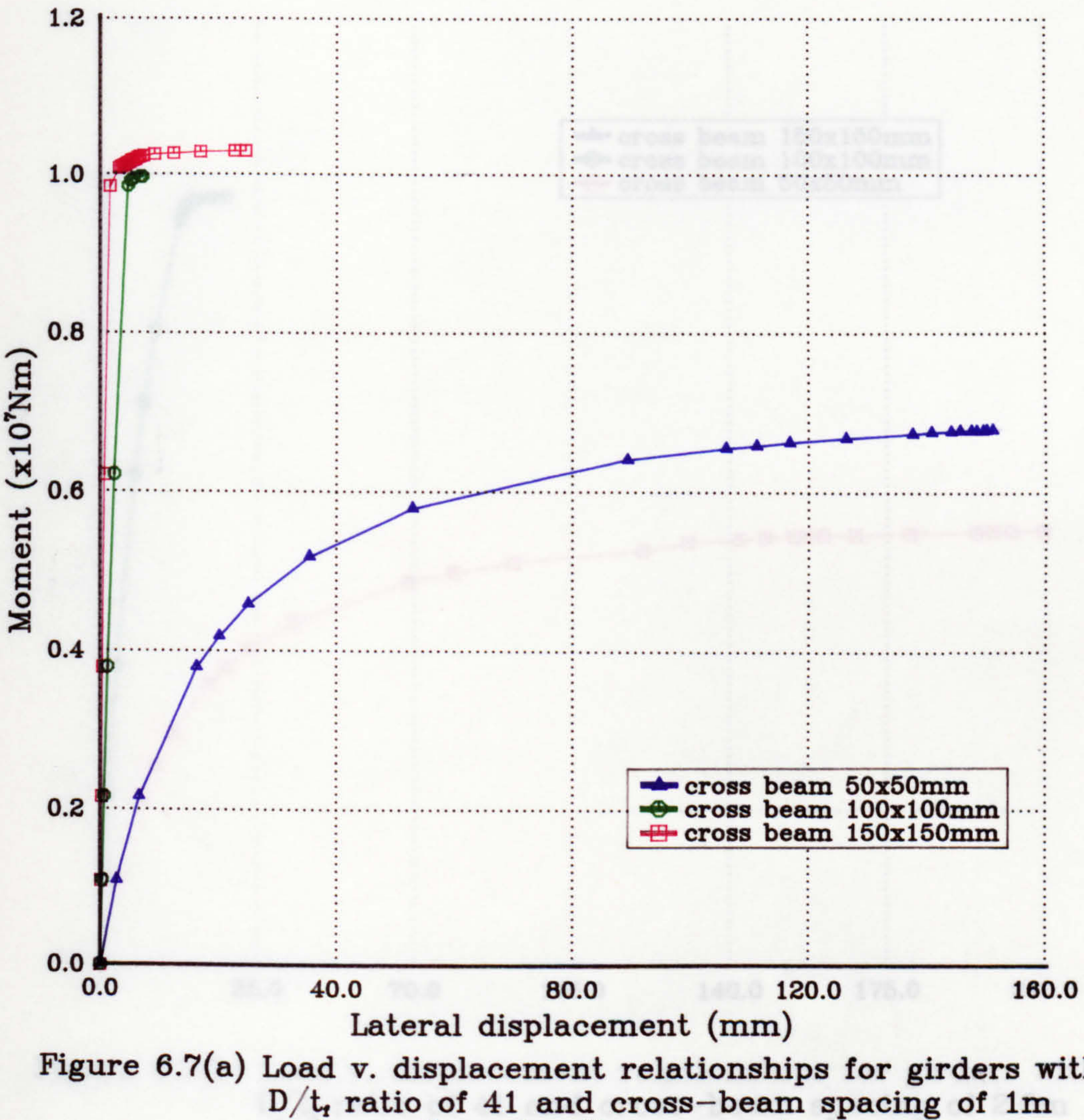

Figure 6.7(a) Load v. displacement relationships for girders with D/t_f ratio of 41 and cross-beam spacing of 1m under uniform bending moment

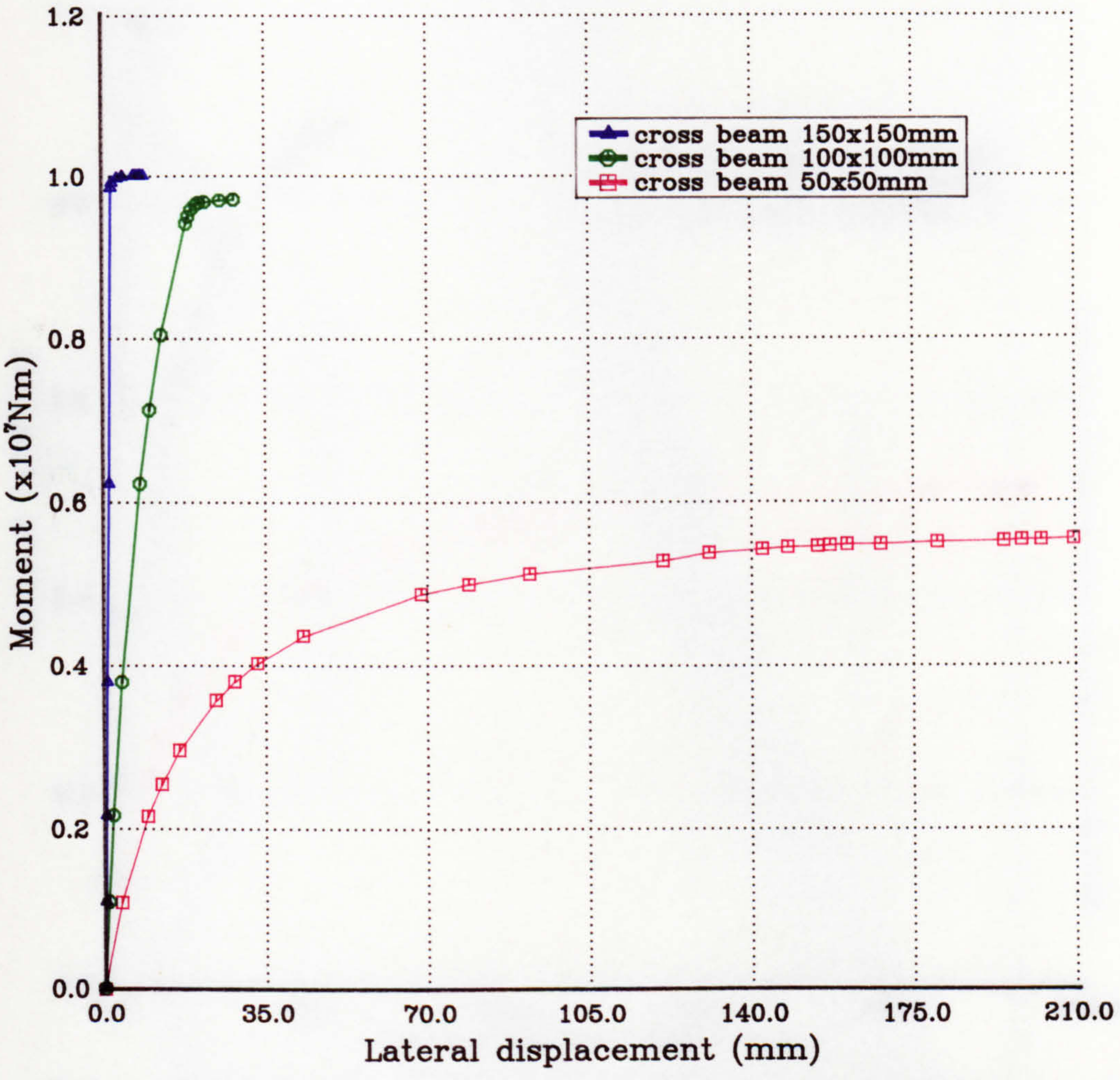

Figure 6.7(b) Load v. displacement relationships for girders with D/t_f ratio of 41 and cross-beam spacing of 2.5m under uniform bending moment

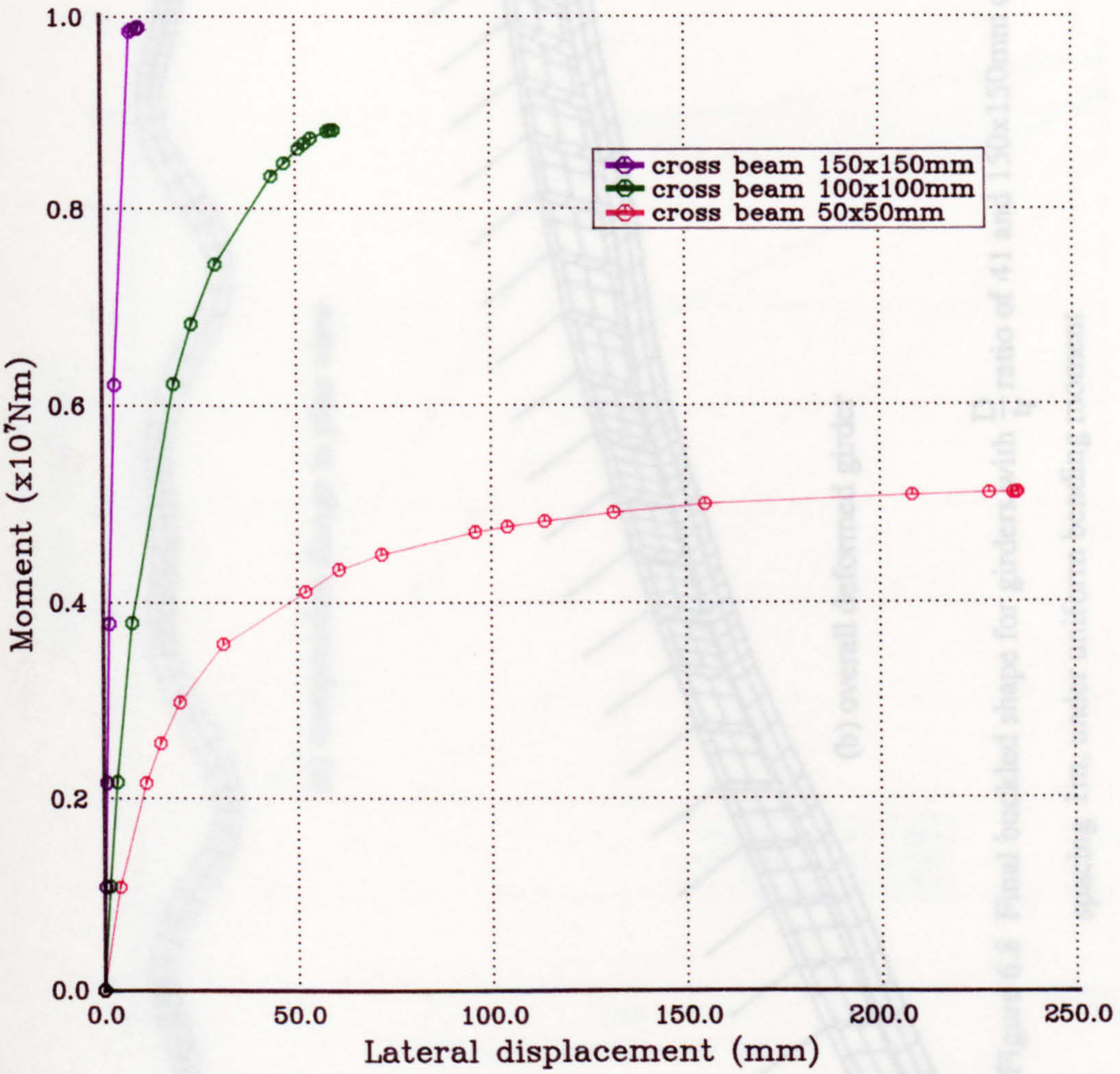

Figure 6.7(c) Load v. displacement relationships for girders with D/t_f ratio of 41 and cross beam spacing 5m under uniform bending moment

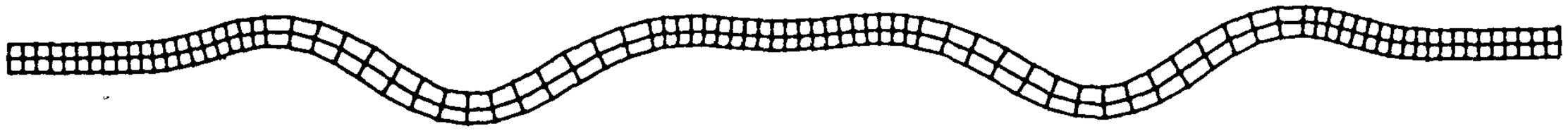

(a) compression flange in plan view

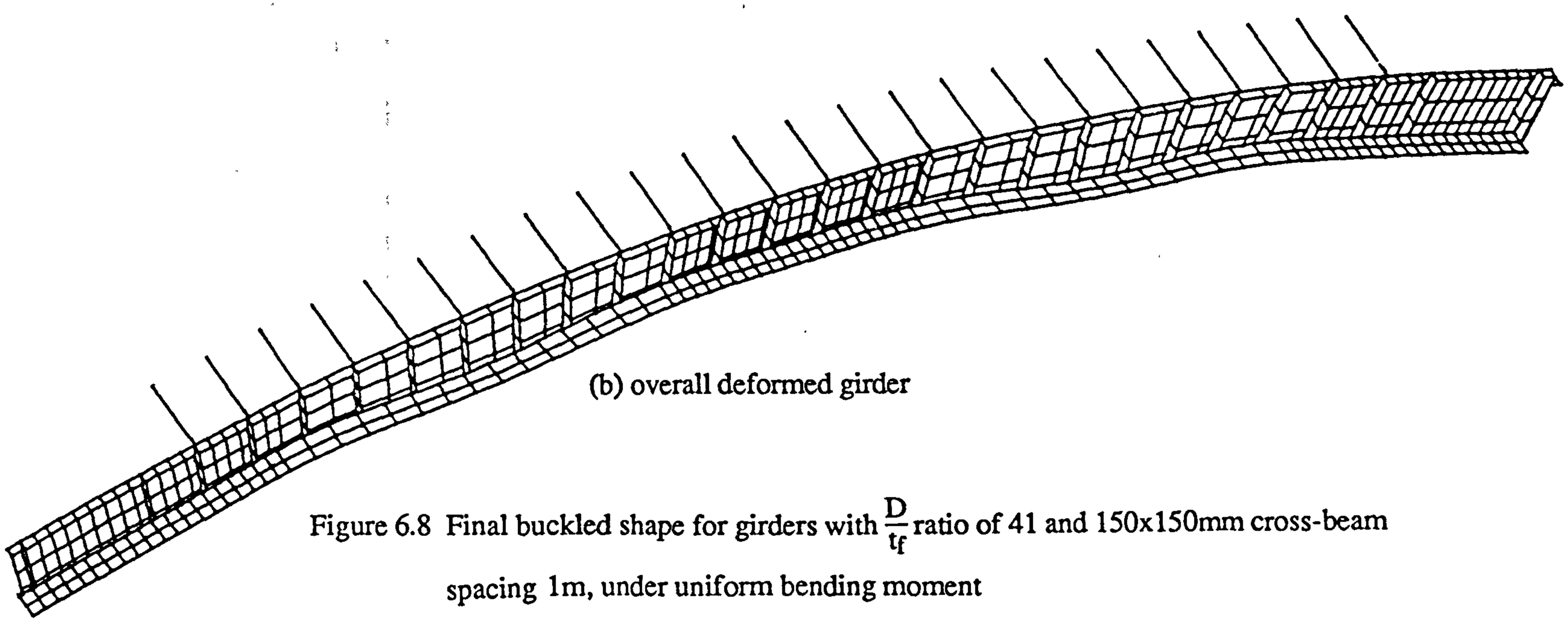

(b) overall deformed girder

Figure 6.8 Final buckled shape for girders with $\frac{D}{t_f}$ ratio of 41 and 150x150mm cross-beam spacing 1m, under uniform bending moment

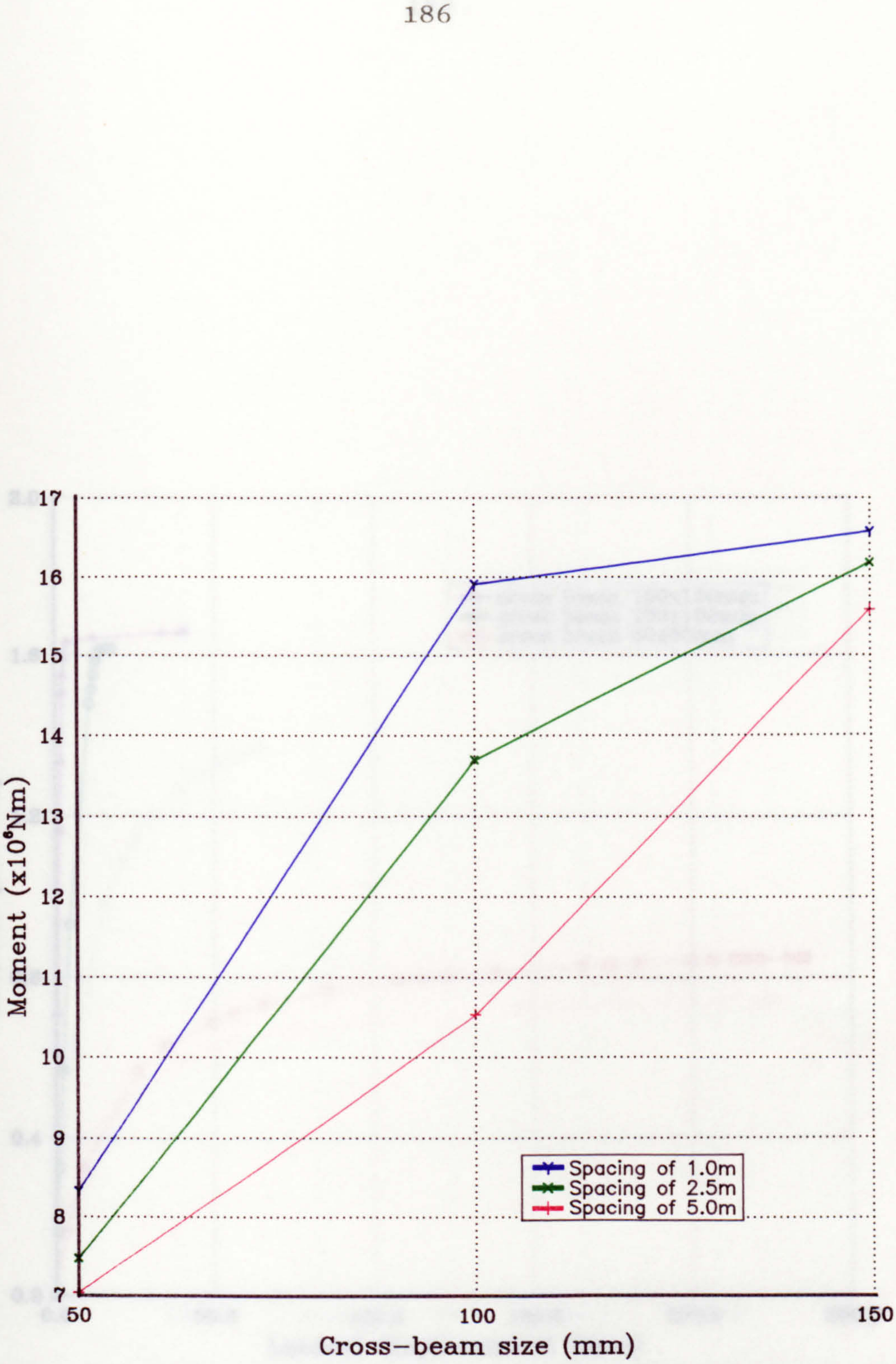

Figure 6.9 Effect of cross-beam size and spacing on bending resistance of girders with D/t_f ratio of 61

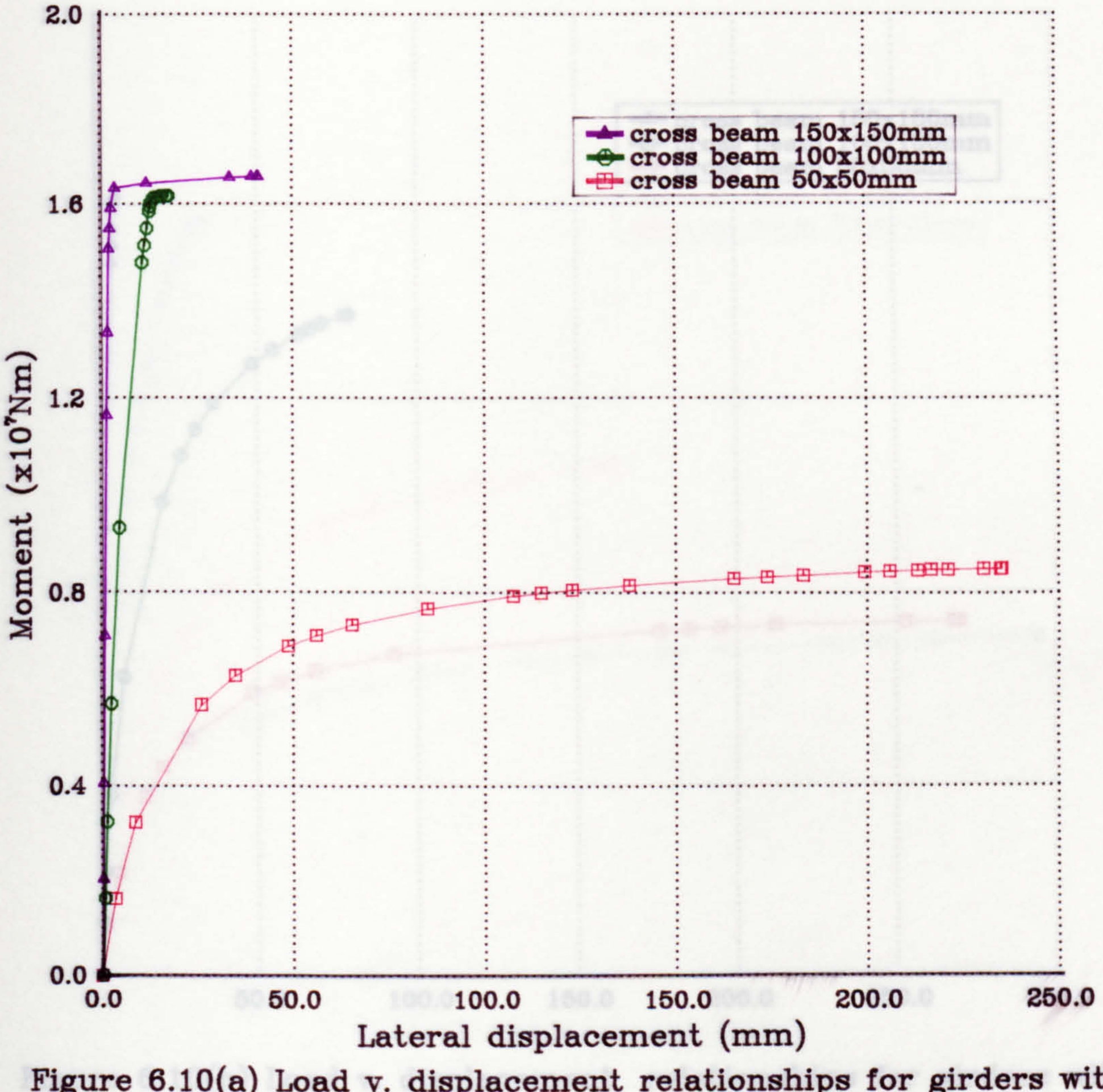

Figure 6.10(a) Load v. displacement relationships for girders with D/t_f ratio of 61 and cross-beam spacing of 1m under uniform bending moment

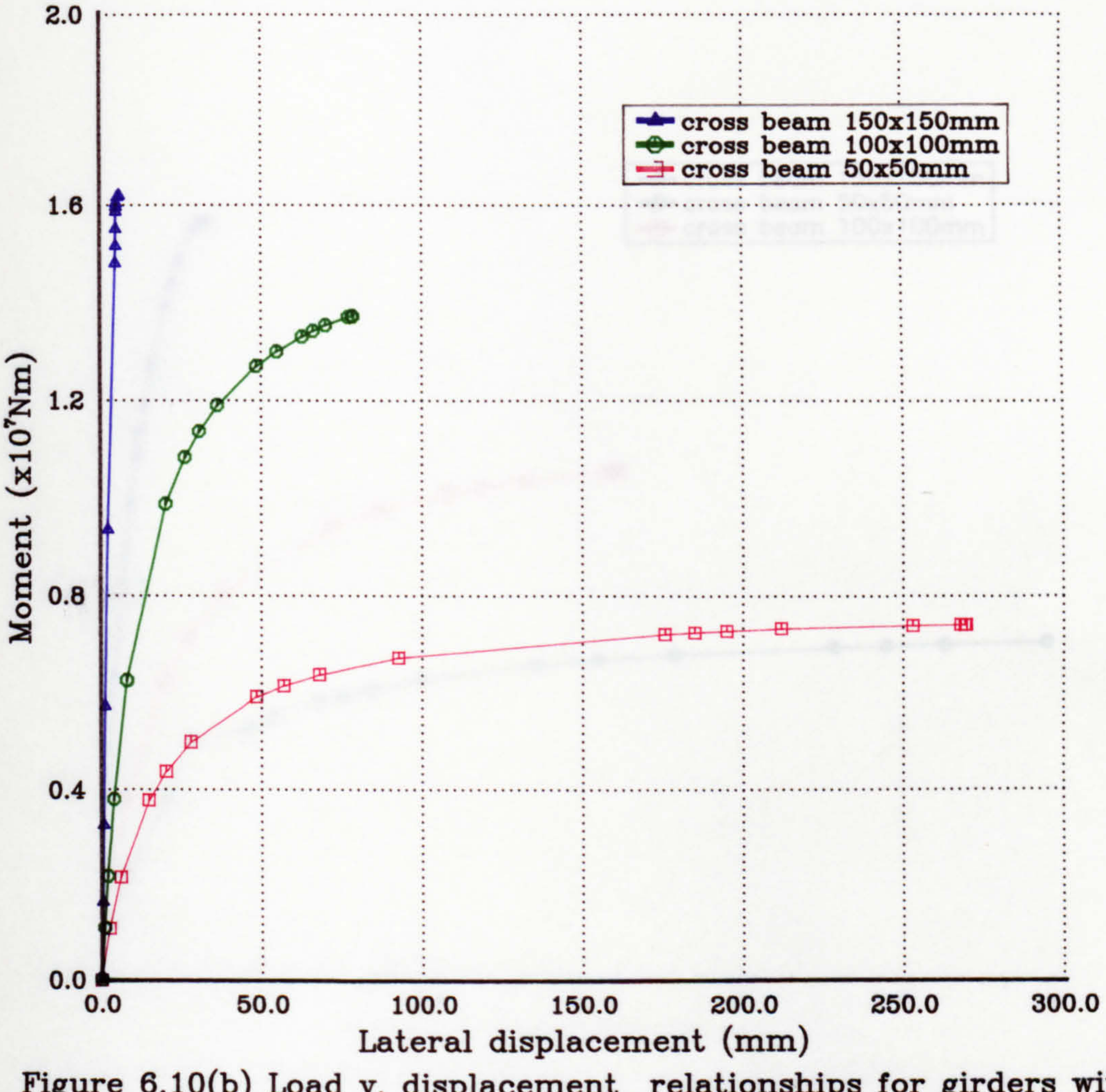

Figure 6.10(b) Load v. displacement relationships for girders with D/t_f ratio of 61 and cross-beam spacing of 2.5m under uniform bending moment

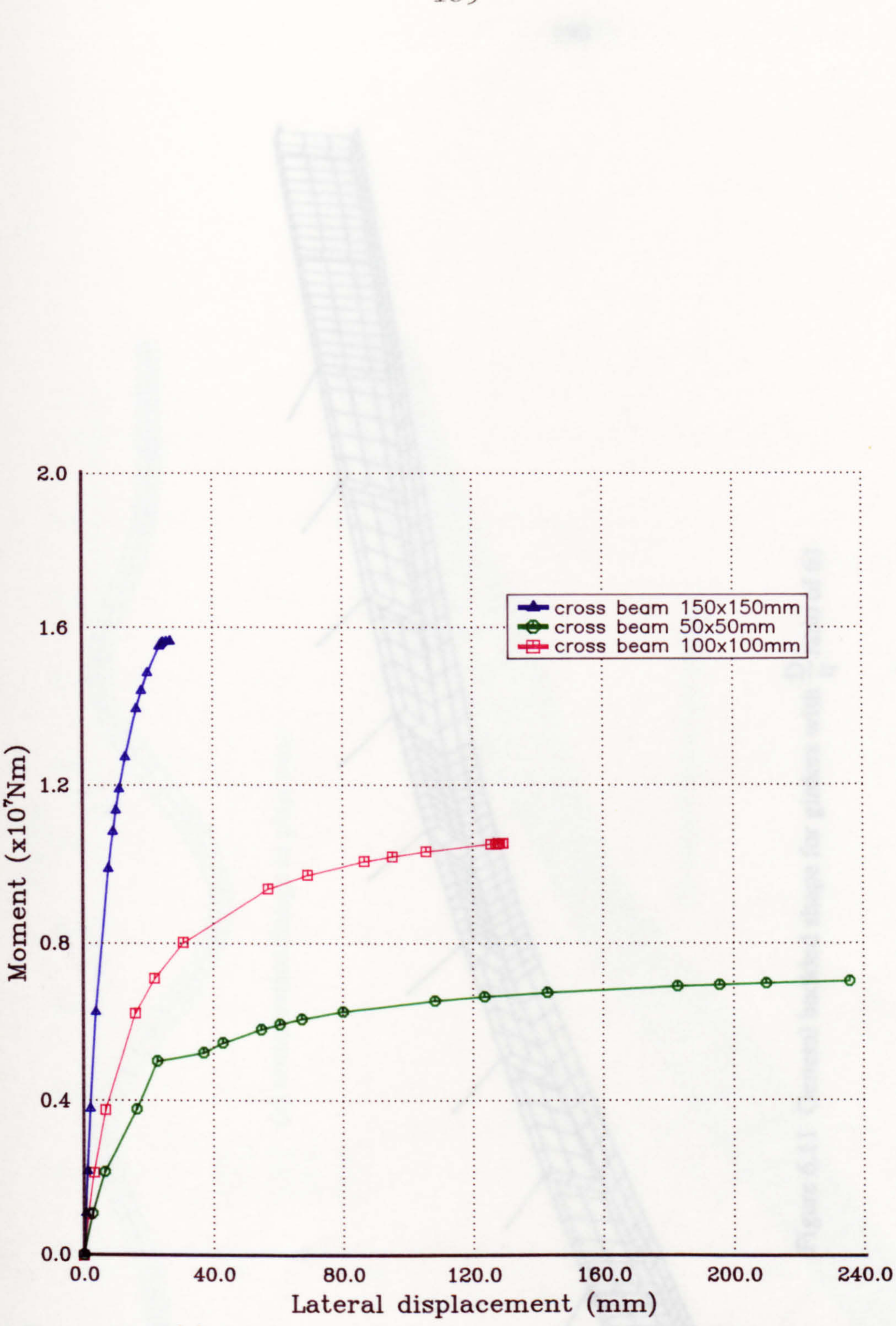

Figure 6.10(c) Load v. displacement relationships for girders with D/t_f ratio of 61 and cross-beam spacing 5m under uniform bending moment

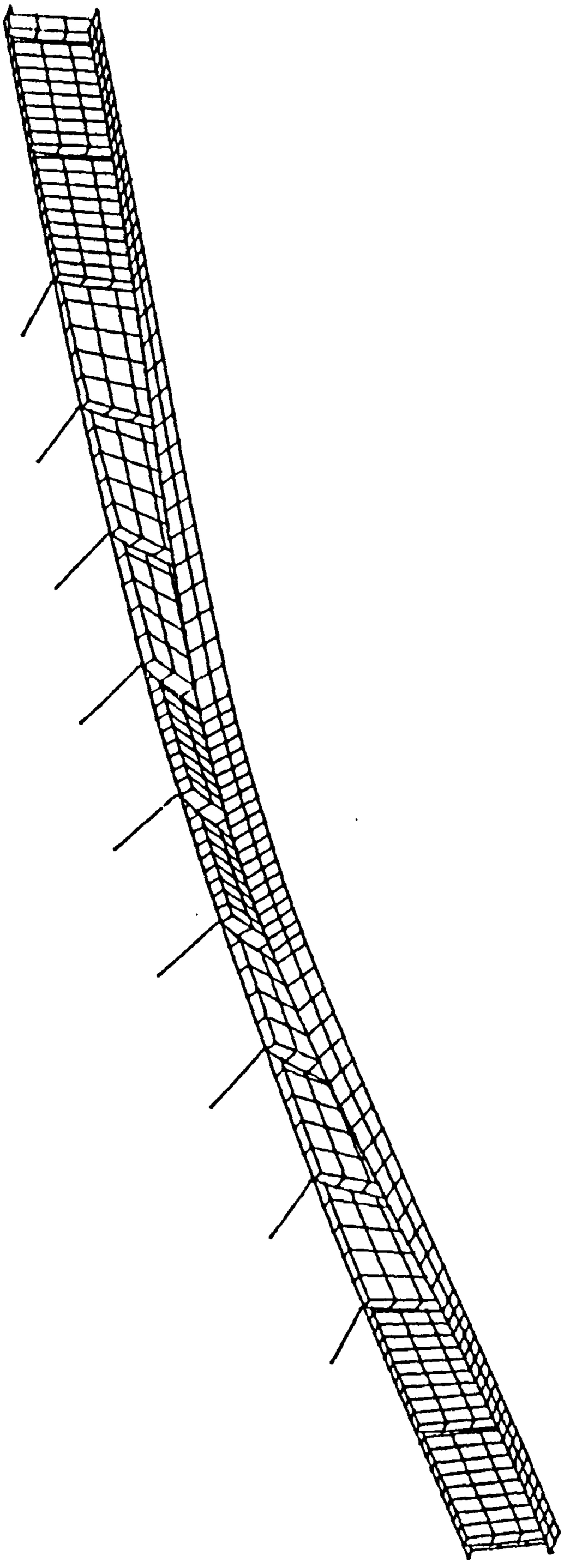

Figure 6.11 General buckled shape for girders with $\frac{D}{t_f}$ ratio of 61

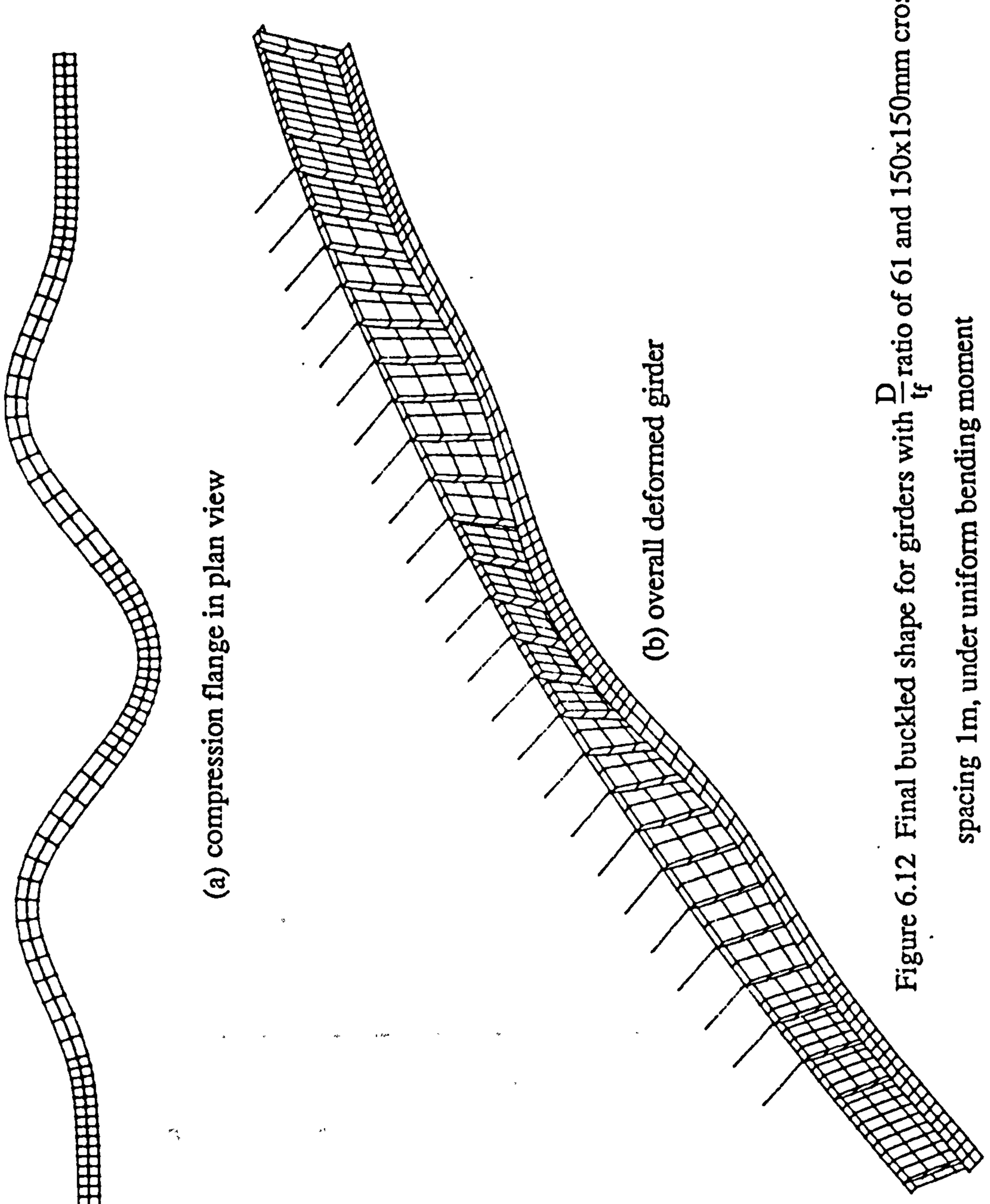

(a) compression flange in plan view

(b) overall deformed girder

Figure 6.12 Final buckled shape for girders with $\frac{D}{t_f}$ ratio of 61 and 150x150mm cross-beam spacing 1m, under uniform bending moment

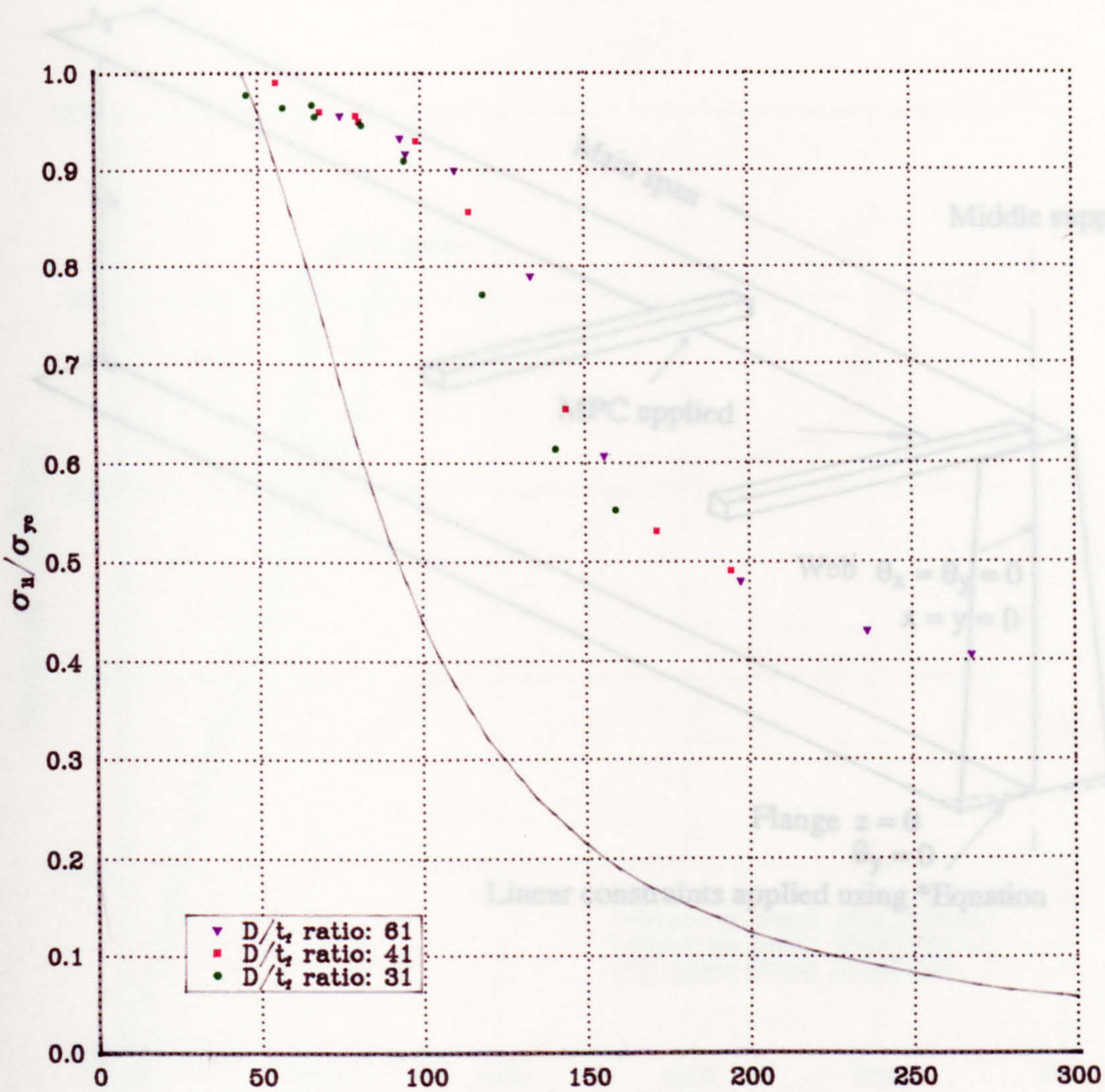

Figure 6.13 Comparison between ABAQUS results and BS5400 design curve

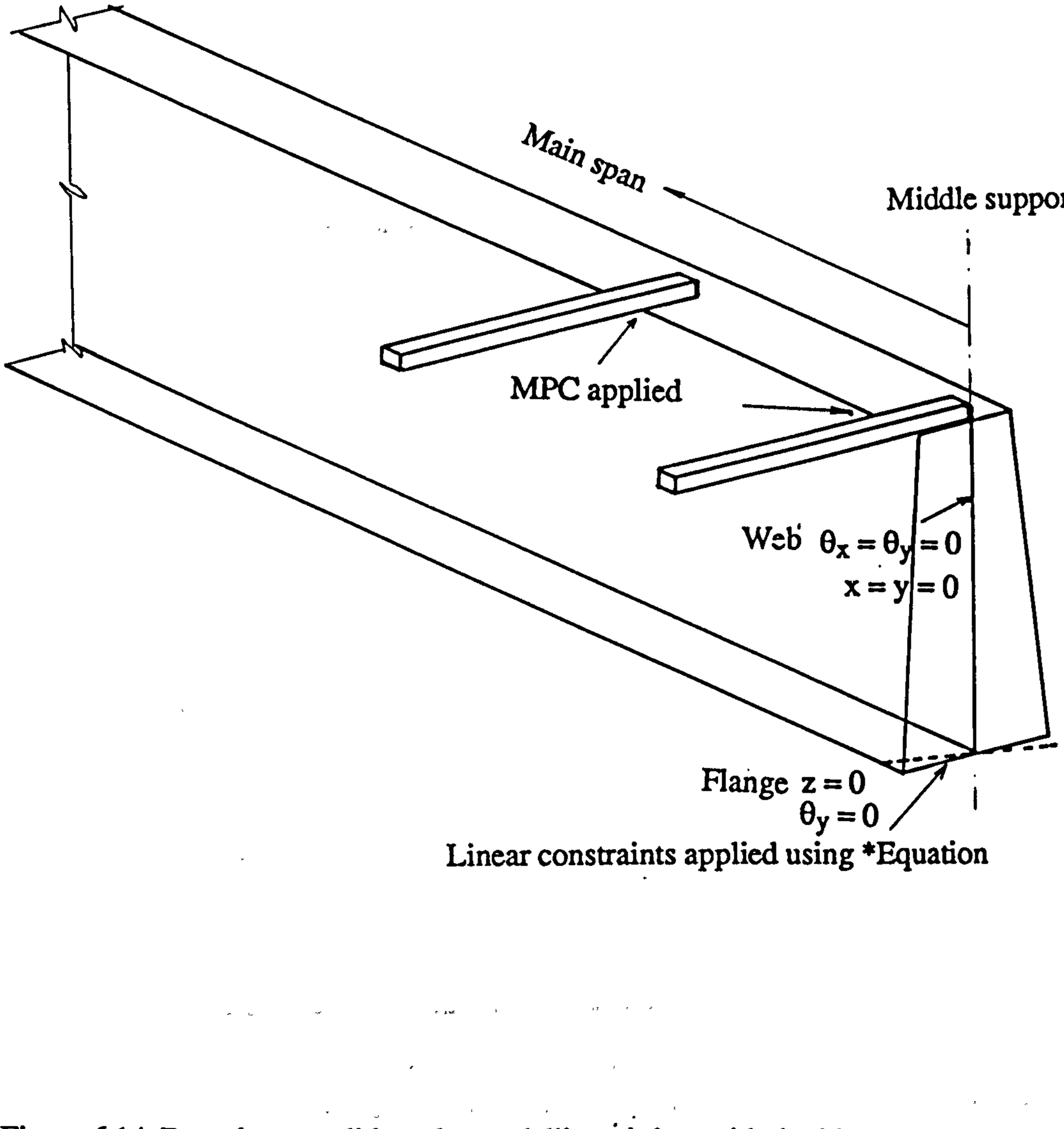

Figure 6.14 Boundary conditions for modelling girders with double span under UDL

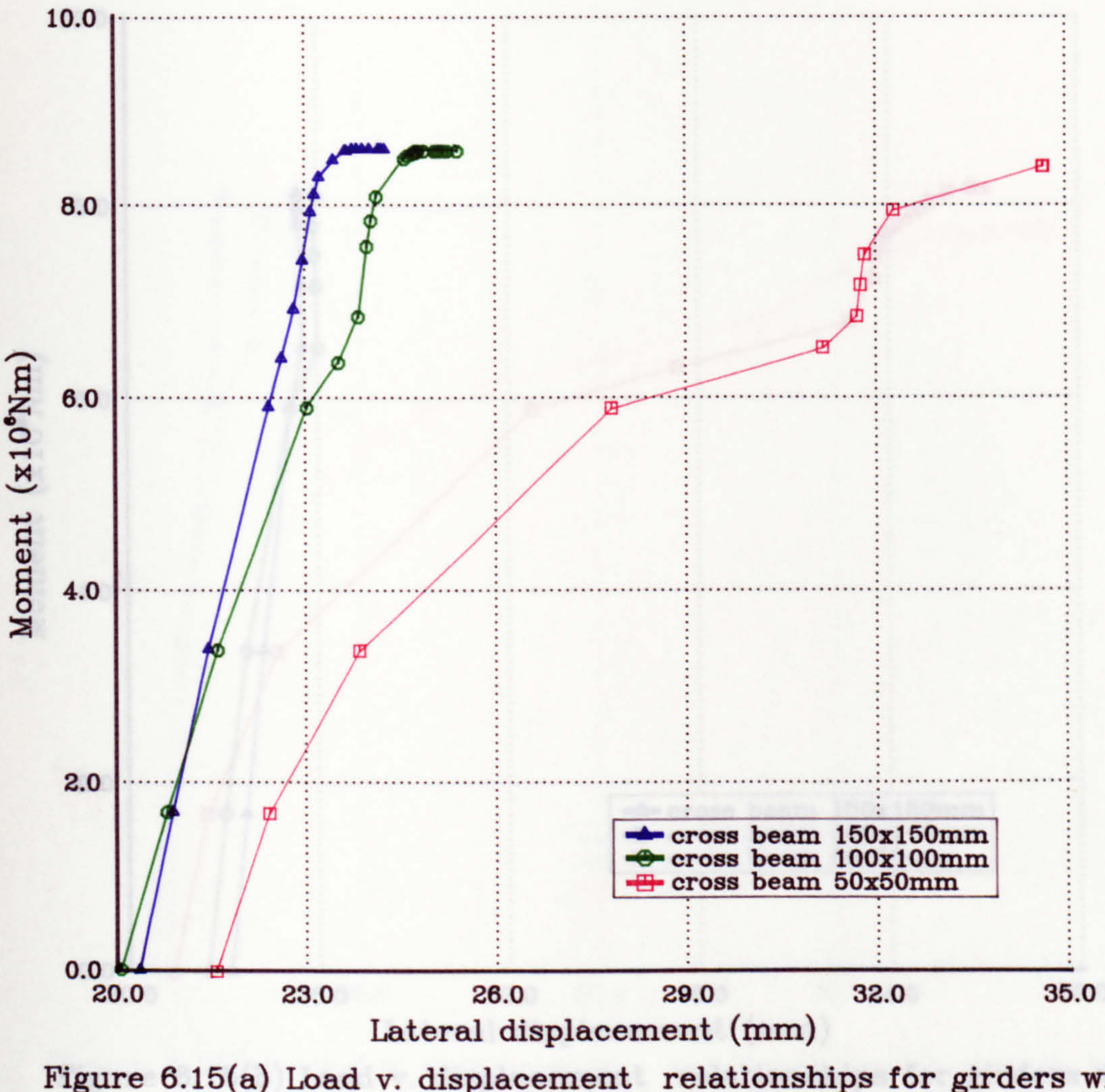

Figure 6.15(a) Load v. displacement relationships for girders with D/t_f ratio of 31 and cross-beam spacing of 1m under UDL on double span

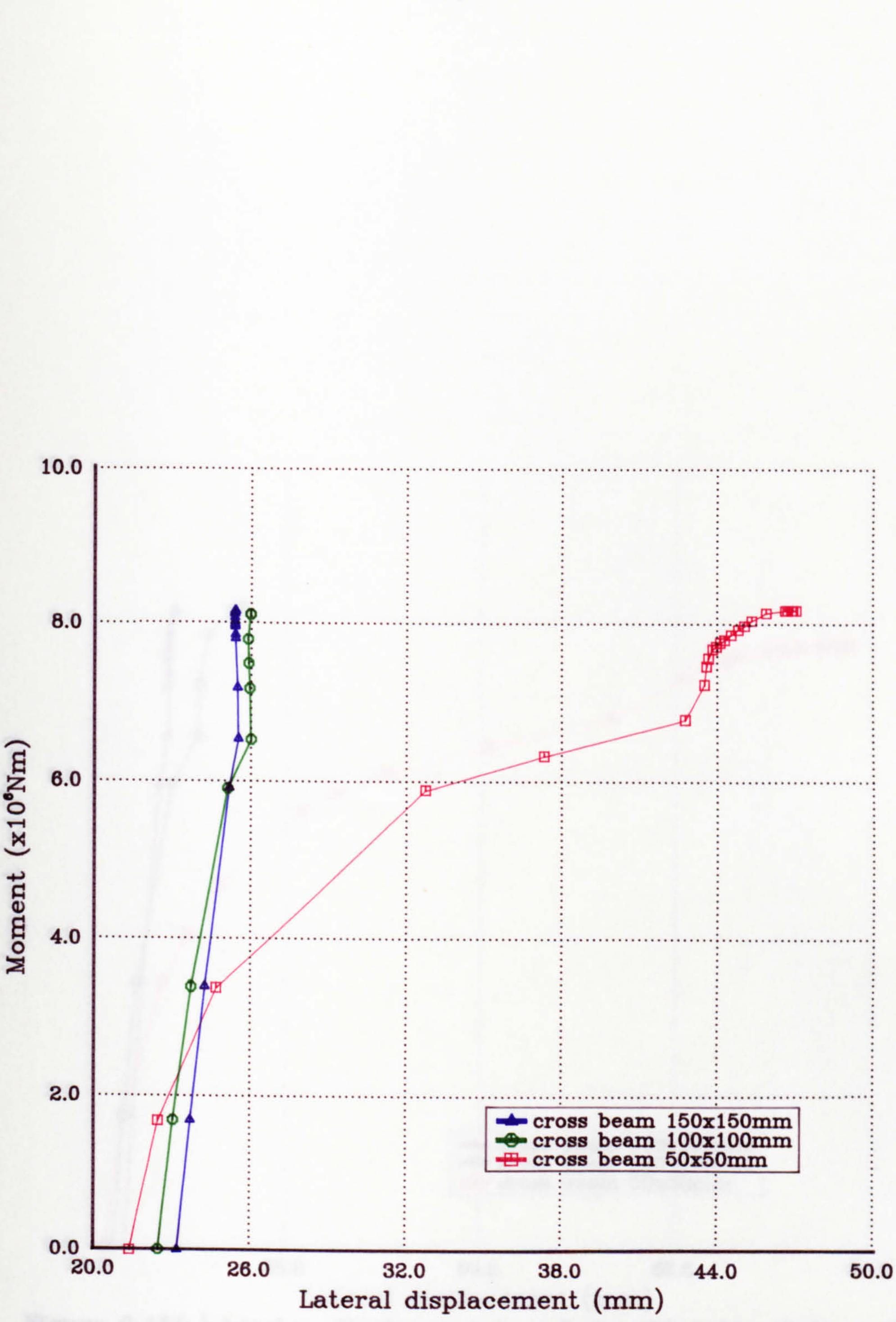

Figure 6.15(b) Load v. displacement relationships for girders with D/t_f ratio of 31 and cross–beam spacing of 2.5m under UDL on double span

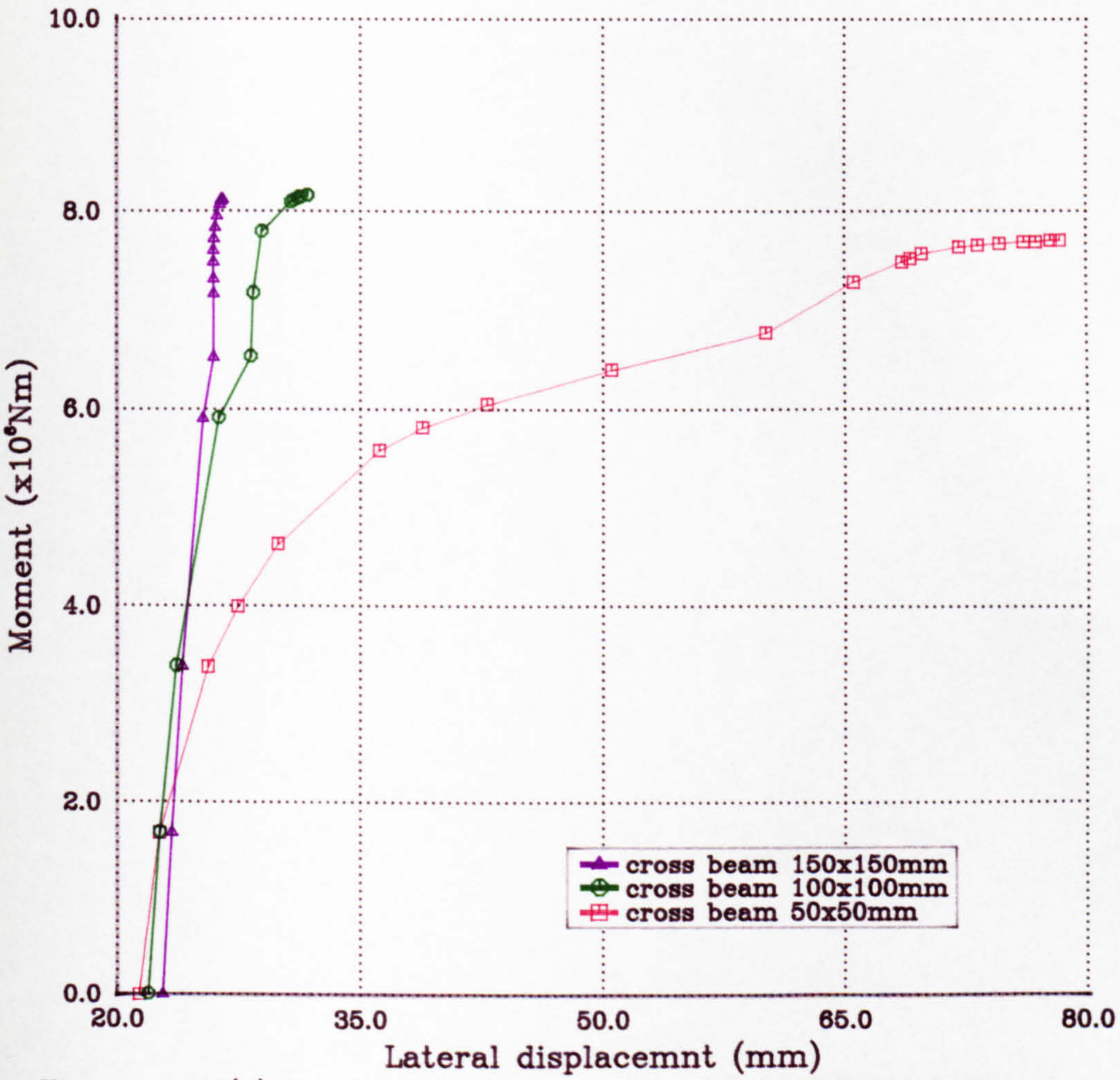

Figure 6.15(c) Load v. displacement relationships for girders with D/t_f ratio of 31 and cross-beam spacing of 5m under UDL on double span

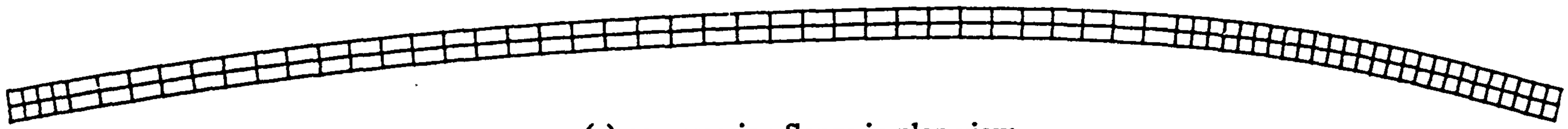

(a) compression flange in plan view

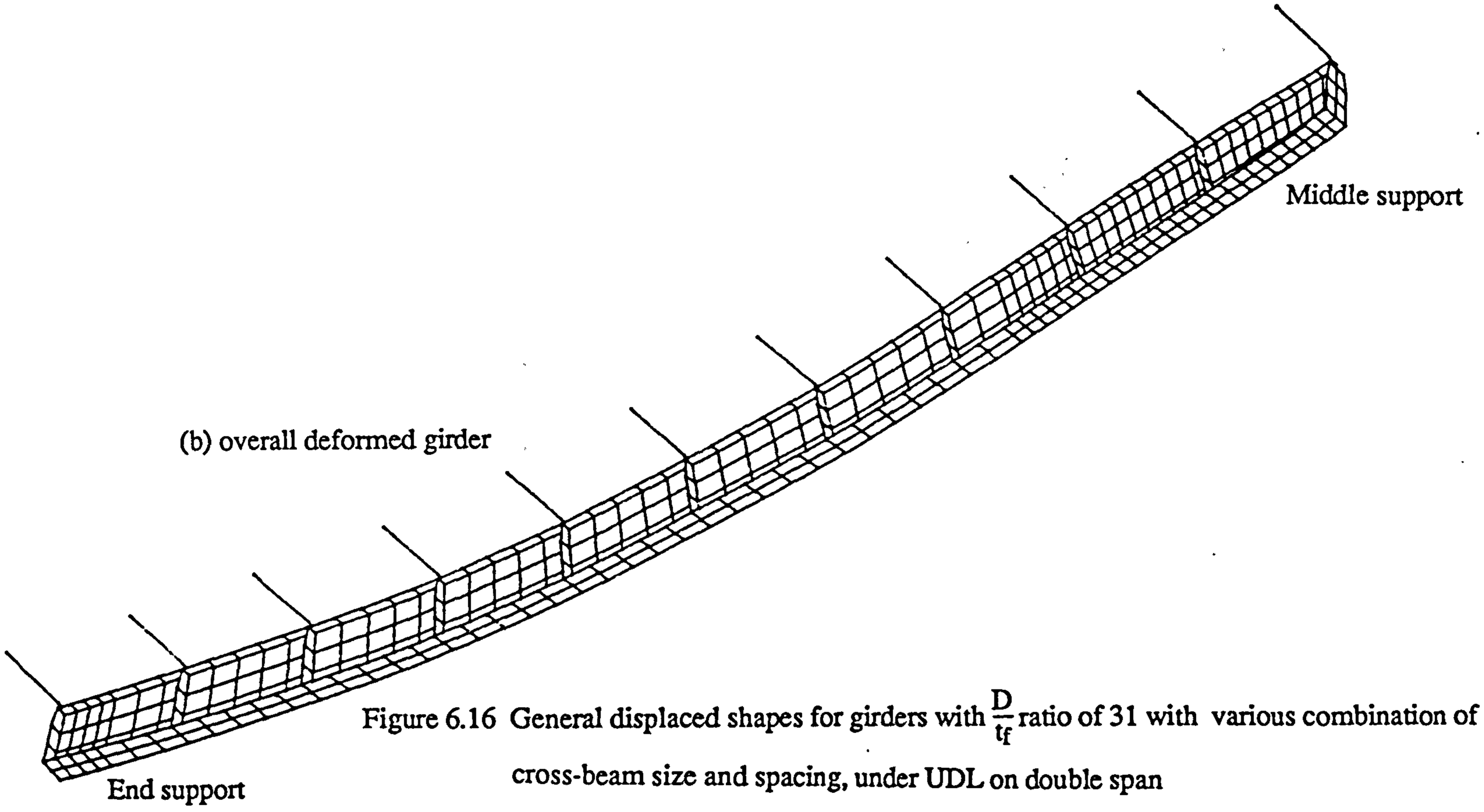

(b) overall deformed girder

Figure 6.16 General displaced shapes for girders with $\frac{D}{t_f}$ ratio of 31 with various combination of cross-beam size and spacing, under UDL on double span

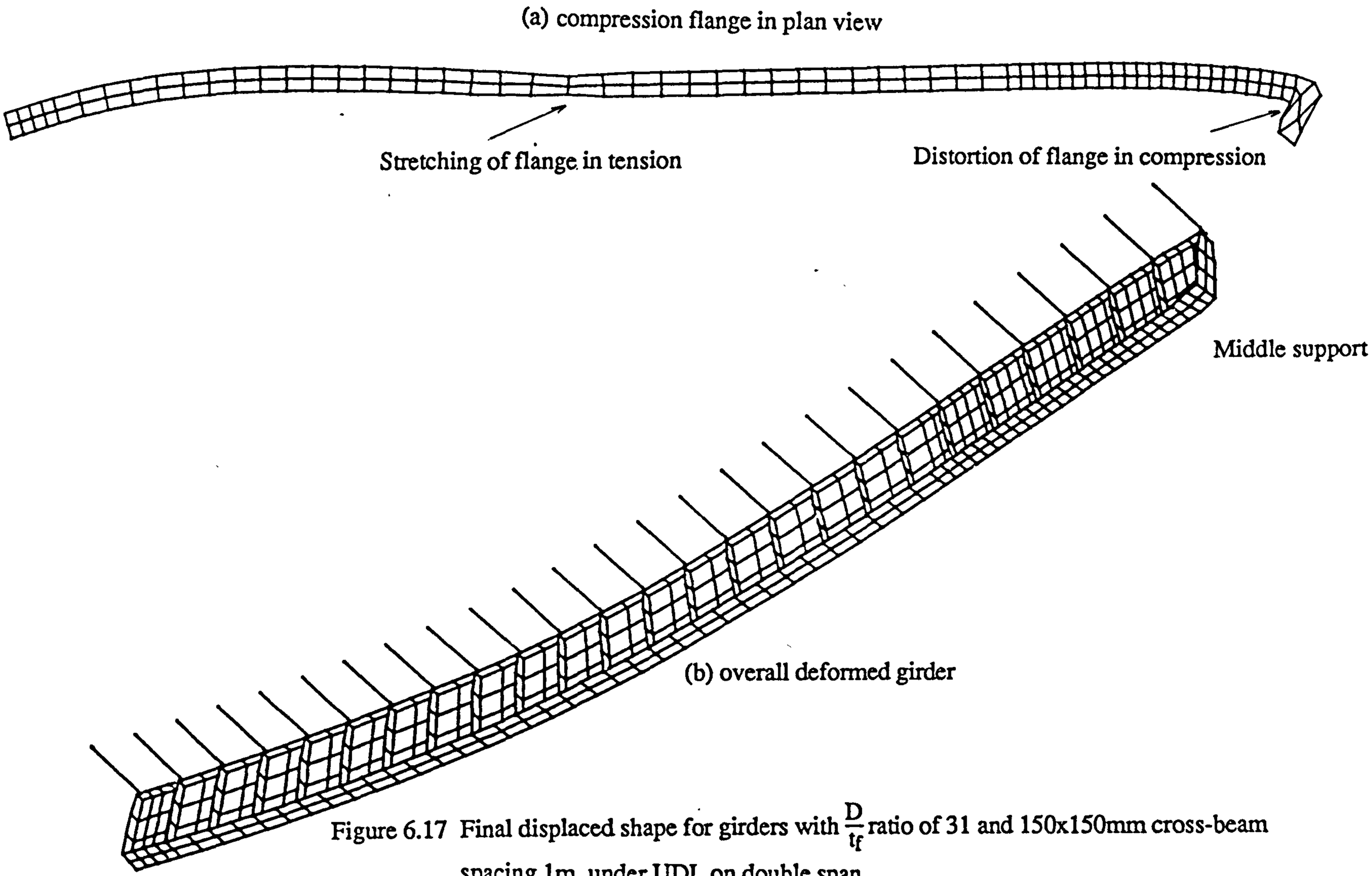

Figure 6.17 Final displaced shape for girders with $\frac{D}{t_f}$ ratio of 31 and 150x150mm cross-beam spacing 1m, under UDL on double span

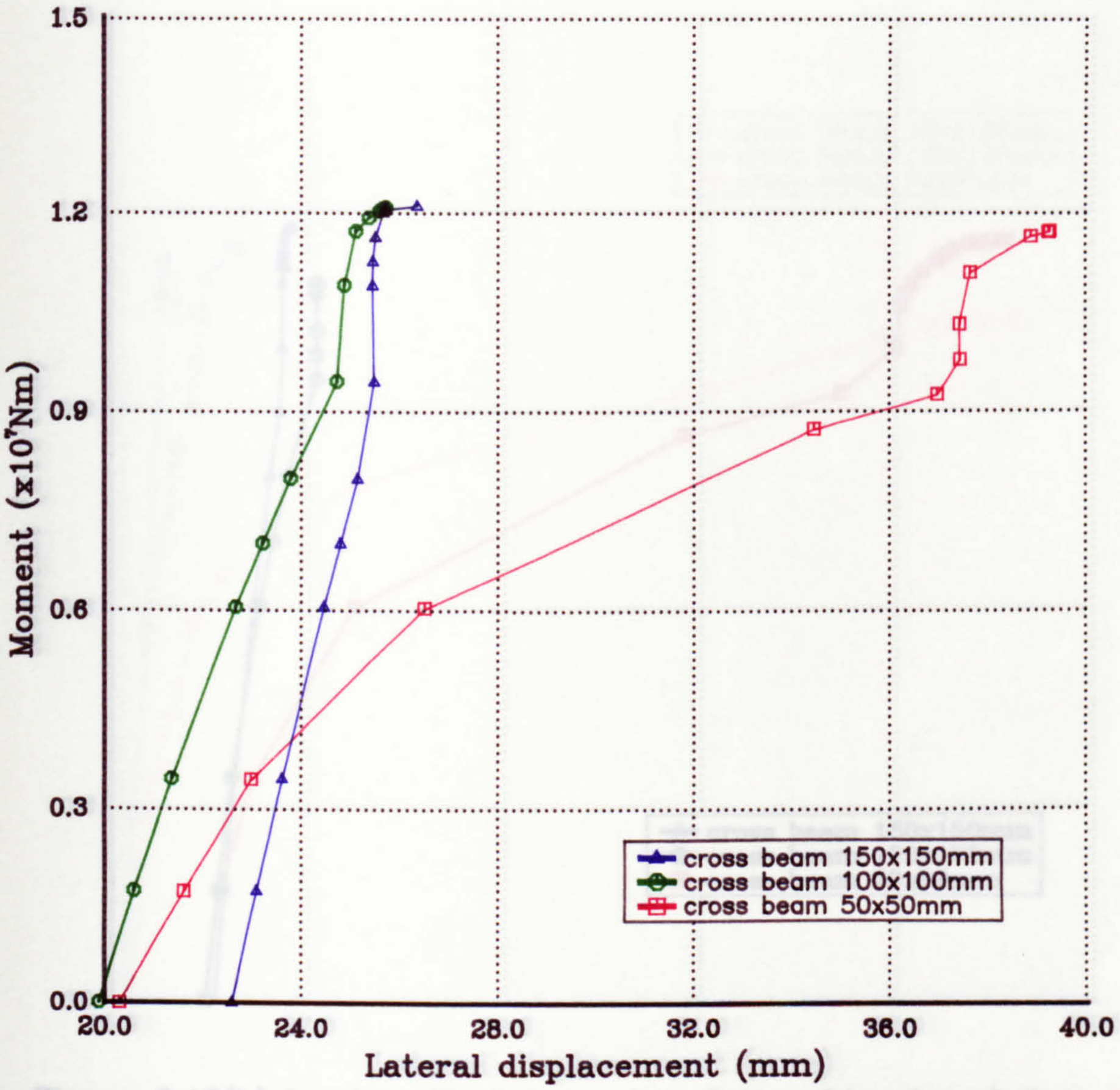

Figure 6.18(a) Load v. displacement relationships for girders with D/t_t ratio of 41 and cross-beam spacing 1m under UDL on double span

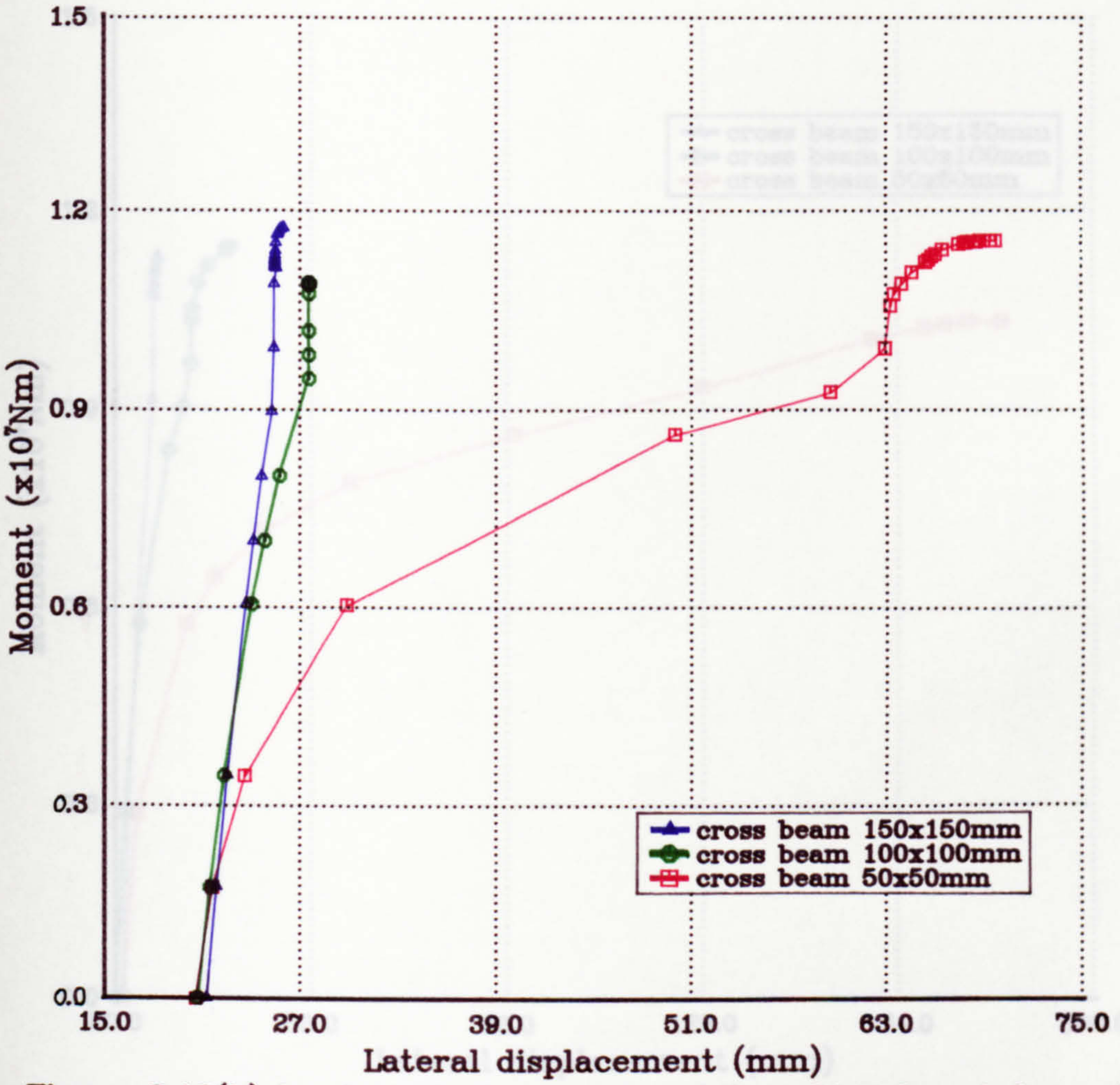

Figure 6.18(b) Load v. displacement relationships for girders with D/t_f ratio of 41 and cross–beam spacing of 2.5m under UDL on double span

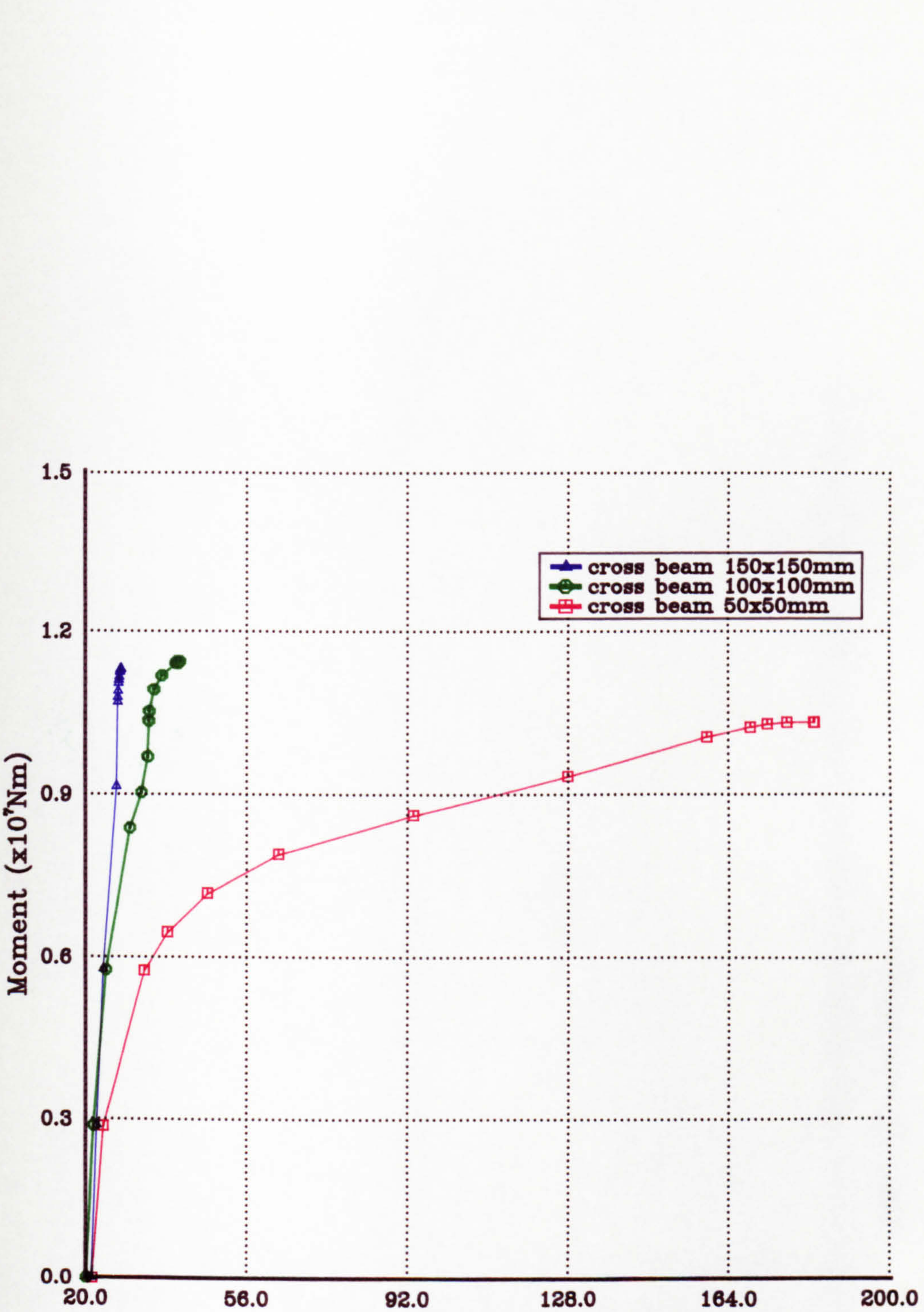

Figure 6.18(c) Load v. displacement relationships for girders with D/t_f ratio of 41 and cross-beam spacing of 5m under UDL on double span

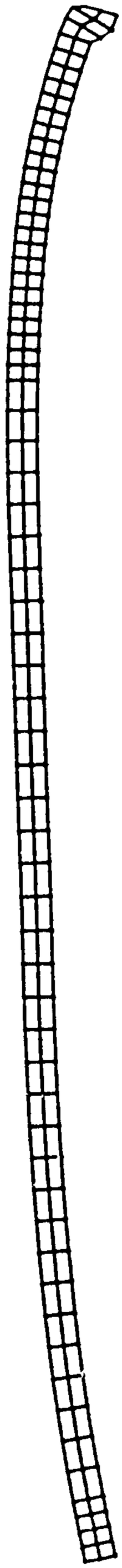

Figure 6.19 General displaced shape of compression flange for girders with $\frac{D}{t_f}$ ratio of 41 under UDL on double span

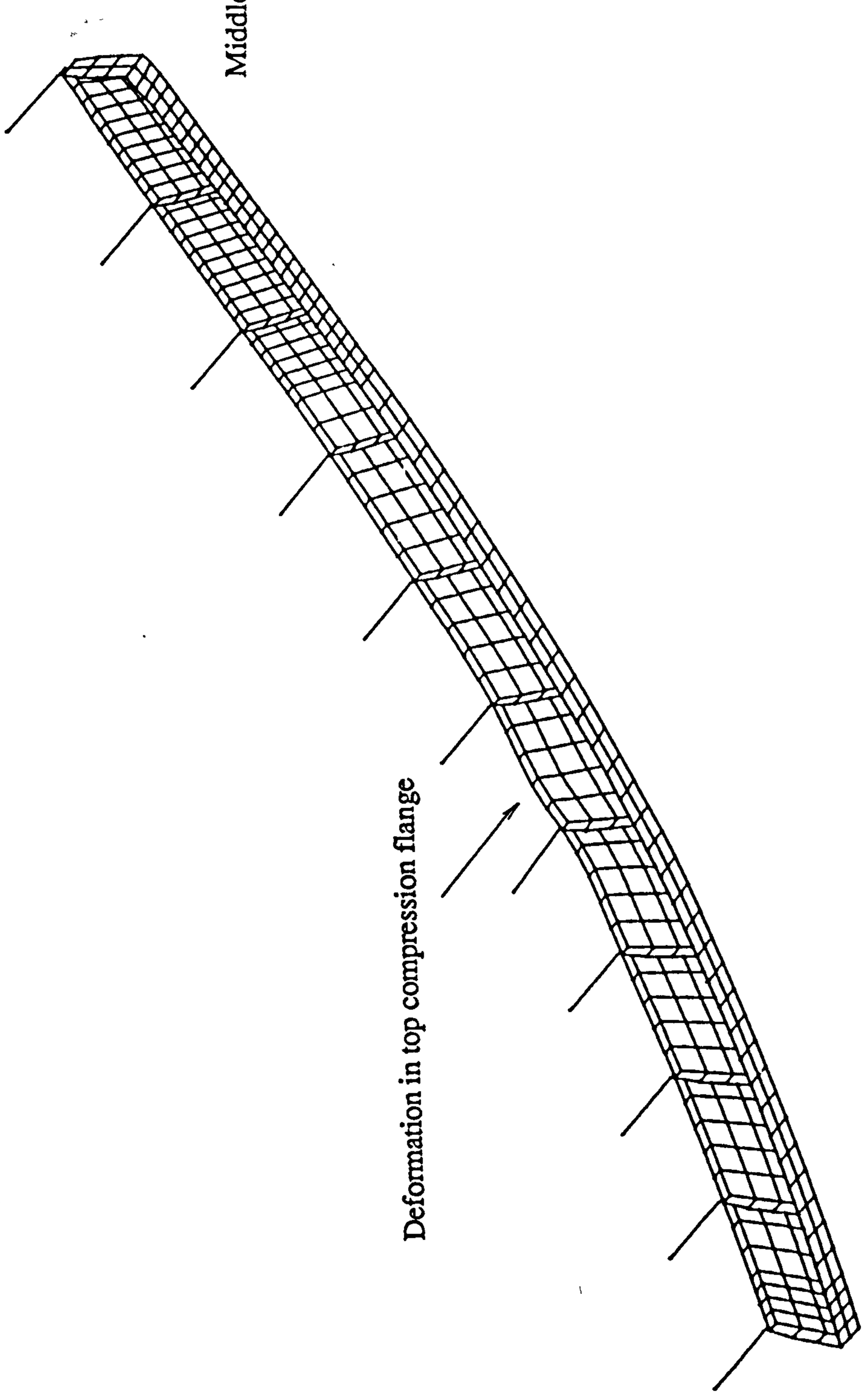

Figure 6.20 General displaced shape for girders with $\frac{D}{t_f}$ ratio of 41 and cross beam spacing 2.5m, under UDL on double span

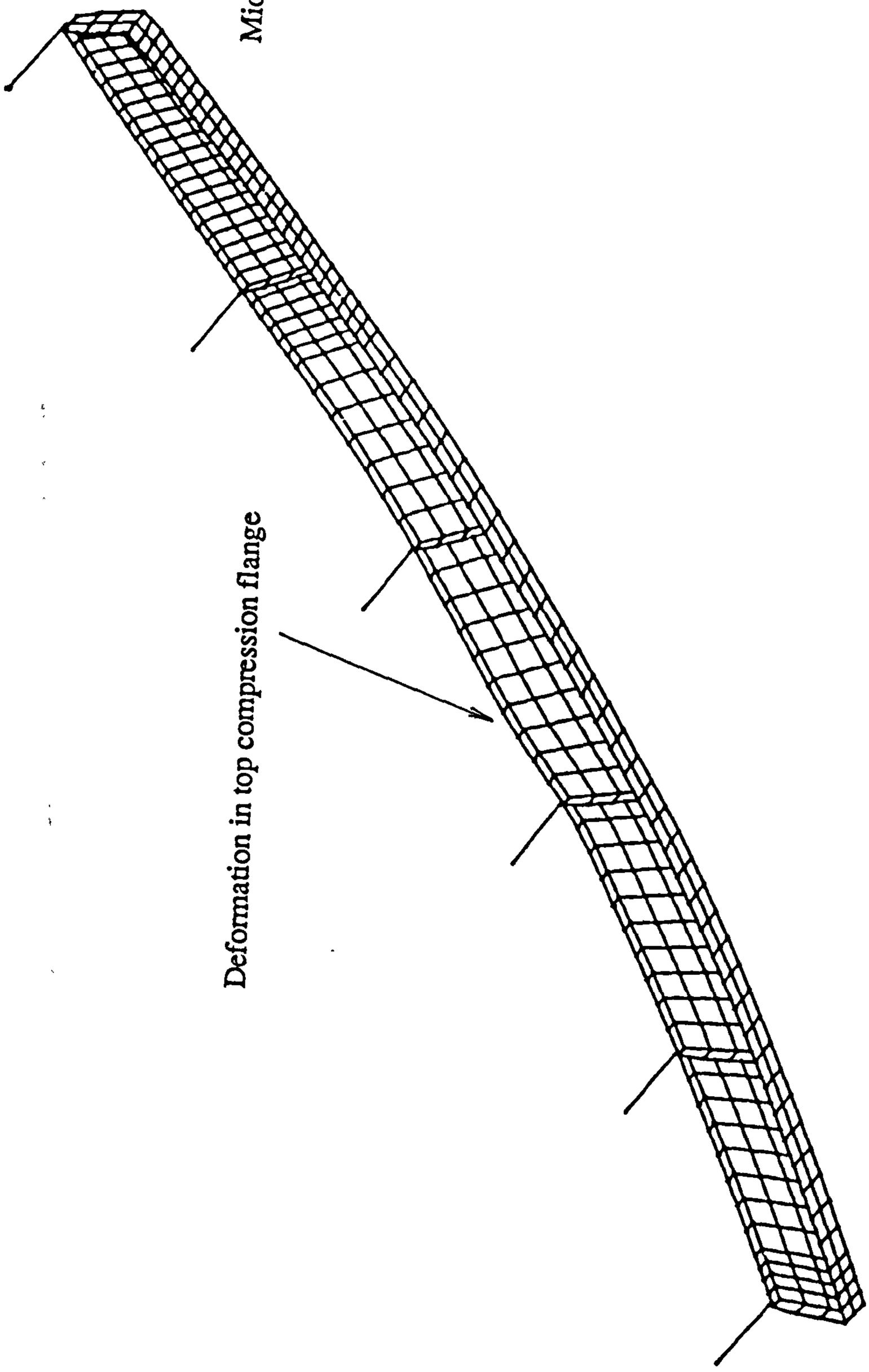

Figure 6.21 General displaced shape for girders with $\frac{D}{t_f}$ ratio of 41 and cross-beam spacing 5m, under UDL on double span

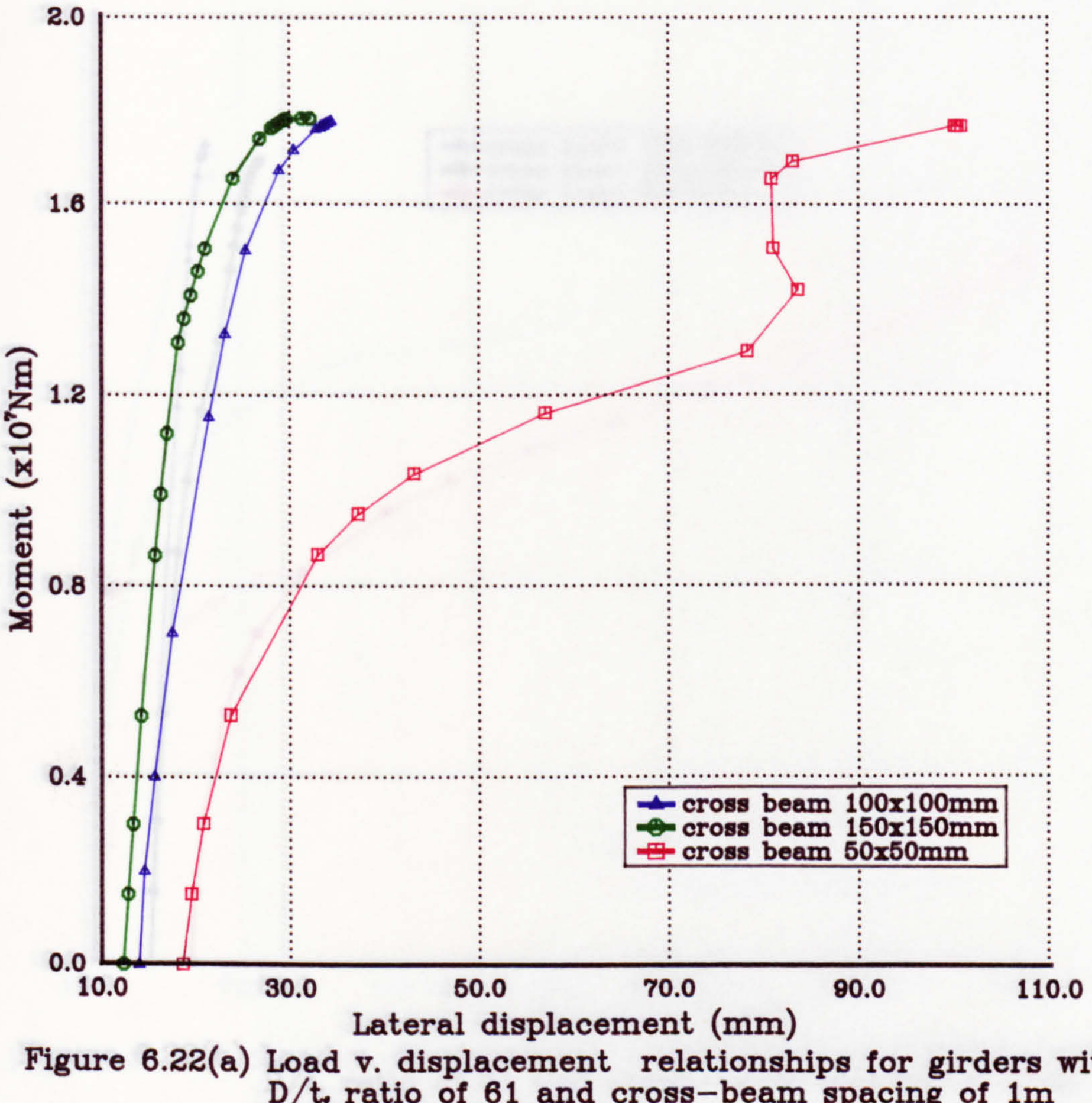

Figure 6.22(a) Load v. displacement relationships for girders with D/t_f ratio of 61 and cross-beam spacing of 1m under UDL on double span

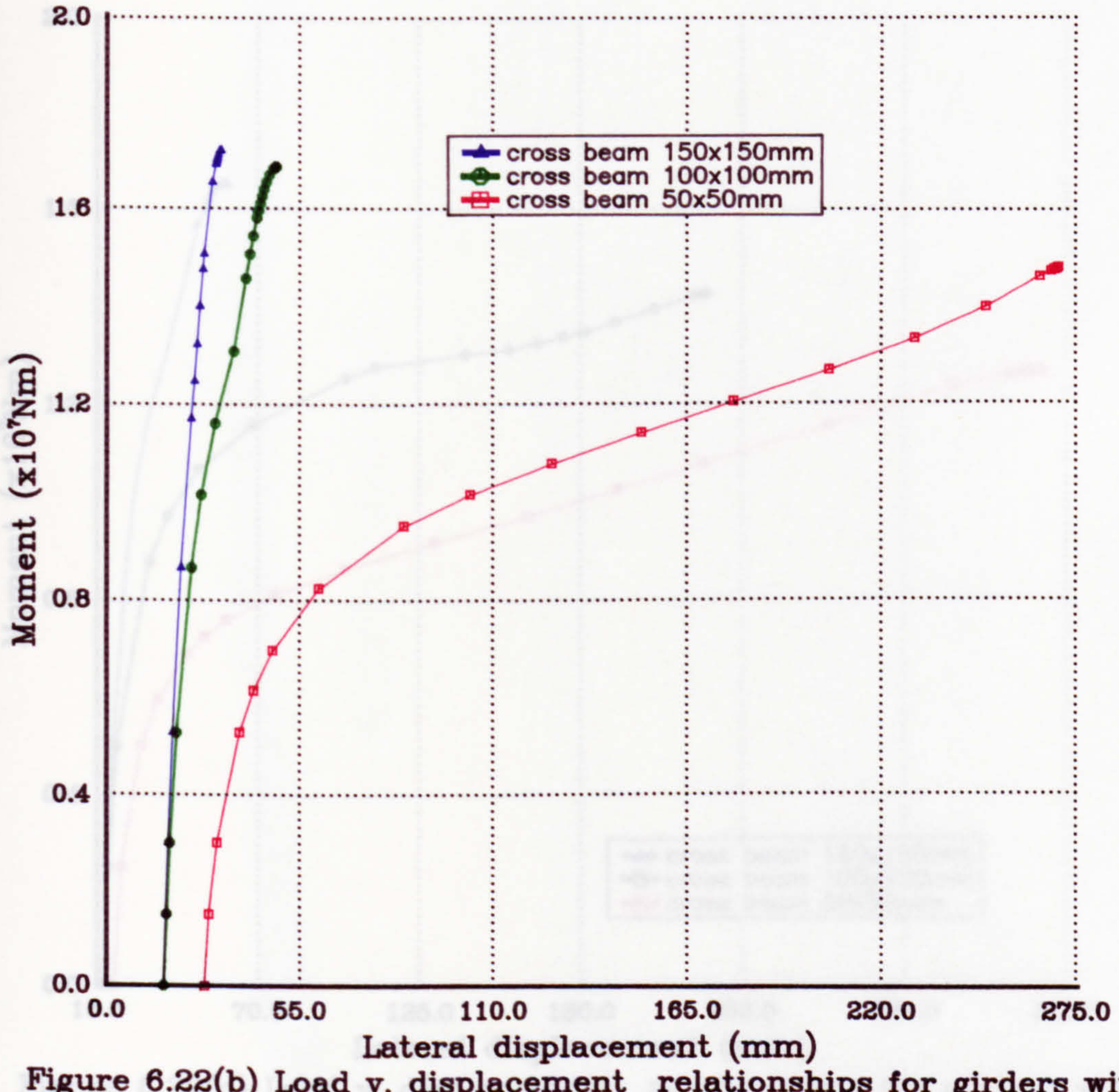

Figure 6.22(b) Load v. displacement relationships for girders with D/t_f ratio of 61 and cross-beam spacing of 2.5m under UDL on double span

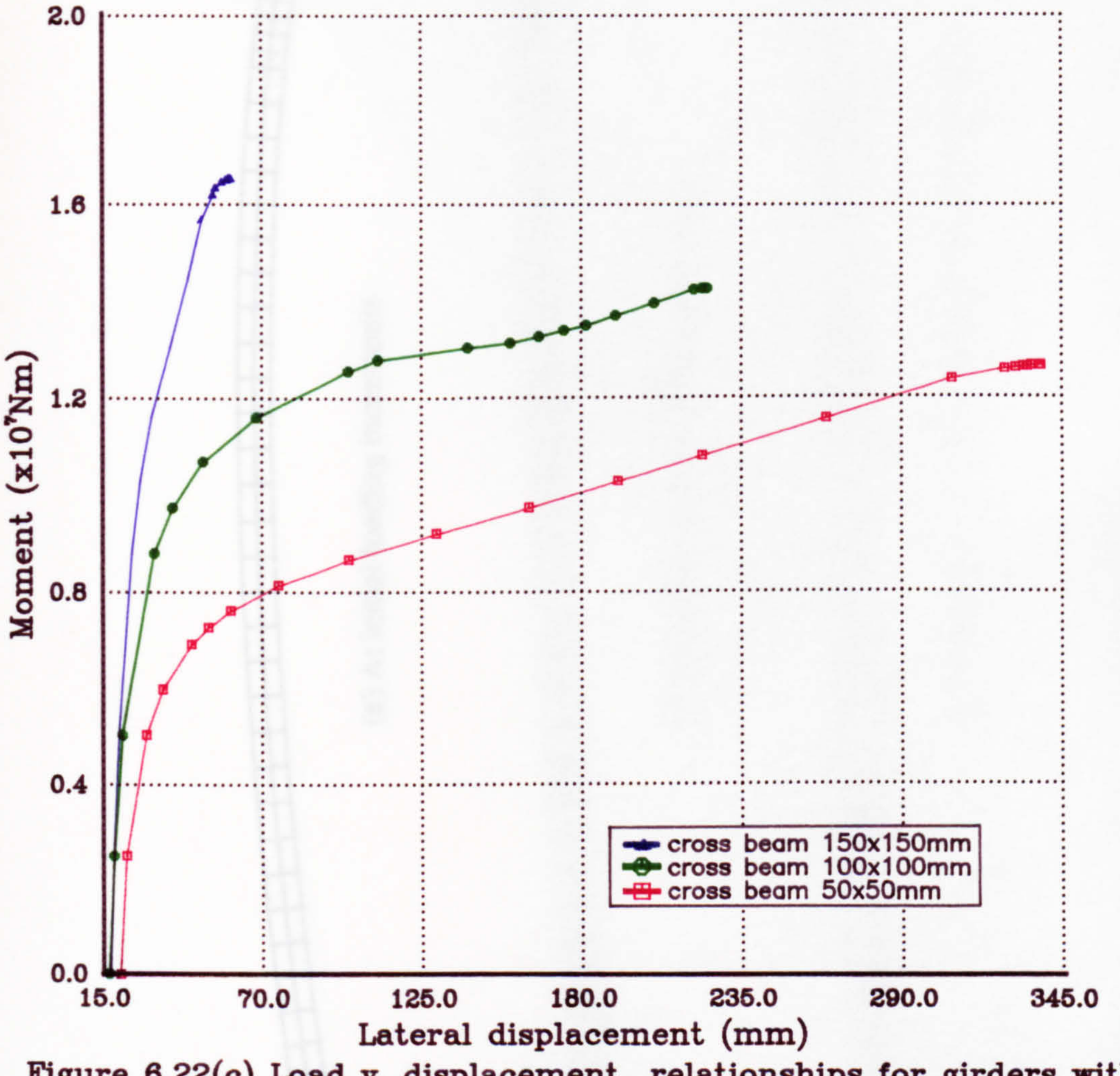

Figure 6.22(c) Load v. displacement relationships for girders with D/t_f ratio of 61 and cross-beam spacing of 5m under UDL on double span

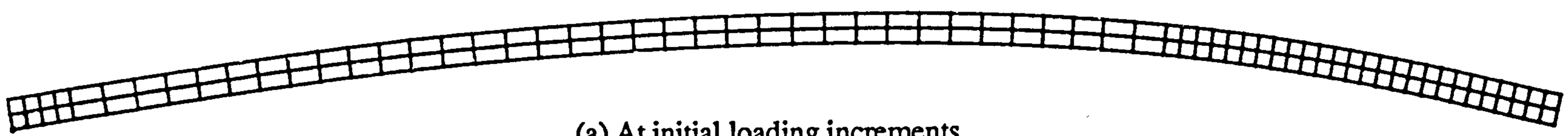

(a) At initial loading increments

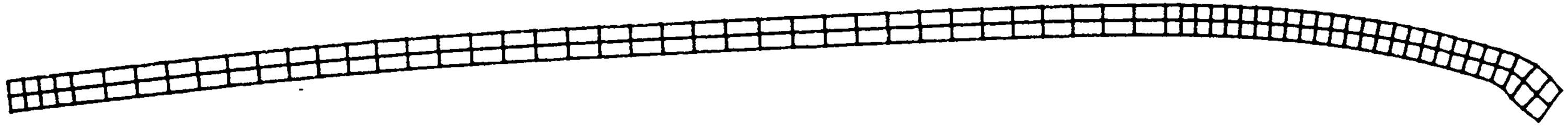

(b) At failure, with 50x50mm cross-beam

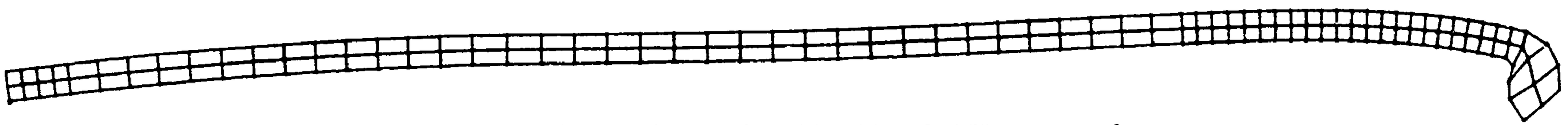

(c) At failure, with 100x100/150x150mm cross-beam

Figure 6.23 Displaced shapes of compression flange in plan view for girders with $\frac{D}{t_f}$ ratio of 61 and cross-beam spacing 1m, under UDL on double span

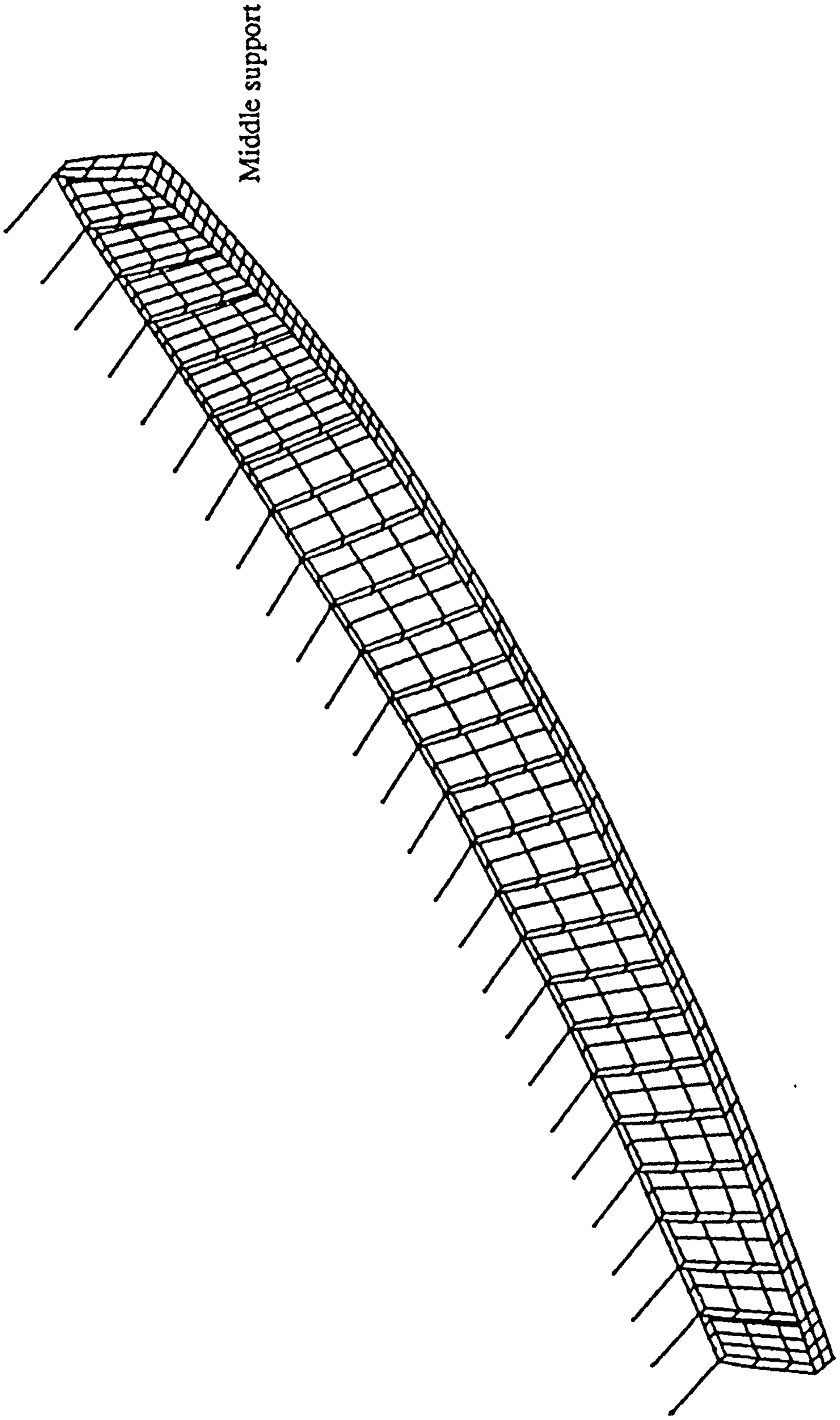

Figure 6.24(a) Final displaced shape for girder with $\frac{D}{t_f}$ ratio of 61 and 50x50mm cross-beam spacing 1m, under UDL on double span

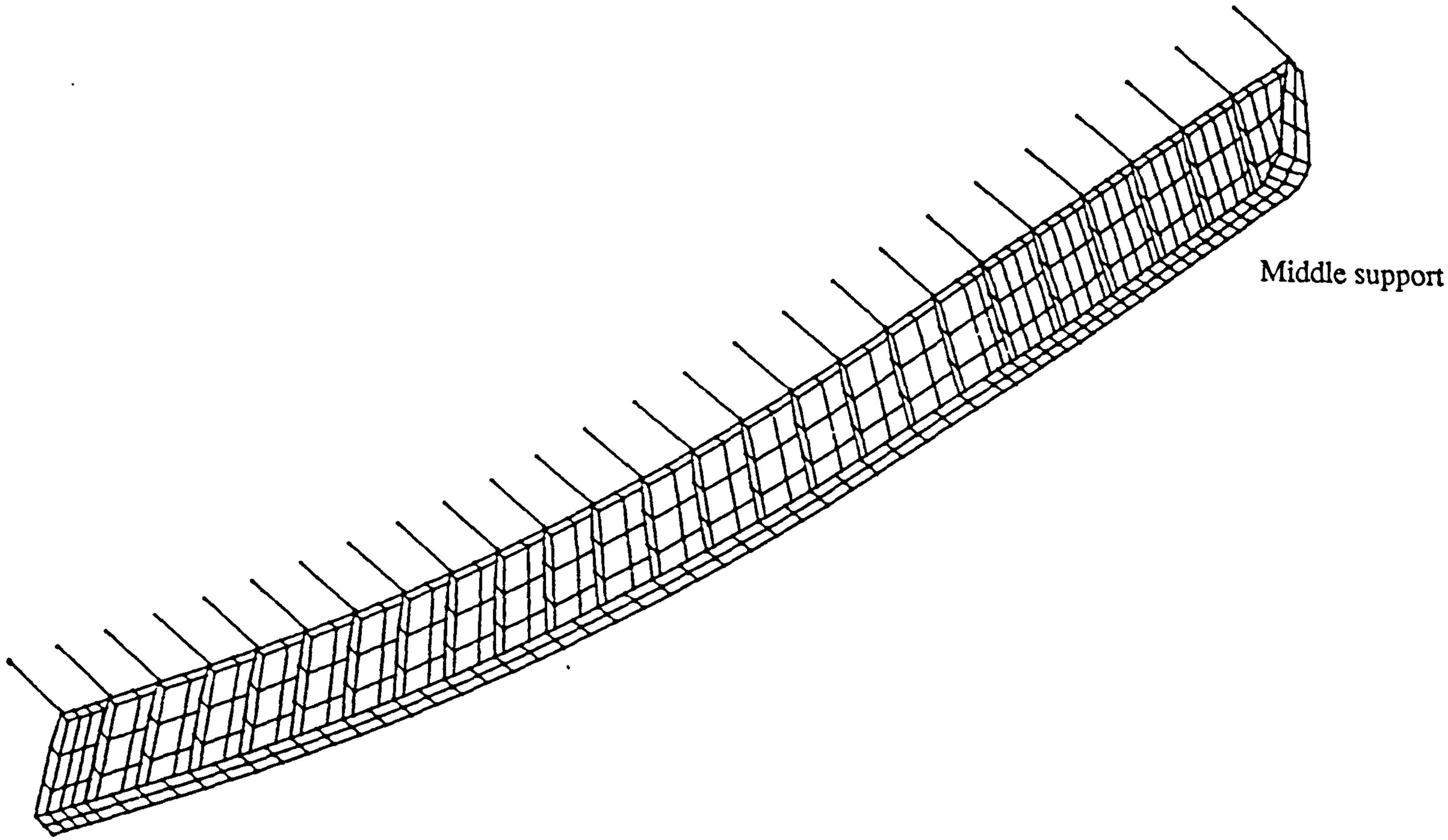

Figure 6.24(b) Final displaced shape for girders with $\frac{D}{t_f}$ ratio of 61 and 100x100/150x150mm cross-beam spacing 1m, under UDL on double span

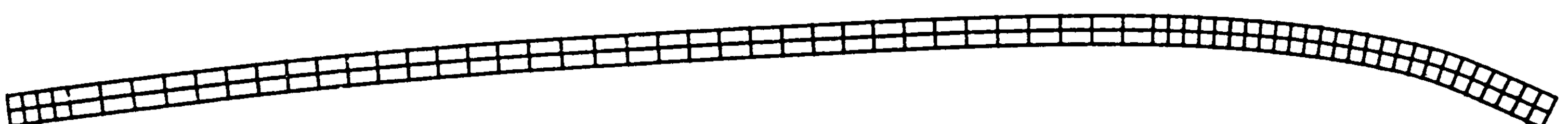

(a) With 50x50mm cross-beam

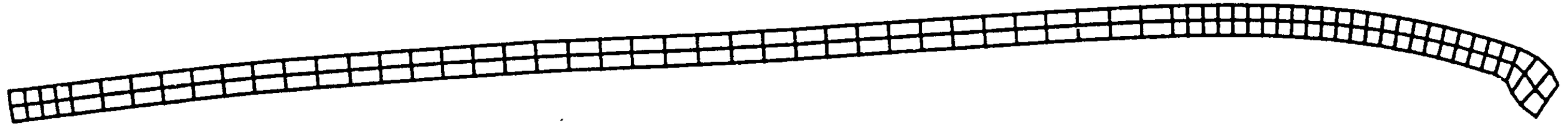

(b) With 100x100mm cross-beam

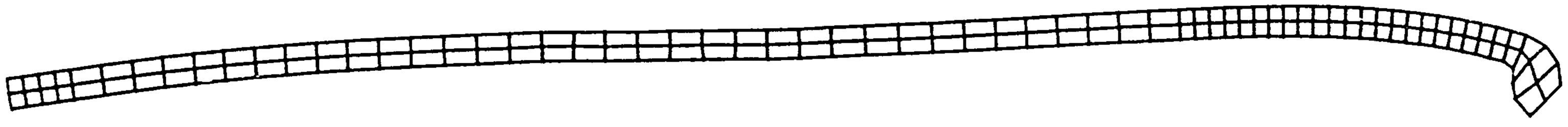

(c) With 150x150mm cross-beam

Figure 6.25 Final displaced shapes of compression flange in plan view for girders with $\frac{D}{t_f}$ ratio of 61 and cross-beam spacing 2.5m, under UDL on double span

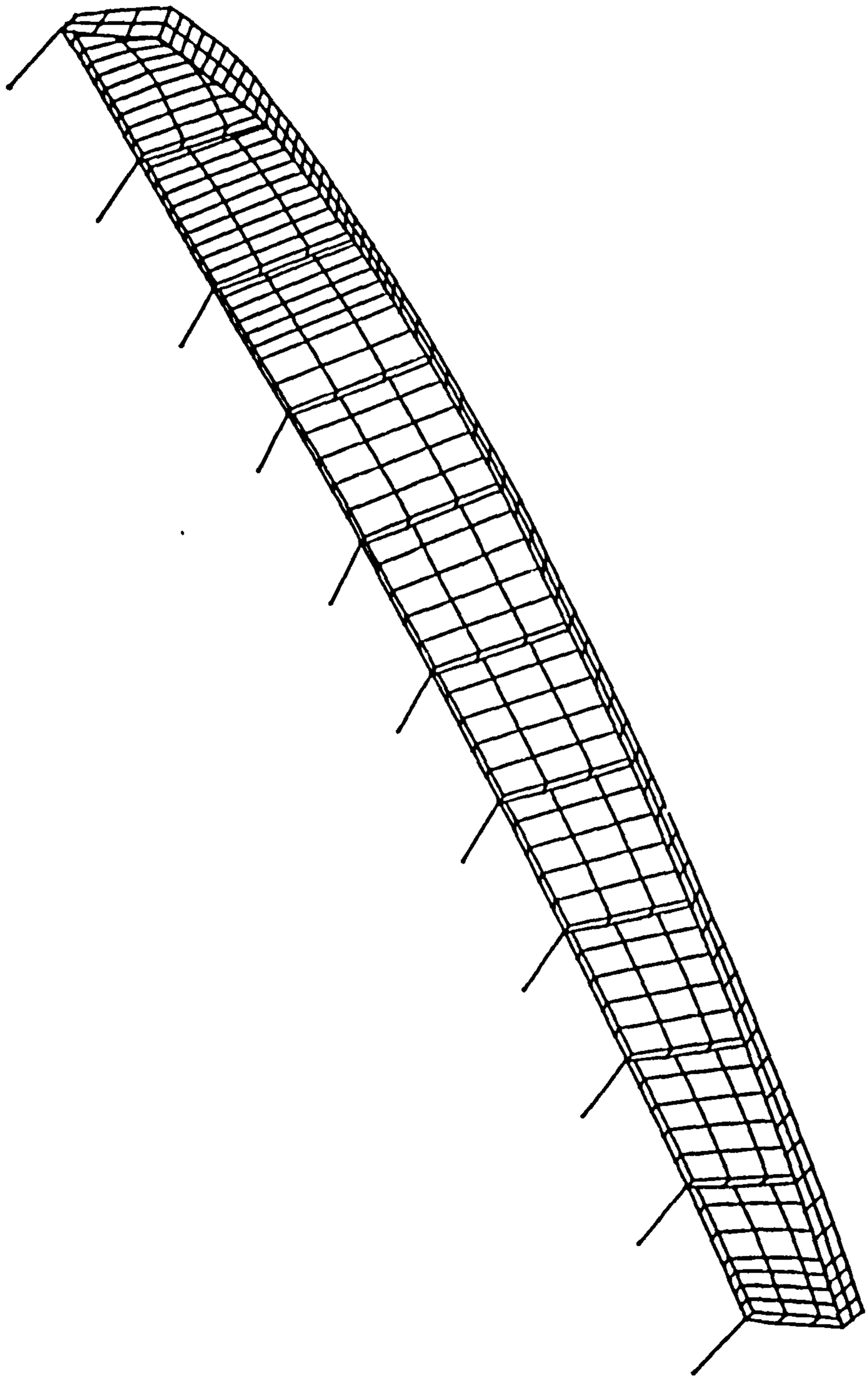

Figure 6.26(a) Final displaced shape for girder with $\frac{D}{t_f}$ ratio of 61 and 50x50mm cross-beam spacing 2.5m; under UDL on double span

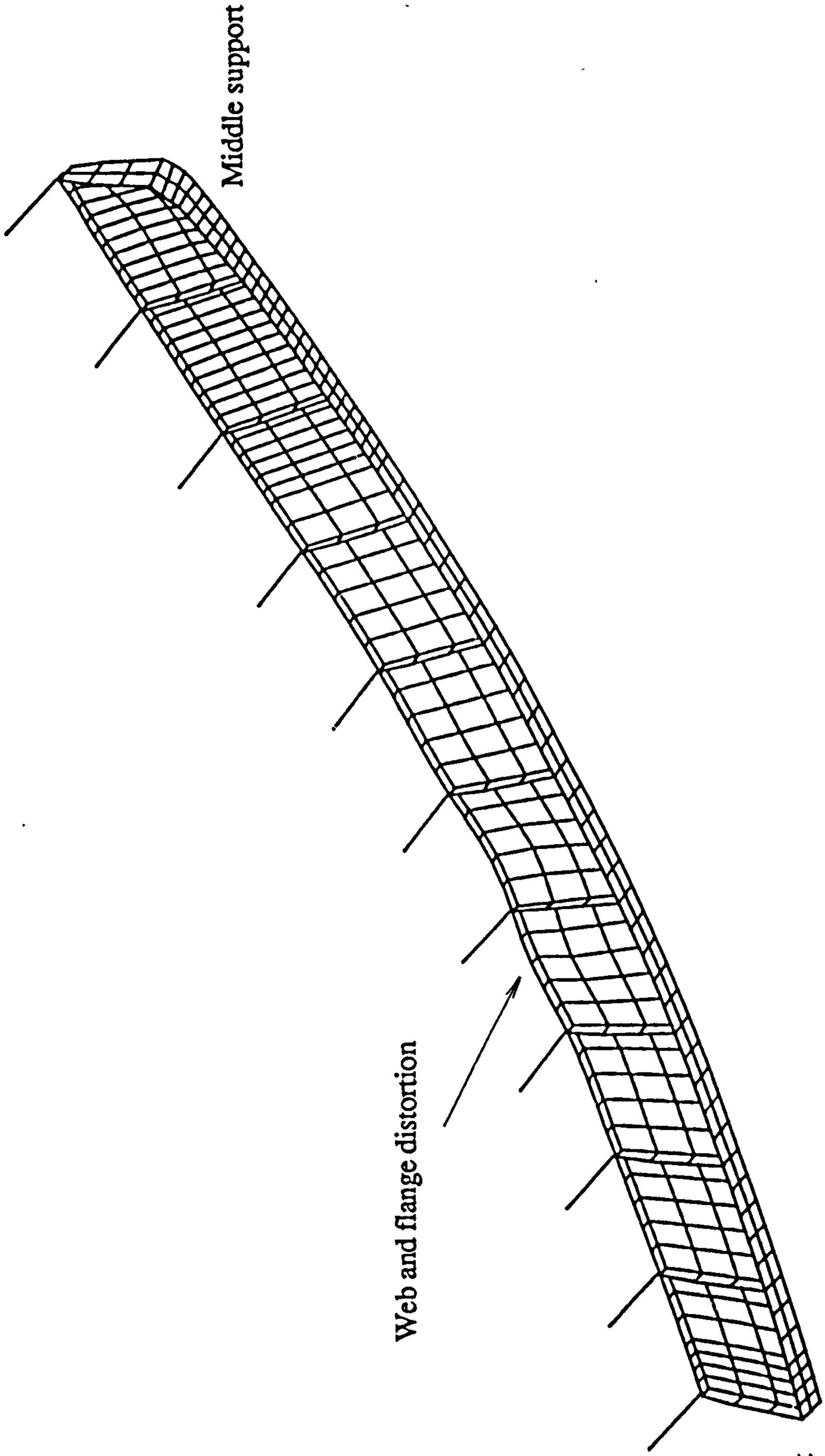

Figure 6.26(b) Final displaced shape for girders with $\frac{D}{t_f}$ ratio of 61 and 100x100/150x150mm cross-beam spacing 2.5m, under UDL on double span

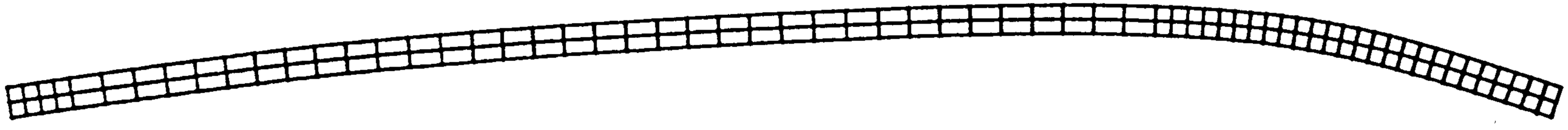

(a) With 50x50mm cross-beam

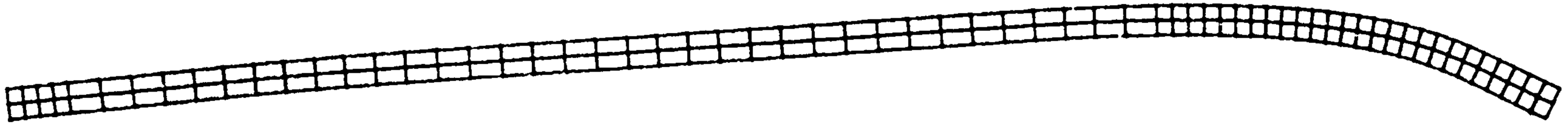

(b) With 100x100mm cross-beam

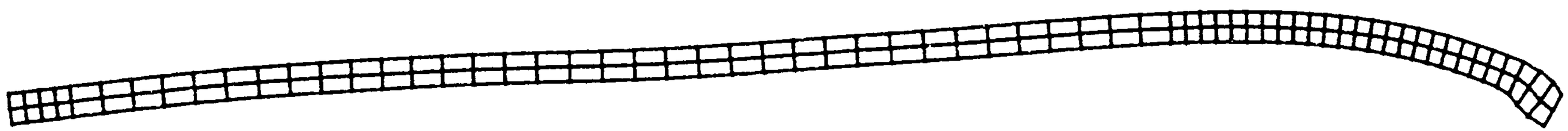

(c) With 150x150mm cross-beam

Figure 6.27 Final displaced shapes of compression flange in plan view for girders with $\frac{D}{t_f}$ ratio of 61 and cross-beam spacing 5m, under UDL on double span

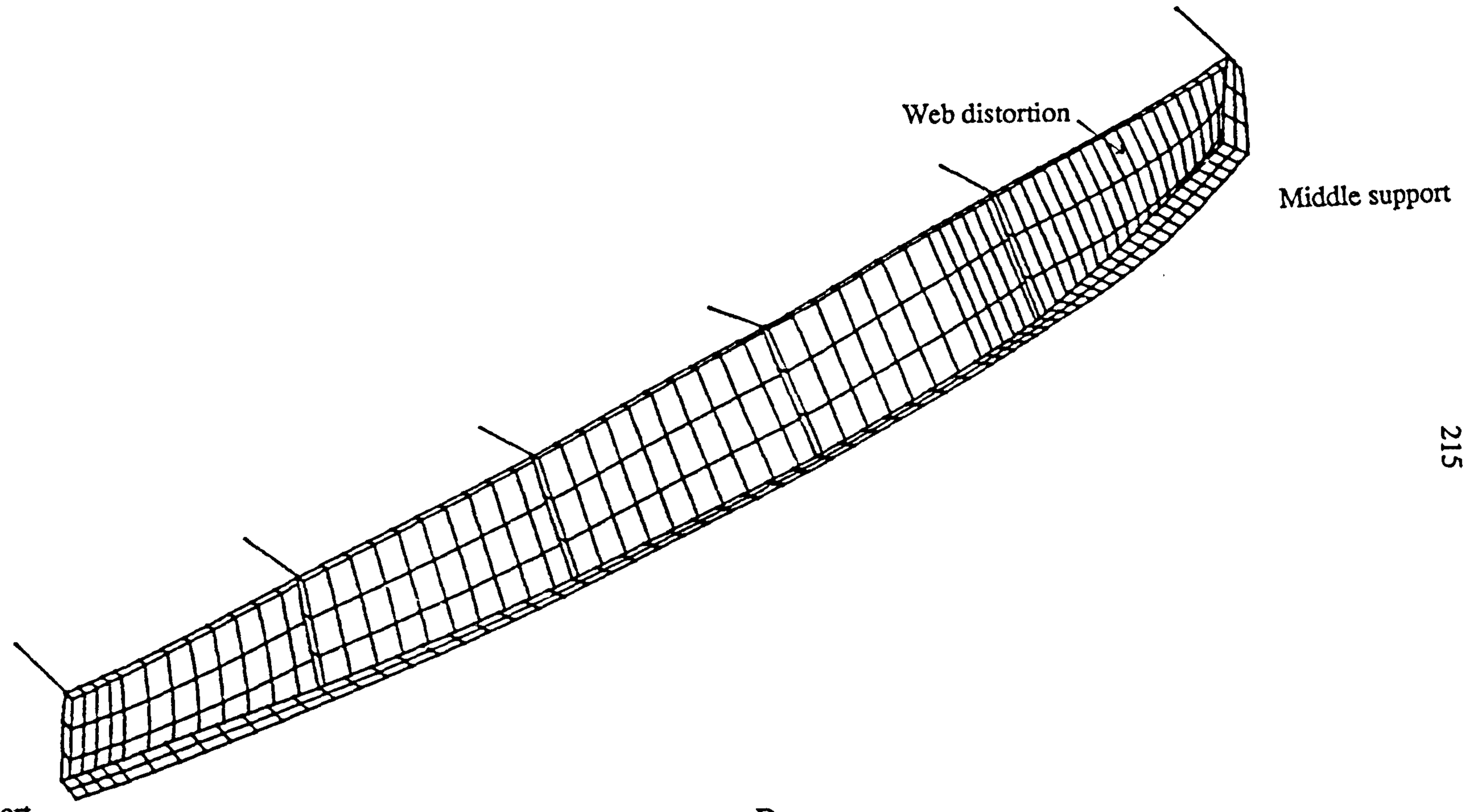

Figure 6.28(a) Final displaced shape for girders with $\frac{D}{t_f}$ ratio of 61 and 50x50/100x100mm cross-beam spacing 5m, under UDL on double span

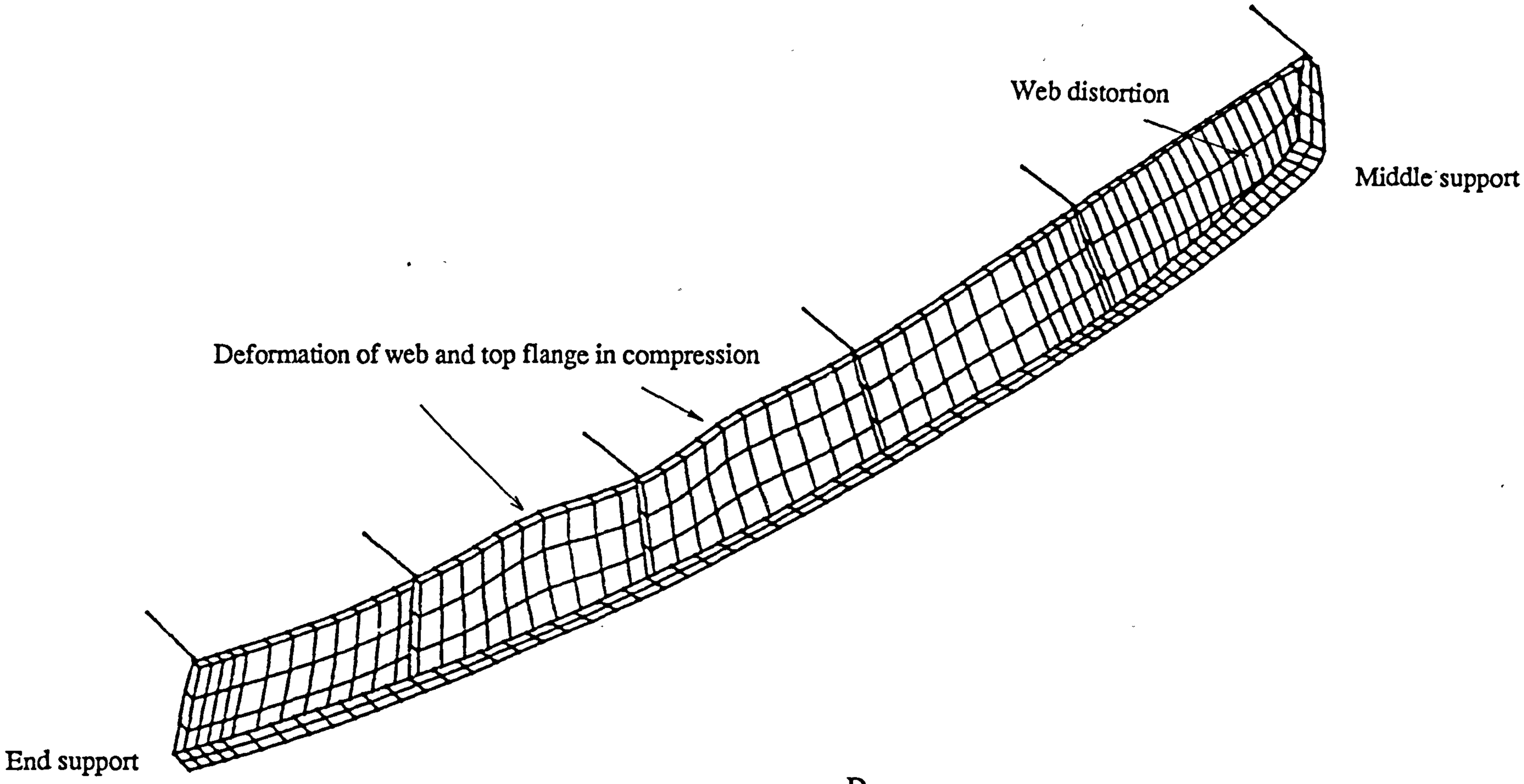

Figure 6.28(b) Final displaced shape for girder with $\frac{D}{t_f}$ ratio of 61 and 150x150mm cross-beam spacing 5m, under UDL on double span

CHAPTER 7

PROPOSED MODIFICATION OF BS5400

7.1 INTRODUCTION

From ABAQUS analyses, it has been shown, in common with the findings of other researchers, that the existing Bridge Code is conservative, especially in the presence of non-uniform bending moment. Putting together the evidence so far, a relatively simple modification is now proposed to improve the design values of I-section girders braced by U-frames. The present design principles and procedures have been retained as far as possible for the convenience of regular BS5400 users.

7.2 STUDY OF UNIFORM BENDING MOMENT CASE

Other than the strut analysis studied by Svensson and Goltermann in which uniform bending moment was considered , no recent work has considered bridge plate girders subject to uniform bending. Although this distribution is rarely encountered in practice, it is still the basic case used for the assessment of beam buckling and is generally taken to be the most severe loading condition. For bridge girders subject to other bending moment profiles, an increased capacity is normally allowed.

Therefore, instead of studying fixed-end girders under UDL and refining the slenderness function β, purely based on these geometrical variations, as Johnson and Bradford or Weston had done, girders under uniform bending were investigated. This study has been presented in the previous chapters as the primary aim of this thesis. The results obtained led to the proposed modification of BS5400, which was itself also based on uniform bending.

After careful examination of the design procedure in the present Code, it was felt that evaluation of effective length, l_e, of the compression flange from the principle of strut on elastic foundation (which is based on flexibility of the web and concrete slab) is appropriate. The finite element model of the Welding Institute test piece which was calibrated against the experimental value has clearly shown this point.

During the Welding Institute test, a horizontal force of 27.0lb was applied transversely at mid-span to the compression flange. As a result, a 0.52mm lateral deflection of the flange at the applied loading position occurred. Applying the same amount of force again to the finite element model, a displacement of 0.79mm was obtained. Therefore, the computer model was more flexible than the test model. The stiffness of individual U-frames of the finite element model was examined by applying transverse unit loads to the compression flange simultaneously at each U-frame position. The lateral displacement of compression flange braced by a central U-frame at mid-span was 0.0211m/N, whereas its theoretical value calculated by using δ as expressed in the Code was 0.0237m/N. The estimation of the U-frame stiffness in BS5400 is based on a summation of deflection due to bending of the web and concrete slab (or cross-beams) with a further allowance for flexibility of the joints between the cross member and the verticals of the U-frames, where appropriate. Therefore, the basis of calculation appears to be reasonably adequate, even in the extreme case of a single U-frame.

Following evaluation of δ and then l_e of the girders, the slenderness parameter λ_{LT} is required for the calculation of the limiting compressive stress. As defined in Clause 9.7.2:

$$\lambda_{LT} = \frac{l_e}{r_y} k_4 \eta \upsilon$$

where r_y is the radius of gyration of the whole beam section about its Y-Y axis;

k_4 depends on the type of beam used;

η is a factor for bending moment distribution; and

υ is a shape factor for the beam and is dependent on $\lambda_F = (\frac{l_e}{r_y})(\frac{t_f}{D})$ and $i = \frac{I_c}{(I_c+I_t)}$.

From Weston's research[26], it was clear that lateral distortional buckling of a beam is more closely related to the radius of gyration of the compression flange about the minor axis of the beam section than it was to the 'radius of gyration of the whole beam section about its minor axis'(as is used in BS5400). In retrospect, it is not surprising that the radius of gyration of the compression flange, only, is more relevant to the particular case of lateral buckling of a compression flange braced by U-frames. This type of buckling has been characterised as a compression flange on an elastic foundation, which comprises translational and rotational springs respectively representing the flexibility of the web and the torsional restraint from the cross-beams or concrete slab. Therefore, the minor radius of gyration of the whole beam section does not, in actual fact, come in as an effective factor, but the radius of gyration of the compression flange is more influential and the term 'lateral distortional buckling' is more appropriate to describe the failure process.

Consequently, the minor radius of gyration of the whole section used in BS5400 should be modified. Williams and Jemah[43] in their modelling of a compression flange on an elastic foundation, using the finite strip method, suggested that 15% of the web should be included in the compression flange for the treatment of such structures. Goltermann and Svensson[42], based on this empirical finding, refined the method previously developed by Svensson and confirmed Williams and Jemah's proposal. Therefore it is suggested that the effective section for lateral buckling of I-section girders be derived from 15% of the web acting in conjunction with the flange in compression. Hence, the minor radius of gyration of the effective section will be higher than the value of the r_y for the entire section. The $\frac{l_e}{r_y}$ value of the girder will then automatically decrease, as will the effective slenderness λ_{LT}.

Despite the fact that in actual bridge girders the $\frac{t_f}{D}$ and $\frac{t_w}{d}$ values are usually of the same order, it was thought that in the type of buckling involving web distortion, the $\frac{t_w}{d}$ rather than $\frac{t_f}{D}$ would be a more suitable factor to take into consideration. Both Johnson and Bradford and Weston's work illustrated this point clearly. $\frac{t_f}{D}$, which is merely an approximation of the torsional index of a section, is applicable to cases where (a) no rotational restraint is applied to the top flange of a girder and (b) lateral torsional buckling merely involves lateral displacement and rotation of an undistorted cross-section.

Combining the above-mentioned findings with results from ABAQUS analysis of various types of girder, leads to the following proposal for changes in λ_F and λ_{LT} as defined in BS5400, Clause 9.7.5.

Although the Perry-Robertson type of expression was derived originally for lateral torsional buckling, it is now employed in respect of lateral distortional buckling even though the two forms of behaviour are quite different. Superimposing results from ABAQUS and the experimental work onto Figure 10 of BS5400 as shown in Figure 7.1, it can be seen that most of the points are above the basic limiting stress curve (with some exceptions when $\lambda_{LT}\sqrt{\frac{\sigma_{yc}}{355}}$ is equal to 45 approximately). The margin between the points and the BS5400 curve increases as the $\lambda_{LT}\sqrt{\frac{\sigma_{yc}}{355}}$ value increases. Therefore, lateral buckling of the compression flange of an I-section girder under U-frame support is not described accurately by a Perry-type formula.

Based on the results from ABAQUS, an empirical curve, modifying the basic limiting stress curve is generated as shown in Figure 7.2. Restating the Perry-Robertson inspired formula:

$(M_{cr}-M_b)(M_p-M_b) = \eta(M_{cr}M_b)$, which can be expressed as:

$$\frac{\sigma_{li}}{\sigma_{yc}} = 0.5[1+(1+\eta)\frac{5700}{\beta^2}-\sqrt{\{1+(1+\eta)\frac{5700}{\beta}\}^2-\frac{22800}{\beta^2}}]$$, as in BS5400.

A correction factor of 0.9 is suggested to increase the existing $\frac{\sigma_{li}}{\sigma_{yc}}$ value to $(\frac{\sigma_{li}}{\sigma_{yc}})_{(1)}$ by expression (7.1)

$$(\frac{\sigma_{li}}{\sigma_{yc}})_{(1)} = 1-[1-(\frac{\sigma_{li}}{\sigma_{yc}})] \times 0.9, \quad . \quad . \quad . \quad . \quad . \quad . \quad . \quad . \quad . \quad . \quad (7.1)$$

when $\lambda_{LT}\sqrt{\frac{\sigma_{yc}}{355}} < 80$;

The value of $(\frac{\sigma_{li}}{\sigma_{yc}})_{(1)}$ will be further increased to $(\frac{\sigma_{li}}{\sigma_{yc}})_{(2)}$ by a second factor of 0.7 as in expression (7.2)

$$(\frac{\sigma_{li}}{\sigma_{yc}})_{(2)} = 0.658-[0.658-(\frac{\sigma_{li}}{\sigma_{yc}})_{(1)}] \times 0.7, \quad . \quad . \quad . \quad . \quad . \quad . \quad . \quad . \quad (7.2)$$

when $\lambda_{LT}\sqrt{\frac{\sigma_{yc}}{355}} > 80$.

Parameter η, being different from the η in the λ_{LT} expression, is assumed to remain as 0.005 (β-45) (which was found from test data for lateral buckling of beams). $\lambda_{LT}\sqrt{\frac{\sigma_{yc}}{355}}$ is still used for β in the Perry formula. k_4 is assumed to be the same for monosymmetrical I-section girders and the factor for the variation of bending moment distribution, η (in λ_{LT} expression), will remain as 1.0 for the case of uniform bending. However, λ_{LT}, under the new definition will be subject to modification for non-uniform bending.

Employing the alterations suggested above, the remainder of the design procedure should follow that specified in the present Code. The proposed modification has been tested by re-analysing all the girders studied previously, amongst which were Deck Form 1 (continuous U-frame bracing, with compression flange larger than tension

flange), Welding Institute Model (discrete U-frames action, with compression flange smaller than tension flange) and Leeds Test 1 (doubly symmetrical section), and the details are presented in the following section.

(a) Deck Form 1

l_e = 10.18m, as shown in Appendix IIA

r_y (compression flange plus 15% web) = 0.132m

$\frac{l_e}{r_y} = 77.12$

$\lambda_F = \frac{l_e}{r_y} x \frac{t_w}{d} = 77.12 x \frac{20}{1080} = 1.43,$

with i = 0.703, ν = 0.8664 from Table 9, BS5400: Part 3

λ_{LT} = 77.12 x 0.8664 x 1.0 x 1.0 = 66.82 compared with 83.37 according to BS5400.

If $\frac{t_f}{D}$ is used, λ_F = 2.347 and ν = 0.842,

λ_{LT} = 64.896, which differs little from 66.82 obtained above.

If the web section is not included in the calculation of r_y, then

r_y (for compression flange only) = 0.144 and

$\frac{l_e}{r_y} = 70.69$, $\lambda_F = \frac{l_e}{r_y} x \frac{20}{1080} = 1.309$, ν = 0.8693 and

$\lambda_{LT} = \frac{l_e}{r_y} x\ 0.8693 = 61.45$

Therefore, neglecting the contribution from the web will reduce the value of λ_{LT} and consequently, increase the ultimate moment capacity of the girder.

The changes in value of λ_{LT}, due to the different definitions, together with the corresponding $\frac{\sigma_{li}}{\sigma_{yc}}$, can be seen in Table 7.1.

Table 7.1 Effect of parameter changes on the limiting stress of Deck Form 1

DECK FORM 1		r_y (m)	λ_{LT}	$\frac{\sigma_{li}}{\sigma_{yc}}$
Using full section (BS5400)	$\frac{t_f}{D}$	0.0997	83.37	0.59
Compression flange with 15% web	$\frac{t_w}{d}$	0.132	66.82	0.802
	$\frac{t_f}{D}$	ditto	64.90	0.820
Compression flange only	$\frac{t_w}{d}$	0.144	61.45	0.860
ABAQUS Result			51.00	0.945

The proposed modifications were tried for other I-section girders. If the dimensions of the tension and compression flanges for Deck Form 1 are kept constant, but the $\frac{t_w}{d}$ ratio is varied, the revised values of critical moment capacity for a set of girders may be compared with the ultimate moment capacities obtained from finite element analysis. The difference between modified λ_{LT} and λ_{LT} according to BS5400 can be seen clearly in Table 7.2.

For the four girders in Table 7.2, the thickness of the concrete slab and the distance between girders used in the calculation of δ were 220mm and 3250mm respectively. However, minor changes in these values will not affect the δ and l_e values significantly. The general presumption is that the concrete deck provides rigid torsional restraint to the top (tension) flange. It is noted that in Weston's finite element modelling, in which the concrete slab was converted into equivalent steel units and combined the with top flange of the girders, he concluded that varying the size of the top flange (meaning top flange and concrete slab), or in other words, varying the torsional rigidity of the section, had negligible effect on the ultimate load capacity of the girders.

Table 7.2 Comparison of proposed bending resistances with BS5400 design values and ABAQUS results for Group C1 under uniform bending moment

JOB	d (mm)	l_e (m)	λ_{LT} modified	λ_{LT} BS5400	$\frac{\sigma_{li}}{\sigma_{yc}}$ BS5400	$\frac{\sigma_{li}}{\sigma_{yc}}$ modified	M_D BS5400 ($x10^6$Nm)	M_D modified ($x10^6$Nm)	M_{ABQ} ABAQUS ($x10^6$Nm)
C1A[1]	980	9.45	61.25	75.91	0.790	0.856	5.64	6.11	6.61
C1B[2]	1080	10.18	66.82	83.37	0.590	0.802	4.22	6.20	7.34
C1C	1365	12.02	80.32	103.71	0.42	0.658	4.28	6.70	9.25
C1D	1715	14.40	98.76	131.15	0.2750	0.520	4.59	8.69	10.62

[1] Apart from C1A, which is a compact section, all sections are non-compact according to BS5400.

[2] C1B is Deck Form 1.

Only two parallel girders were assumed in the evaluation of δ and the coefficient u for the number of girders used was taken as 0.5 rather than 0.3. Thus, a higher δ resulted and the moment capacity was lower than for a greater number of girders. In the finite element modelling of continuous U-frames, because of the boundary conditions imposed on the top flange, the modelling is more relevant to those cases where three or more girders are in use. As a result, moment capacities of the girders estimated by the proposed modification should be even closer to those obtained from the finite element analysis.

The modified bending resistances of the girders are obtained by multiplying the limiting stress and the elastic section modulus with respect to the extreme compression fibre without taking account of $\frac{D}{2y_t}$. In cases where the size of the compression flange is greater than that of the tension flange, $\frac{D}{2y_t}$ is always less than 1.0. The actual bending moment resistance should in fact be reduced according to BS5400.

(b) Leeds Test 1

Considering 15% web plus the compression flange, $r_y = 3.704$mm

$\frac{l_e}{r_y} = 92.81$ and $\lambda_F = \frac{l_e}{r_y} \times \frac{t_w}{d} = 106.4 \times \frac{1}{70} = 1.326$

$\therefore \upsilon = 0.978$ and

$\lambda_{LT} = 81.69$ using $k_4 = 0.9$ for double symmetrical section

$\lambda_{LT}\sqrt{\frac{\sigma_{yc}}{355}} = 51.67$, using $\sigma_{yc} = 142.73 Nmm^{-2}$

$\frac{\sigma_{li}}{\sigma_{yc}} = 0.99$

If $k_4 = 0.8$ is used, $\lambda_{LT} = 72.61$ and $\lambda_{LT}\sqrt{\frac{\sigma_{yc}}{355}} = 45.92$

therefore $\frac{\sigma_{li}}{\sigma_{yc}} = 0.99$

A second group of I-section girders with equal flange size of 375x35mm was analysed for further examination of the suitability of this proposed design. Taking $k_4 = 0.9$, the proposed moment capacities of girders are relatively low in comparison with the ABAQUS results. An arbitrary modification is thus proposed for the coefficient k_4 in the λ_{LT} expression for cases where such equal flange sections were used. If the k_4 of 0.9 in the present Code for an I-section symmetrical about both axes is reduced to 0.8, less conservative moment capacities of girders will be obtained. Table 7.3 shows the difference in the proposed values using a revised k_4 value.

When using the proposed modification of the Code, even with k_4 taken as 0.9, there was a significant increase in the $\frac{\sigma_{li}}{\sigma_{yc}}$ value when λ_{LT} was high. The moment capacity of a larger section (C2A) became greater than a smaller section (C2C) reversing the order of magnitude obtained by design according to BS5400, which did not make sense, as shown in the sixth column.

Although insignificant improvement was obtained for girders with higher λ_{LT} value when k_4 was changed from 0.9 to 0.8, a moderate increase of bending resistance is achieved when λ_{LT} is low.

Table 7.3* Comparison of proposed bending resistances with BS5400 design values and ABAQUS results for Group C2 under uniform bending moment

	Design to BS5400				
	d (mm)	l_e (m)	λ_{LT}	$\frac{\sigma_{li}}{\sigma_{yc}}$	M_D (x10^6Nm)
C2A	1715	11.60	119.57	0.325	3.68
C2B	1365	9.69	93.77	0.49	4.14
C2C	1080	8.03	75.17	0.68	4.29

*For doubly symmetrical girders, $\frac{D}{2y_t}$ is equal to 1.0

Table 7.3 cont'd

	Design to Proposed Modification of BS5400						ABAQUS
	k4= 0.9			k4=0.8			
	λ_{LT}	$\frac{\sigma_{li}}{\sigma_{yc}}$	M_D (x10^6Nm)	λ_{LT}	$\frac{\sigma_{li}}{\sigma_{yc}}$	M_D (x10^6Nm)	M_D (x10^6Nm)
C2A	110.69	0.50	5.67	98.39	0.51	5.78	8.64
C2B	89.64	0.59	4.98	79.68	0.66	5.58	7.49
C2C	73.85	0.71	4.49	65.64	0.82	5.18	6.18

(c) Welding Institute Model

$l_e = 1.443$m

when the compression flange and 15% of web are used,

$r_y = 0.0136$m and $\frac{l_e}{r_y} = \frac{1.443}{0.01361} = 106.05$

$\lambda_F = 1.697$

With i = 0.296 and υ = 1.229

$\lambda_{LT} = 1.229 \times 106.05 = 130.38$

and $\lambda_{LT}\sqrt{\frac{\sigma_{yc}}{355}} = 146.79$ for $\sigma_{yc} = 450 N/mm^2$

$\frac{\sigma_{li}}{\sigma_{yc}} = 0.53$

If compression flange only is used, r_y will be 0.01732m

and the resultant λ_{LT} will be 104.48,

$\lambda_{LT}\sqrt{\frac{\sigma_{yc}}{355}} = 117.63$ and $\frac{\sigma_{li}}{\sigma_{yc}} = 0.57$

From the above calculation, it is found that for sections with smaller compression flange than tension flange, by neglecting the web section, a less conservative ultimate moment capacity will be obtained. Another group of girders with compression flange of 250x35mm but tension flange of 375x35mm were examined using ABAQUS, the ultimate moment capacities reached in the finite element analysis were compared with the proposed values, with and without 15% of web taken into consideration in Table 7.4.

$\frac{D}{2y_t}$ was not taken into consideration in the evaluation. For girders with compression flange smaller than tension flange, $\frac{D}{2y_t}$ is greater than 1.0. Therefore, higher bending resistances than those tabulated should be obtained.

In general, through this proposed modification for various types of I-section, a substantial increase in $\frac{\sigma_{li}}{\sigma_{yc}}$ ratio will be achieved by (a) correction of $\frac{\sigma_{li}}{\sigma_{yc}}$, especially when λ_{LT} is high; and (b) reduction of the slenderness ratio λ_{LT}, particularly for sections with compression flange larger than or equal to the tension flange. It can be seen that a safety margin is still maintained because the proposed $\frac{\sigma_{li}}{\sigma_{yc}}$ values are, with rare exceptions, lower than those obtained from the finite element analyses. Thus, together with the safety factors used in the current Code, the resultant safety margin will be sufficient for practical design.

Table 7.4 Comparison of proposed bending resistances with BS5400 design values and ABAQUS results for Group C3 under uniform bending moment

	Proposed Moment Capacity ($x10^6$Nm)		ABAQUS Result ($x10^6$Nm)
	compression flange plus 15% web	compression flange only	
C3A	2.92	3.08	4.43
C3B	2.55	2.85	4.42
C3C	1.67	2.37	4.50

After testing the proposed modification on continuously braced girders, its applicability to discrete U-frames was also considered. The moment capacities of girders analysed in Chapter 6 were calculated using the new proposal and the results are compared with BS5400 and ABAQUS values in Tables 7.5, 7.6 and 7.7.

In these tables, the bending resistances in column 5 were obtained from multiplication of the limiting stress $\frac{\sigma_{li}}{\sigma_{yc}}$ and elastic section modulus of the cross-section with respect to the extreme compression fibre. According to BS5400, the bending resistance of these non-compact girders (marked with *) should only be taken as $\sigma_{yt}Z_{xt}$ (ie, $6.57x10^6$Nm) because the value of $\sigma_{yc}Z_{xc}\frac{D}{2y_t}$ is higher than $6.57x10^6$Nm.

From the stress output from ABAQUS analysis, in which the von Mises yield criterion was used as a measure of plasticity, it was seen that the stress blocks for these girders were neither perfectly elastic nor plastic. Approximately, the central third of the girder web remained elastic while the remainder yielded. (A more accurate proportion could be obtained if a more refined mesh was used in the web region.) The question therefore, arises as to what is the correct section modulus for this type of section. In the classification of sections in BS5400, it is clear that there is no place for such semi-compact sections.

Table 7.5 Comparison of proposed bending resistances with BS5400 design values and ABAQUS results for Group D31 under uniform bending moment

JOB	l_e (m)	λ_{LT}	$\frac{\sigma_{li}}{\sigma_{yc}}$	M_D Proposed (x10^6Nm)	M_D BS5400 (x10^6Nm)	M_D ABAQUS (x10^6Nm)
D31/1	15.62	99.76	0.55	4.24	2.29	5.95
D31/2	7.90	52.59	0.95	7.32*	6.07	7.48
D31/3	5.36	35.52	1.0	7.74*	7.08	7.55
D31/4	19.64	122.72	0.465	3.60	1.72	4.75
D31/5	9.94	66.12	0.81	6.27	4.33	7.31
D31/6	6.74	44.55	1.0	7.74*	6.30	7.45
D31/7	23.35	142.79	0.42	3.21	1.36	4.27
D31/8	11.85	76.75	0.69	5.37	3.43	7.03
D31/9	8.01	52.78	0.94	7.25*	5.51	7.38

Table 7.6 Comparison of proposed bending resistances with BS5400 design values and ABAQUS results for Group D41 under uniform bending moment

JOB	l_e (m)	λ_{LT}	$\frac{\sigma_{li}}{\sigma_{yc}}$	M_D Proposed (x10^{6}Nm)	M_D BS5400 (x10^{6}Nm)	M_D ABAQUS (x10^{6}Nm)
D41/1	17.64	116.22	0.48	5.04	2.25	6.83
D41/2	8.19	55.46	0.91	9.56	6.07	9.97
D41/3	6.04	40.98	1.0	10.51	8.72	10.32
D41/4	22.18	143.44	0.42	4.41	1.67	5.55
D41/5	11.21	75.32	0.71	7.46	4.41	9.69
D41/6	7.59	51.44	0.95	9.98	7.35	10.01
D41/7	26.38	167.55	0.38	3.99	1.27	5.12
D41/8	13.33	88.99	0.58	6.10	3.48	8.82
D41/9	9.03	61.07	0.86	9.04	5.97	9.89

Table 7.7 Comparison of proposed bending resistances with BS5400 design values and ABAQUS results for Group D61 under uniform bending moment

JOB	l_e (m)	λ_{LT}	$\frac{\sigma_{li}}{\sigma_{yc}}$	M_D Proposed (x10^{6}Nm)	M_D BS5400 (x10^{6}Nm)	M_D ABAQUS (x10^{6}Nm)
D61/1	21.42	149.00	0.406	7.17	2.14	8.33
D61/2	10.80	76.61	0.69	12.26	7.82	15.91
D61/3	7.37	52.41	0.95	16.71	11.20	16.57
D61/4	26.93	184.90	0.36	6.39	1.48	7.47
D61/5	13.58	96.05	0.56	9.95	3.54	13.70
D61/6	9.26	65.78	0.81	14.33	8.15	16.18
D61/7	32.03	216.72	0.34	5.95	1.15	7.05
D61/8	16.15	113.61	0.49	8.73	3.29	10.55
D61/9	11.02	78.16	0.68	11.94	6.09	15.60

7.3 STRUTS ON ELASTIC FOUNDATION

In 1985, Svensson produced a series of curves for effective length factor $\frac{l_e}{l}$ versus spring stiffness βl based on eigenvalue analysis of struts supported laterally by elastic springs. Various loading cases (or more precisely, various forms of axial loading) were investigated.

Similarly, in the present work, elastic eigenvalue analysis using ABAQUS was carried out for a set of struts, braced by translational springs of varied stiffness. However, only four types of loading were considered. The effective length factor of the

struts (for the case of uniform axial compressive force) together with the spring stiffness are plotted in Figure 7.3.

It can be seen that the two analyses are in reasonably close agreement.

Re-arranging the l_e expression in Clause 9.6.5 or Clause 9.6.6 ,

$l_e = 2.5k_3(EI_c\delta l_u)^{0.25}$ for the discrete U-frames or

$l_e = 2.5k_3(EI_c\delta)^{0.25}$ for the continuous U-frames,

l_e can be written as $2.5k_3(\frac{EI_c}{k})^{0.25}$, where $\frac{1}{k} = \delta l_u$ or discrete U-frames or $\frac{1}{k} = \delta$ for continuous U-frames.

$$\frac{l_e}{l} = \frac{2.5k_3}{l}(\frac{EI_c}{k})^{0.25}$$

Let $(\frac{EI_c}{k})^{0.25} = \frac{1}{\beta}$

then $\frac{l_e}{l} = \frac{2.5k_3}{\beta l}$

Assuming the compression flange is restrained against rotation, ie, k_3=1.0

$$\frac{l_e}{l} = \frac{2.5}{\beta l} \quad . \quad . \quad . \quad . \quad . \quad . \quad . \quad . \quad . \quad . \quad . \quad . \quad (7.3)$$

where βl is a relative U-frame stiffness (relative, that is, to the lateral bending stiffness of the compression flange).

Plotting $\frac{l_e}{l}$ versus βl in the same graph as shown in Figure 7.3, it is interesting to note the relationship between the curve from BS5400 which is based on uniform bending, namely curve **a** (ie, expression (7.3)), and those obtained from the eigenvalue analysis of struts under uniform bending, namely curves **b1** and **b2**.

The margin between curve **a** and curve **b1** or **b2** is, in general, uniform but the gap is reduced when the relative spring stiffness βl becomes greater. However, it is incorrect to think that the $\frac{l_e}{l}$ value from BS5400 is in relatively constant ratio to the $\frac{l_e}{l}$ value from eigen analysis. As the stiffness of the spring decreases, BS5400 seems to suggest that the effective length will increase (ie, the ultimate moment capacity will decrease) rather rapidly. Consequently, a more conservative prediction of l_e values and ultimate load capacities is generated. Nevertheless, there is still a reasonable correlation between curve **b1** or **b2** and curve **a** obtained from the currently used l_e expression in

BS5400. This supports the appropriateness of using the effective length concept in relation to U-frame bracing.

7.4 STUDY OF UDL CASE

From Figure 9(b) of the Code, it is indicated that the factor for non-uniform moment due to a double span under UDL should be taken as 0.668. If this value is used, the standard curve $\frac{2.5}{\beta l}$ should be multiplied by 0.668 to produce curve **c**, which can be expressed as $\frac{1.67}{\beta l}$, in Figure 7.4.

From the eigenvalue analysis of a strut with identical moment gradient, ie, the case of double span under UDL , it can be seen, from the curves **d1** and **d2** plotted in Figure 7.4, that there is a drastic decrease in the $\frac{l_e}{l}$ value in comparison with the case of uniform bending, especially when the relative spring stiffness βl decreases. Thus, the beneficial effect of non-uniform moment is obvious.

On closer examination of the curves obtained for various moment gradients, it is found that they do not lie at a constant distance below the curve **c** and a simple mathematical formulation can be written to approximate them as:

$$\frac{l_e}{l} = \frac{2.5}{(\beta l + 3)} - 0.03 \quad . \quad . \quad . \quad . \quad . \quad . \quad . \quad . \quad . \quad . \quad . \quad . \quad (7.4)$$

with some allowance for safety margin. This expression is represented as curve **d** in Figure 7.4. The value of $\frac{l_e}{l}$ from curve **c** is always greater than those from eigenvalue analyses and curve **d**, particularly when βl is small. This indicates that the suggested values of l_e from BS5400 are conservative or over-conservative in extreme cases.

Therefore, for girders of double span under UDL, a reduction of the effective length according to relative spring stiffness βl, ie, $EI_c\delta l_u$ or $EI_c\delta$ for discrete or continuous U-frames respectively will firstly be calculated by equation (7.4) or from Figure 7.4. This effective length will then be employed together with the correction for r_y and $\frac{t_w}{d}$ as suggested in the uniform bending moment situation to give a value for λ_{LT}. Using the modified curve for BS5400 or equations (7.1) and (7.2), the limiting stress $\frac{\sigma_{li}}{\sigma_{yc}}$ may be obtained.

Bending resistance of girders in Group C1 is calculated and tabulated in Table 7.8 according to the above suggestions. It can be seen that the proposed values are much higher than the current design values and very close to results from ABAQUS.

Table 7.8 Comparison of proposed bending resistances with BS5400 design values and ABAQUSresults for Group C1 under UDL

JOB	l_e (m)	λ_{LT} BS5400	M_D BS5400 ($x10^6$Nm)	βl	l_e Reduced (m)	λ_{LT} Modified	M_D* Proposed ($x10^6$Nm)	M_D ABAQUS ($x10^6$Nm)
C1A	9.45	53.08	6.64	6.614	5.75	37.79	7.14	7.34
C1B	10.18	55.68	6.96	6.139	6.09	40.51	8.05	8.59
C1C	12.02	72.61	7.34	5.20	6.87	43.41	10.09	11.4
C1D	14.40	91.99	8.52	4.34	7.76	53.76	15.82	15.59

*Not including effect of $\frac{D}{2y_t}$

Table 7.9 Comparison of bending resistances* with different section factors

	Not including effect of $\frac{D}{2y_t}$	Including effect of $\frac{D}{2y_t}$	Using $Z_{xt}\,\sigma_{yt}$	ABAQUS
C1B	8.05	7.45	6.57	8.59
C1C	10.09	9.39	8.80	11.4
C1D	15.82	12.80	10.29	15.59

* Unit: $x10^6$Nm

The effect of $\frac{D}{2y_t}$ is shown in Table 7.9. The bending resistances are lowered. However, if complying with the clause in BS5400 by allowing for non-compact sections,

the ultimate bending resistances should all be no greater than $Z_{xt}\sigma_{yt}$, that is, the values in column 3. Therefore, the question raised in the case of uniform bending arises again.

For sections with equal compression and tension flange, the corresponding proposed values for moment of resistance were calculated. The difference according to k_4 value and corresponding ABAQUS results are compared in Table 7.10.

Table 7.10 Comparison of proposed bending resistances with BS5400 design values and ABAQUS results for Group C2 under UDL

	Proposed Bending Resistance M_D ($x10^6$Nm)		ABAQUS M_D ($x10^6$Nm)
	k_4=0.9	k_4=0.8	
DF1J	9.00	10.95	13.07
DF1M	8.28	8.45	10.25
DF1N	6.32	6.32	7.61

The bending resistance of girders braced by discrete U-frames studied in Chapter 6 (with double span under UDL) were evaluated by the proposed design procedure with modification of effective length at the initial stage of design. The results are compared with those from BS5400 and ABAQUS in Tables 7.11, 7.12 and 7.13.

Table 7.11 Comparison of proposed bending resistances with BS5400 design values and ABAQUS results for Group D31 under UDL

JOB	l_e (m)	λ_{LT}	$\frac{\sigma_{li}}{\sigma_{yc}}$	M_D Proposed (x10^{6}Nm)	M_D BS5400 (x10^{6}Nm)	M_D ABAQUS (x10^{6}Nm)
D31/1	8.18	53.87	0.93	7.19	4.89	8.43
D31/2	5.02	33.29	1.0	7.74	7.74	8.58
D31/3	3.51	23.33	1.0	7.74	7.74	8.60
D31/4	9.36	61.34	0.86	6.62	3.79	8.19
D31/5	5.98	39.60	1.0	7.74	7.12	8.11
D31/6	4.34	28.80	1.0	7.74	7.74	8.16
D31/7	10.26	67.00	0.80	6.19	2.90	7.70
D31/8	6.79	44.91	1.0	7.74	6.38	8.16
D31/9	5.04	33.42	1.0	7.74	7.72	8.12

Table 7.12 Comparison of proposed bending resistances with BS5400 design values and ABAQUS results for Group D41 under UDL

JOB	l_e (m)	λ_{LT}	$\frac{\sigma_{li}}{\sigma_{yc}}$	M_D Proposed (x10⁶Nm)	M_D BS5400 (x10⁶Nm)	M_D ABAQUS (x10⁶Nm)
D41/1	8.80	59.52	0.87	9.14	4.94	11.73
D41/2	5.13	34.85	1.0	10.52	10.52	12.09
D41/3	3.93	26.73	1.0	10.52	10.52	12.11
D41/4	9.99	67.37	0.80	8.38	3.73	11.55
D41/5	6.54	44.35	1.0	10.52	8.20	10.91
D41/6	4.82	32.75	1.0	10.52	10.46	11.74
D41/7	10.89	69.63	0.78	8.14	2.94	10.33
D41/8	7.88	50.0	0.95	9.98	6.94	11.45
D41/9	5.55	37.68	1.0	10.52	9.68	11.31

Table 7.13 Comparison of proposed bending resistances with BS5400 design values and ABAQUS results for Group D61 under UDL

JOB	l_e (m)	λ_{LT}	$\frac{\sigma_{li}}{\sigma_{yc}}$	M_D Proposed (x10^6Nm)	M_D BS5400 (x10^6Nm)	M_D ABAQUS (x10^6Nm)
D61/1	9.81	69.64	0.78	13.69	4.86	17.71
D61/2	6.36	45.21	1.0	17.66	14.66	17.82
D61/3	4.69	33.43	1.0	17.66	16.78	17.87
D61/4	11.00	71.02	0.67	11.86	3.44	14.80
D61/5	7.47	53.13	0.93	16.47	9.37	16.91
D61/6	5.66	40.31	1.0	17.66*	14.66	17.25
D61/7	11.87	84.13	0.63	11.18	2.73	12.66
D61/8	8.35	59.35	0.87	15.44*	7.24	14.24
D61/9	6.46	45.92	0.99	17.49*	12.36	16.55

Generally speaking, the new proposal gives values very close to those obtained from finite element analysis, barring three cases (marked with *) in Table 7.13. In all calculations of bending resistance, $\frac{D}{2y_t}$ was not taken into account for ease of comparison. Repeatedly, the classification of sections in BS5400 under-valued the moment capacity of girders. A more effective, or rather, an improved section modulus should be employed for true representation of bending capacity.

7.5 SUMMARY

Following experimentation on various geometric properties of sections, a modified design proposal, based on the present BS5400 principles for design of I-section girders under U-frame support has been suggested and is summarised below.

In dealing with lateral stability of a compression flange braced by U-frames, the general design procedure in the current Code should still be followed. However, some alterations to the current design method are proposed:

(1) The Perry-Robertson curve used in Figure 10 of BS5400 should be modified according to expressions (7.1) and (7.2).

(2) The slenderness parameter required for calculation of the limiting compressive stress should be redefined as:

$$\lambda_{LT} = \frac{l_e}{r_y} k_4 \eta \upsilon ,$$

where l_e is defined as in the Clause 9.6.5 or 9.6.6;

r_y should be taken as the radius of gyration of the whole compression flange plus 15% of the web about the Y-Y axis defined in Figure 1 of BS5400.

For cases with compression flange smaller than the tension flange, r_y should be based on the compression flange, only, to allow for increased compression in the web.

(3) The slenderness factor, υ, should be based on:

$$\lambda_F = (\frac{l_e}{r_y})(\frac{t_w}{d})$$

where t_w and d are the thickness and depth of the web respectively. The use of parameter i and Table 9 in the Code remain the same.

(4) Coefficient 'k_4 for an I-section symmetrical about both axes (with t_f not greater than twice the web thickness)' may be reduced from 0.9 to 0.8. Otherwise, it remains as 1.0.

(5) For two continuous spans under UDL, the coefficient suggested by the Standard has been examined. A reduction of effective length due to the presence of moment variation is proposed in expression (7.4). Coefficients for other loading cases have not been studied and therefore, further comment cannot be made.

Finite element analysis of a wide range of girders was carried out to check the effect of these proposals. The ultimate capacities obtained from ABAQUS proved that

the proposed modifications give a sound prediction of the ultimate moment capacity of a uniform I-section girder.

Problems with the classification of a section and thus the relevant section modulus to use, have not be tackled rigorously. Further investigation is needed for full confirmation of the proposal.

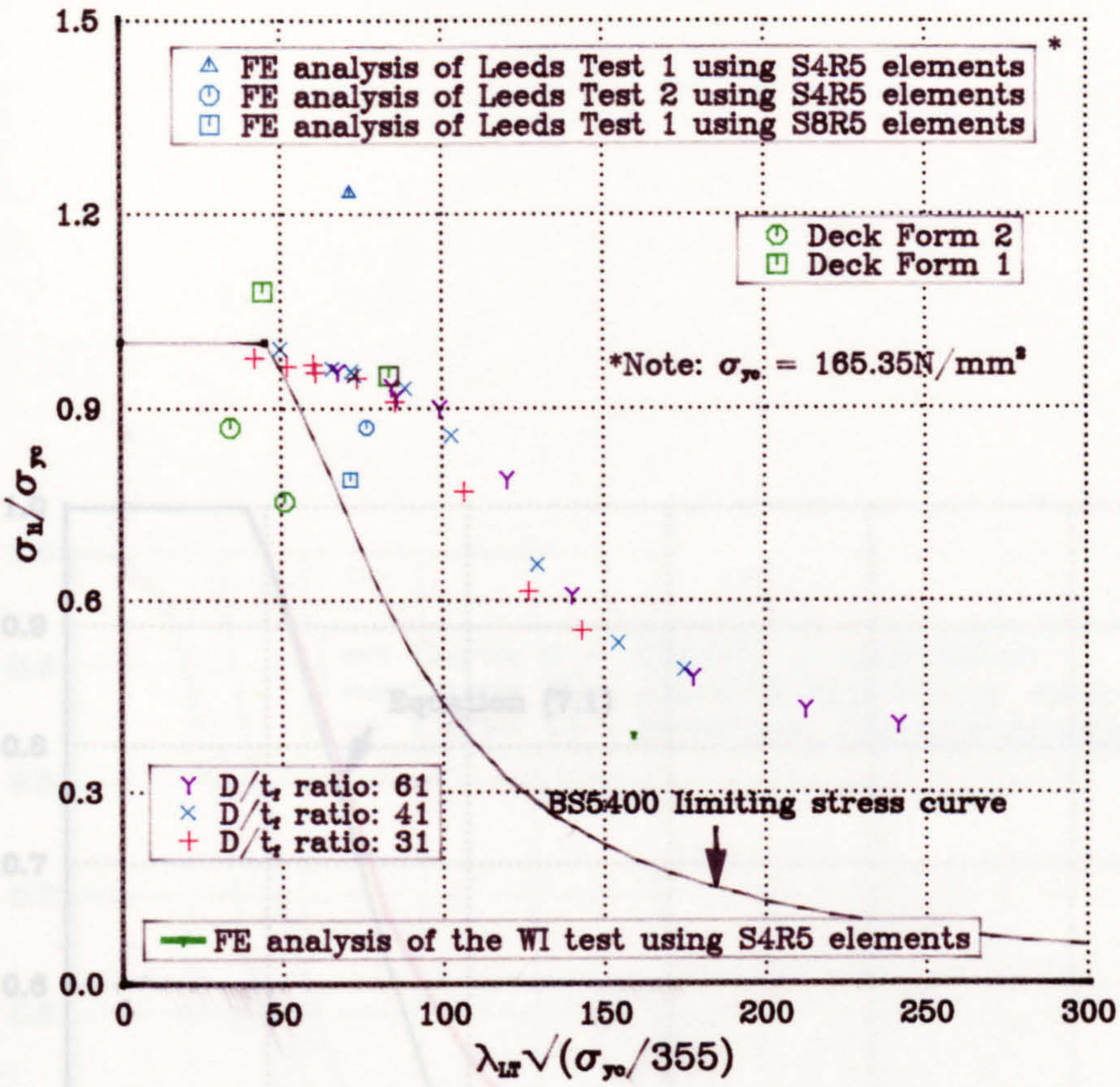

(a) Summary of ABAQUS results

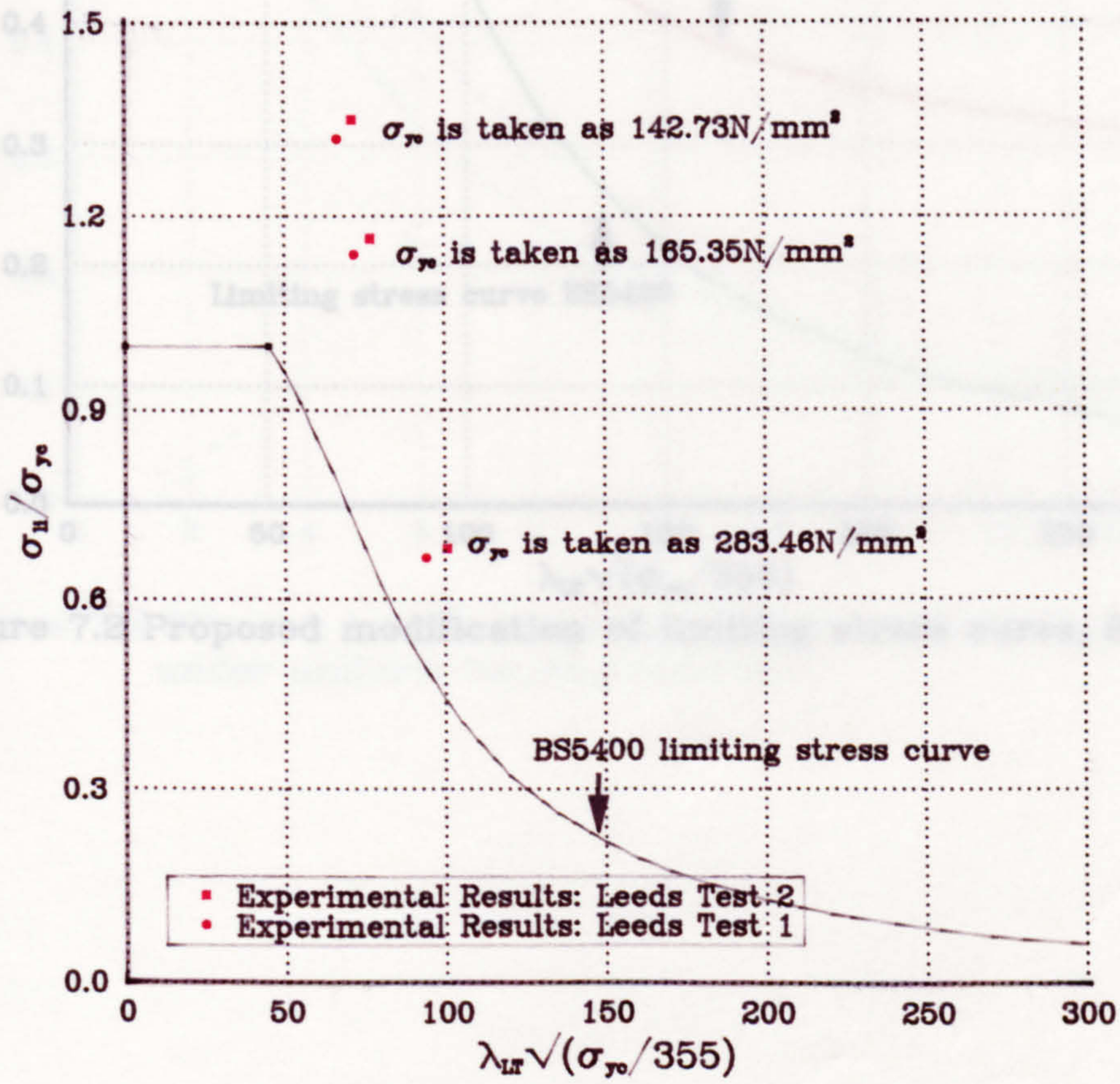

(b) Effect of yield stress

Figure 7.1 Comparison of test and ABAQUS results with design curve

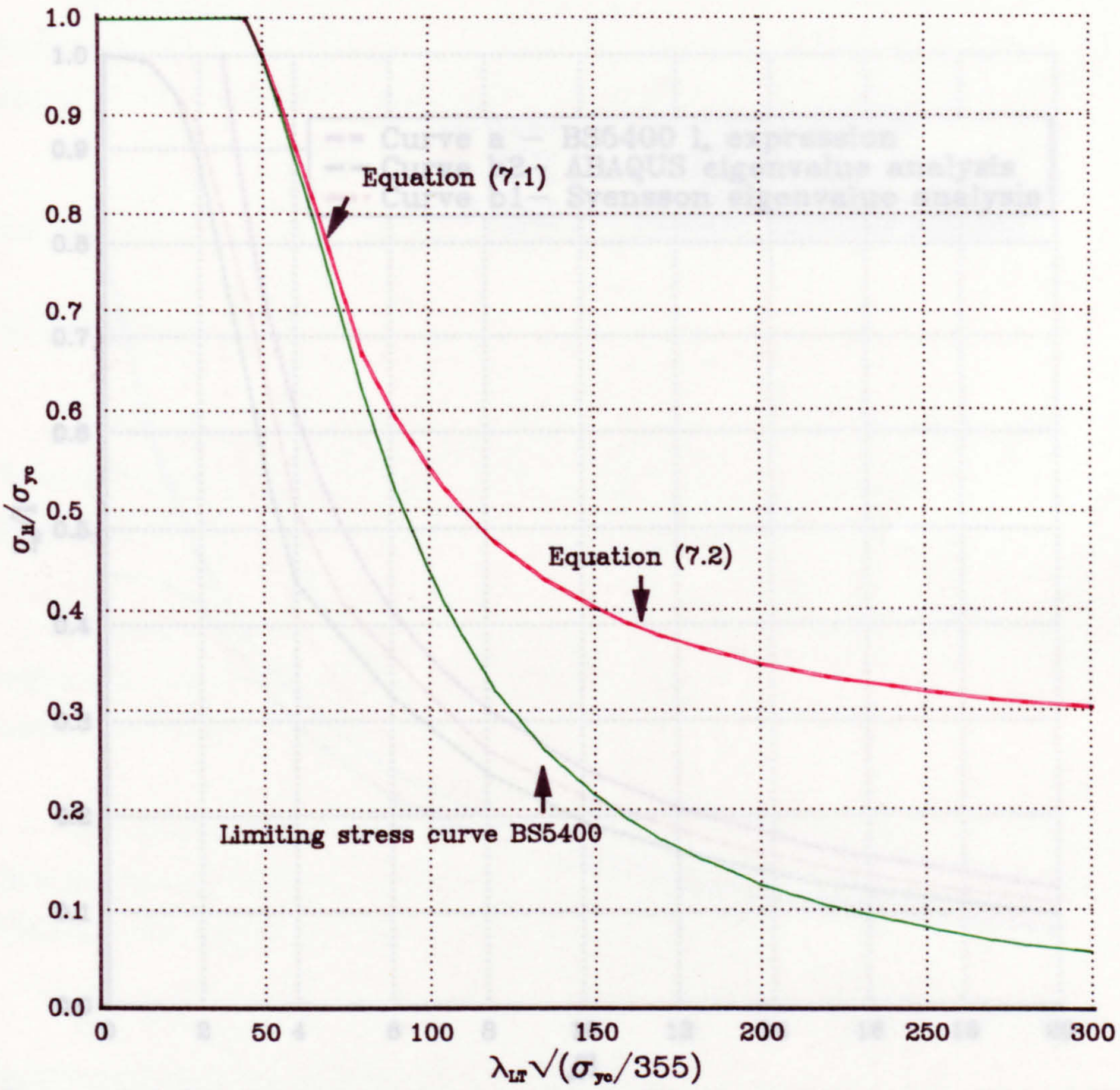

Figure 7.2 Proposed modification of limiting stress curve, BS5400: Part 3

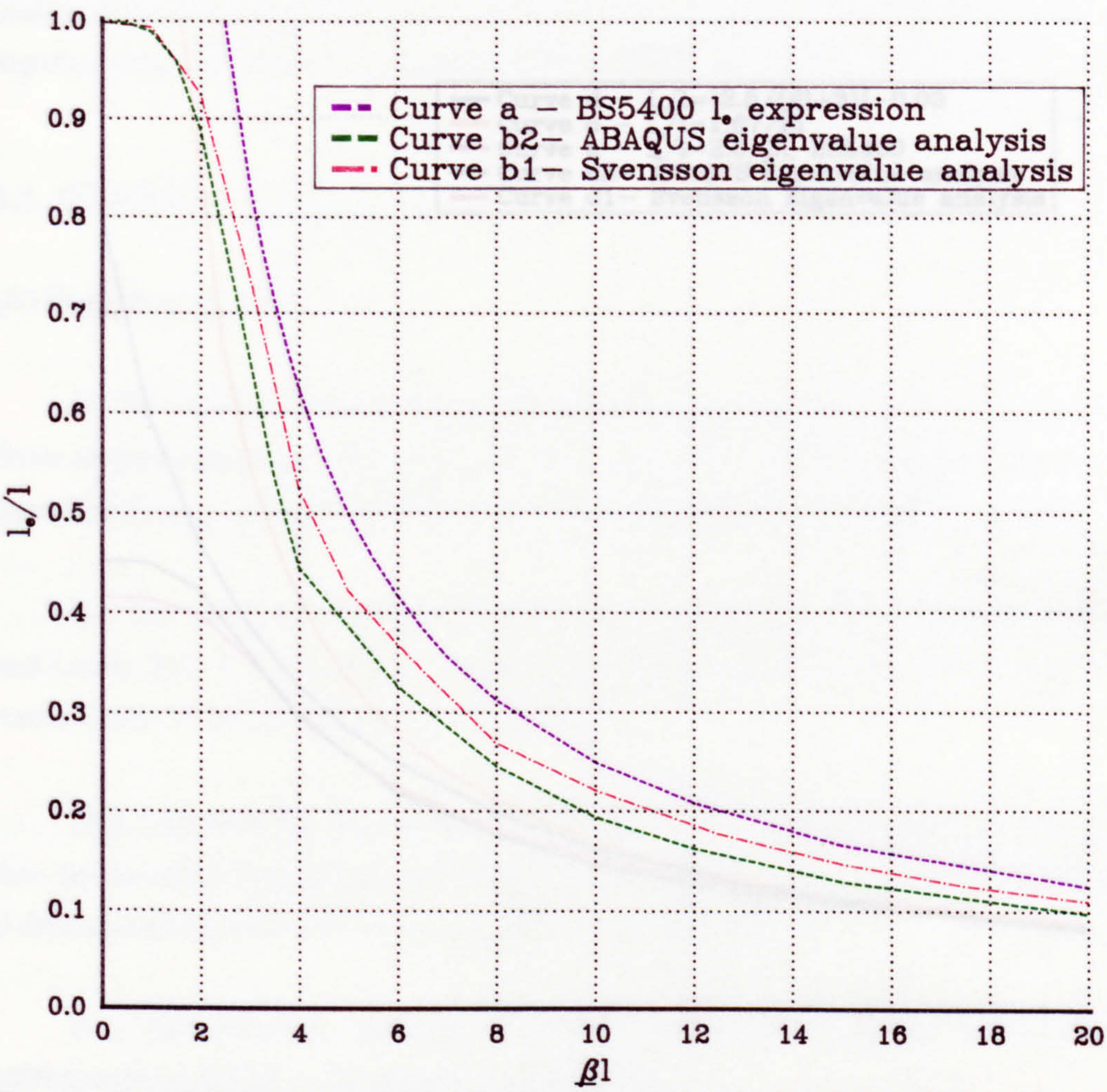

Figure 7.3 Effective length v. spring stiffness relationships for girders under uniform bending moment

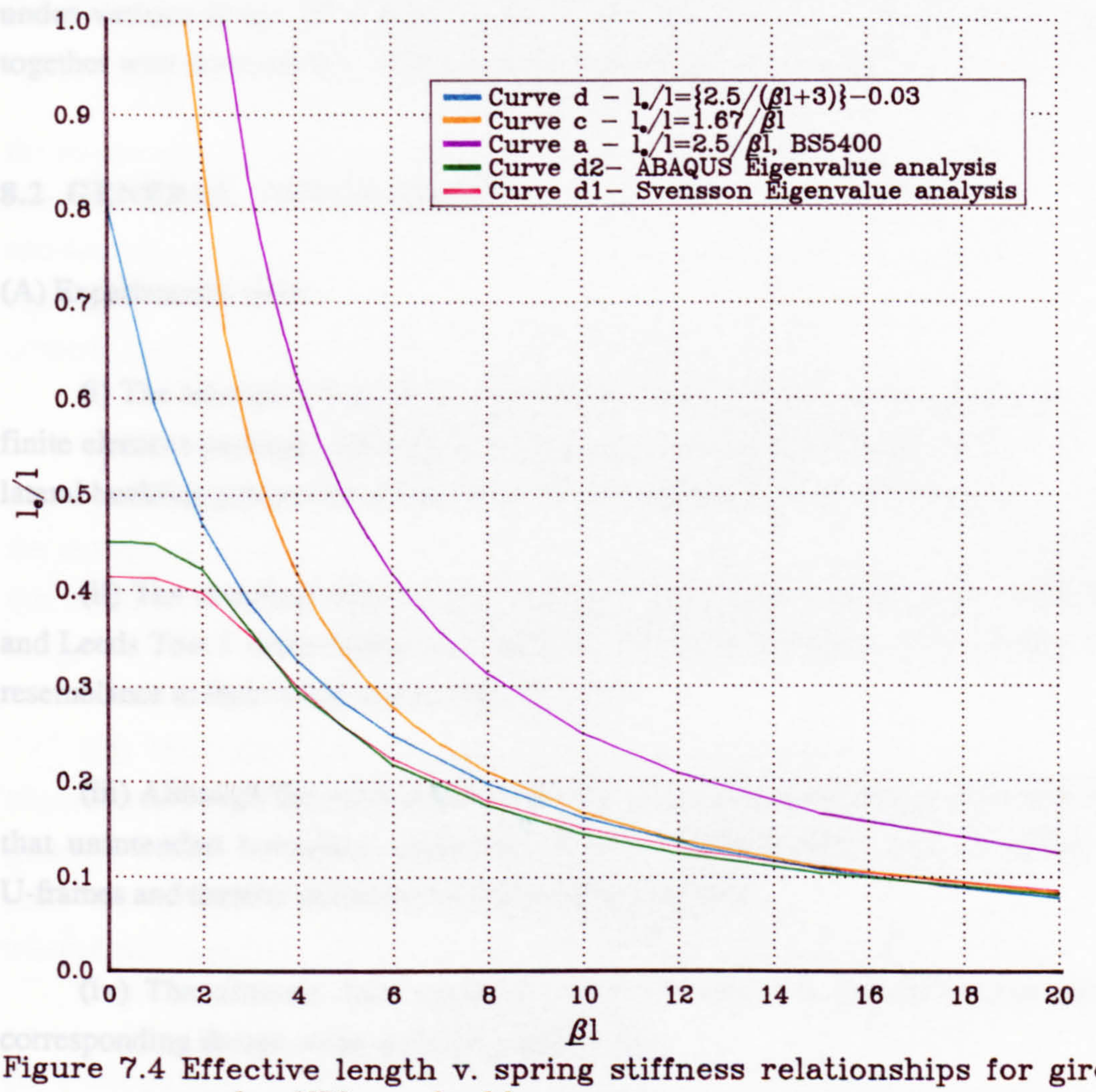

Figure 7.4 Effective length v. spring stiffness relationships for girders under UDL on double span

CHAPTER 8

CONCLUSION

8.1 INTRODUCTION

The general findings of the experimental and analytical investigation of girders under various forms of U-frame bracing are summarised in the following sections together with reservations. Suggestions for further study are also outlined.

8.2 GENERAL CONCLUSIONS

(A) Experimental work

(i) The laboratory tests were valuable not only in validating the performance of the finite element package, ABAQUS, but also in providing a physical visualisation of the lateral buckling process for compression flanges restrained by U-frame action.

(ii) The coupling effect of the U-frames was clearly demonstrated in the WI test and Leeds Test 1 when failure was reached. The buckled shape of the flanges bore no resemblance to their initial lateral imperfections.

(iii) Although the outcome of Leeds Test 2 was less satisfactory, it at least showed that unintended boundary conditions could override natural cross-coupling of the U-frames and thereby influence lateral buckling behaviour.

(iv) The ultimate load capacity in all the tests was approximately twice the corresponding design value according to BS5400.

(B) Finite element idealisation of experimental work.

(i) In the finite element idealisation of laboratory tests, a reasonable correlation between the two sets of results showed that ABAQUS was capable of rendering valid analysis of girders with lateral instability problems.

(ii) From a comparison of models exclusively using first and second order elements, it was found that the former was more cost-effective than the latter.

(iii) Modelling of one-quarter of a doubly symmetrical U-frame structure can save CPU time, but local yielding at points of stress concentration may increase difficulties in obtaining a convergent solution.

(iv) The lateral buckling mode was sensitive to applied boundary conditions. Therefore, accurate prediction of buckling modes for real structures is seldom possible.

(C) Finite element idealisation of typical bridge configurations.

(i) With regard to the modelling of girders braced by different forms of restraints to the tension flange, it was found that in the case of uniform bending moment, the bracing effect of individual types of restraints (torsional or translational) was considered to be satisfactorily dealt with in BS5400. However, when the effects of these restraints were combined, distortion of the girder web occurred and the BS5400 values were more conservative in comparison with ABAQUS results.

(ii) The ultimate bending resistance of girders was very much increased in the presence of non-uniform bending moment. Local distortion of the compression flange in the vicinity of the central support was always more influential than lateral buckling and this hindered the formation of anything less than a single half-wave in the compression flange.

(iii) The effect of torsional restraint was found to be more significant than that of translational restraint in the case of uniform bending. However, this was not so when girders were subjected to variation of bending moment distribution due to UDL. In this case, the effect of torsional restraint was negligible in comparison with that of translational restraint.

(D) Finite element idealisation of girders braced by discrete U-frames.

(i) It is clear that the BS5400 design values for bending resistance of girders are over-conservative, particularly in the case of girders with a high value of slenderness or subject to moment variation. Also, the bending resistance of a girder does not increase (or decrease) monotonically with increase in cross-beam size (or reduction in spacing). Only a small increase was achieved after reaching the optimum beam size and

the effect of spacing was not influential. In the case of moment variation, neither of these two factors were significant.

(ii) Final buckling modes always consisted of an odd-number of half-waves (in most cases, one single half-wave unless the slenderness of the girder was approximately 45 to 55). Therefore, buckled shapes were always symmetrical about mid-span. (However, an anti-symmetrical buckling mode might be achieved with restraints applied to stop the longitudinal floating of the structure at one end instead of at mid-span.)

(iii) Strong bracing generates swift increase in lateral deflection at failure and the excessive early displacement produced by using weaker bracing is thus reduced. The general expression for lateral torsional buckling of bare steel girders (which depends on $\frac{D}{t_f}$ ratio and is characteristically represented by the Perry-Robertson formula) may not be suitable for girders braced by cross members. A modified Perry-type of formula could be used to describe the results obtained from ABAQUS.

(E) Proposed modification of the BS5400 design rules for lateral buckling of I-section girders braced by U-frames.

The above-mentioned results based on analytical and experimental study have led to a proposed modification of the existing design method (see Chapter 7) which is briefly as follows:

(i) Two geometric parameters $\frac{l_e}{r_y}$, (where r_y is the radius of gyration of compression flange plus 15% girder web for I-sections with compression flange larger than tension flange) and $\frac{t_w}{d}$ are introduced in place of $\frac{l_e}{r_y}$ and $\frac{t_f}{D}$ used in BS5400 because they are more relevant to lateral buckling of a girder with U-frame bracing. $\frac{l_e}{r_y}$ and $\frac{t_f}{D}$ are more closely related to lateral buckling of bare steel beams in which no web distortion occurs. Thus, there are corresponding changes in the λ_{LT} and λ_F values.

(ii) A modification of the limiting design stress curve is suggested, introducing two empirical coefficients (see section 7.2) to minimise undue conservatism in the present approach.

(iii) For double span girders braced by U-frames under UDL, a modified effective length may be obtained from a proposed chart for calculating the bending resistance of girders.

(iv) A reduction of the k_4 value is suggested for girders of double symmetry in the calculation of λ_{LT}.

Details of the proposal are stated in section 7.4.5.

8.3 FURTHER WORK

(1) In the proposed modification, it is assumed that the imperfection constant (which was obtained from empirical data for bare steel girders) is applicable to the case of U-frame braced girders. The shape function (which is related to $\frac{l_e}{r_y}$ and $\frac{t_f}{D}$ for bare steel girders) is also assumed to have the same relationship with the newly defined parameters $\frac{l_e}{r_y}$ and $\frac{t_w}{d}$. These assumptions need to be verified.

(2) A wider range of girders with variation of parameters such as section properties and span length (with compact and non-compact sections), material properties (including initial residual stresses, strain hardening effects and initial imperfections), effects of end stiffeners and end constraints should be studied carefully to verify the accuracy of the proposed modification. This could be done (as a parametric study) by modifying finite elements models used.

(3) Further study of other forms of bending moment distribution should be carried out so that additional charts (to Figure 7.4) can be produced for the estimation of effective length under non-uniform moment distribution.

(4) Restraining forces at supports of U-framed girders have not been examined. There are queries about the adequacy of the Code's provision. Therefore, an investigation into this based on finite element analysis should be carried out.

(5) Although combined torsional and translational restraints were used to simulate restraint of the concrete slab on the tension flange, it would be more exact if cracking behaviour of the concrete could be modelled in the study of lateral buckling of the compression flange.

(6) Study was limited to two parallel running girders. Lateral buckling in skew symmetrical girders braced by U-frames or U-frames formed by three or more girders needs to be investigated.

APPENDIX I

A LIST OF A TYPICAL ABAQUS JOB

```
**----------JOB CONTROL CARD----------
//WT1 JOB ,, USER=ELCENRY, PASSWORD=xxxxxx, MSGLEVEL=(2,1),
//TIME=XXX
/*VP2
.....
**----------DATA CARD----------
*HEADING: IDEALISATION OF THE WELDING INSTITUTE TEST
***----------Nodes Generations----------
*NODE
1,0., 0.237, 0.254
2,0., 0.277, 0.254
3,0., 0.317, 0.254
.....
*NSET, GENERATE, NSET=TENS
1,87,1
.....
*NCOPY, CHANGE NUMBER=, OLD SET=NOA, REFLECT=MIRROR,
NEW SET=NOC
2.805,0.,0.,2.805,0.,3.
2.805,4.,0.
.....
***----------Elements Generation----------
*ELEMENT, TYPE=S4R5
1,1,4,5,2
57,102,105,5,2
.....
```

```
*ELEMENT, TYPE=B31
224,142,143
.....
*ELGEN, ELSET=ELTA
1,2,1,1,28,3,2
.....
*ELCOPY, ELEMENT SHIFT=2000, OLD SET=ELTA, SHIFT NODE=2000,
NEW SET = ELTC
.....
***----------Material Properties----------
*MATERIAL, NAME=STEEL
*ELASTIC
2.05E11,0.3
*PLASTIC
3.55E8
.....
***----------Element properties----------
*SHELL SECTION, ELSET=ELTAC, MATERIAL=STEEL
0.004
.....
*BEAM SECTION, SECTION=RECT, ELSET=ELBAC, MATERIAL=STEEL
0.015,0.015
1.0,0.0,0.0
.....
***----------Constraints between Nodes----------
*MPC
7,TENSMPC1, BEAM2
7,TENSMPC2, BEAM1
.....
***----------Boundary Conditions----------
*BOUNDARY
END1,2
MIDSPAN,1
SUPPORT1,3
YSYMM
.....
```

```
***----------Load Application----------
*STEP, NLGEOM, INC=20, CYCLE=10, MONOTONIC
*STATIC, PTOL=15.0
0.1,1.0,0.0001
*CLOAD, AMP=LOAD1
4,3,-1.
.....
***----------Node and Element Output----------
*NODE PRINT, NSET=COMP 13, FREQ=3
U
.....
*EL PRINT, ELSET=ELCA, FEQ=3
MISES
.....
***----------Graphical Output----------
*PLOT,FREQ=3
DEFORMED COMPRESSION FLANGES
*VIEWPOINT
1.,1.,0.
*DISPLACED
U,,1
*DETAIL, ELSET=ELCAC, NSET=COMPAC
.....
*END STEP
/*
***----------Conversion and Transfer of Graphic Outputs----------
//ABAPLOT EXEC ABQ47GIN
//    N='ELCENRY.WIT1NL.PLOT1',
//    S='ELCENRY.JOB.GINO.SAVDRA2'
//*
//FTP1    EXEC BATCHTSO
FTPTR(0) LOCAL(JOB.GINO.SAVDRA2) LUSER(ELCENRY) LPSWD
FILE(CEN5RMY.WIT)SITE(MCC.CMS)USER(ELECLHP)PSWD(XXXXXX)
 NOSAVE
```

APPENDIX II

EVALUATION OF BENDING RESISTANCE FOR DECK FORM 1 AND 2 ACCORDING TO BS5400

A. DECK FORM 1

(a) Classification of the section

Position of the elastic neutral axis of the girder = 621.7mm

$x = 1080 + 35 - 621.7 = 493.3mm$

$t_w = 20mm$

Assuming the yield stress of the steel, $\sigma_{yw} = 355Nmm^{-2}$,

$$28x20x\sqrt{\frac{\sigma_{yw}}{355}} = 480mm < 493.3mm$$

Therefore, the web is non-compact.

$$b_{fo} = \frac{(500-20)}{2} = 240mm$$

$7t_{fo} = 7x35 = 245mm > 240mm$

Therefore, the flange is compact.

Thus as a whole, the cross section of the girder is non-compact.

(b) Evaluation of the Critical Moment of Resistance

$l_e = 2.5K_3 (EI_c\delta)^{0.25}$

where $\delta = \frac{d^3}{3EI_1} + \frac{uBd_2^2}{EI_2}$

$d_1 = 1080 + 35 + \frac{35}{2} = 1132.5mm$

$d_2 = 1132.5 + \frac{220}{2} = 1242.5mm$

$I_1 = \frac{t_w^3}{12} = \frac{1000x20^3}{12} = 6.67x10^5mm^4$

$I_2 = \frac{1000x220^3}{12x10} = 8.87x10^5mm^4$, to equivalent steel unit,

therefore, neglecting the flexibility in the joints.

$$\delta = \frac{1132.5^3}{3Ex6.67x10^5} + \frac{0.5x3250x1245.5^2}{Ex8.87x10^7}$$

$\delta = 3.45x10^{-3} + 1.38x10^{-4}$

$\delta = 3.68x10^{-3}$ mm/N.

$I_c = \frac{35x500^3}{12} = 3.65x10^{-4}m^4$

and thus,

$l_e = 2.5k_3(E \times 3.565x10^{-4} \times 3.68x10^{-6})^{0.25}$, $E = 2.05x10^{11}Nm^{-2}$

$l_e = 10.18m$

$\lambda_{LT} = \frac{l_e}{r_y}k_4\eta\upsilon$

$I_y = 5.19x10^{-4}m^4$, $A_s = 0.05225m^2$

$r_y = 0.099688m$

Take $k_4 = 1.0$, and $\eta = 1.0$ for uniform bending moment

$\lambda_F = \frac{let_f}{r_yD} = 3.108$, where D = 1.150m

i = 0.703, for the shape of the girder

therefore, $\upsilon = 0.8164$, from Table 9, BS5400: Part 3

$\lambda_{LT} = 0.8164x1.0x1.0x\frac{10.18}{0.099688} = 83.37$

From Figure 10, in BS5400: Part 3

$\frac{\sigma_{li}}{\sigma_{yc}} = 0.59$

Take $\sigma_{yc} = 355Nmm^{-2}$,

$\sigma_{li} = 0.59x355 = 209.45Nmm^{-2}$

$\frac{D}{2y_t} = 0.925$

Since the section is non-compact, the bending resistance M_D is the lesser of $Z_{xt}\sigma_{xt}$ and $Z_{xc}\sigma_{xc}$

$I_x = 0.0115m^4$

$Z_{xc} = \frac{I_x}{y_c} = 0.02179$

$Z_{xt} = \frac{I_x}{y_t} = 0.0185$

$Z_{xc}\sigma_{xc} = 0.02179x209.45x0.925 = 4.22x10^6Nm$

$Z_{xt}\sigma_{xt} = 0.0185x355.0 = 6.57x10^6Nm$

Therefore $M_D = 4.22x10^6Nm$

In the calculation for the δ value, it can be seen that contribution from the presence of concrete is small (only approx 4% of the final value of δ)

For the bending moment distribution due to UDL, from Figure 9 in BS5400: Part 3,

$M_A = \frac{WL}{8}$,

$M_M = -\frac{WL}{8}$, and

$M_B = 0$

thus $\frac{M_A}{M_M} = -1$, and $\frac{M_B}{M_A} = 0$

$\eta = 0.66785$

and $\lambda_{LT} = 0.8146 \times 0.66785 \times 1.0 \times \frac{10.18}{0.099688} = 55.24$

$\frac{\sigma_{li}}{\sigma_{yc}} = 0.96$

$\sigma_{li} = 355 \times 0.96 = 340.8 N/mm^2$

$Z_{xc}\sigma_{xc} = 0.02179 \times 340.8 \times 0.925 = 6.88 \times 10^6 Nm$

Therefore, $M_D = 0.0185 \times 355 = 6.57 \times 10^6 Nm$

B. DECK FORM 2

(a) Classification of the section

Position of the elastic neutral axis of the girder = 1626.78mm

$x = 2500 + 50 - 1672.64 = 877.36mm$

$t_w = 25mm$

Assuming the yield stress of the steel = 355 Nmm^{-2},

$28 \times 25 \times \sqrt{\frac{\sigma_{yw}}{355}} = 700 \text{ mm} < 877.36mm$

Therefore, the web is non-compact.

$b_{fo} = \frac{(1200-25)}{2} = 587.5mm$

$7t_{fo} = 7 \times 70 = 490mm < 587.5mm$

Therefore, the flange is non-compact.

The cross section of the girder is non-compact.

(b) Evaluation of the Critical Moment of Resistance

$l_e = 2.5K_3 (EI_c \delta l_u)^{0.25}$, for discrete U-frame actions because of the presence of the web stiffeners, where l_u, the spacing of the stiffeners, is 3.0m .

$\delta = \frac{d_1^3}{3EI_1} + \frac{uBd_2^2}{EI_2}$

$d_1 = 2500 + 50 + \frac{70}{2} = 2585mm$

$$d_2 = 2585 + \frac{370}{2} = 2770\text{mm}$$

Considering the effect of transverse web stiffeners, the axis of bending is assigned to be x_1, and

$x_1 = 72.92\text{mm}$

Therefore I_1 of the effective web section = $3.34\text{x}10^{-4}\text{m}^4$

$$b = \frac{6000}{8}\text{ x } 2 = 1500\text{mm}$$

$$I_2 = \frac{1500\text{x}370^3}{12\text{x}10} = 6.33\text{x}10^{-4}\text{m}^4\text{, to the equivalent steel unit,}$$

therefore, neglecting the flexibility in the joints.

$$\delta = \frac{2585^3}{3\text{Ex}3.344\text{x}10^8} + \frac{0.5\text{x}6000\text{x}2770^2}{\text{Ex}6.33\text{x}10^8}$$

$$\delta = 8.399\text{x}10^{-5} + 1.7734\text{x}10^{-4}$$

$$\delta = 2.613\text{x}10^{-4}\text{ mm/N.}$$

$$I_c = \frac{70\text{x}1200^3}{12} = 0.01008\text{m}^4\text{ and thus,}$$

$$l_e = 2.5K_3(\text{E x } 0.01008 \text{ x } \frac{2.613\text{x}10^{-4}}{1000}\text{ x } 3.0)^{0.25}$$

$$l_e = 15.86\text{m}$$

$$\lambda_{LT} = \frac{l_e}{r_y}k_4\eta\upsilon$$

$$I_y = 0.01184\text{m}^4$$

$$A_s = 0.184\text{m}^2$$

$$r_y = 0.253\text{m}$$

Take $k_4 = 1.0$, and $\eta = 1.0$ for uniform bending moment

$$\lambda_F = \frac{l_{et_f}}{r_y D} = 1.436\text{ , where D} = 2500 + 70 + 50 = 2.62\text{m}$$

$i = 0.851$, for the shape of the girder

therefore $\upsilon = 0.8118$, from Table 9, BS5400: Part 3

$$\lambda_{LT} = 0.8118\text{x}1.0\text{x}1.0\text{x}\frac{15.86}{0.253} = 50.89$$

From Figure 10, in BS5400

$$\frac{\sigma_{li}}{\sigma_{yc}} = 0.945$$

Take $\sigma_{yc} = 355\text{Nm}^{-2}$,

$$\sigma_{li} = 0.945\text{x}355 = 335.475\text{Nmm}^{-2}$$

$$\frac{D}{2y_t} = 0.805$$

Since the section is non-compact, the critical moment of resistance M_D is the lesser of $Z_{xt}\sigma_{xt}$ and $Z_{xc}\sigma_{xc}$

$I_x = 0.2130m^4$

$Z_{xc} = \frac{I_x}{y_c} = 0.2145$

$Z_{xt} = \frac{I_x}{y_t} = 0.1309$

$Z_{xc}\sigma_{xc} = 0.2145x334.475x0.805 = 5.79x10^7Nm$

$Z_{xt}\sigma_{xt} = 0.1309x355 = 4.65x10^7Nm$

Therefore $M_D = 4.65x10^7Nm$

In the calculation for δ value, it can be seen that the contribution from the presence of concrete can become dominant as the flexibility of the concrete deck is increased by the increase in the spacing between girders or reduction of the flexibility of the web with the presence of transverse web stiffeners.

For the bending moment distribution due to UDL, from Figure 9(b) in the code,
$\eta = 0.66785$, as calculated in Deck Form 1,
and $\lambda_{LT} = 0.8118x0.66785x1.0x\frac{15.86}{0.253} = 33.98$

$\frac{\sigma_{li}}{\sigma_{yc}} = 1.0$

$\sigma_{li} = 355Nmm^{-2}$

The critical bending moment resistance M_D, taken as the lesser of :$Z_{xc}\sigma_{xc}$ and $Z_{xt}\sigma_{xt}$, is $4.65x10^7Nm$

It is interesting to note that, according to BS5400, the design values for critical moment of resistance of Deck Form 2 both under uniform bending and moment distribution due to UDL are exactly the same, even though the modification factor for variation of moment along the span was taken into consideration.

Table 1 Design values for Critical Moment of Resistance of Deck Form 1 and 2 according to BS5400

	Deck Form 1 ($x10^6Nm$)	Deck Form 2 ($x10^7Nm$)
Uniform Bending Moment	4.22	4.65
Moment due to UDL	6.57	4.65

LIST OF REFERENCES

1. BS5400: Part 3, *Code of Practice for The Design of Steel Bridges*, British Standard Institution, London, 1982.

2. Johnson, R. P., and Buckby, R. J., *Composite Structures of Steel and Concrete, Volume 2: Bridge*, 2nd Edition, Collins, 1986.

3. Kirby, K. A., and Nethercot, D. A., *Design for Structural Stability*, Constrado Monographs, Collins, 1979.

4. Narayanan, R.(ed.), *Beams and Beam Columns: Stability and Strength*, Applied Science Publishers, London, 1983.

5. Flint, A. R., 'The Influence of Restraints on the Stability of Beams', *J. Struct. Engr.*, Vol, XXIX, September 1951, pp235-246.

6. Winter, G., 'Lateral Bracing of Columns and Beams', *Trans. A.S.C.E.*, Vol. 125, 1960, pp807-845.

7. Travers Morgan, 'An Investigation Into Bracing Systems And Use of U-frame on Steel Bridges', *Transport and Road Research Laboratory*, 1990.

8. Timoshenko, S. P., and Gere, J. M., *Theory of Elasticity*, 3rd Edition, McGraw-Hill, New York, 1970.

9. Nethercot, D. A., 'Design of Beams and Plate Girders - Treatment of Overall and Local Flange Buckling', *The Design of Steel Bridges*, ed. by Rockey, K. C. and Evans, H. R., Granda, 1981.

10. Duffield, C. F., Hutchinson, G. L. and Stevens, L. K., 'Elastic Torsional Buckling of Through Plate Girder Rail Bridges', *Proc. Pacific Structural Steel Conference*, Auckland, New Zealand, August 1986, pp27-42.

11. Nethercot, D. A., 'Design: Bracings', *ECCS/BCSA International Symposium On Steel Bridges*, London, February 1988, pp13/1-13/13.

12. Bleich, F., *Buckling Strength of Metal Structures*, Engineering Societies Monographs, McGraw-Hill, London, 1952.

13. Allen, H. G., and Bulson, P. S., *Background to Buckling*, McGraw-Hill, London, 1980.

14. Hancock, G. J., 'Distortional and Lateral Buckling of I-Beams', *J. Struct. Div., Proc. A.S.C.E.*, Vol. 104, No. ST11, November 1978, pp1787-1798.

15. Hancock, G. J., Bradford, M. A., and Trahair, N. S.,'Web Distortion and Flexural-Torsional Buckling', *J. Struct. Div., Proc. A.S.C.E.*, Vol. 106, No. ST7, July 1980, pp1557-1571.

16. Bradford, M. A., 'Distortional Buckling Strength of Elastically Restrained Monosymmetrical I-Beams', *Thin-Walled Structures*, ed. by Rhodes, J., and Walker, A. G., Elsevier, 1990.

17. Bradford, M. A.,'Buckling Strength of Partially Restrained I-Beams', *Journal of Structural Engineering, Proc. A.S.C.E.*, 115 (5), May 1989, pp1272-1276.

18. Lawson, R. M., and Nethercot, D. A., 'Lateral Stability of I-Beams Restrained by Profiled Sheetings', *The Structural Engineer*, Vol. 63B, No. 1, March 1985, pp1-8.

19. Nethercot, D. A. and Trahair, N. S., 'Design of Diaphragm Braced I-Beams', *J. Struct. Div., Proc. A.S.C.E.*, 101, ST10, October 1975, pp2045-2061.

20. Kerensky, O. A., Flint, A. R., and Brown, W. C., 'The Basis for Design of Beams and Plate Girders in the Revised British Standard 153', *Structural and Building Engineering Division, Proc. Inst. Civil Engrs.*, Part 3, Vol. 5, 1956, pp396-461.

21. Longbottom, E. and Heyman, J., 'Experimental Verification of the Strengths of Plate Girders Designed in accordance with the Revised British Standard 153: Test on Full-Size and on Model Plate Girders', *Structural and Building Engineering Division, Proc. Inst. Civil Engrs.*, Part 3, No. 5, 1956.

22. Johnson, R. P., and Bradford, M. A., 'Distortional Lateral Buckling of Unstiffened Composite Bridge Girders', *Instability and Plastic Collapse of Steel Structures*, ed. by Morris L.J., 1982, pp569-580.

23. Climenhaga, J. J., and Johnson, R. P., 'Local Buckling in Continuous Composite Beams', *The Structural Engineer*, Vol. 50, No.9, September 1972, pp367-374.

24. Bradford, M. A., and Johnson, R. P., 'Inelastic Buckling of Composite Bridge Girders near Internal Supports', *Proc. Inst. Civil Engrs.*, Part 2, No. 83, March 1987, pp143-159.

25. Hope-Gill, M. C., and Johnson, R. P., 'Tests on Three-span Continuous Composite Beams', *Proc. Inst. Civil Engrs.*, Part 2, No. 61, 1976, pp367-381.

26. Weston G., Lateral Buckling in Diaphragmed-braced Beams and Continuous Composite Bridge Girders, Ph.D. Thesis, Department of Civil and Structural Engineering, University of Sheffield, 1987.

27. Weston G., Nethercot, N. A., and Crisfield, M. A., 'Lateral Buckling in Continuous Composite Bridge Girders', *The Structural Engineer* , Vol. 69, No. 5 March 1991, pp70-87.

28. Weston, G., and Nethercot, D. A., 'Continuous Composite Bridge Beams - Stability of the Steel Compression Flange in Hogging Bending', *ECCS Colloquium on Stability of Plate and Shell Structures*, Ghent University, April 1987, pp47-51.

29. Crisfield, M. A., 'Large-deflection Elasto-plastic Buckling Analysis of Plates Using Finite Element', *TRRL*, Report LR 593, 1973.

30. Crisfield, M. A., 'Large-Deflection Elasto-Plastic Buckling Analysis of Eccentrically Stiffened Plates Using Finite Element', *TRRL*, Report 725, 1976.

31. Crisfield, M. A., 'Ivanov's Yield Criterion for Thin-Plates and Shell Using Finite Elements', *TRRL*, Report 919, 1979.

32. Svensson, S. E., 'Lateral Buckling of Beams Analysed As Elastically Supported Column Subject to a Varying Axial Force', *Journal of Constructional Steel Research* Vol. 5, 1985, pp179-193.

33. Fan, C. K. R., Buckling In Continuous Composite Beams. Ph.D. Thesis, Department of Engineering, University of Warwick, 1990.

34. Hamada, S., and Longworth, J., 'Buckling of Composite Beams in Negative Bending', *J. Struct. Div., Proc. A.S.C.E.*, Vol. 100, No. ST11 November 1974, pp2205-2222.

35. Ansourian P., 'Experiments on Continuous Composite Beams', *Proc. Inst. Civil Engrs.*, Part 2, No. 71, 1981, pp25-51.

36. Trahair, N. S., 'Elastic Lateral Buckling of Continuously Restrained Beam-Columns', *The Profession of a Civil Engineer.*, ed. by Campbell-Allen D., and Davis E.H., Sydney University Press, 1979.

37. Trahair, N. S., and Nethercot, D. A., 'Bracing Requirements in Thin-Walled Structures.', *Development in Thin-Walled Structures*, Vol. 1 ed. by Rhodes J., and Walkers A.G., Applied Science Publishers, London, 1982 pp91-131.

38. Medland, I. C. and Segedin, C. M., 'Inter-Braced Column-Beams Steel Framed Structures', *Steel-concrete composite structures - Stability and Strength*, ed. by Narayanan, R., Elseview, London, 1988.

39. Tong, G. S., and Chen, S. F., 'Elastic Buckling of inter-braced Girders', *Journal of Constructional Steel Research* , 14(2), 1989, pp87-105.

40. Nakamura, T., 'Strength and Deformability of H-Shaped Steel Beams and Lateral Bracing Requirements', *Journal of Constructional Steel Research*, No.9, 1988, pp217-228.

41. ECCS, Second International Colloquium on Stability, Introductory Report, Liege, Belgium, 1977.

42. Goltermann, P., and Svensson, S. E., 'Lateral Distortional Buckling: Predicting Elastic Critical Stress', *J. Struct. Div., Proc. A.S.C.E*, Vol. 114, No. 7, July 1988, pp1606-1625.

43. Williams, F. H., and Jemah, A. K., 'Building Curves for Elastically Supported Columns with Varying Axial Force to Predict Lateral Buckling of Beams', *Journal of Structural Steel Research*, No.7(2), 1987, pp133-147.

44. Nakamura, T., and Wakabayashi, 'Lateral Buckling of Beams Braced by Purlins', *Inelastic Instability of Steel Structures and Structural Elements US-Japan Joint Seminar*, Tokyo, May 25-27, 1981.

45. Nakamura, T., and Wakabayashi, M., 'Lateral Buckling of Steel Beams with Reinforced Concrete Slab', *Proc. Pacific Structural Steel Conference*, Auckland, New Zealand, 1986, pp395-406.

46. Wakayabashi, M., and Nakamura, T., 'Buckling of Lateral Braced Beams', *Engineering Structure*, Vol. 5, April 1983, pp108-118.

47. Johnson, R. P., and Fan, C. K. R., 'Distortional Lateral Buckling of Continuous Composite Beams', *Proc. Inst. Civil Engrs.*, Part 2, March 1991, pp131-161.

48. Travers Morgan, 'An Investigation into Bracing System and the Use of U-Frames - Laboratory Test Model', February 1989.

49. The Welding Institute, 'Ultimate Load Test on $\frac{1}{10}$ Scale Model of a Steel Plate Girder Bridge Braced with U-Frame', December 1989.

50. Hibbitt, Kaarlsson and Sorensen Inc., *ABAQUS Theory Manual*, Version 4.7, 1989.

51. Hibbitt, Karlsson and Sorensen Inc., *ABAQUS User's Manuals, Part 1*, Manchester Computing Centre, September, 1989.

52. Hibbitt, Karlsson and Sorensen Inc., *ABAQUS User's Manuals, Part 2*. Manchester Computing Centre, September, 1989.

53. Hibbitt, Karlsson and Sorensen Inc., *ABAQUS User's Manuals, Part 3*. Manchester Computing Centre, September, 1989.

54. Manchester Computing Centre, *ABAQUS Finite Element System*, VPS 604, September 1989.

55. Manchester Computing Centre, *File Transfer Between the Amdàhl VPS and JANET NETWORK*, VPS 801, February 1989.

56. Davies, J. D., Somerveille, I. J. and Zienkiewicz, O. C., 'Analysis of Various Types of Bridges by the Finite Element Method', *Developments in Bridge Design and Construction*, ed. by Rockey, K. C., Bannister, J. L., and Evans, H. R., 1980.

57. Evans, H. R., Peksa, D. O., and Taherian A. R., 'The Analysis of Non-Linear and Ultimate Load Behaviour of Plate Structure by Finite Element Method', *Eng. Comput.*, Vol. 2, December 1985, pp271-284.

58. Crisfield, M. A., 'Some approximations in the non-linear analysis of rectangular plates using finite elements', *TRRL*, Supplementary Report 51 UC, 1974.

59. Travers Morgan, *Notes and Sketches of Steel Bridge Arrangements*, December 1988.